17β-estradiol degradation photoinduced by iron complex, clay and iron oxide minerals: effect of the iron complexing agent ethylenediamine-N,N'-disuccinic acid

Jing Li

Numéro d'Ordre : 2030

UNIVERSITE BLAISE PASCAL

U. F. R. Sciences et Technologies

ECOLE DOCTORALE DES SCIENCES FONDAMENTALES

N°: 644

THESE EN COTUTELLE

Avec l'Université de Wuhan (Chine)

Présentée pour obtenir le grade de

DOCTEUR D'UNIVERSITE

Spécialité : Chimie Physique et chimie de l'environnement

Par

Jing LI

Diplômée de Master

17β-ESTRADIOL DEGRADATION PHOTOINDUCED BY IRON COMPLEX, CLAY AND IRON OXIDE MINERALS: EFFECT OF THE IRON COMPLEXING AGENT ETHYLENEDIAMINE-N,N'-DISUCCINIC ACID

Rapporteurs:	Pr. Jean-Marc CHOVELON
	Pr. Hui ZHANG
Examinateurs:	Pr. Nansheng DENG
	Dr. Gilles MAILHOT
	Pr. Feng WU
	Dr. Marcello BRIGANTE

ABSTRACT

Light-induced transformation in aqueous solutions or suspensions/on soil surface is an important degradation pathway for many pollutants and may result in efficiency losses. It is well known that polycarboxylate-iron complexes are high photoactivity species, which could undergo rapid photochemical reactions under sunlight irradiation leading to the formation of oxidative species and degradation of pollutants. Several polycarboxylate-iron complexes such as Fe(III)-oxalate, Fe(III)-citrate as photocatalyst are well studied. Recently, because of the widely used in the various area and high concentration detected existing in the environment, aminopolycarboxylic acids (APCAs) has aroused the scientists much interests. APCAs may present behavior similar to that of polycarboxylic acid. The photolysis of Fe-EDTA/NTA is studied by several authors. EDDS is one of natural occurring APCAs, which has been proposed as a safe and environmentally benign replacement for EDTA for environmental remediation products. EDDS could form strong complex with iron, and the physicochemcial properties of Fe(III)-EDDS have been reported. However, the photochemical process of Fe(III)-EDDS is poor understood.

Clay and iron oxide minerals are widespread in nature and possess particular structural and surface charge characteristics. Clay and iron oxide minerals play an important role in the earth-chemical transformation and cycles of pollutants, involving in the adsorption, hydrolysis, auto-oxidation and photocatalytical redox processes in the environment. The clay and iron oxides minerals, either as active catalysts or supports, have been widely used as heterogeneous catalysts for the oxidation of organic pollutants. Iron is one of the elements commonly found in the clay minerals and the main component in iron oxides. Carboxylate could not only form complexes with soluble iron in the clay and iron oxides mineral suspensions, but also form surface complexes with the structure iron in the minerals, promoting the dissolution of the iron oxide in minerals under irradiation. In the same time, the surface properties of minerals will be changed due to the carboxylate-minerals complex formation. In this work, we first introduce EDDS into the clay (Natural Montmorillonite and Montmorillonite KSF) and iron oxides mineral (Goethite) and studied the photoactivity of the EDDS-clay/iron oxides mineral system using 17β-Estradiol (E2) as the model pollutant.

E2 is one of the endocrine-disrupting chemicals (EDCs) and is well-known to exhibit very potent estrogenic activity even at a very low concentration (~10^{-9} M, in vitro). Due to the harmful effect of E2 and the widespread occurrence in the aquatic environment, people pay

more and more attention to the removal of E2 in the wastewater. Several advanced oxidation processes (AOPs) have been applied succesufully for oxidation and mineralization of E2, such as TiO_2-mediated photocatalysis, photo-Fenton catalytic reactions, O_3/UV process, ozonation, electrochemical oxidation process. However, no reference reported using EDDS-Fe(III)/clay/iron oxides to degradation of E2 under irradiation.

The objective of this work is to understand the photochemical process and the reaction mechanism of E2 degradation in the presence of light and Fe(III)/clay/iron oxides-EDDS complexes, which can produce basic knowledge that could be used to predict the fate of organic pollutant in natural environments and also expand the view of wastewater treatment. Main experiment contents and conclusions of this dissertation are as follows.

(1) In the first part of this work, the properties of Fe(III)-EDDS was studied and the model minerals (Montmorillonite KSF, natural Montmorillonite, Goethite) were characterized with X-ray powder diffraction (XRD), X-ray fluorescence (XRF), Transform infrared (FT-IR) and Transmission electron microscopy (TEM), etc. The experimental results indicated that pH was an important parameter for the speciation of Fe(III)-EDDS. Under 365 nm irradiation, the Fe(III)-EDDS complexes at different pH were easily photolyzed. During the irradiation, the absorbance of Fe(III)-EDDS at λ = 240 nm decreases faster at lower pH, but it seems that at higher pH, there are more new species formed in the solution. The iron contents in the form of Fe_2O_3 existing in the KSF, NM, Goethite are 4.76%, 4.28%, 100% respectively. But the amount of free iron ions in the minerals was in the order: KSF > Goethite >NM. The BET surface area of the minerals were Goethite (71 m^2 g^{-1}) > NM (32 m^2 g^{-1}) > KSF (5 m^2 g^{-1}). The isoelectric points (PI) of KSF, NM, Goethite is about 5, 2 and 4 respectively. The acido-basic properties of the surface of the three solids are rather different. Indeed, once in suspension the solid modified the solution pH. Values of 7.7, 9.0 and 3.7 are respectively measured for Goethite, NM and KSF. The quite different properties of the minerals help understand the photochemical process of the EDDS-minerals systerm.

(2) The quantum yield of $^{\bullet}OH$ and the degradation of E2 in homogeneous irradiated Fe(III)-EDDS system was investigated. For the first time, the quantum yield of $^{\bullet}OH$ was detected by photolysis of Fe(III)-EDDS. The quantum yield of $^{\bullet}OH$ was independent of the concentration of Fe(III)-EDDS. Lower wavelength and higher concentration of O_2 favored the quantum yields of $^{\bullet}OH$. The quantum yield of $^{\bullet}OH$ radical formation was higher at higher pHs between 3.0 and 9.0. This result is particularly interesting in terms of the natural environment. Correspondingly, E2 could be photodegraded by the photolysis of

Fe(III)-EDDS, which is influenced by the concentration of Fe(III)-EDDS, pH, O_2 and the concentration of Fe(III). The Fe(III)-EDDS complex would be of importance for the transformation of organic compounds in the environment due to its higher photoactivity at pHs more relevant to the environment. The reaction rate constants with $^{\bullet}OH$ of E2 and EDDS were also measured to be 6.7×10^{9} $M^{-1}s^{-1}$ and 2.0×10^{8} $M^{-1}s^{-1}$ respectively. Although the reaction rate constant of $k_{E2,\bullet OH}$ is about ten times higher than the $k_{EDDS,\bullet OH}$, due to the ten times higher concentration of EDDS used than that of E2 in our experiments, the competition between EDDS and E2 reacting with $^{\bullet}OH$ should not be ignored. Several photoproductions was detected by LC-MS. The photodegradation mechanism was deduced in this work. Attacking by Hydroxyl radical was thought to be the main degradation pathway of E2.

(3) The quantitative determination of $^{\bullet}OH$ radicals in the Montmorillonite suspensions under irradiation of a 250 W metal halide lamp ($\lambda \geq 365$ nm) was investigated for the first time. Low pH value facilitated the formation of hydroxyl radicals in the pH range of 2.0 to 10.0. The $^{\bullet}OH$ concentration increased with increasing the concentration of Montmorillonite in aqueous solutions in the range of 0 to 20.0 g L^{-1}. Higher concentration like 25.0 g L^{-1} of Montmorillonite inhibited the $^{\bullet}OH$ production. Iron, predominantly free iron in the clays, is believed to be one of the most important factors determining $^{\bullet}OH$ formation. Structural irons in Montmorillonite have also contributions to $^{\bullet}OH$ formation but especially in the presence of carboxylate ions. The formation of $^{\bullet}OH$ from Montmorillonite under irradiation of near UV and visible light indicates that clays might play important role not only in transfer through adsorption but also in transformation through oxidation of organic compounds on the surface of clay particles in air, water, soil or even top sediments.

(4) The adsorption and photocatalytic degradation process of E2 in the suspension of Montmorillonite KSF, Natural Montmorillonite (NM) and Goethite were studied. The adsorption of E2 on the minerals is fast and weak. The results followed the Langmuir equation in the KSF and Goethite suspensions, and the Freundlich equation in NM suspensions. EDDS influence slightly the E2 adsorption on the minerals. However, the influence of E2 adsorption on the degradation process was not found. The E2 degradation rate was influenced by the concentration of minerals and pH. The degradation of E2 was decreased with increasing the pH and in the basic pH there was almost no E2 degradation. The optimal pH for the E2 degradation was around 3.0 in all the three minerals. The results indicated that the iron in the minerals was involved in the photocatalytic process.

(5) The photocatalytic degradation process of E2 in the suspension of Montmorillonite KSF, Natural Montmorillonite and Goethite in the presence of EDDS were studied. In these three minerals-EDDS suspensions, the degradation of E2 significantly increased at near-neutral pH and basic pH (pH 5.0 to 9.0). On the contrary without EDDS, the optimal pH is limited in the acid pH (3.0 to 4.0). The degradation kinetics of E2 follows the Langmuir-Hinshelwood rate law in all the three minerals-EDDS system. Small amount of minerals is enough to get good degradation efficiency in the presence of EDDS, i.e. KSF 0.1 g L^{-1}, NM 0.1 g L^{-1} and Goethite 0.1 g L^{-1}. The concentration of EDDS is a very important factor influencing the efficiency of E2 degradation. EDDS plays an important role for keeping ferrous iron soluble at cirumneutral pH and the photochemical process of the minerals-EDDS can continue. During the E2 degradation, EDDS also is degraded. Oxygen is a very important factor that affects the photodegradation of E2. Oxygen takes part in the photochemical process in such system. Without oxygen, the hydroxyl radicals barely could be formed. After adding 2-propanol into the suspension, there was almost no E2 degradation, indicating that the main degradation pathway of E2 was the reaction with $^{\bullet}OH$. Thus all these results show that the concentration of minerals and EDDS, solution pH and oxygen must be taken into account as major parameters to improve the efficiency of the mineral-EDDS photochemical process.

Based on the above results, EDDS-Fe(III)/mineral systems are effective photocatalysis system for the removal of the organic pollutants. The most specialties of the EDDS-Fe(III)/mineral photochemical system are their high photocatalysis efficiency in the neutral pH range, even in the basic pH. And iron, the minerals and EDDS widely exist in the nature environment. Thus, they are promising ways for the removal of the contaminations in the nature aqueous environment.

Keywords: Clay, Iron oxides, EDDS, Hydroxyl radical, 17β-Estradiol, Photodegradation

Acknowledgements

This project has been carried out within the framework of the cooperation program, between Wuhan University and Blaise Pascal University. Part of my work was carried out in the Laboratory of Environmental Science directed by Prof. Nansheng DENG. and Feng Wu. The other part was carried out in Laboratoire de Photochimie Moléculaire et Macromoléculaire UMR CNRS 6505 from Blaise Pascal University led by Dr. Claire RICHARD. I would sincerely like to thank them for providing the good experimental conditions, supervision, and help.

I cordially express my thanks to Prof. Nansheng DENG and Dr. Feng WU, who give me a lot of help during my study in Wuhan University. Thanks a lot for their great support and helpful guide on my thesis. I learned a lot from them.

I'm honored to express my gratitude to Dr. Gilles MAILHOT who provided the scientific responsibility of this thesis. He has offered me valuable ideas and suggestions to prepare my thesis. He is always available when I have troubles. His hard-working, conscientiousness, full of ideas deeply impressed me and influenced on me. I spent a very happy time in Clermont-Ferrand.

I want to sincerely thank Ms. Lei WNAG, Mr. Changbo Zhang, Mr.Yanxiang LIU, Ms. Zhang'E PENG, Ms. Beibei WANG, Mr. Xu ZHANG, Mr. Li GUO, Mr. Xiaofei XUE, Ms. Yixin LIN, Mr. Lijie BAI, Mr. Xuwei WU, Mr. Zhiping WANG, Mrs. WenYu HUANG who are my colleague in the lab and friends of Wuhan University. I am very grateful to Mrs. Mei Xiao and Mrs. Lin Zhang, who give me many help in Wuhan University.

I also wish to express my thanks to all members of the laboratory in France Madam Benedicte MAILHOT, Mr. Mohamed SARAKHA, Mrs. Bernadette LAVEDRINE, Mr. Guillaume VOYARD, Mr. Jean-Philippe DEBOUT, Mr. Pascal WONG WAH CHUNG, Mrs. Alexandra TER HALLE, Mr. Vincent VERNEY, Mr. Ghislain GUYOT, Mr. Marius PARAZOLS, Mr. Christian COELHO, Ms. Marie SIAMPIRINGUE, Mr. Boris EYHERAGUIBEL, Ms. Eliana SILVA, Ms. Monica MABSILVA, Mr. Sebastien BELLINCK and Mr. Michal KOLAR, and to the people that I forgot the name and that I have not mentioned. Thanks for their friendship and help for me when I stay in Blaise Pascal

University.

I would like to take the opportunity to thank my friends, who lived in France, for their kindly help. They are Ms. Jing Li, Ms. Lei Fu, Ms. Mr. Wei ZHANG, Mrs. Jing MAI, Ms. Yun DENG, et al.

Thanks for the fund support of China Scholarship Council (CSC) affiliated with the Ministry of Education of the P. R. China. Thanks also go to the Education Service of China Embassy in Paris.

I am immensely grateful to my parents, my sister and my husband. I love you so much.

CATALOGUE

I

INTRODUCTION

I-Introduction

Clay and iron oxide minerals are widespread in nature and possess particular structural and surface charge characteristics. As abundant environmental friendly raw materials, they are used in various areas, such as industry, agriculture, engineering and construction applications, environmental remediation, and geology. These uses depend on one or more of the unique properties of the minerals. Moreover, as the important components in the soil, atmospheric aerosols, the suspended particle of water and the sediments, clay and iron oxide minerals play an important role in the earth-chemical transformation of pollutants, involving in the adsorption, hydrolysis, auto-oxidation and photocatalytical redox processes in the environment.

In recent years, the photoactivity of the clay and iron oxides minerals has attracted a great interest among the researchers. The clay and iron oxides minerals, either as active catalysts or supports, have been widely used as heterogeneous catalysts for the oxidation of organic pollutants. Research of clay and iron oxides minerals photochemical detoxification has mainly focused on three types: (1) raw minerals photocatalysis; (2) Photo-Fenton-like reaction; (3) other modified clay/iron oxides photocatalysis. Much attention has been paid to the photo-Fenton-like reaction and the modified clay photocatalysis due to their high photocatalytic activity as well as their prospective application to wastewater detoxification. As far as we know, there are few studies concerning raw clay photocatalysis and the mechanism is unclear.

Iron is the most abundant transition metal in the earth's crust. Iron is present under a variety of forms in water ranging from soluble to colloidal and particulate species. Most of the iron in natural waters exists in the form of insoluble ferric oxides and (hydr)oxides. The concentration of dissolved iron is very low and most of the dissolved iron is associated with strong organic ligands in natural waters. Polycarboxylates such as citrate, malonate, and oxalate are common constituents of precipitation, fog, surface waters and soil solutions. Polycarboxylates can form strong complexes with Fe^{3+} and enhance the dissolution of iron in natural water through photochemical processes. Moreover, such polycarboxylate complexes undergo rapid photochemical reactions under sunlight irradiation leading to the formation of oxidative species and degradation of pollutants.

Aminopolycarboxylic acids (APCAs) may present behavior similar to that of polycarboxylic acid. Aminopolycarboxylic acids have the ability to solubilize and inactivate

metal ions by complex formation. For that reason, they are used in a wide variety of domestic products, industrial applications and soil remediation. Ethylenediamine-*N*,*N'*-disuccinic acid (EDDS) is one of natural occurring APCAs. Ethylenediamine-*N*,*N'*-disuccinic acid (EDDS) is a structural isomer of EDTA, and exists as three stereo isomers, namely [S,S]-EDDS, [R,R]-EDDS and [R,S/S,R]-EDDS. Among them, [S,S]-EDDS is readily biodegradable. Recently S,S-EDDS(*S*,*S*-ethylenediaminedisuccinic acid) has been proposed as a safe and environmentally benign replacement for EDTA for environmental remediation products as it is also a strong complexing agent.

Iron is one of the elements commonly found in the clay minerals and the main component in iron oxides. Carboxylate could not only form complexes with soluble iron in the clay and iron oxides mineral suspensions, but also form surface complexes with the structure iron in the minerals, promoting the dissolution of the iron oxide in minerals under irradiation. In the same time, the surface properties of minerals will be changed due to the carboxylate-minerals complex formation. Thus, introducing the carboxylates into the clay and iron oxides minerals would have an important influence on the degradation and transformation of pollutant.

17β-Estradiol (E2) is a well-known natural endocrine disrupting compounds (EDCs). E2 is also of major concern as environmental contaminant due to the very potent estrogenic activity even at very low concentration (~10^{-9} M, in vitro). E2 is produced and released into the environment by humans, livestock, and wildlife. It has been detected in several sewage treatment plants (STP), surface water and groundwater. In addition, most of the E2 concentration detected in these waters is high enough to exist harmful effect to human and wildlife. Due to the harmful effect of E2 and the widespread occurrence in the aquatic environment, people pay more and more attention to the removal of E2 in the wastewater. Advanced oxidation processes (AOPs) have been thought to be the most efficient method for oxidation and mineralization of E2. Several AOPs have been studied and applied for the treatment of E2, such as TiO_2-mediated photocatalysis, photo-Fenton catalytic reactions, O_3/UV process, ozonation, electrochemical oxidation process.

The objective of this work is to understand the photochemical process and the reaction mechanism of E2 degradation in the presence of light and Fe(III)/clay/iron oxides-EDDS complexes, which can produce basic knowledge that could be used to predict the fate of organic pollutant in natural environments and also expand the view of wastewater treatment.

In the first part of this work, the properties of Fe(III)-EDDS was studied and the model

minerals (Montmorillonite KSF, natural Montmorillonite, Goethite) were characterized with X-ray powder diffraction (XRD), X-ray fluorescence (XRF), Transform infrared (FT-IR) and Transmission electron microscopy (TEM), etc.

Secondly, the quantum yield of $^{\bullet}OH$ and the degradation of E2 in homogeneous irradiated Fe(III)-EDDS system were investigated. The main factors, Fe(III)-EDDS concentration, irradiation wavelength, oxygen, and pH were studied. The reaction rate constants with $^{\bullet}OH$ of E2 and EDDS were measured by competition kinetics with 2-propanol.

Thirdly, the formation of $^{\bullet}OH$ in the Montmorillonite suspensions under irradiation with a 250 W metal halide lamp ($\lambda \geq 365$ nm) was quantitatively determined. The degradation of E2 in heterogeneous irradiated Montmorillonite KSF, natural Montmorillonite, Goethite/EDDS system are presented. The effect of mineral concentration, EDDS concentration, pH, oxygen, 2-propanol, initial E2 concentration on the E2 degradation were investigated. During the irradiation, except the concentration of E2 was detected, the concentration of EDDS and iron were also followed.

II

BIBLIOGRAPHY STUDY

II-Bibliography study

A-Clay and iron oxide minerals in the environment

A-1 Properties of clay and iron oxides

A-1-1 The structure and properties of clay

Clay minerals are ubiquitous in soils, sediments, atmospheric aerosols in the troposphere (Sposito *et al*., 1999; Thomas, 2005). Clay minerals have been mined and well known to humanity as the raw materials used to make Chinese porcelain since the Stone Age. But until the early 20th century, people start to research clay minerals consciously. Recently, they have gained much more attention and renewed interest from science and academia as well as industry for their unique and interesting properties (Shichi and Takagi, 2000).

Clay minerals are layer-type phyllosilicates, with particle dimension smaller than 2 μm which is the colloidal size range (Zen and Kumar, 2004). The aluminum(III) cations are bonded to an octahedral arrangement of oxygen anions. Repetition of these AlO_6 units in two dimensions forms an octahedral layer. Likewise, a tetrahedral layer is formed from SiO_4 silicate units (Laszlo, 1987). Tetrahedral (T) and octahedral (O) sheets are combined to create TO or TOT layers, which are separated by an interlayer space. Each layer has a net negative charge, which is compensated by exchangeable cations placed in the interlayer space (Mashlan *et al*., 2009). Clay minerals are classified not only by the differences in their layered structures but also by the types of substituted metals, amounts and kinds of exchangeable ions within the interlayer, and the impurities present. The Classification of clay minerals is shown in Table II-A-1.

Montmorillonite is one of the minerals in the smectite type. The chemical composition of Montmorillonite consists of high amount of SiO_2, $A1_2O_3$, H_2O and small amount of Fe_2O_3, CaO, MgO, K_2O, MnO, FeO, TiO_2, P_2O_5 and so on. The layer structure of Montmorillonite consists of two silica tetrahedral sheets and an alumina octahedral sheet, as shown in Figure II-A-1. Stacking of the layers of around 1 nm thickness by a weak dipolar force leads to interlays between the layers (Qin *et al*., 2005). The interlayers are occupied by exchangeable metal ions (e.g. Na^+, K^+, Ca^{2+}, Mg^{2+}), neutralizing the net negative charges which are generated by partial substitution of Al^{3+} with Mg^{2+} at the octahedral sites. It is well known

that Montmorillonite particles carry two kinds of electric charges: a variable (pH dependent) charge resulting from proton adsorption/desorption reactions on the surface of hydroxyl groups and a structural negative charge resulting from isomorphous substitutions within the clay structure (Liu et al, 2008). The OH groups and O atoms on the broken edges of Montmorillonite hydrolyze and form Lewis acid or Lewis base functional groups that are the sources of the pH-dependent charge. The substitution of Fe^{2+} and Mg^{2+} atoms for Al^{3+} in the octahedral layer creates a positive charge deficit, giving to the overall structure a net negative charge. The isomorphic substitution is the origin of the permanent charges that exist on the surface of Montmorillonite. The particle size of Montmorillonite is about 0.2-1μm and has specific areas of the order of 500 m^2g^{-1}, sometimes as high as 760 m^2g^{-1} (Odom I.E. 1984). Due to the so small crystals of Montmorillonite, they may remain suspended in the liquid indefinitely, so that a colloid state is attained. The ability to impart high viscosity and to develop thixotropy is unique properties of naturally occurring Montmorillonite. As a consequence of the negative potential and a specifically large surface area, Montmorillonite has very important cation adsorption, cation exchange, intercalation and swelling properties (Pinnavaia 1983). Montmorillonite has a large cation exchange capacity. The cation exchange capacity (CEC) of relatively pure Montmorillonite ranges between 70 and 130 meq/100 g. The intercalation properties of clay minerals as host materials can construct organically modified layer surface of clay minerals. Now, the scientists have understood these properties of Montmorillonite better. They focus their research on the modification of Montmorillonite to prove the activity of them and expand the application of them in the industry, agriculture and environment.

Table II-A-1 Classification of clay minerals (Shichi and Takagi, 2000)

Clay	Ideal composition $M_{int}(M_{oct})(M_{tetra})O_1(OH)_m \cdot nH_2O$[a]	Layer type	Schematic structure[b]
1:1			
Kaolinite group (charge density ~ 0 per unit)			
Kaolinite	$(Al_2)(Si_2)O_5(OH_4)$	Dioctahedral	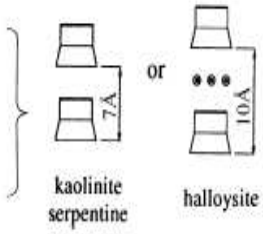
Halloysite	$(Al_2)(Si_2)O_5(OH_4)\cdot 2H_2O$	Dioctahedral	
Serpentine group (charge density ~ 0 per unit)			
Serpentine	$(Mg_6)(Si_4)O_{10}(OH)_8$	Trioctahedral	
2:1			
Pylophyllite group (charge density ~ 0 per unit)			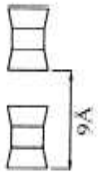
Pyrophyllite	$(Al_2)(Si_4)O_{10}(OH)_2$	Dioctahedral	
Talc	$(Mg_3)(Si_4)O_{10}(OH)_2$	Trioctahedral	
Smectite group (charge density: x ~ 0.2–0.6 per unit)			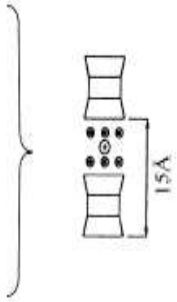
Montmorillonite	$M_x(Al_{2-x}Mg_x)(Si_4)O_{10}(OH)_2\cdot nH_2O$	Dioctahedral	
Beidellite	$M_x(Al_2)(Si_{4-x}Al_x)O_{10}(OH)_2\cdot nH_2O$	Dioctahedral	
Nontronite	$M_x(Fe_2^{3+})(Si_{4-x}Al_x)O_{10}(OH)_2\cdot nH_2O$	Dioctahedral	
Saponite	$M_x(Mg_3)(Si_{4-x}Al_x)O_{10}(OH)_2\cdot nH_2O$	Trioctahedral	
Hectorite	$M_x(Mg_{3-x}Li_x)(Si_4)O_{10}(OH)_2\cdot nH_2O$	Trioctahedral	
Vermiculite group (charge density: x ~ 0.6–0.9 per unit)			
Dioctahedral vermiculite	$M_x(Al_{2-y}Fe_4^{3+})(Si_{4-x}Al_x)O_{10}(OH)_2\cdot nH_2O$	Dioctahedral	
Trioctahedral vermiculite	$M_x(Mg_3)(Si_{4-x}Al_x)O_{10}(OH)_2\cdot nH_2O$	Trioctahedral	
Mica group (charge density: x ~ 0.6–1 per unit)			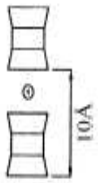
Mica (muscovite)	$K(Al_2)(Si_3Al)O_{10}(OH)_2$	Dioctahedral	
Illite	$K_x(Al_2)(Si_{4-x}Al_x)O_{10}(OH)_2$	Dioctahedral	
Biotite	$K[(Mg, Fe^{2+})(Fe^{3+}, Al, Ti)](Si, Al)_4O_{10}(OH)_2$	Trioctahedral	
Chlorite group			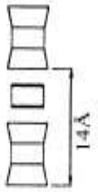
Cookeite	$[LiAl_2(OH)_6][(Al_2)(Si_3Al)O_{10}(OH)_2]$	Dioctahedral	
Clinochlore	$[Mg_2Al\ (OH)_6][(Mg_3)(Si_3Al)O_{10}(OH)_2]$	Trioctahedral	
Chamosite	$[Fe_2Al\ (OH)_6][(Mg_3)(Si_3Al)O_{10}(OH)_2]$	Trioctahedral	
Channel type			
Sepiolite	$M^{2+}_{(x+y+2z)/2}(Mg_{8-y-z}M_y^{3+}\square_z)$ $(Si_{12-x}M_x^{3+})O_{30}(OH)_4(OH_2)_4\cdot 8H_2O$		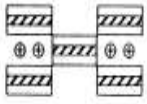
Palygorskite	$M^{2+}_{(x-y+2z)/2}(Mg_{5-y-z}M_y^{3+}\square_z)$ $(Si_{8-x}M_x^{3+})O_{20}(OH)_2(OH_2)_4\cdot 4H_2O$		

[a] M_{int}: intercalated metal cations; M_{oct}: cations occupying octahedral position; M_{tetra}: cations occupying tetrahedral position.
[b] ⏢: tetrahedral sheet; □: octahedral sheet; ▬: OH surface; ⊙: H_2O; ⊕: interlayer cation.

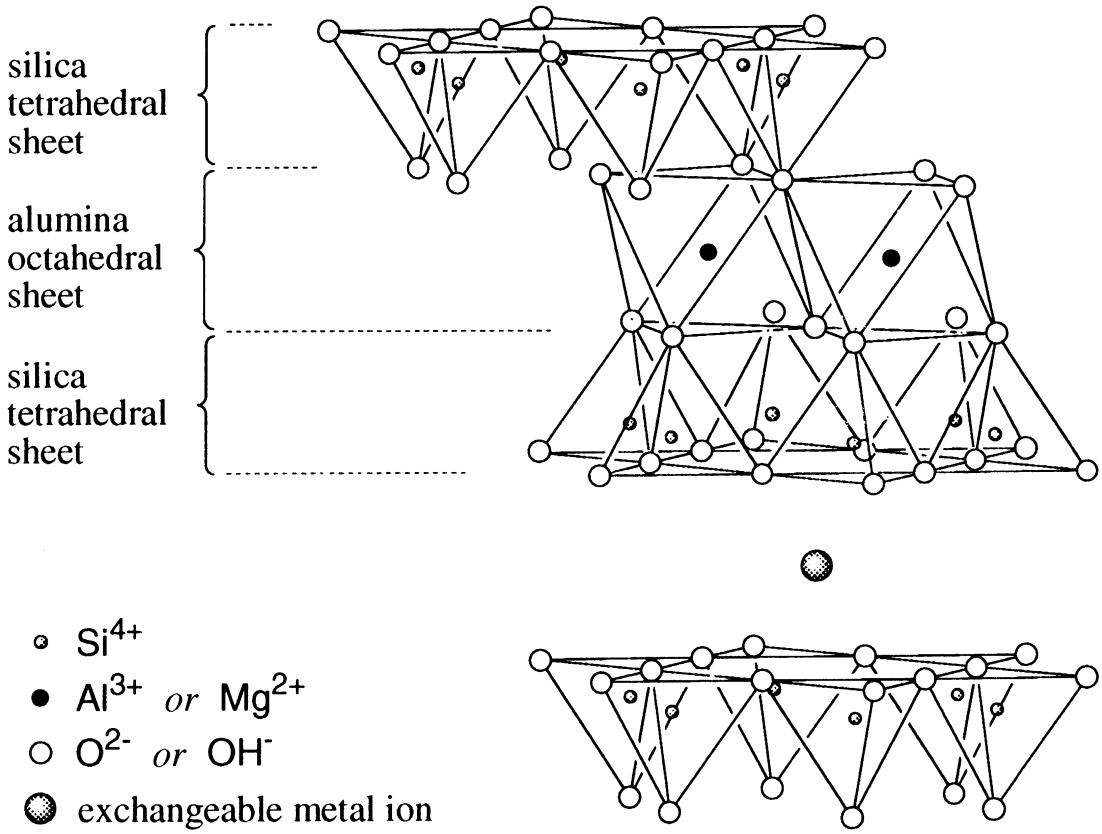

Figure II-A-1 Crystal structure of Montmorillonite

A-1-2 Iron in clay minerals

Iron is one of the elements commonly found in the clay minerals. As we all know that the iron in the natural environment plays a central role in many biological and chemical processes. Iron present in the clay also plays also important role, being active sites or enhancing the reactivity of the clay surface in many processes, especially the redox and photocatalysis processes (Cheng *et al*., 2008). Iron in the clay minerals is present in three different chemical environments within the clay structure and at the mineral surface (Figure II-A-2): (1) interlayer iron cations that balance the negative charges of the clay layers, and are exchangeable with other cations; (2) structural iron that substitutes aluminum in the octahedral lattice; (3) iron complexed by surface hydroxyl groups on the edge of a clay sheet (complexed iron) (Song *et al*., 2006; Gates and Slade, 2002) Different kinds of clay minerals contain the different content and oxidation state of iron in the different chemical environments. For example, Montmorillonite usually contains structural iron to an extent of about 3% by weight compared to about 20% or more in Nontronite.

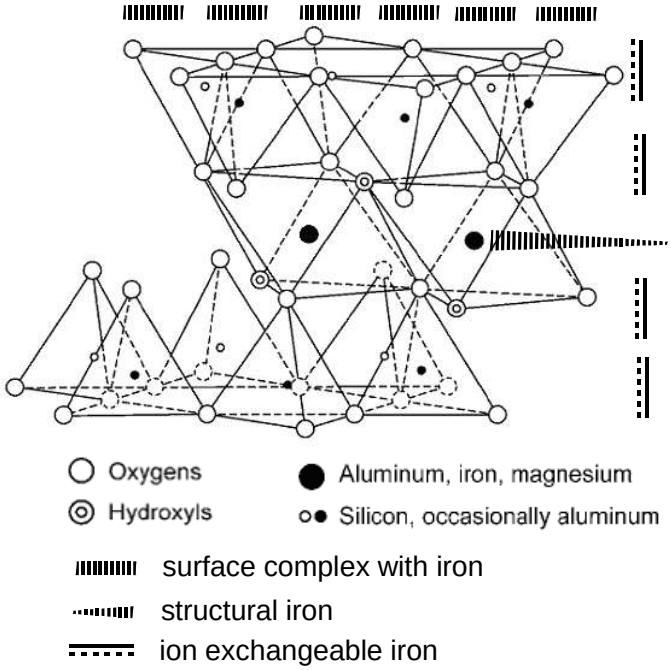

Figure II-A-2 The chemical environment of iron in 2:1 clay

Iron in clay minerals may play different roles under different nature and experimental conditions. The three different types of iron species may exhibit different reactions in a chemical process. Structural and surface-bound Fe(II) of clay minerals is known to play a significant role in reductive transformation of many reducible pollutants, such as chlorinated compounds, nitroaromatic compounds (NACs), chromium(VI), technetium(VI), uranium(VI), oxamyl and related carbamate pesticides (Kriegman-King and Reinhard,1992; Hofstetter *et al*., 2003; Buerge and Hug, 1999; Amonette, 2003). Taylor *et al*. (2000) found that reduced ferruginous Smectite (sample SWa-1) reduces Cr^{6+} to Cr^{3+} with an efficiency of 79% of the idealized 1:3 ratio of Cr^{6+} reduced to structural Fe^{2+} oxidized. Hofstetter *et al*. (2003) investigated the accessibility and reactivity of the three types of Fe(II) species in suspensions of two different clay minerals containing either ferrous iron-bearing Nontronite or iron-free hectorite. It was found that the NACs were reduced to anilines by both structural and surface iron species, while the interlayer exchangeable Fe(II) ions did not contribute to the reduction of NACs. The Iron-bearing clays have been found to be active heterogeneous Fenton catalysts (Feng, 2004). It is believed that the iron species in the clay play also very important role in the photocatalysis reactions for the degradation of organic pollutants. Cheng *et al*. (2008) found that the iron species in layered clays are active for catalytically oxidizing synthetic dyes with H_2O_2 under visible irradiation and the reactivity of the iron species greatly depends on their chemical environments. The exchangeable interlayer iron ions in the clay exhibit much better ability to catalyze the mineralization of malachite green

(MG) than the structural iron. The addition of foreign ligands of iron ions in clay suspensions could accelerate the degradation of MG due to the enhancement in the electron transfer between the dye and the structure Fe(III). Song *et al*. (2006) examined the reactivity of iron-bearing clays to catalyze the decomposition of hydrogen peroxide under light irradiation. It was found that free iron oxides on clay surface efficiently catalyzed the decomposition of H_2O_2 under UV light irradiation but structural iron in the octahedral lattice showed poor reactivity. The simple pathways of H_2O_2 decomposition catalyzed by iron-oxides and structure iron in clay shows in scheme II-A-1. Wu *et al*. (2008) detected the formation of hydroxyl radicals in Montmorillonite suspensions under irradiation. They found that iron, predominantly free iron in the clays, is one of the most important factors determining $^{\bullet}OH$ formation. Structural irons in Montmorillonite have contributions to $^{\bullet}OH$ formation, especially in the presence of carboxylate ions. Although the reactivity of iron species in the clay has been attracted much more attention no matter in the redox processes or photocatalysis processes, the mechanism is still not very clear. Much more work need to do.

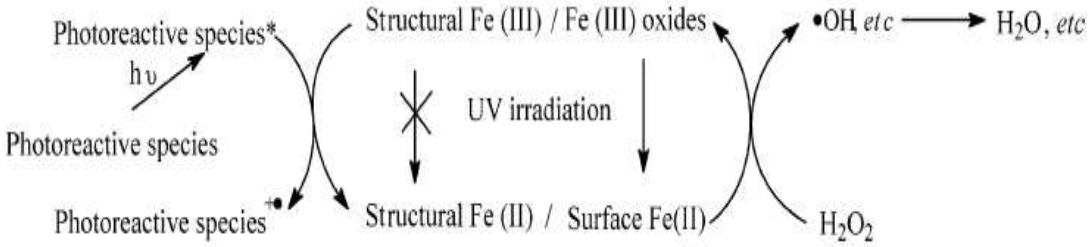

Scheme II-A-1 Pathways of H_2O_2 decomposition catalyzed by iron-bearing clay (Wu *et al*.,2008)

A-1-3 The structure and properties of iron-oxides

The iron oxides are a class of minerals produced by the chemical interaction between Fe and O and/or OH. Iron oxide minerals are widespread in nature, appearing in soils, rocks, sediments, atmosphere, fresh and salt water systems (Cornell and Schwertmann, 2003; Banfield and Zhang, 2001). Iron oxides in the nature exist as oxides, hydroxides, or oxyhydroxides. There are about fourteen iron oxides that have been recognized in nature, they are shown in Table II-A-2. The iron oxides could be transformed from other iron oxides by heating. The basic mineralogical structure of iron oxides is an octahedron, in which each iron atom is surrounded by O and OH ions (Schwertmann and Cornell, 1991). Most of iron oxides are often in the size range of clay particles (less than 2 μm), so they occur as dust in

the atmosphere and as colloids in aqueous solutions. Iron oxides have a high affinity for anions such as AsO_4^{3-}, CO_4^{2-}, Cl^-, PO_4^{3-} and the iron in iron oxides could be partly replaced by other cations such as Al^{3+}, Mn^{3+}, Cr^{3+}, V^{3+}, Zn^{2+}, Cu^{2+}, Co^{3+} (Cornell and Schwertmann, 2003). Iron oxides could absorb light 200-800 nm and have an optical band gap of 2-2.5 eV. Most of them have semiconductor properties and then can behave as photocatalysts (Mazellier and Bolte, 2000). Iron oxides can be dissolved by reaction with various combinations of protons, organic and inorganic ligands, and reductants upon illumination or not (Stumm, 1992). Once dissolved, iron may stay in solution if it is complexed with organic ligands with a high affinity for iron, or reprecipitate. According their properties and widespread in nature, they play a vital role in a variety of chemical and biological processes in aquatic and edaphic ecosystems and have widely used in industry, art pigment and sources of iron for steel production.

Table II-A-2 The iron oxides in the nature

	Oxide Name	Formula
Oxides	Wustite	FeO
	Hematite	α-Fe_2O_3
		β- Fe_2O_3
	Maghemite	γ- Fe_2O_3
		ϵ- Fe_2O_3
	Magnetite	Fe_3O_4
Hydroxides	Bernalite	$Fe(OH)_3$
	Iron(II) Hydroxide	$Fe(OH)_2$
oxyhydroxides	Goethite	α- FeOOH
	Akaganéite	β- FeOOH
	Lepidocrocite	γ- FeOOH
	Feroxyhyte	δ- FeOOH
		δ'- FeOOH
	Ferrihydrite	$Fe_5HO_8 \cdot 4H_2O$

Goethite (α-FeOOH) was studied in this thesis. It is one of the most thermodynamically stable forms of iron oxides and plentiful in the earth's crust. The structure of Goethite consists of double bands of edge-sharing $FeO_3(OH)_3$ octahedra, with the double bands linked by corner-sharing to form spaces crossed by hydrogen bridges, as shown in Figure

II-A-3. The other main properties of goethite were shown in Table II-A-3 (Schwertmann and Cornell, 1991). Previous works have explored abiotic and biotic reduction of goethite (Liu *et al*., 2001; Dong *et al*., 2003), organic compounds and metal adsorption on goethite (Yost and Anderson, 1984; Nowack and Sigg, 1996), dissolution of goethite (Wiederhold *et al*., 2006; Houben 2003), transport and conversion of chemical species by goethite (Chun *et al*., 2006; Chun *et al*., 2005; Amonette *et al*., 2000; Lu 2000), and synthesis of the thermodynamic energies of goethite (Rarida and Das, 1996; Laberty and Navrotsky, 2005). In this work, the photoactivity of goethite is studied.

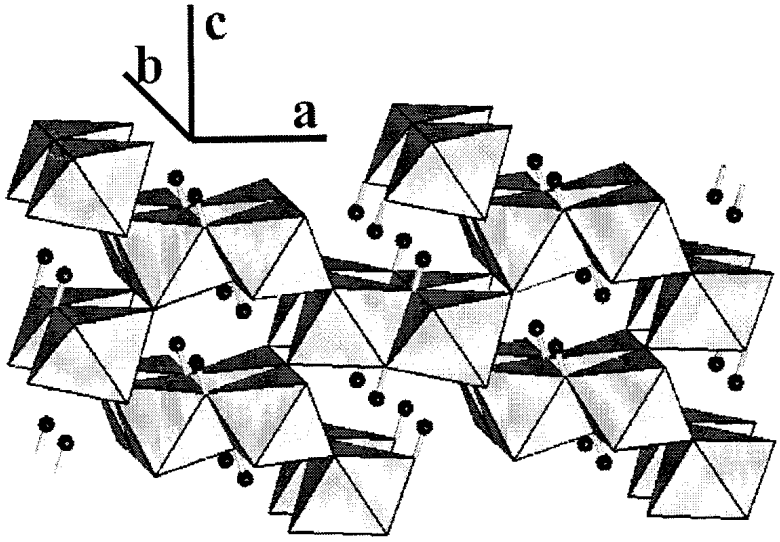

Figure II-A-3 The structure of Goethite (Dots represent H atoms)

Table II-A-3 General properties of Goethite

	Goethite
Formula	α- FeOOH
color	yellow
Solubility product (pFe + 3 pOH)	43.3-44.0
Standard free energy of formation ΔG_f° (kJ mol^{-1})	-489
Particle size	≤ 1 μm
shape	acicular
Specific surface area	20-30 m^2g^{-1}
Density	4.26 g cm^{-3}
Crystal structure	orthorhombic
Unit cell dimension(nm)	a = 0.4607, b = 1.254, c = 0.307
Formula units/unit cell	4

A-2 Photochemical behavior of clay and iron oxide minerals

As we mentioned above, clay and iron oxide minerals are widespread in the natural environment and possess particular structural and surface charge characteristics. So, they play an important role in the transformation of organic molecules in the aquatic and edaphic system. In recent years, the high photoactivity of the clay and iron oxides minerals has attracted a great interest among the researchers. The clay and iron oxides minerals, either as active catalysts or as supports, have been widely used as heterogeneous catalysts for the oxidation of organic pollutants. Research of clay and iron oxides minerals photochemical detoxification has mainly focused on three types: (1) raw minerals photocatalysis (2) Photo-Fenton-like reaction (Clay/iron oxide minerals/UV/H_2O_2 or carboxylate) (3) other modified clay/iron oxides photocatalysis. We will introduce these applications of clay and iron oxides as photocatalyst in detail below.

A-2-1 Raw clay and iron oxides photocatalysis

The reports about the clay and iron oxides used as heterogeneous catalysts alone are very limited. Katagi (1990) investigated the photodegradation of the organophosphorus fungicide tolclofos-methyl (I) on kaolinite and Montmorillonite solid surface under the irradiation of a 500-W xenon lamp. He found that photoinduced oxidation of I was the dominant degradation pathway on the clay minerals. The hydrogen peroxide was detected on the irradiated clays. The active oxygen species formation was suggested by the following reactions:

$$O_2 + \text{clay} \xrightarrow{hv} O_2^{\bullet-} + (\text{clay})^+ \quad (1)$$

$$O_2^{\bullet-} + H_2O \rightarrow HO_2^{\bullet} + OH^- \quad (2)$$

$$HO_2^{\bullet} + H_2O \rightarrow H_2O_2 + {}^{\bullet}OH \quad (3)$$

Katagi (1993) examined photodegradation of the pyrethroid insecticide esfenvalerate (I) in clay suspensions (kaolinite and Montmorillonite) with a xenon lamp ($\lambda > 290$ nm). The results showed that the suspended clays slightly accelerated the photolysis rate with a significant epimerization at the benzyl carbon of I to form the (2*S*, *aR*)-isomer (II). Hydroxyl radical was generated by exposure of the suspended clays to UV light and participated in the formation of the desphenyl derivative of I. It was suggested that the clay surface played a significant role in the photoproduction of hydroxyl radical and that the different ways of

adsorption of I to each clay might control photoreactions on the surfaces. Miller and Zepp (1979) reported that suspended clays could enhance the photolysis rate of a chemical via efficient light scattering. Our group has done some systematic work to study the photoactivity of the raw clays and the mechanism. The degradation of Orang II/ chloroform/ phenol/ Bisphenol A in Montmorillonite KSF (KSF) suspensions under irradiation ($\lambda \leq 365$ nm) were investigated (Li *et al*., 2008; Li *et al*., 2010; Liu *et al*., 2008a; Liu *et al*., 2008b). We found that for all the pollutants, high efficiency of the photodegradation was achieved and the degradation of the organic pollutants is due to the oxidation by hydroxyl radical formed in the KSF suspensions. The photodegradation was greatly influenced by the KSF concentration, the pH of the suspensions and the adsorption of pollutants on the KSF surface. The optimal concentration of KSF for the degradation of organic pollutants changed with the different experimental condition. Normally, the acid pH of the KSF suspensions is favor for the degradation of organic pollutants, which is due to more iron dissolved in the acid pH and the high photoactivity of the iron species ($Fe(OH)^{2+}$) at pH 3 (reaction (1)). The high amount of hydroxyl radicals formation in

$$Fe(OH)^{2+} \xrightarrow{h\upsilon} Fe^{2+} + {}^{\bullet}OH \quad (1)$$

aqueous KSF suspensions were also determined and the free iron ions in KSF were thought to be the main source of the hydroxyl radicals. So, from the above researches of the clays as photocatalyst, we can see that although they are proved that the raw clay could be a high efficient photocatalyst, the mechanistic analysis of photodegradation by clays has just begun, and they are still remain many issues to be clarified (Katagi, 2004).

Most of the iron oxides have semiconductor properties and can behave as photocatalyst though a very efficient positive holes-electrons recombination takes place (Leland and Bard, 1987). The photochemical process of iron oxides with the strong electron donors such as S(IV), benzoate, oxalate or dissolved organic carbons is well known (Voelker *et al*., 1997; Waite and Morel, 1984). But only a few papers were published related to the degradation of pollutants by iron oxides without any strongly absorbed organic materials. Mazellier and Bolte 2000, studied the oxidation of 2,6-dimethylphenol with the system goethite/UV and concluded that the process proceeds without any intervention of OH radicals. The substrate being oxidized by the positive holes formed on the surface of the irradiated goethite. The pathway of 2,6-dimethylphenol degradation is shown in Figure II-A-4. Andreozzi *et al*. (2003) investigated the photooxidation of 2-aminophenol in aqueous solution in the

presence of goethite at different pH (3.0 – 8.0) and catalyst loads (100 - 500 mg L^{-1}). Also the intervention of OH radicals in the photodegradation of 2-aminophenol has been ruled out. The dependence of the system reactivity has been found to be strictly correlated to the capability of the substrate to adsorb on the catalyst surface. Wang *et al*. (2009) studied the photodegradation of polycyclic aromatic hydrocarbons (PAH) by several iron oxides (α-FeOOH, α-Fe_2O_3, γ-Fe_2O_3, γ-FeOOH). The results showed that using these iron oxides as photocatalyst, the photodegradation of PAHs was due to the oxidation by hydroxyl radicals, which was shown in the following reactions:

$$\text{Iron oxides} + h^+ \rightarrow e^- + h^+ \quad (1)$$

$$H_2O + h^+ \rightarrow H^+ + {}^{\bullet}OH \quad (2)$$

$$O_2 + e^- \rightarrow O_2^{\bullet -} \quad (3)$$

$$O_2^{\bullet -} + H^+ \rightarrow HO_2^{\bullet} \quad (4)$$

$$2\ HO_2^{\bullet} \rightarrow H_2O_2 + O_2 \quad (5)$$

$$H_2O_2 + e^- \rightarrow OH^- + {}^{\bullet}OH \quad (6)$$

$$\text{PAHs} + {}^{\bullet}OH \rightarrow \text{degradation products} \quad (7)$$

Chartterjee *et al*. (1994) attributed the degradation of phenol by colloidal Fe_2O_3 suspension to the formation of hydroxyl radicals. However, no strong evidence has been put forward in this study for the initial mechanism of pollutant degradation. For the previous studies, we can see that the photoinduced pollutant degradation occurring on the iron oxides is mainly through a semiconductor photocatalysis. And photodegradation of pollutant by the positive holes formed on the surface of the irradiated iron oxides or by the $^{\bullet}OH$ formed mainly depends on the chemical properties of the pollutants.

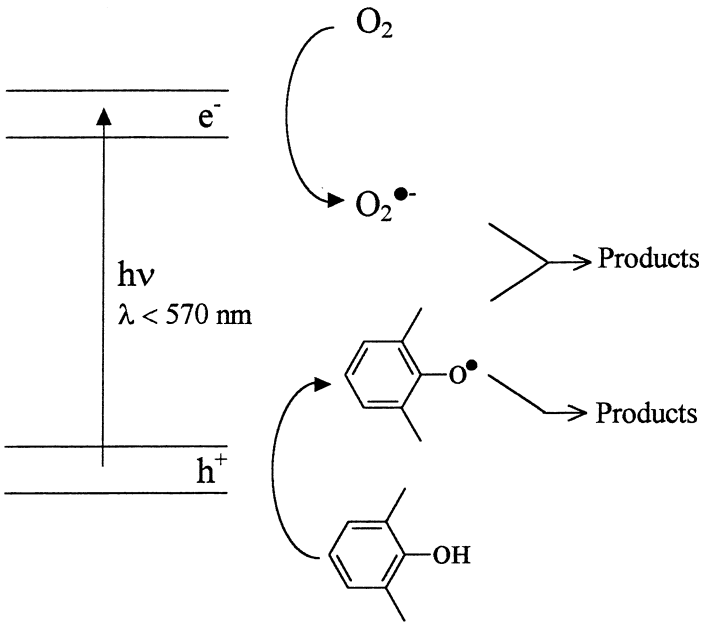

Figure II-A-4 Pathway of DMP degradation at the surface of goethite (Mazellier and Bolte, 2000).

A-2-2 Heterogeneous Photo-Fenton-like catalysis

Photo-Fenton reaction as one kind of advanced oxidation technology (AOT) has been paid more attention over the past several decades (Walling and Amaranth, 1982; Sun and Pignatello, 1993; Lu *et al*., 1999). The Photo-Fenton reactions involve in situ generation of reactive radicals, notably hydroxyl radicals ($^{\bullet}OH$) that are highly oxidative and capable of decomposing a wide range and variety of organic compounds owing to their high oxidation potential (E^0 = + 2.80 V) (Ramírez *et al*., 2007). The formation of hydroxyl radicals and the regeneration of Fe^{2+} by photoreduction of Fe^{3+} in the photo-Fenton reactions may be expressed by the following equations:

$$Fe^{2+} + H_2O_2 \rightarrow Fe^{3+} + {}^{\bullet}OH + OH^- \quad (1)$$

$$H_2O_2 \xrightarrow{h\upsilon} 2\,{}^{\bullet}OH \quad (2)$$

$$Fe(OH)^{2+} \xrightarrow{h\upsilon} Fe^{2+} + {}^{\bullet}OH \quad (3)$$

The homogeneous Photo-Fenton reaction has succeeded in the treatment of organic pollutants in waste water under both UV and visible light irradiation in acidic solution (Balmer and Sulzberger, 1999; Wu *et al*., 1999; Huston and Pignatello, 1996). However, the homogeneous photo-Fenton reaction has two drawbacks: (1) it is limited to acidic pH range and the optimum pH is 2.5 - 3.0, so it is difficult to apply the homogeneous Fenton process to in situ environmental remediation. (2) After the reaction, a high amount of ferric

hydroxide sludge was produced, creating disposal and other problems (Li *et al*., 2004). Therefore, to overcome such drawbacks and to synthesize reusable catalyst, many efforts have been made to develop efficient heterogeneous photo-Fenton catalysts, including iron-containing minerals or iron-coated particles (Barrault *et al*., 2000; Baldrian *et al*., 2006; Matta *et al*., 2007).

As we mentioned above, the natural clay minerals normally contained the iron in their structures and surface. And the pillared clays interlayered by iron cations also were developed. Clay and oxide minerals, either as such or as supports of iron species, have been widely serve as heterogeneous catalysts in the photo-Fenton-like reaction (Table II-A-4).

Table II-A-4 Clays and iron oxides as heterogeneous catalysts for the decomposition of various organic compounds via photo-Fenton-like reactions

Compound	Catalyst	Process	Reference
Orange II	Bentonite clay-based Fe nanocomposite film	Catalyst/H_2O_2/ UVC	Feng *et al*., 2005
Orange II	Laponite clay-based Fe nanocomposite	Catalyst / H_2O_2/UV	Feng *et al*., 2003
methylene blue	iron-pillared montmorillonite	Catalyst / H_2O_2/UV	De León *et al.*, 2008
acidblack 1	Series of pillared Laponite clay-based Fe nanocomposites	Catalyst/H_2O_2/UVC(254 nm)	Sum *et al*., 2004
reactive brilliant orange X-GN	Iron pillared montmorillonite	Catalyst /H_2O_2/UV	Chen *et al*., 2009
reactive brilliant orange X-GN	Iron pillared vermiculite	Catalyst /H_2O_2/ visible light ($\lambda \geq$ 420 nm)	Chen *et al*., 2010
Rhodamine B	iron-bearing soil clays	Catalyst/H_2O_2/ visible light (λ > 450 nm)	Wang Z.H. *et al*., 2009
Phenol	Fe-treated laponite	Catalyst/ H_2O_2/ UVC (254 nm) or UVA (360 nm)	Lurascu *et al*., 2009
Ciprofloxacin	Laponite clay-based Fe nanocomposite	Catalyst / H_2O_2/UV	Bobu *et al*., 2008

pentachlorophenol	Goethite Hematite	Catalyst/oxalate/UVA	Lan *et al.*, 2010
Mordant Yellow 10	Goethite	Catalyst / H_2O_2/UV	He *et al.*, 2002
Diuron	Goethite	Catalyst/oxalate/UV(λ> 300 nm)	Mazellier and Sulzberger, 2001
Methylene blue	Maghemite Hematite	Catalyst/oxalate/UV, visible and solar irradiation	Gulshan *et al.*, 2010
polycyclic aromatic hydrocarbons	Goethite Hematite Lepidocrocite Maghemite	Catalyst/oxalate/UV	Wang *et al.*, 2009
bisphenol A	Lepidocrocite Hematite The mixed of Maghemite and Hematite.	Catalyst/oxalate/UV	Li *et al.*, 2007
orange I	Lepidocrocite Four mixed iron oxides	Catalyst/oxalate/UV	Lei *et al.*, 2006
2-mercaptobenzothiazole	Maghemite	Catalyst/oxalate/UVA	Wang *et al.*, 2008
2-mercaptobenzothiazole	Lepidocrocite	Catalyst/oxalate/UV(365 nm)	Liu *et al.*, 2006

As shown in Table II-A-4, the researches on the heterogeneous photo-Fenton process using clay and iron oxides as catalyst mainly focus on two types which are catalyst/H_2O_2/UV and catalyst/oxalate/UV. In the Catalyst/H_2O_2/UV process, H_2O_2 is the most important factor to form the hydroxyl radicals and sufficient hydrogen peroxide has to be added to make the system be efficient (Chamarro *et al.*, 2001). However, H_2O_2 is an acute reactive reagent and cannot stand in nature for a long time (Liu *et al.*, 2006). This factor limits the application of the Catalyst/H_2O_2/UV process in the remediation of organic pollutants in nature. It is well known that clay/iron oxides and oxalate coexisted in natural environments. Compared with the catalyst/H_2O_2/UV, catalyst/oxalate/UV can form H_2O_2 in situ and normally has the higher efficiency for the degradation of organic compounds (Lan

et al., 2010). Actually, not just oxalate, other carboxylates also can substitute for H_2O_2 in the photo-Fenton-like system. In the homogeneous system, except Fe-oxalate, some iron-carboxylate complexes such as Fe-citrate, Fe-tartrate, Fe-NTA has been well known to have a high photoactivity and have been applied to degrade organic and inorganic pollutants. As we see, in the heterogeneous system, the reports are just limited in the catalyst/oxalate/UV system. Therefore, exploring other more catalyst/carboxylate/UV process is demanded and interesting.

In these heterogeneous photo-Fenton-like systems, the operation does not require strict control of pH as is the case in the homogeneous Fenton process (Garrido-Ramí *et al*., 2010). Several authors have reported that the photodegradation of pollutants could happen at pH values between 3 and 9 in the heterogeneous photo-Fenton-like system (Table II-A-4). During the irradiation, small amount of iron could be released into the solution through the photoreduction reactions, but which can not bear comparison with the amount of immobilized iron in the clay and iron oxides minerals. Most of the catalyst could be reused several times. The photochemical process involves the mechanism though the homogeneous reaction in aqueous solution and the heterogeneous reaction on the surface of clay and iron oxide. For the catalyst/H_2O_2/UV process, two mechanisms for the oxidation of the pollutant involving the hydroxyl radicals which are proposed by Feng *et al*. (2003) and He *et al*. (2002).

According to Feng *et al*. (2003), the reactions are initiated by the photo reduction of Fe^{3+} on the surface of clay to Fe^{2+} under UV irradiation. The Fe^{2+} formed on the surface of clay accelerates the decomposition of H_2O_2, forming $^{\bullet}OH$ radicals, and at the same time, the Fe^{2+} on the surface of the clay is oxidized to Fe^{3+}. These $^{\bullet}OH$ radicals attack the Orange II adsorbed on the surface of clay, resulting in the formation of reaction intermediates from the degradation of Orange II. Finally, the intermediates are completely oxidized into CO_2 and H_2O.

$$Fe^{3+} \text{ on the surface of clay} \xrightarrow{h\upsilon} Fe^{2+} \text{ on the surface of clay} \quad (1)$$

$$Fe^{2+} \text{ on the surface of clay} + H_2O_2 \rightarrow Fe^{3+} \text{ on the surface of clay} + {}^{\bullet}OH + OH^- \quad (2)$$

$$\text{clay-Orange II} + {}^{\bullet}OH \rightarrow \text{Intermediates} \quad (3)$$

$$\text{Intermediates} + {}^{\bullet}OH \rightarrow CO_2 + H_2O \quad (4)$$

According to He *et al*. (2002), the possible surface and solution reaction in this heterogeneous photo-Fenton system was summarized in Scheme II-A-2. The reactions are initiated by the formation of a precursor surface complex of H_2O_2 with the oxide surface

metal centers. The iron surface is immobilized and octahedrally coordinated by O^{2-} and OH^- (Flynn, 1984). The O–O bond of the surface complex undergoes a cleavage under UV irradiation leading to the generation of Fe(IV) species and hydroxyl radicals. Since the Fe(IV) complex is unstable, it reacts immediately with H_2O forming another active hydroxyl radical (Meunier *et al.*, 1992). The photolysis of Fe(III) generates Fe(II), followed by Fe(II) reoxidation by H_2O_2.

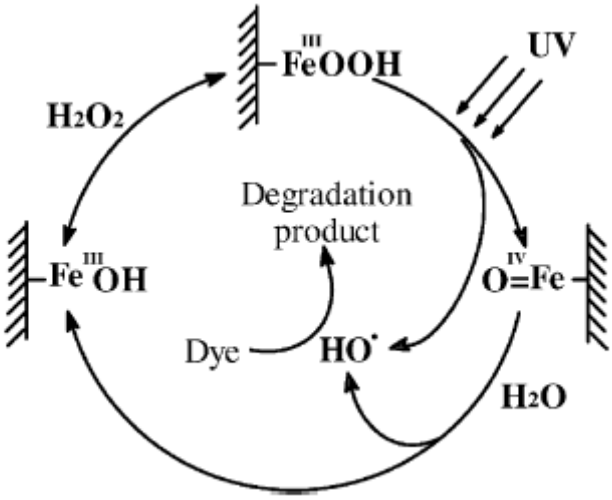

Scheme II-A-2 Fe cycling in the Goethite/H_2O_2/UV system(He *et al.*, 2002).

For the catalyst/oxalate/UV system, the photochemical process for the degradation of pollutants is well determined (Wang *et al.*, 2008; Lei *et al.*, 2006; Mazellier and Sulzberger, 2001). Mazellier and Sulzberger (2001) give a very clearly light-induced iron cycling in the iron oxides/oxalate/UV system, which is shown as Scheme II-A-3.

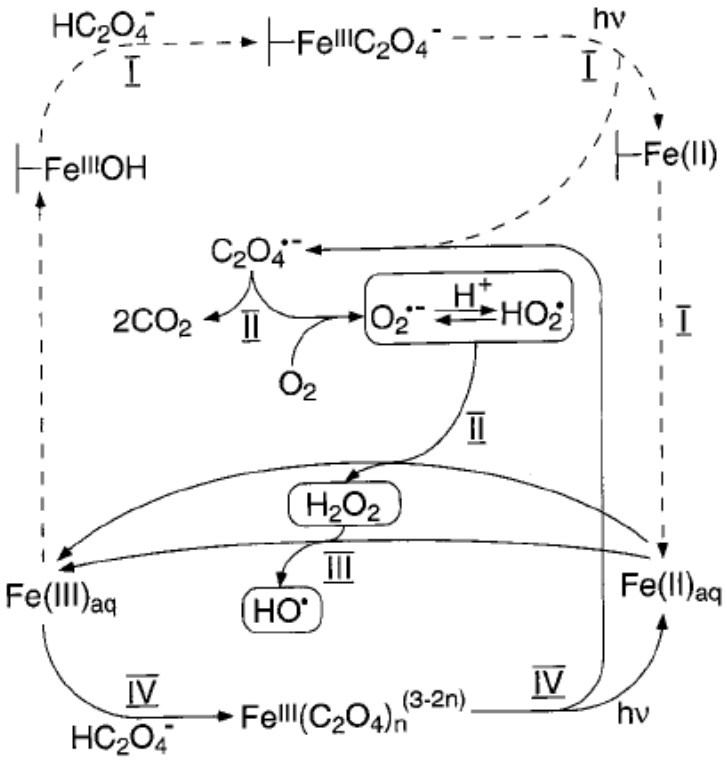

Scheme II-A-3 Fe cycling in the Goethite/oxalate /UV system (Mazellier and Sulzberger, 2001)

The specific photoreaction in this process is shown as follows:

$$\text{Iron oxide} + n H_2C_2O_4 \leftrightarrow [\equiv Fe(C_2O_4)_n]^{(2n-3)-} \quad (1)$$

$$[\equiv Fe(C_2O_4)_n]^{(2n-3)-} \xrightarrow{h\nu} Fe(C_2O_4)_2^{2-} (\text{or} \equiv Fe(C_2O_4)_2^{2-}) + (C_2O_4)^{\bullet -} \quad (2)$$

$$Fe^{III}(C_2O_4)_n^{3-2n} + h\nu \rightarrow [Fe^{II}(C_2O_4)_{(n-1)}]^{4-2n} + (C_2O_4)^{\bullet -} \quad (3)$$

$$(C_2O_4)^{\bullet -} \rightarrow CO_2 + CO_2^{\bullet -} \quad (4)$$

$$CO_2^{\bullet -} + O_2 \rightarrow CO_2 + O_2^{\bullet -} \quad (5)$$

$$O_2^{\bullet -} + H^+ \rightarrow HO_2^{\bullet} \quad (6)$$

$$O_2^{\bullet -} + Fe^{3+} \rightarrow Fe^{2+} + O_2 \quad (7)$$

$$O_2^{\bullet -} / HO_2^{\bullet} + nH^+ + Fe^{2+} \rightarrow Fe^{3+} + H_2O_2 \quad (8)$$

$$Fe^{2+} + H_2O_2 \rightarrow Fe^{3+} + OH^- + {}^{\bullet}OH \quad (9)$$

The first essential step was the specific adsorption of oxalate on the surface of the iron oxides. During the photochemical reaction, dissolved Fe(II) and Fe(III) species, adsorbed Fe(II) and Fe(III) species, the superoxide and hydroperoxyl radicals ($O_2^{\bullet -}/HO_2^{\bullet}$) are the key intermediates formed through the reactions, as shown in Eqs. (1)–(6). H_2O_2 can be obtained by the dismutation of $O_2^{\bullet -}/HO_2^{\bullet}$, as Eqs. (7) and (8). After H_2O_2 was formed, the classical Fenton reaction happened with Fe(II) species, to form $^{\bullet}OH$, as Eq. (9).

The efficiency of clay/iron oxide minerals in catalyzing the decomposition of the organic pollutants through the photo-Fenton-like reaction is influenced by several parameters, such

as hydrogen peroxide/ oxalate concentration, type and surface area of the mineral, solution pH, different light sources, and pollutant characteristics. For example, De León *et al*. (2008) observed that the smaller-sized particle fraction of the starting mineral could increase the catalytic activity in methylene blue discoloration by photo-Fenton processes. Investigating the oxidation of 2-mercaptobenzothiazole in the Lepidocrocite/oxalate/UV system, Liu *et al*. (2006) found that when the oxalate concentration was increased from 0 to 1.0 mM, the rate of degradation increased. However, when the concentration of oxalate was further increased from 1.0 to 3.0 mM, the rate of decomposition declined. This was due to the competition between the oxalate and 2-mercaptobenzothiazole reacting with hydroxyl radicals. In a word, the heterogeneous Photo-Fenton-like system is very complicated. In order to achieve the best efficiency for the degradation of pollutants, all the main factors should be evaluated.

A-2-3 Other modified clay/iron oxides photocatalysis

Due to special layer structure and colloid properties of clay minerals, they are widely used as hosting/support materials. In the past few years, the introduction of organic or inorganic cations into clay minerals, especially Montmorillonite, has been developed to prepare various porous pillared materials (Ding *et al*., 2008). Numerous articles have been reported to introduce the semiconductor, such as TiO_2, CdS, Fe_2O_3 ,ZnS into the clay minerals to get the high efficiency photocatalyst (Chen *et al*., 2001; Xiao *et al*., 2007). Among the semiconductor-pillared clay, TiO_2-clay has been paid the most attention. Immobilization of TiO_2 into clay minerals can reduce electron–hole recombination and increases the adsorption of organic pollutant onto the catalyst surface. This result increases the photocatalytic activities of TiO_2-clay. Otherwise, the TiO_2-clay could use the solar light as the light source and is easily recovered and reuse. Therefore, TiO_2-clay have been widely applied into the photocatalytic degradation of various pollutants, such as dyes (Daniel *et al*., 2007; Sun *et al*., 2002), volatile organic components (VOCs) (Ménesi *et al*., 2008; Ooka *et al*., 2003), phenol (Zhu *et al*., 2005), herbicides (Belessi *et al*., 2007).

Surface modified clay minerals with dyes also found to exhibit high photocatalytic activities. Song *et al*. (2006) found that the methyl viologen (MV^{2+}) intercalated clay could either produce or deplete of hydrogen peroxide (H_2O_2) under UV light irradiation. The intercalated MV^{2+} is excited by UV irradiation and then captures electrons from clay hosts, forming $MV^{+\bullet}$. In iron free clay, $MV^{+\bullet}$ rapidly reduces dissolved molecular oxygen to

$O_2^{\bullet-}/HO_2^{\bullet}$, subsequently, H_2O_2 was produced. When Fe(III) is present in clay, it is reduced to Fe(II) by $MV^{+\bullet}$ leading to the decomposition of H_2O_2. Madhavan and Pitchumani (2002) investigated the photooxidation of electron-rich substrates such as quinone, 1-naphthol and anthracene to the corresponding 1,4-quinones with clay-bound methylene blue/ rose bengal. It was found that under oxygen atmosphere, electrophilic oxidant of singlet oxygen was formed. The pathway of the substrate was the A [4 + 2] cycloaddition between singlet oxygen and the substrate, followed by its subsequent cleavage.

Not as clay minerals, there are rare reports about the modified iron oxides photocatalyst. Wu *et al*. (2007) investigated the adsorption and catalytic transformation of chromium on Mn substituted goethite. It was found that Mn-substituted goethite may act as a p-type semiconductor, having the similar redox process as TiO_2 and could photoreduce the Cr (VI) effectively.

B-Iron-carboxylate complex

B-1 EDDS: one of naturally occurring aminopolycarboxylic acids (APCAs)

Aminopolycarboxylic acids, an important group of chelating agents, are compounds that contain several carboxylate groups bound to one or more nitrogen atoms. The major chemical property of APCAs is their ability to form stable and water-soluble complexes with many metal ions (Bucheli-Witschel and Egli, 2001). For that reason, they are used in a wide variety of domestic products, industrial applications and soil remediation (Bucheli-Witschel and Egli, 2001). Among the APCAs, the most widely used of these are EDTA, with an estimated annual use of 55.6×10^3 metric tons in the USA and Western Europe, and NTA with an estimated annual use of 40.3×10^3 metric tons. Therefore, much attention has been paid to the environmental fate of APCAs, especially EDTA and NTA. EDTA is very persistent in the environment due to its low biodegradability (Schmidt *et al*., 2004). Means *et al*. (1980) reported a half-life of 6 months for EDTA. This can cause a rather high risk of metal leaching to the groundwater (Nowack 2002). A combined widespread use of fertilizers and slow decomposition has led to background concentrations of EDTA in European surface waters in the range 10–50 mg L^{-1} (Kari *et al*., 1995). As reported, photochemical oxidation is the only effective way for removal of EDTA and its derivatives. The Fe(III)-EDTA complex is the only EDTA species that undergoes direct photolysis in the environment

(Frank and Rau, 1990; Kari *et al*., 1995). So the photochemistry reaction of Fe(III)-EDTA has been extensively studied (Kocot *et al*., 2007; Metsärinne *et al*., 2001; Kocot *et al*., 2006). NTA is easily biodegradable, having half-lives from 3 to 7 days under aerobic conditions (Bucheli-Witschel and Egli, 2001). However, it is under scrutiny due to possible adverse health effects (Ebina *et al*., 1986). Recently the easily biodegradable chelating agent S,S-EDDS (*S,S*-ethylenediamine-*N,N'*-disuccinic acid) has been proposed as a safe and environmentally benign replacement of EDTA for environmental remediation products as it is also a strong complexing agent (Velupula *et al*., 2007; Zhang *et al*., 2008).

Ethylenediamine-*N,N'*-disuccinic acid (EDDS) is one of natural occurring APCAs. It is isolated from culture filtrate of the actinomycete *Amycolatopsis orientalis*. Transport of EDDS into this actinomycete was also demonstrated. Ethylenediamine-*N,N'*-disuccinic acid (EDDS) is a structural isomer of EDTA, and exists as three stereoisomers, namely [S,S]-EDDS, [R,R]-EDDS and [R,S/S,R]-EDDS. Among them, [S,S]-EDDS is readily biodegradable. Other stereoisomers of ethylenediamine disuccinic acid are either non-biodegradable (R,R) or only partially biodegradable (R,S, S,R), so the SS-isomer is generally used. Indeed, mineralization of EDDS in sludge-amended soil was completed in 28 days with a calculated half-life of 2.5 days (Jaworska *et al*., 1999). In addition, several metal-EDDS complexes are readily biodegradable (Vandevivere *et al*., 2001). Also, EDDS is reported to photodegrade markedly faster than EDTA, both in the laboratory and in field experiments (Metsärinne *et al*., 2001). This is because the photodegradation of EDDS is independent of its speciation, whereas the photodegradation of EDTA depends on its existence as Fe(III)-EDTA species. [S,S]-EDDS could form stable hexadentate chelates with transition metals. Stability constants for heavy metals with EDDS in comparison to EDTA and NTA are presented in Table II-B-1. EDDS has lower affinity for Mg and Ca than EDTA, which enhances its applicability for intended mobilization of metals. EDDS can readily solubilize metals from soil and at pH 7 it was shown to be better at solubilizing Cu and Zn than EDTA at equimolar ratios of chelating agent to metals (Tandy *et al*., 2004). The toxicity of [S,S]-EDDS to fish and daphnia is low (EC50 > 1000 mg L^{-1}) (Jaworska *et al*., 1999). [S,S]-EDDS was recently introduced as an ingredient of industrial detergents. Presently, it is the only commercially available chelate that is naturally present in soil, where it is readily decomposed into benign degradation products. Due to its environmental friendly and also the strong metal chelating ability, Octel (Octel Performance Chemicals, a Manufacturer/Exporter) have designed and built a process and plant to make EDDS in the

UK to serve the growing market need for biodegradable chelating agent.

Table II-B-1 Stability constants (log K) of 1:1 complexes of NTA, EDTA and [S, S] with di- and trivalent metal ions determined for an ionic strength of 0.1 M (Bucheli-Witschel and Egli, 2001)

	NTA	EDTA	EDDS
Mg^{2+}	5.5	8.8	5.8
Ca^{2+}	6.4	10.6	4.2
Mn^{2+}	7.5	13.8	9.0
Zn^{2+}	10.7	16.4	13.5
Co^{2+}	10.4	16.3	14.1
Cu^{2+}	12.9	18.7	18.4
Pb^{2+}	11.3	17.9	12.7
Cd^{2+}	9.8	16.4	10.8
Al^{3+}	11.4	16.5	
Fe^{2+}	8.3	14.3	
Fe^{3+}	15.9	25.0	22.0
Ni^{2+}	11.5	18.5	16.8

B-2 Fe(III)-EDDS

As we mentioned above, EDDS could form complex with Fe(III) with a stability constants of 22.0. The stoichiometric ratio of Fe(III)-EDDS complex is 1:1 (Zhang, 2009). The structure of the Fe(III)-EDDS complex is shown in Figure II-B-1. EDDS's six donor sites form both five- and six-member chelate rings around the metal ion: two NC_2OFe rings, two NC_3OFe rings, and one C_2N_2Fe ring (Pavelčik and Kettman, 1983). Orama *et al*. (2002) studied the distribution of complexes in the solution with the concentration of Fe^{3+}/EDDS in 1:1 (as Figure II-B-2) and the conditional stability constants for several complexes of [*S*,*S*]-EDDS *vs.* pH (Figure II-B-3). The values of $\log K'_{ML} \geq 6$ are often considered as a criterion for an efficient complexation. With this assumption, the approximate pH ranges suitable for the use of EDDS as a chelating agent complexing with Fe(III) are 3-9.

Metsärinne *et al*. (2001) studied the photodegradation of Fe(III)-EDTA and Fe(III)-EDDS complexes under different conditions. It was found that the rate of photodegradation of Fe(III)-EDDS is faster in lake water than in distilled water. That is may be due to iron, fulvic and humic acids contained in the lake water. These compounds could lead to the indirect

photolysis of the iron complex. The rate of photodegradation of Fe(III)-EDDS is fast at pH 3.1 rather than 6.5. This is because at pH 3.1 EDDS form stable complexes with Fe(III)-ions, while at pH 6.5, iron is partly transformed into iron hydroxide and is therefore not available for complexation. But the pathway of Fe(III)-EDDS degradation was not introduced.

Zhang (2009) applied the Fe(III)-EDDS to be a photocatalyst. It was found that Fe(III)-EDDS was easily photolyzed under irradiation and $^{\bullet}OH$ was formed during photodegradation of Fe(III)-EDDS. But no matter the Fe(III)-EDDS as a pollutant or as a photocatalyst, the photochemisty of Fe(III)-EDDS is poorly understood.

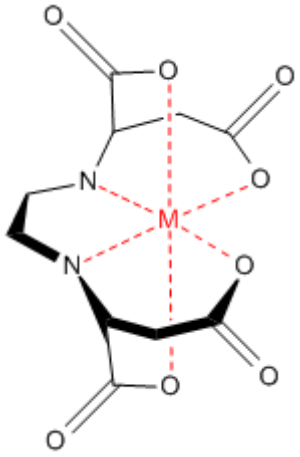

Figure II-B-1 Structure of Fe(III)-EDDS complex (M: Fe)

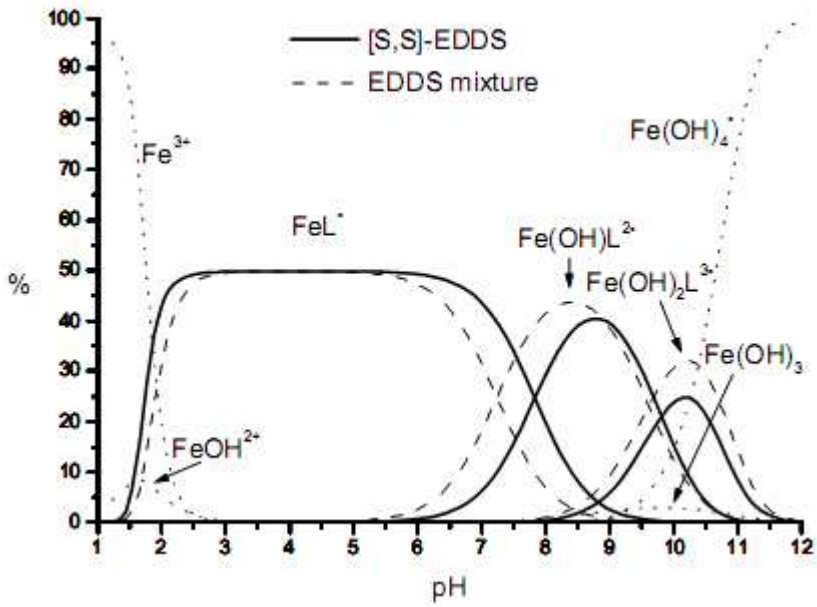

Figure II-B-2 Distribution diagram of Fe(III)-EDDS aqueous solution as a function of pH values range from 0 to 12 (Orama *et al.*, 2002)

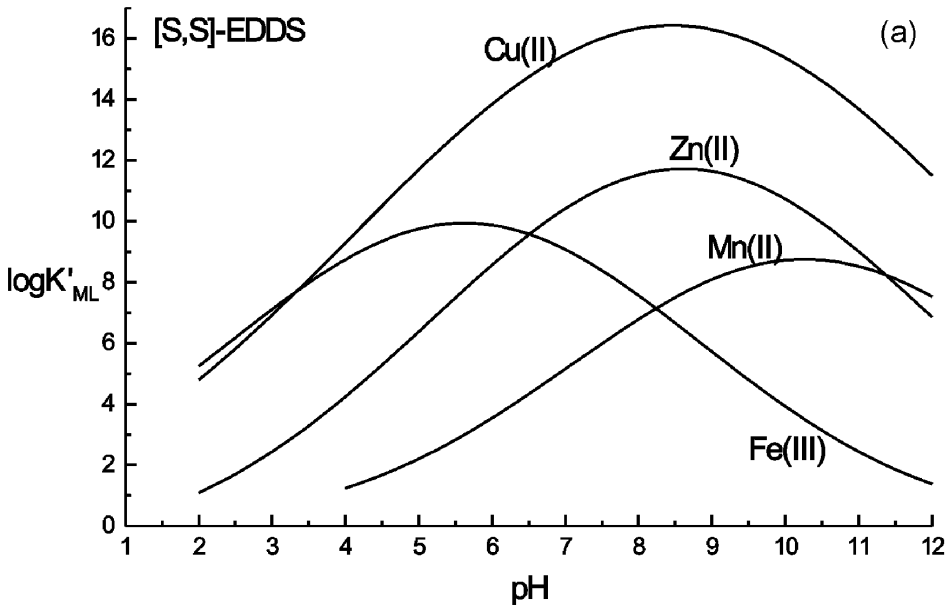

Figure II-B-3 Conditional stability constants for ML complexes of [*S,S*]-EDDS *vs.* pH (Orama *et al.*, 2002)

B-3 The photochemistry of iron-carboxyate complex

Iron is the most abundant transition metal in the earth's crust. Iron is present under a variety of forms in water ranging from soluble to colloidal and particulate species. Most of the iron in natural waters exists in the form of insoluble ferric oxides and (hydr)oxides (Barbeau, 2006). The concentration of dissolved iron is very low and most of the dissolved iron is associated with strong organic ligands in natural waters (Achterberg *et al*., 2001; Cieśla *et al*., 2004). Polycarboxylates such as citrate, malonate, and oxalate are common constituents of precipitation, fog, surface waters and soil solutions (Kawamura *et al*., 1985). Polycarboxylates can form strong complexes with Fe^{3+} and enhance the dissolution of iron in natural water through photochemical processes. Moreover, such polycarboxylate complexes undergo rapid photochemical reactions under sunlight irradiation leading to the formation of oxidative species (Faust and Zepp, 1993; Panias *et al*., 1996). Therefore, in the presence of polycarboxylates, photochemical redox cycling of iron in the aqueous solution was significantly altered (Figure II-B-4).

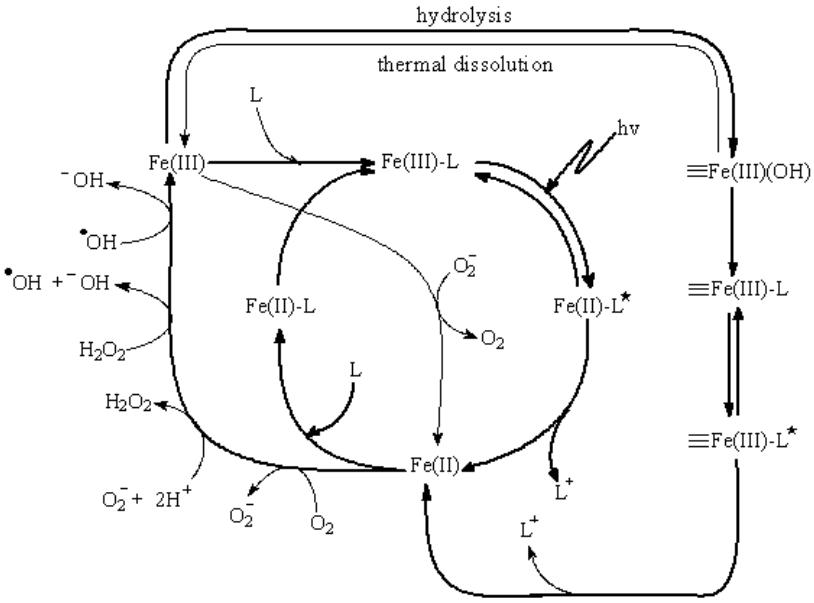

Figure II-B-4. Mechanism of photochemical redox cycling of iron in the aqueous solution. Fe(II)-L and Fe(III)-L represent Fe(II) and Fe(III) complexed with Ligand. (Abida, 2005)

Up to now, photolysis of Fe- Polycarboxylates as one of the advanced oxidation process (AOPs) has received much attention (Zhou *et al*., 2004; Chen *et al*., 2007; Ou *et al*., 2008; Zhang *et al*., 2009). For instance, Zhou *et al*. (2004) investigated the photooxidation of diethylstilbestrol (DES) by Fe-oxalate complex under a 250 W high-pressure mercury lamp. The photodegradation of DES in the Fe(III)-oxalate complex system is more efficient than in the Fe(III)-OH complex system (aquacomplexes). Ou *et al*. (2008) also found that the presence of Fe(III)-citrate complex enhanced the photodegradation rate of atrazine as a result of $^{\bullet}OH$ radical attack. Silva *et al*. (2007) observed that besides the high efficiency of the herbicide tebuthiuron (TBH) degradation was achieved using the ferric citrate complex in the solar photo-Fenton process, the ferric citrate complex also offers the advantage of application at a pH of up to 7.5.

It was reported that light irradiation of Fe(III)-Polycarboxylate complexes could produce both Fe(II) and ligand-free radical by the ligand-to-metal charge transfer (LMCT) reactions (reaction (1)). Then the reducing radical could react with Fe(III) species or O_2 to form Fe(II) species or superoxide radical $O_2^{\bullet-}$ (reaction (2)) respectively. The relative rates of the reactions of the reducing radical with O_2 or Fe(III) are very important for determining the steady state concentration of Fe(II) and $O_2^{\bullet-}$. The radical $O_2^{\bullet-}$ and its acid conjugated form $HO_2^{\bullet}$ (pKa = 4.8 for the $HO_2^{\bullet}$/ $O_2^{\bullet-}$) can participate in further reactions, including generation of H_2O_2 (reactions (3) to (6)) (Bielski *et al*., 1985). The yield of H_2O_2 depends critically on competition between H_2O_2-producing reactions (reactions (3) to (6)) and O_2-producing

reactions (reactions (7) and (8)).

$$Fe(III)\text{-}L + h\nu \rightarrow [Fe(III)\text{-}L]^{*} \rightarrow Fe(II) + L^{\bullet} \quad (1)$$

$$L^{\bullet} + O_2 \rightarrow O_2^{\bullet-} + L' \quad (2)$$

$$Fe(II) + O_2^{\bullet-} + 2\,H_2O \rightarrow Fe(III) + H_2O_2 + 2\,OH^- \quad k = 1.0 \times 10^7\ M^{-1}s^{-1} \quad (3)$$

$$Fe(II) + HO_2^{\bullet} + H_2O \rightarrow Fe(III) + H_2O_2 + OH^- \quad k = 1.2 \times 10^6\ M^{-1}s^{-1} \quad (4)$$

$$HO_2^{\bullet} + O_2^{\bullet-} + H_2O \rightarrow H_2O_2 + O_2 + OH^- \quad k = 9.7 \times 10^7\ M^{-1}s^{-1} \quad (5)$$

$$HO_2^{\bullet} + HO_2^{\bullet} \rightarrow H_2O_2 + O_2 \quad k = 8.3 \times 10^5\ M^{-1}s^{-1} \quad (6)$$

$$Fe(III) + HO_2^{\bullet} \rightarrow Fe(II) + O_2 + H^+ \quad k < 1 \times 10^3\ M^{-1}s^{-1} \quad (7)$$

$$Fe(III) + O_2^{\bullet-} \rightarrow Fe(II) + O_2 \quad k = 5 \times 10^7\ M^{-1}s^{-1} \quad (8)$$

From these reactions it seems very likely that the concentrations of $HO_2^{\bullet}/O_2^{\bullet-}$ and Fe(III)/Fe(II) and as a consequence the formation of H_2O_2 in water are intertwined. In fact in such system it is well known that $^{\bullet}OH$ can be formed by oxidizing Fe(II) with H_2O_2 also called Fenton reaction (reaction (9)) (Gallard *et al*., 1998).

$$H_2O_2 + Fe(II) \rightarrow Fe(III) + {}^{\bullet}OH + OH^- \quad k = 63\ M^{-1}s^{-1} \quad (9)$$

Zhang (2009) presents a very clear reaction scheme for the photolysis of Fe(III) complexes of polycarboxylates (oxalate, malonate, citrate) (Figure II-B-5). From the scheme, we can see that iron concentration, pH and oxygen are all important parameters that influence the reactions.

Aminopolycarboxylic acids (APCAs) may present behavior similar to that of polycarboxylic acid (Abida *et al*., 2006). Abida studied the photochemical impact of Fe(III) –nitrilotriacetic acid complex (FeNTA) on the fate of 4-chlorophenol (4-CP) in natural waters. It was found that the quantum yields of the photodecomposition of the FeNTA complex and of Fe(II) formation, by an intra-molecular photoredox process are high. The radical species $^{\bullet}OH$ and $CO_3^{\bullet-}$ are responsible of the 4-CP degradation. Iron organic complexes like FeNTA can play a significant role on the fate of the organic compounds present in natural waters.

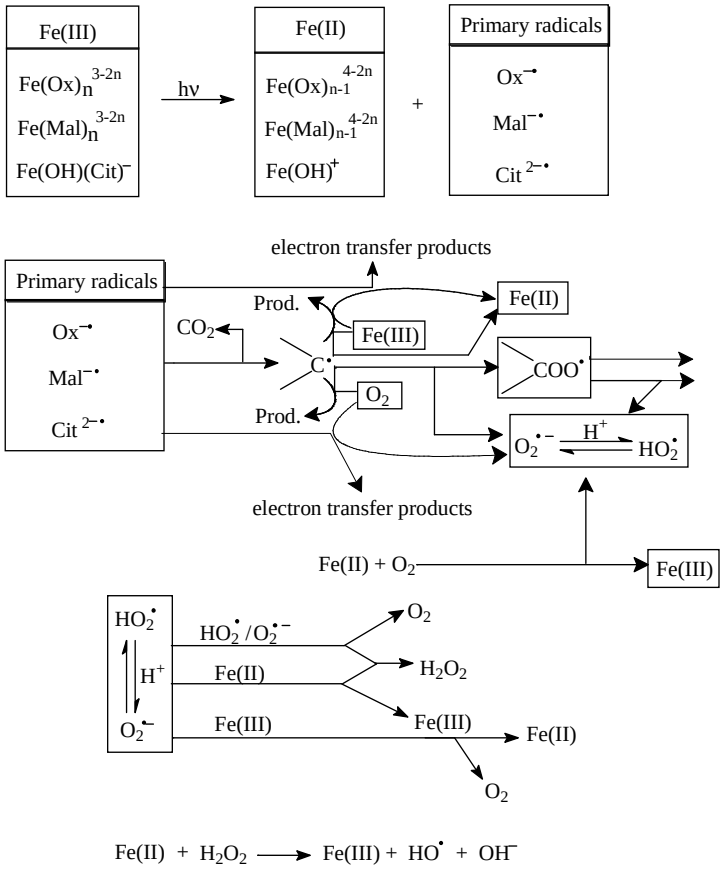

Figure II-B-5 Reaction scheme for the photolysis of Fe(III)-polycarboxylate complexes (Zhang, 2009)

C-Endocrine disrupting compounds

Endocrine disrupting compounds (EDCs) are chemicals with the potential to elicit negative effects on the endocrine systems of humans and wildlife (Kavlock, 1999). Research of EDCs in the past decade has grown immensely since the publication of the book "Our stolen future" (colborn *et al*. 1996). The US Environmental Protection Agency (EPA) defines an EDC as "An exogenous" agent that interferes with the synthesis, secretion, transport, binding, action, or elimination of natural hormones in the body that are responsible for the maintenance of homeostasis, reproduction, development, and/or behavior (USEPA, 1997, p. 1). Various types of natural and synthetic chemical compounds have been identified as EDCs, such as pharmaceuticals, pesticides, industrial chemicals, personal care products and heavy metals (Giesy *et al*., 2002). Table II-C-1 introduces several examples of EDCs (Chang *et al*., 2009; Bondgaard, and Bjerregaard, 2005). EDCs could be released into the environment by humans, animals, and industry; mainly through sewage treatment systems before reaching the receiving bodies (Liu, *et al*., 2009). EDCs have been detected in

influents and effluents of sewage treatment plants (Baronti, *et al*., 2000; Jeannot *et al*., 2002), surface water (Liu *et al*., 2004; Zhou *et al*., 2007), as well as drinking water (Kuch and Ballschmiter, 2001). Considering their wide spread over the environment and potential impacts, it is very important to remove them from the environment or degrade them.

Table II-C-1 Examples of various types of EDCs classified

Class	Compoud
Steroid	Estrone, 17β-estradiol, Estriol, Testosterone, Androstenedione, Ethynylestradiol
Pharmaceutical	Acetaminophen, Hydrocodone, Diclofenac, Sulfamethoxazole
Personal care product	Caffeine, Oxybenzone
Industrial chemicals	Bisphenol A, Phthalate, Nonylphenol
Pesticides	Atrazine, DDT, Alachlor, Amitrole, Metribuzin, Carbaryl, Banol
Combustion by-product	Dioxin
Heavy Metal	TBT, Hg, Cd, Pb

C-1 E2 in the environment

17β-Estradiol (E2) is a well-known natural EDC. E2 is also of major concern as environmental contaminant due to the very potent estrogenic activity even at very low concentration (~10^{-9} M, in vitro) (Arnold *et al*., 1996; Ohko *et al*., 2002). It have been reported that concentration of E2 in water as low as 30 ng L^{-1} for 21 days induced vitellogenin (an egg yolk precursor protein typically associated with sexually mature females) synthesis and abnormal testicular growth in male fathead minnows (Panter *et al*.,1998; Panter *et al*., 2000). Exposure to E2 levels as low as 1 ng L^{-1} in environment is sufficient to cause the feminization of male trout and the development of intersex roach in rivers (Desbrow *et al*., 1998; Routledge *et al*., 1998). Meanwhile, it is a confirmed animal carcinogen with neoplastigenic, tumorigenic, and teratogenic effect (Lewis, 1991).

E2 is produced and released into the environment by humans (e.g. animals urine and feces, contraceptive pill residues, hormone replacement therapy residues), livestock (e.g., animal manure), and wildlife (Ying *et al*., 2002; Desbrow *et al*., 1998). It is reported that on an average, 1.6 µg d^{-1}, 2.3–3.5 µg d^{-1}, 259 µg $d^{-1}$of E2 is excreted by human males, females, pregnant women respectively (Johnson *et al*., 2000). In urine of cattle, the E2 concentration

was found to be 13 ng L^{-1} on average (Erb *et al*., 1977). The human source of E2 can enter the environment from the wastewater and sewage treatment plant (Desbrow *et al*., 1998; Zheng *et al*., 2008). After the typical sewage treatment, part of E2 could be removed, but most of them will be released into surface waters. The disposal of animal manure to agricultural land also could lead to releasing E2 into surface and ground water (Bushe´e *et al*., 1998; Shore *et al*.,1995). E2 has been detected in several sewage treatment plants (STP), surface water and ground water. Table II-C-2 shows the concentration of E2 detected in several water systems. The concentration of E2 in effluent of STP, surface water, ground water, drinking water in different areas ranged from the below detection limit to 158 ng L^{-1}. And most of the E2 concentration list in the table II-C-2 is high enough to exist harmful effect to human and wildlife.

Table II-C-2 Concentration of E2 in various water systems

Waters	Location	Concentration(ngL^{-1})	Reference
Efflunet of STP	Japan	4.6-14	Kobayashi *et al.*, 2006
	Italy	0.35-3.5	Baronti *et al*., 2000
	Italy	1.6	D'Ascenzo *et al.*, 2003
	Austria	<LOD-30	Clara *et al.*, 2005
	US	<10-20	Tabak *et al*., 1981
	US	1.5-5.4	Robert *et al*., 2007
	Canada	0.2-14.7	Servos *et al*., 2005
	Italy	3-8	Lagana *et al*., 2004
	Canadian	<LOD-158	Fernandez *et al*., 2007
	Netherlands	<0.1-5.0	Belfroid *et al.*, 1999
	Germany	<0.15-5.2	Kuch and Ballschmiter, 2001
Surface water	Japan	<LOD-27/24	Tabata *et al.*, 2001
	Germany	0.15-3.6	Kuch and Ballschmiter, 2001
	Italy	0.11	Baronti *et al*., 2000
	Netherlands	<0.3-5.5	Belfroid *et al.*, 1999
Ground water		n.d-45	Swartz *et al.*, 2006
		n.d-0.79	Hohenbum *et al.*, 2004
		6-66	Perterson *et al*., 2000
		13-8	Wicks *et al*., 2004
Drinking water		0.2-2.1	Kuch and Ball schmiter, 2001
		2.6	Roefer *et al.*, 2000
		<LOD-2.6	Morteani *et al.*, 2006

LOD = limit of detection

C-2 E2 degradation

Due to the harmful effect of E2 and the widespread occurrence in the aquatic environment, people pay more and more attention to the removal of E2 in the wastewater. The conventional chemical process, biological process and sorption process could not achieve the removal of E2 effectively and adequately (Kim *et al*., 2007). In addition, the sorption of E2 on the sludge after the treatment causes further concern of the sludge management. Advanced oxidation processes (AOPs) have been thought to be the green and most efficient method for oxidation and mineralization of pollutants (Katsumata *et al*., 2004; Daneshvar *et al*., 2003; Macounová *et al*., 2003). AOPs are based on the generation of very reactive species such as hydroxyl radical ($^{\bullet}OH$) that oxidizes a broad range of pollutants quickly and non-selectively. Several AOPs have been studied and applied for the treatment of E2, such as TiO_2-mediated photocatalysis, photo-Fenton catalytic reactions, O_3/UV process, ozonation, electrochemical oxidation process.

Among the AOPs, TiO_2-mediated photocatalysis was the most extensively reported method for degradation of E2. TiO_2 is an efficient, nontoxic, stable and economical photocatalyst. When near ultraviolet UV light impinges on TiO_2 surfaces, electron-hole pairs will be generated which exhibit strong oxidizing power and could results in the production of hydroxyl radicals and superoxide radicals (Jaeger and Bard, 1979). Ohko *et al*. (2002) reported that 10^{-6} M of E2 was totally mineralized to CO_2 in 1.0 g L^{-1} TiO_2 suspension under UV irradiation (365 nm) for 3h. 10ϵ-17β-Dihydroxy-1,4-estradien-3-one and testosterone like species were elucidated as intermediate products by GC/MS analysis. The intermediates produced during the photocatalytic reactions did not exhibit any potent estrogenic activity in the treated water. Zhang *et al*. (2007) investigated the TiO_2-assisted photodegradation of E2 and in two UV-photo-reactors. 97% of E2 was degraded within 4 h of irradiation in reactor 1 (150 w, 238-579 nm), while 98% of E2 disappeared within 1 h in reactor 2 (15 w, 253 nm). The wavelength of UV-light has a big influence of the E2 photodegradation. Coleman *et al*. (2004) reported 0.05-3 μM E2 were 98% destroyed in 3.5 h with virtually all the estrogenic activity being removed. Thus TiO_2 photocatalysis can be applied to water treatment to effectively remove E2 without producing biologically active intermediates.

The degradation of E2 by a homogeneous/heterogeneous photo-Fenton process has been reported. Feng *et al*. (2005) reported that E2 could be decomposed efficiently in UV–vis/Fe(III)/H_2O_2 system. Under the condition of 10.0 μM Fe(III), 1000 μM H_2O_2 and pH 3.0, the degradation efficiency of 18.4 μM E2 reach 75.2% after the irradiation of 160

min. Zhao *et al*. (2008) investigated the E2 degradation under weak UV irradiation in the presence of α-FeOOH loaded resin (α-FeOOHR) and H_2O_2. The results showed that α-FeOOHR not only degraded E2 but also removed the estrogenic activity originating from E2, its degradation intermediates, and its products. Detailed reaction pathways are proposed, as shown in Scheme II-C-1.

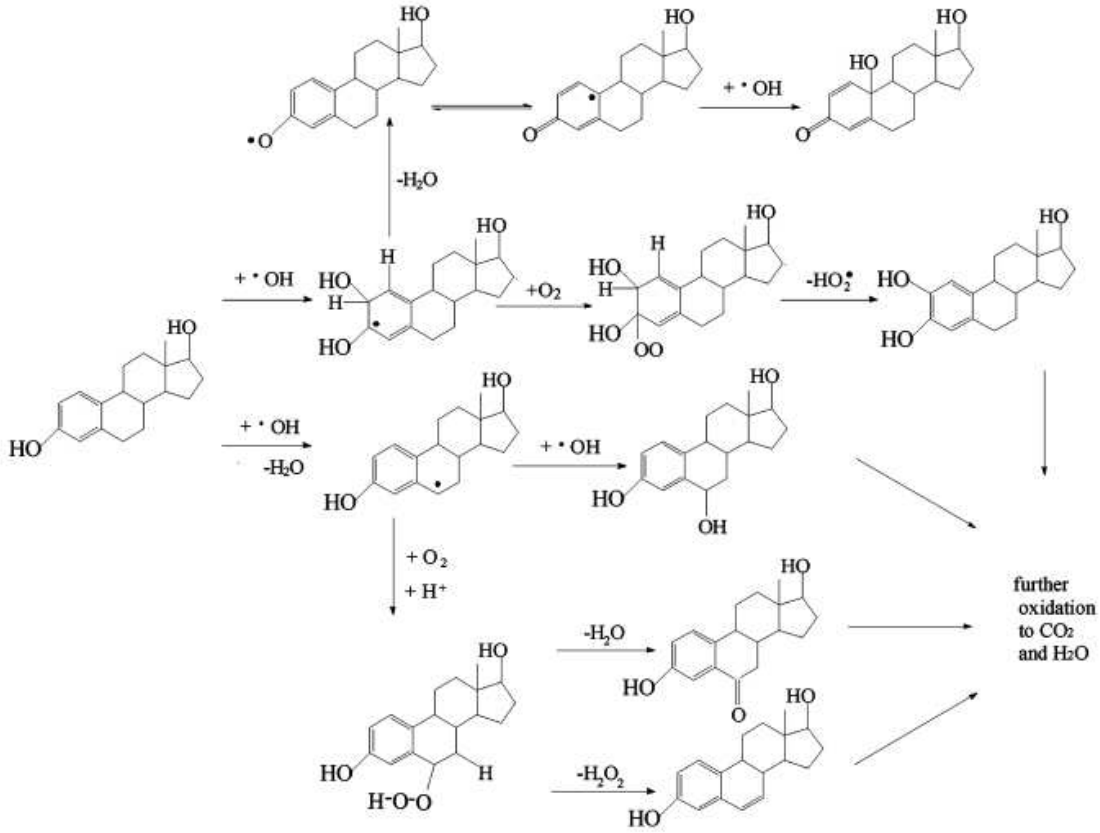

Scheme II-C-1 Simplified mechanism of E2 photodegradation (Zhao *et al*., 2008)

Degradation of E2 by O_3/UV process and ozonation was also reported. Deborde *et al*. (2005) reported that E2 exhibited high rate constants with ozone. The reactivity of ozone with ionized E2 and neutral E2 was 3.89×10^{9} $M^{-1}s^{-1}$ and 1.01×10^{5} $M^{-1}s^{-1}$ respectively. At pH 7 and 20 ± 2 ^{o}C, O_3 exposures of only ~ 2×10^{-3} mg min^{-1} L^{-1} were calculated to achieve ≥ 95% E2 removal efficiency. Bila *et al*. (2007) investigated the degradation of E2 and the removal of estrogenic activity by the ozonation process in three different pHs (3, 7 and 11). High removals (>99%) were achieved with low ozone dosages in the three different pHs. However, complete removal of estrogenic activity was only obtained at pH 3. Due to different chemical pathways and different oxidants (O_3 and $^{\bullet}$OH radical), different by-products are formed at different pHs. Irmak *et al*. (2005) showed that the time needed for complete conversion of 0.1 mM of 17β-estradiol was 55 min for the applied O_3 dose of 15.78×10^{-3} mM min^{-1}.

Electrochemical oxidation as one of the AOPs method offers several advantage such as environmental compatibility, versatility, energy efficiency and amenability to automation. But the effective degradation of organic pollutants of electrochemical technology is often limited by the electrode material and its stability. One reference was checked for the degradation of E2 using electrochemical oxidation. Murugananthan *et al*. (2007) reported electrochemical degradation of aqueous solutions containing E2 using boron-doped diamond (BDD) anode with a working solution volume of 250 mL under galvanostatic control. 500 µg dm^{-3} E2 was completed degraded within a reaction time of 40 min at 25 mA cm^{-2} current density with 0.1 M Na_2SO_4 as supporting electrolyte.

III

MATERIALS AND METHODS

III-Materials and methods

A-Reagents

Ferric perchlorate ($Fe(ClO_4)_3 \cdot 9H_2O$), Fluka, > 97%.

S, S'-Ethylenediamine-N, N'-disuccinic acid trisodium salt solution, (EDDS), 30% in water, Fluka.

17β-Estradiol (E2), Sigma, > 98%

$Fe(NO_3)_3$ $9H_2O$, Sigma-Aldrich, > 99%.

Disodium terephthalate, Alfa Aesar GmbH & Co KG, > 99%

Copper(II) sulfate pentahydrate, Merck, > 99%.

Tetrabutylammonium hydrogen sulfate, Acros Organics, > 98%

2-Hydroxyterephthalic acid, Atlantic, > 98%

$FeSO_4 \cdot (NH_4)_2SO_4 \cdot 6H_2O$, Aldrich, 99%.

Sodium hydroxide, Prolabo, > 97%.

Sulfuric acid, Merck, > 95%.

Perchloric acid, Merck, > 97%.

1, 10-phenanthroline, Aldrich, > 99%.

Ascorbic acid, made in Germany, E.Merck, Dermstadt, > 99.7%

Isopropanol, Aldrich, > 99.5%.

Sodium nitrate, Fluka, ≥ 99%

Hydrogen peroxide 30%, Fluka, not stabilized (7722-84-1)

CH_3COONa, Merck.

Acetic acid, Carlo Erba reagent, 96%

Goethite (α-FeOOH), synthesized in LPMM laboratory

Montmorillonite KSF (KSF), Alfa Aesar.

Montmorillonite, naturally occurring mineral (MN), Alfa Aesar.

Montmorillonite, Sanding Clay Products Inc. (Shaoxing, Zhejiang, PRC).

B-Preparation of materials and solutions

B-1 Synthesis of goethite

The method of Goethite synthesize is in agreement with the paper of Atkinson R.J. *et al*. (1968). 180 g $Fe(NO_3)_3 \cdot 9H_2O$ were dissolved in 730 mL Milli-Q water; when dissolution was complete, 250 mL of 3 M NaOH were added rapidly. Then the solution was stirred with magnetic bar for 2 days at ambient temperature. After aging, saturated NaOH were used to adjust the pH between 12 and 13. After precipitation, the bottle was placed in a bath at 60°C up to 4 days. During this period, the solution was not stirred. Then the suspension was centrifuged and washed several times until the pH was set to 7.5. The iron oxides were dry in an oven at 45°C for one night. During all the synthesis period, the exposition under light was avoided.

B-2 Preparation of stock solutions

(a) Estrogen (E2) stock solution (20 µM)

0.0028 g of E2 was diluted to 500 ml by adding an appropriate volume of Milli-Q water and then put the flask in the ultrasonic bath for several hours to make E2 dissolved.

(b) [S, S']-stereoisomer of ethylenediaminedisuccinic acid (EDDS) stock solution (10 mM)

1.1940 g of EDDS was diluted to 100 mL by adding an appropriate volume of Milli-Q water to get the desired concentration of EDDS.

(c) Fe(III) stock solution (2 mM)

Great care was taken to prepare the solutions of Fe(III) in order to prevent evolution and/or precipitation of Fe(III). A certain quantity of $Fe(ClO_4)_3 \cdot 9H_2O$ (0.2582 g) was diluted to 250 mL by adding an appropriate volume of Milli-Q water to get the desired concentration of Fe(III) and the pH value of the stock solution was adjusted to pH 2.0 with perchloric acid.

(d) Ferric-EDDS complex stock solution (2 mM)

40 mL of 10 mM EDDS and 40 mL of 10 mM $Fe(ClO_4)_3 \cdot 9H_2O$ were mixed and diluted to 200 ml by adding an appropriate volume of Milli-Q water.

(e) Fe (II) stock solution (0.45 mM)

0.0882 g of $FeSO_4 \cdot (NH_4)_2SO_4 \cdot 6H_2O$ was diluted to 500 mL by adding an appropriate volume of Milli-Q water to get the desired concentration of Fe (II).

(f) Acetic sodium buffer

For actinometry

The buffer of acetic sodium was prepared by mixing 600 mL of acetic sodium (1 N) and

360 mL of sulfuric acid (1 N) with end volume of 1 L by adding an appropriate volume of Milli-Q water.

For Fe detection

The buffer of sodium acetate -acetic acid was prepared by mixing 82 g acetate sodium and 31 mL acetic acid with end volume of 500 mL by adding an appropriate volume of Milli-Q water.

(j) Potassium ferrioxalate

Potassium ferrioxalate used for actinometry was prepared from potassium oxalate and ferric chloride, according to the procedure proposed by Calvert and Pitts (1966), and carefully stored in the dark.

(H) Disodium terephthalate (TA, 10 mM)

0.2101 g of TA was dissolved to 100 mL by adding an appropriate volume of Milli-Q water.

(i) 2-Hydroxyterephthalic acid (TAOH, 0.1 mM)

0.00183 g of TAOH was diluted to 100 mL by adding an appropriate volume of Milli-Q water.

B-3 Preparation of reaction solutions

All the reaction solutions were prepared with Milli-Q water. The pH values were adjusted with perchloric aid (1 N) and NaOH (1 N) by a JENWAY 3310 pH-meter to ± 0.01 pH unit.

The suspensions of Goethite were dispersed by using an ultrasonic disperser for 2 min. The suspensions of Montmorillonite (MN) were dispersed by a glass rod for several minutes. After the irradiation, the mineral suspensions were centrifuged at 12000 rpm for 30 min.

When necessary, reaction solutions were deaerated or oxygenated by purging with argon or oxygen before irradiation. The purging time is 30 min.

C-Irradiation

C-1 Ferrioxalate actinometry

The light intensity I_0 was measured by ferrioxalate potassium ($K_3Fe(C_2O_4)_3$) actinometer (Calvert and Pitts, 1966). This method depends on the photochemical reactivity of $K_3Fe(C_2O_4)_3$ in the acid solution. Under irradiation, Fe(III) was reduced to Fe(II) and

oxalate ion was oxidized to CO_2. The reactions are as follows:

$$\left[Fe^{3+}(C_2O_4)_3\right]^{3-} \xrightarrow{h\upsilon} \left[Fe^{2+}(C_2O_4)_2\right]^{2-} + C_2O_4^{\bullet -} \quad (1)$$

$$\left[Fe^{3+}(C_2O_4)_3\right]^{3-} + C_2O_4^{\bullet -} \longrightarrow \left[Fe^{3+}(C_2O_4)_3\right]^{2-} + C_2O_4^{2-} \quad (2)$$

$$\left[Fe^{3+}(C_2O_4)_3\right]^{2-} \longrightarrow \left[Fe^{2+}(C_2O_4)_2\right]^{2-} + 2\,CO_2 \quad (3)$$

Fe^{2+} can form stable red complex with 1, 10-phenanthroline. Fe(II) concentrations were determined by complexometry using $\varepsilon_{510} = 1.118 \times 10^4$ mol^{-1} L cm^{-1} for the complex of Fe(II) with *o*-phenanthroline. The principle of this assay is the following: after irradiation of a volume (V_1) of ferrioxalate potassium solution (0.006 mol L^{-1}) for a time *t* (expressed in seconds), we added at 2 mL (V_2) of this irradiated solution, 1 mL of acetate buffer, and 0.5 mL of 1, 10-phenanthroline (0.1% by mass). The solution is then filled with pure water up to 5 mL (V_3). After agitation, the solutions were kept in the dark for 1h and then the UV-vis measurement was carried out at 510 nm in a cell with an optical path equal to *l*.

The number of Fe(II) formed during the photo reaction was calculated with the following formula:

$$n_{Fe^{2+}} = \frac{6.023 \cdot 10^{20} \cdot V_1 \cdot V_3 \cdot \log(I_0 / I_T)}{V_2 \cdot l_{510} \cdot \varepsilon_{510}} = \frac{6.023 \cdot 10^{20} \cdot V_1 \cdot V_3 \cdot OD_{510}}{V_2 \cdot l_{510} \cdot \varepsilon_{510}}$$

With $OD_{510} = (OD_{solution} - OD_{balnk})_{510}$, the value of the absorbance at 510 nm of the blank is obtained with the same solution of potassium ferrioxalate, but not irradiated and prepared as before.

The number of Fe^{2+} formed is proportional to the fraction of absorbed light by the solution during this time *t*. Then the intensity emitted by the system, in photons per second for the volume V_1, is equal to:

$$I_0 = \frac{n_{Fe^{2+}}}{\phi_{Fe^{2+}} \cdot t \cdot (1 - 10^{-OD})} \quad \textbf{photons s}^{\textbf{-1}}$$

$(1\text{-}10^{-OD})$ is the percentage of photons absorbed by the solution at the wavelength of irradiation at time t = 0.

Then:

$$I_0 = \frac{6.023 \cdot 10^{20} \cdot V_1 \cdot V_3 \cdot OD_{510}}{V_2 \cdot l_{510} \cdot \varepsilon_{510} \cdot \phi_{Fe^{2+}} \cdot t \cdot (1 - 10^{-DO})} \quad \textbf{photons s}^{\textbf{-1}} \textbf{ for } \mathbf{V_1} \textbf{ mL}$$

These photonic flows were expressed in photons s^{-1} cm^{-2}, because with parallel beam, V_1 can be assimilated to the length of the optical path of the cell ℓ irr; these flows were

monitored throughout this work.

So,

$$I_0 = \frac{6.023 \cdot 10^{20} \cdot V_3 \cdot l_{irr} \cdot DO_{510}}{V_2 \cdot l_{510} \cdot \varepsilon_{510} \cdot \phi_{Fe^{2+}} \cdot t \cdot (1 - 10^{-DO})} \quad \textbf{photons s}^{-1}\ \textbf{cm}^{-2}$$

C-2 Irradiation with monochromator

For the determination of quantum yields of hydroxyl radicals, solutions were irradiated in monochromatic parallel beam in 1 cm (path length) quartz cell. The light source was a xenon lamp (1600W) equipped with a Schöffel monochromator. Figure III-C-1 gives a picture of the monochromatic irradiation device. The monochromatic irradiations were carried out separately at wavelength 365, 313 and 296 nm. The light intensity was measured by ferrioxalate actinometry (Calvert and Pitts, 1966). The photon flux of the monochromatic irradiation at different wavelength is listed in Table III-C-1. When necessary, solutions were deaerated or oxygenated by bubbling with argon or oxygen for 30 min before irradiation.

Figure III-C-1 Picture of the monochromatic irradiation device

Table III-C-1. Photonic flux at 365, 313 and 296 nm

λirr (nm)	365	313	296
I_0 (10^{15} photon·s^{-1}·cm^{-2})	4.25	1.40	0.83

All the quantum yield calculations depend on the following formulas (1), (2), (3) and (4):

$$\Phi = \frac{\Delta C \cdot 6.023 \cdot 10^{20} \cdot l}{I_a \cdot \Delta t \cdot f} \qquad (1)$$

$$\frac{I_a}{I_0} = 1 - 10^{-DO_{\lambda irr}} \qquad (2)$$

So we can get formula (3).

$$\Phi = \frac{\Delta C \cdot 6.023 \cdot 10^{20} \cdot l}{I_0 \cdot \Delta t \cdot (1 - 10^{-DO_{\lambda irr}}) \cdot f} \qquad (3)$$

Where $1\text{-}10^{-OD\lambda irr}$ represents the percentage of the light absorption at the wavelength of irradiation by the solution when t = 0, I_0 is the number of the photons entering the reaction cell per second determined by actinometry and ℓ is the length of irradiation cell in cm. ΔC is the amount of HTPA produced during the irradiation period Δt. *f* is the yield of HTPA produced in the reaction of •OH with TPA. In oxygen-containing solutions and oxygen-free solutions *f* is equal to 35% and 84% respectively (Fang *et al*., 1996; Millington and Kirschenbaum, 2002). For the quantum yields, the experimental error was estimated to 5%.

C-3 Irradiation centered at 365 nm

For the photodegradation of E2, the irradiation experiments were performed in a home-made photoreactor placed in a cylindrical stainless steel container. The reaction device consists of four tubes (Philips TLD 15W / 05), whose emission spectrum is from 300 to 500 nm with a maximum irradiation at 365 nm (Figure III-C-2). These four tubes were separately placed in the four different axes, while the photoreactor, a water-jacketed Pyrex tube of 2.8 cm diameter, was placed in the center of the setup (Figure III-C-3). The solution (usually 100 mL) was continuously magnetically stirred with a magnetic bar during irradiation to insure its homogeneity.

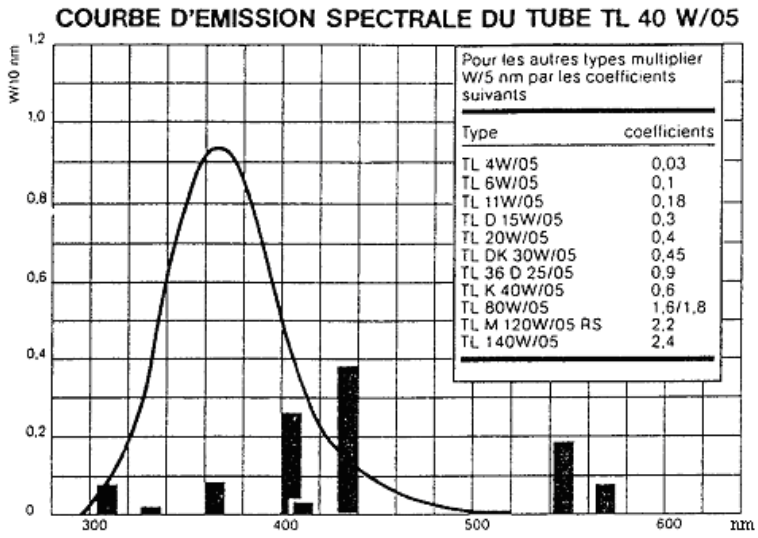

Figure III-C-2. Emission spectra of tube Philips, TLD 15W/05.

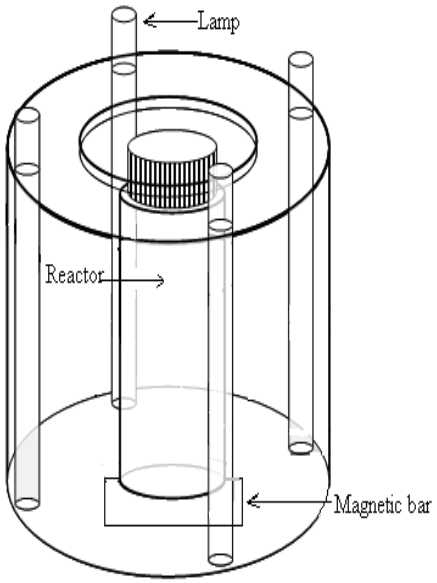

Figure III-C-3 Home-made photoreactor with four tubes (Philips TLD 15W / 05)

C-4 Irradiation with Metal halide lamp

For the quantitative determination of hydroxyl radical formation in the Montmorillonite (Shaoxing, Zhejiang, PRC), the experiments was set up in a photoreactor as shown in Figure III-C-4. The photoreactor was designed with a cylindrical cell (25.5 cm length, 9.5 cm diameter, 4 mm wall thickness), and the lamp with a glass-jacket was fixed through the central axes of the cell. The light source was a 250 W metal halide lamp (MHL, $\lambda \geq 365$ nm, 250 W, Wuhan Yaming lamp Co. Ltd., China). The surface area of the lamp is about 320 cm^2, and exposed area of the solution is about 690 cm^2. The light intensity was 34 $\mu W\ cm^{-2}$,

which was detected by an irradiance meter (FS type, Peixian Photoelectric Instruments Co. Jiangsu, PRC). A total volume of 400 mL of suspension containing 7 mM benzene and desired amount of montmorillonite was prepared. The pH values of the suspension were adjusted from 2.0 to 10.0 using 0.01 M HCl or NaOH. Then, the aqueous clay suspensions were transferred to the photochemical reaction chamber and photolyzed under a Metal Halide Lamp for a period of 6 h. The temperature of the irradiated solution was maintained at 25 ± 1 ^{o}C by circulating water and a magnetic stirrer was used to agitate the suspension during irradiation. An aliquot of 2 mL was withdrawn at different time and centrifuged at 10000 rpm for 30 min. Control experiments were carried out under identical conditions, but in the dark. Determination of the blank was also carried out in a similar manner without clay.

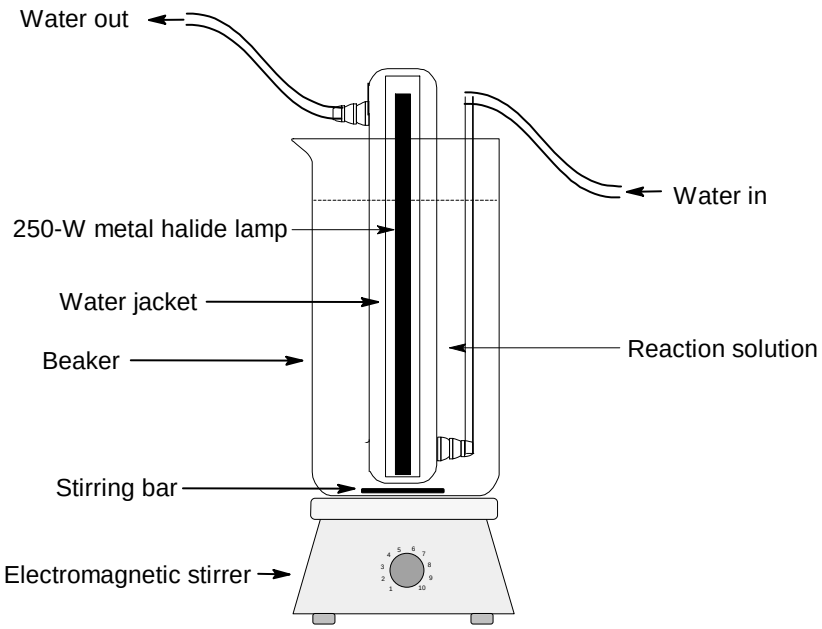

Figure III-C-4 Scheme of the experimental setup for photooxidation of benzene. Lamp: 250-W metal halide lamp, $\lambda_{ex} \geq 365$ nm, $I = 34$ µW cm^{-2}.

D-Analysis method

D-1 Minerals

Powder X-ray diffraction patterns were recorded on a Siemens D501 diffractometer using CuKα radiation (λ = 1.5415 Å). Patterns were recorded over the 2.0-70 2θ range in steps of 0.08° with a counting time per step of 4 seconds. The chemical compositions of the samples were analyzed by a S4 PIONEER X-ray fluorescence spectrometer (XRF). Transform

infrared (FT-IR) spectra were measured in the range 400-4000 cm^{-1} on a FTIR Nicolet 5700 spectrometer (Thermo Electon Corporation) equipped with a Smart Orbit accessory. Transmission electron microscopy (TEM) images were taken using a Hitachi 7650 microscope at an acceleration voltage of 80 kV. To prepare the samples, a drop of the solution containing the materials was deposited on a carbon coated grid and let to dry. Nitrogen adsorption- desorption were performed at -196 °C with a Micromeritics ASAP 2020. Before analysis, samples were pre-treated at 80 °C under vacuum for 12 h. The surface areas were estimated by using the Brunauer-Emmett-Teller method.

D-2 Chemicals

D-2-1 Spectroscopy methods

UV-vis Spectrophotometer

The UV–visible spectra of the solutions were recorded on a Cary 300/3 double beam spectrophotometer.

Fluorescence spectrometer

The fluorescence spectra of the solutions were recorded on a LS 55 luminescence spectrometer (Perkin Elmer).

For measurements of TAOH, the excitation wavelength was set at 315 nm and the emission wavelength at 433 nm. The excitation and emission band passes were both set at 10 nm.

D-2-2 Chromatographic methods

Two HPLC systems were used for product analysis:

HPLC Alliance chromatograph equipped with waters 2475 Multi λ Fluorescence detector, waters 2487 Dual λ Absorbance detector and waters 2695 separations Module.

HPLC (LC-10AT, Shimadzu, Japan)

Two HPLC columns were used in the work:

A NUCLEODUR 100-5 C18 of 4.6 mm (ID)×150 mm (length) with a particle diameter of 5 µm.

A Kromasil C18 column of 4.6 mm (ID)×150 mm (length) with a particle diameter of 5

μm.

The conditions of HPCL for the analysis are the following:

a. To analyze E2, a mixture of water containing 3‰ formic acid and acetonitrile (55/45, v/v) was used as mobile phase and the flow rate was 1.0 mL min^{-1}. The UV detection wavelength was set at 280 nm and the fluorescence detection was set at 280 nm excitation and 300 nm emission.

b. To analyze EDDS, the mobile phase was a methanol: formate buffer (2 mM tetrabutylammonium hydrogen sulfate and 15 mM sodium acetate, pH adjusted to 4.0 with acetic acid) (20:80, v/v) and the flow rate was 1.0 mL min-1. The detection wavelength was set at 254 nm.

c. To analyze TAOH, a mixture of water containing 3‰ formic acid and acetonitrile (80/20, v/v) was used as mobile phase and the flow rate was 1.0 mL min^{-1}. The UV detection wavelength was set at 254 nm and the fluorescence detection was set at 320 nm excitation and 434 nm emission.

d. To analyze Phenol, the mobile phase was methanol/water mixture (70/30, v/v) at a flow rate of 1.0 mL min^{-1}. The formation of phenol from benzene was monitored at 280 nm.

D-2-3 Dosage methods

Fe(II) and total iron

Fe(II) concentration was determined by complexometry with *ortho*-phenanthroline, using ε = 1.118×10^4 L mol^{-1} cm^{-1} for the Fe(II)-phenanthroline complex (Calvert and Pitts, 1966). Fe^{3+} ions were reduced to Fe^{2+} with excess of ascorbic acid to determine the total concentration of iron ions.

A certain quantity of $Fe(NH_4)_2SO_4$ solution was used as Fe(II) sources to make a calibration curve (as shown in Figure III-D-1). The molar absorption coefficient was 11420 L mol^{-1} cm^{-1}, which is nearly the same as the reference value $\varepsilon_{510\,nm}$ = 11180 L mol^{-1} cm^{-1}. By means of the calibration curve, it was carefully checked that no interference in the analysis was observed when E2 or EDDS was present in the solution.

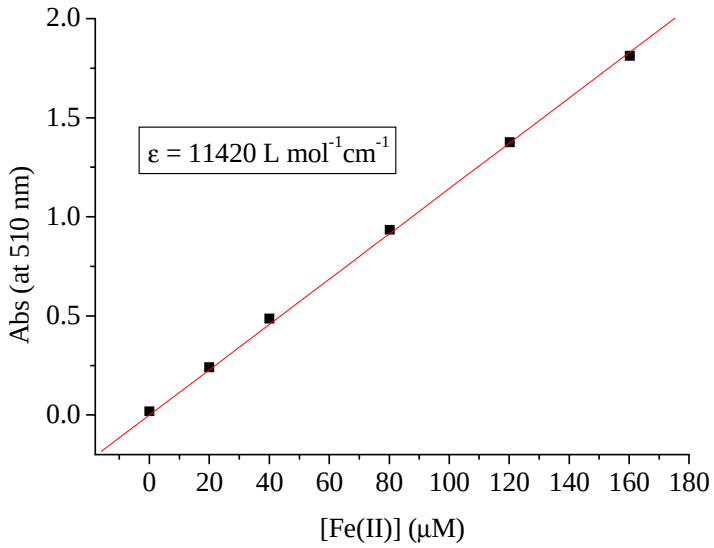

Figure III-D-1 Calibration curve of Fe(II) concentration

Hydroxyl radicals

Scavenging of •OH by TA

Terephthalic acid dianion (TA) has proven to be an especially convenient hydroxyl radical trap, which can be used to estimate relative amounts of hydroxyl radicals (•OH) formed under varying conditions (Barreto *et al.*, 1995; Fang *et al.*, 1996). TA which is not fluorescent, gives a single fluorescent product 2-hydroxyterephthalic acid (TAOH) in the reaction with the hydroxyl radical as described by the following reaction:

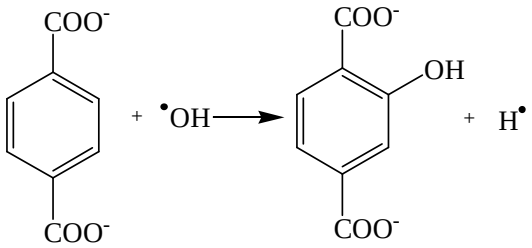

Reaction of TA to form TAOH is highly specific towards •OH; other common oxygen radical species, such as the superoxide anion and organic hydroperoxides, have failed to produce TAOH fluorescence directly (Millington and Kirschenbaum, 2002). Because of the symmetrical structure of TA, there is only one form of the monohydroxylated adduct.

In the experiments, high concentration of TA (0.5 mM) was used in order to make sure trap all of the hydroxyl radicals formed. The concentrations of photochemically formed hydroxyl radicals were determined as:

$$C_{OH} = C_{TAOH} / f$$

f is the yield of TAOH produced in the reaction of $^{\bullet}OH$ with TA. In oxygen-containing solutions and oxygen-free solutions *f* is equal to 35% and 84% respectively (Fang *et al*., 1996; Millington and Kirschenbaum, 2002).

The concentration of TAOH was detected by Fluorescence spectrometer and HPLC. It should be noticed that when using the fluorescence spectrophotometer, the fluorescence intensity of TAOH was influenced by the pH and the iron concentration in the solution. The Calibration curve of TAOH using HPLC detected was shown in Figure III-D-2.

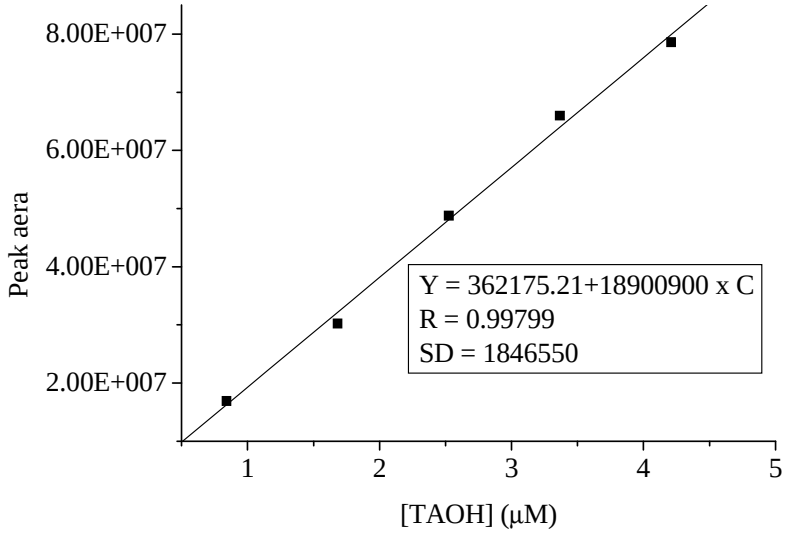

Figure III-D-2 Calibration curve of TAOH

Scavenging of $^{\bullet}OH$ by benzene

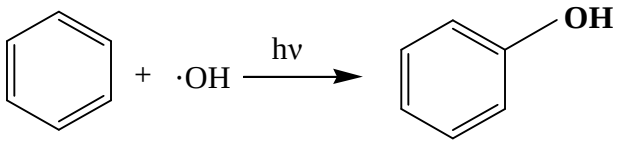

Aromatic hydroxylation is one of the typical reactions of $^{\bullet}OH$ and is used for detection of $^{\bullet}OH$ in the case of Fenton reaction and of the photolysis of aqueous solution of HNO_2, NO_3^- and NO_2^- (Arakaki *et al*., 1999). Benzene is very unreactive toward O_2 ($1\Delta g$) (Zepp *et al*., 1987). The hydroxylation of benzene by $^{\bullet}OH$ to produce phenol is a selective process. Given the high reactivity of benzene with $^{\bullet}OH$ ($k \approx 8 \times 10^9$ L.mol^{-1}.s^{-1}) (Kochany and Bolton, 1992; Pan and Schuchmann,1993) and under the conditions of these experiments, virtually all of the $^{\bullet}OH$ should have been scavenged by benzene. The destruction rate of phenol by direct photolysis and by peroxyl radicals, $O_2(^1\Delta_g)$ and other oxidants is expected to be slow by

comparison to the rate of phenol formation from the •OH through the oxidation of benzene (Liu *et al*., 2004). It was thought that •OH-mediated oxidation of benzene forms phenol with a nearly 100% yield (Faust and Allen, 1993; Joseph *et al*., 2001; Wang *et al*., 2006), and thus the concentrations of photochemically formed hydroxyl radicals were determined as

$$C_{OH} = C_{Phenol}$$

Where, C_{Phenol} is the concentration of phenol at time t. Figure III-D-3 shows the calibration curve of phenol.

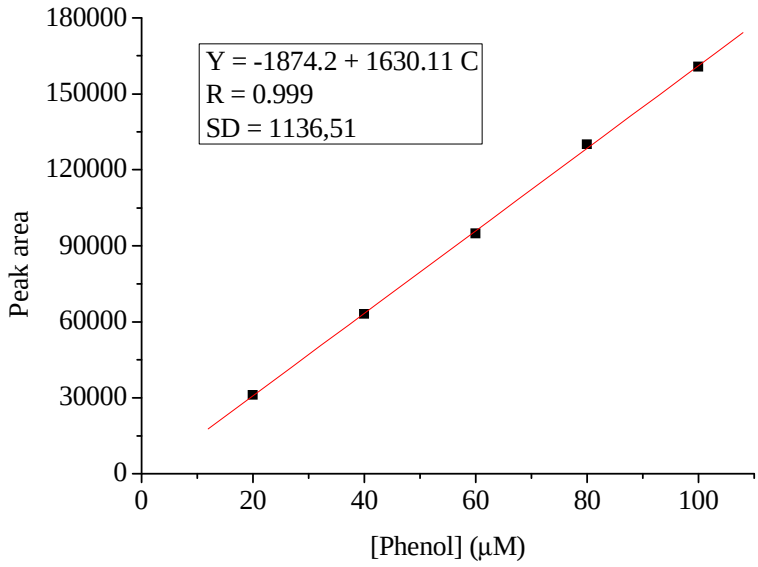

Figure III-D-3 Calibration curve of phenol

EDDS

The determination of EDDS is based on the conversion of EDDS to Cu(II)-EDDS followed by HPLC and detected with a UV detector. A 10 mM of a $CuSO_4$ stock solution was prepared. Metal complex solutions were prepared by mixing the desired proportions of Cu(II) and appropriate complexing agents and diluting with deionized water. The concentration of Cu(II) was kept at 0.5 mM. The solutions were kept in a refrigerator and left to stand over night to ensure complete complexation. The Calibration curve of EDDS was shown in Figure III-D-4.

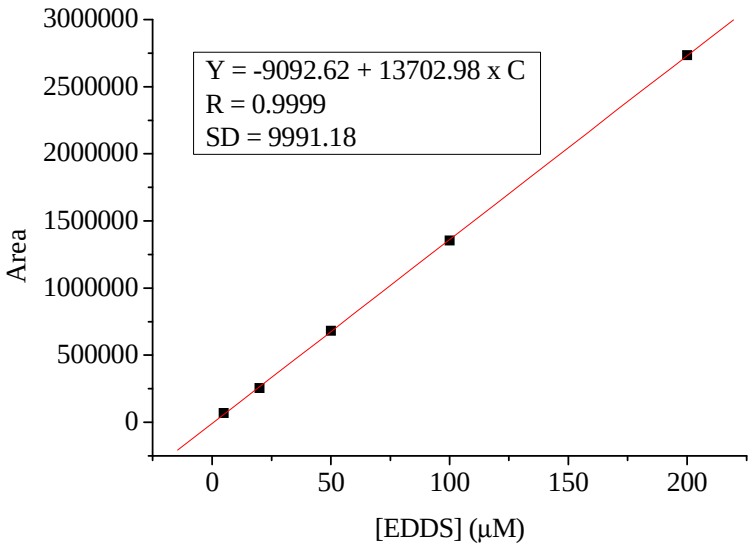

Figure III-D-4 Calibration curve of EDDS concentration

IV

RESULTS AND DISCUSSION

IV-Results and discussion

IV-A Physicochemical property of E2, Fe(III)-EDDS, and Minerals

A-1 Property of 17*β*-estradiol

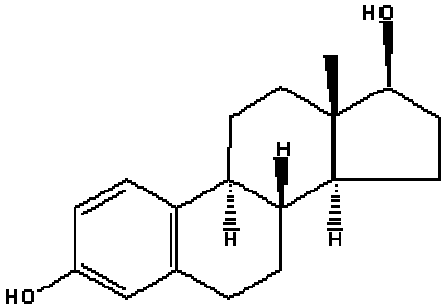

17*β*-estradiol (E2)

The UV-visible spectrum of the solutions with different concentrations of E2 is presented in Figure IV-A-1. It has one band with maximum absorption at 278 nm. No absorption was observed at $\lambda > 300$ nm. The molar absorption coefficients ε is equal to 1900 L mol^{-1} cm^{-1} at 278 nm as shown in Figure IV-A-2.

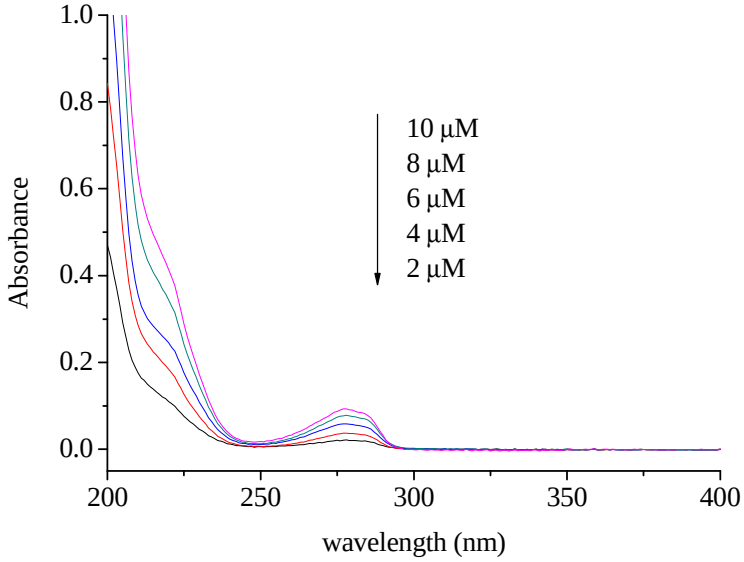

Figure IV-A-1 The UV-Visible absorption spectrum of E2 solution with different concentration

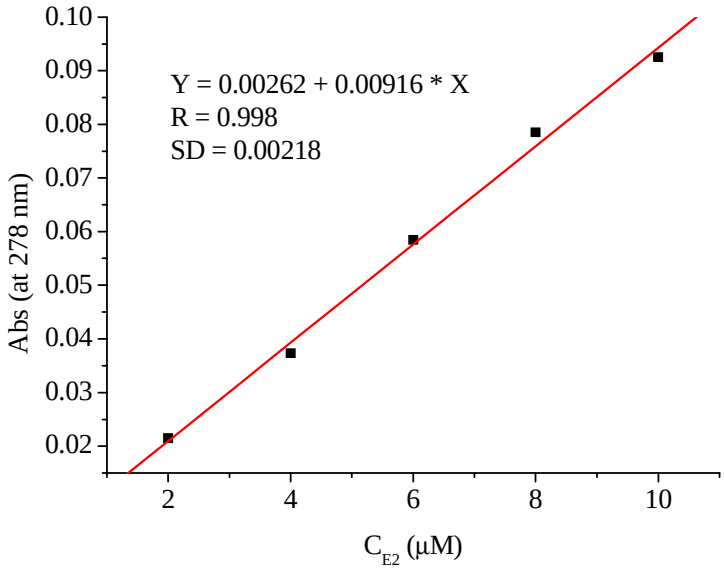

Figure IV-A-2 Molar absorption coefficients at 278 nm.

The other important chemical and physical properties of E2 were shown in table IV-A-1. The water solubility of E2 is very low. In this work, no organic solution was used to help dissolving E2 in the water solution. The maximal concentration of E2 in water can be reached to 20 μM under the ultrasonic waves.

Table IV-A-1 Chemical and physical properties of E2

17*β*-estradiol	
CAS number	50-28-2
molecular formula	$C_{18}H_{24}O_2$
molecular weight	272.39
melting point	178-179 °C
Odor and appearance	Odorless; white to pale yellow crystals
λ_{max}	278 nm
logKow	4.01
pKa	10.4
Solubility in	alcohol, acetone, dioxane, fixed alkali hydroxides, sparingly soluble in vegetable oils
Water solubility	3.99 mg L^{-1} or 14.66 μM

A-2 Properties of Fe(III)-EDDS

A-2-1 Properties of EDDS

Ethylenediamine-*N*,*N'*-disuccinic acid (EDDS), like EDTA and DTPA is a member of the aminopolycaroxylate group of compounds. It is a structural isomer of EDTA, and exists as three stereo isomers, namely [S,S]-EDDS, [R,R]-EDDS and [R,S/S,R]-EDDS (Figure IV-A-3). Among them, [S,S]-EDDS is readily biodegradable. It has been proposed as a safe and environmentally benign replacement of EDTA for environmental remediation product as it is also a strong complexing agent. In this work, [S,S]-EDDS was used.

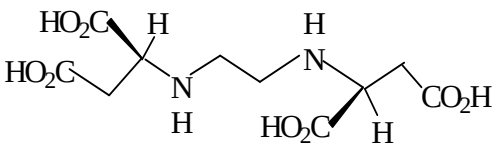

[S, S]-EDDS

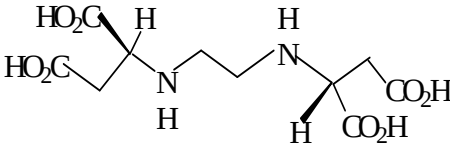

[R, S]-EDDS or [S, R]-EDDS

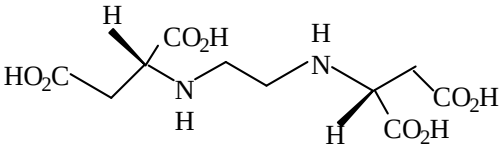

[R, R]-EDDS

Figure IV-A-3 Chemical structures of the different stereoisomers of EDDS.

UV-Visible absorption spectra of EDDS as function of pH was shown in Figure IV-A-4. The results show that the absorbance increases between 200 and 240 nm when the pH increases. This effect was accelerated at basic pH. Table IV-A-2 lists the EDDS dissociation constants of EDDS in the form of pKa, which is the negative of the logarithm of the acid dissociation constant Ka (Vandevivere *et al*., 2001).

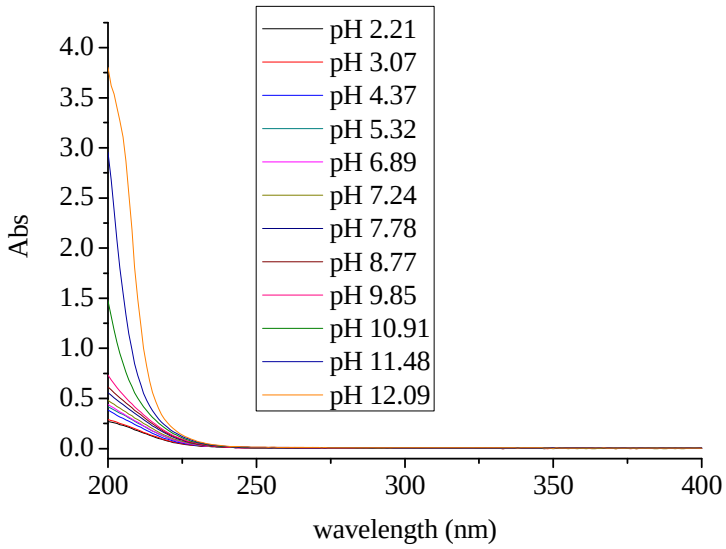

Figure IV-A-4 UV-Visible absorption spectra of EDDS as function of pH ([EDDS] = 0.2 mM).

Table IV-A-2 pKa of ethylenediamine-disuccinic acid (EDDS) (25°C, 0.1 M KNO_3). (Vandevivere *et al.*, 2001)

	pKa
pK_1	2.4
pK_2	3.9
pK_3	6.8
pK_4	9.8

Consequently, EDDS equilibrium in the solutions is described here, Eq. (1) - (4). For simplification, EDDS molecules were substituted by H_4A.

$$H_4A \rightarrow H^+ + H_3A^- \qquad K_1 \qquad (1)$$

$$H_3A^- \rightarrow H^+ + H_2A^{2-} \qquad K_2 \qquad (2)$$

$$H_2A^{2-} \rightarrow H^+ + HA^{3-} \qquad K_3 \qquad (3)$$

$$HA^{3-} \rightarrow H^+ + A^{4-} \qquad K_4 \qquad (4)$$

Using the following equilibrium equation and the equilibrium constants from Vandevivere *et al.*, 2001, the distribution diagram was calculated and shown in Figure IV-A-5. Between pH 2.4 to 3.9, pH 3.9 to 6.8, pH 6.8-9.8, $[H_3A^-]$, $[H_2A^{2-}]$, $[HA^{3-}]$ was the dominate species respectively.

$$\delta_0 = \frac{[H_4A]}{C} = \frac{[H^+]^4}{[H^+]^4 + K_1[H^+]^3 + K_1K_2[H^+]^2 + K_1K_2K_3[H^+] + K_1K_2K_3K_4}$$

$$\delta_1 = \frac{[H_3A^-]}{C} = \frac{K_1[H^+]^3}{[H^+]^4 + K_1[H^+]^3 + K_1K_2[H^+]^2 + K_1K_2K_3[H^+] + K_1K_2K_3K_4}$$

$$\delta_2 = \frac{[H_2A^{2-}]}{C} = \frac{K_1K_2[H^+]^2}{[H^+]^4 + K_1[H^+]^3 + K_1K_2[H^+]^2 + K_1K_2K_3[H^+] + K_1K_2K_3K_4}$$

$$\delta_3 = \frac{[HA^{3-}]}{C} = \frac{K_1K_2K_3[H^+]}{[H^+]^4 + K_1[H^+]^3 + K_1K_2[H^+]^2 + K_1K_2K_3[H^+] + K_1K_2K_3K_4}$$

$$\delta_4 = \frac{[A^{4-}]}{C} = \frac{K_1K_2K_3K_4}{[H^+]^4 + K_1[H^+]^3 + K_1K_2[H^+]^2 + K_1K_2K_3[H^+] + K_1K_2K_3K_4}$$

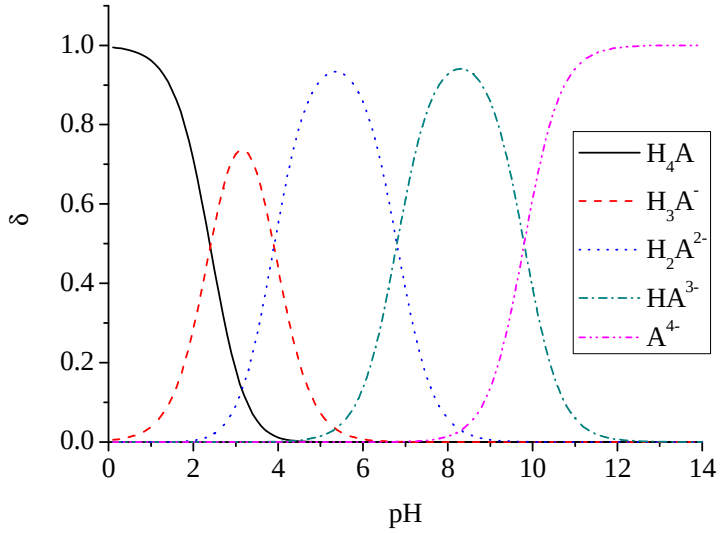

Figure IV-A-5 Distribution diagram of EDDS aqueous solution as a function of pH values range from 0 to 14, calculated with equilibrium constants from Vandevivere *et al*. (2001) at 25 □.

A-2-2 Properties of Fe(III)-EDDS

Our laboratory have done some work on the physicochemical properties of Fe(III)-EDDS complex. Fe (III) is complexed by EDDS with a ratio 1:1 (Zhang, 2008). The Fe(III)-EDDS complex is stable in the dark and at room temperature at least 10 days.

The UV-Visible spectrum of Fe(III)-EDDS solution with different concentration (pH = 3.88) was shown in Figure IV-A-6. The complex has one band with maximum absorption at 239 nm. No absorption was observed at $\lambda > 500$ nm. The molar absorption coefficients ε is equal to 6530 L mol^{-1} cm^{-1} at 239 nm as shown in Figure IV-A-7.

Figure IV-A-8 shows the UV-Visible absorption spectra of aqueous solutions with 0.1 mM Fe(III)-EDDS complex changes with the modification of pH value from 1.74 to 11.06. The

stability constants of Fe(III)-EDDS complex in aqueous 0.1 M NaCl at 25 ^{o}C are given table IV-A-3 (Orama M. *et al*., 2002). The distribution diagram of Fe(III)-EDDS aqueous solution as a function of pH values range from 0 to 12 was shown in Figure IV-A-5 (Orama M. *et al*., 2002). FeL^{-} was the dominant species between pH 2-8. The approximate pH ranges suitable for the use of EDDS as a chelating agent complexing with Fe(III) are 3-9.

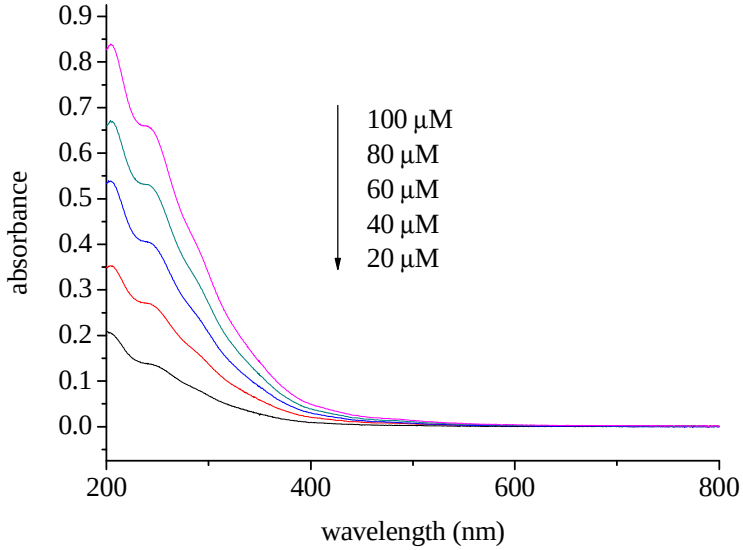

Figure IV-A-6 UV-Visible spectrum of Fe(III)-EDDS solution with different concentration (pH = 3.88)

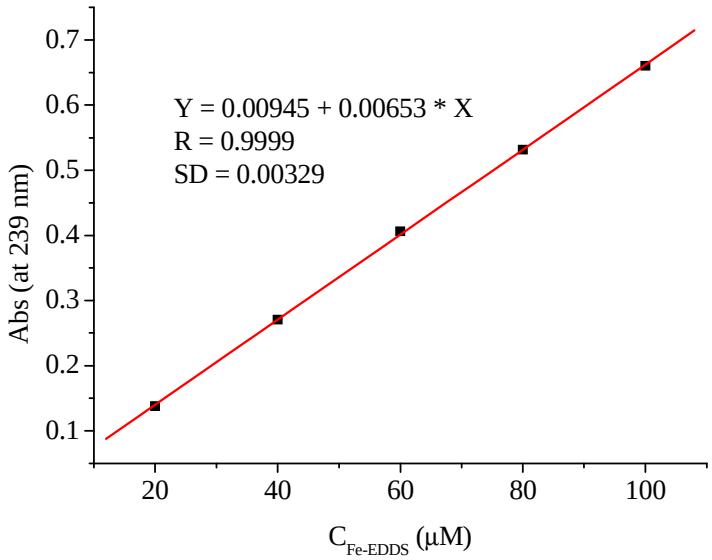

Figure IV-A-7 Molar absorption coefficients at 239 nm

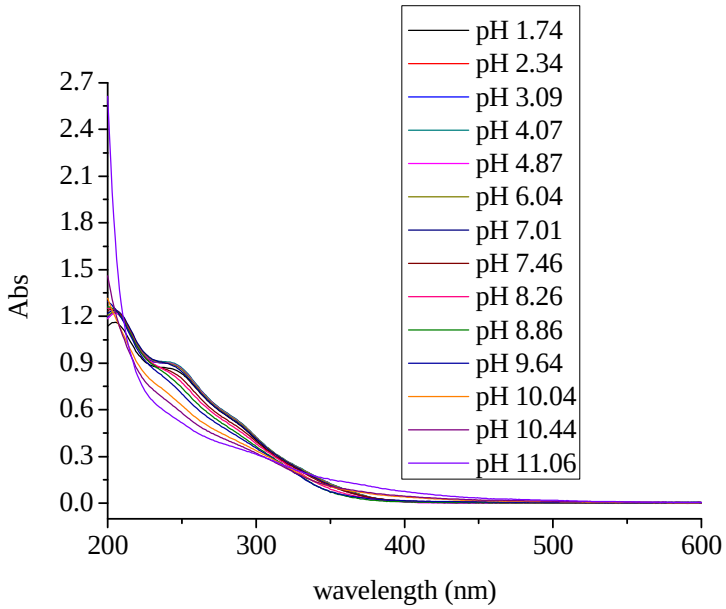

Figure IV-A-8 UV-Visible absorption spectra of Fe(III)-EDDS solution under different pH (Fe(III)-EDDS 10^{-4} M)

Table IV-A-3 Stability constants of Fe(III)-EDDS complex in aqueous 0.1 M NaCl at 25 ^{o}C.

Reaction	Log (K+3σ) [S,S]-EDDS
$Fe^{3+} + L^{4-} \rightarrow FeL^{-}$	20.6 ± 0.2
$Fe(OH)L^{2-} + H^{+} \rightarrow FeL^{-}$	7.9 ± 0.1
$Fe(OH)_2L^{3-} + H^{+} \rightarrow Fe(OH)L^{2-}$	9.9 ± 0.1

Photolysis of Fe (III)-EDDS complex (0.1 mM) was studied in the aqueous solution under different pH. The Results were shown in Figure IV-A-9. These results indicated that under 365 nm, these complexes were easily photolyzed and it provided the possibility for the formation of excited state complexes and further generated many kinds of radicals. Figure IV-A-10 showed the absorbance at λ = 240 nm of the Fe(III)-EDDS complex at the different time under the different pH during irradiation. The results shows that at lower pH, the absorbance at λ = 240 nm decreases faster. But it seems that at higher pH, there are more new species formed in the solution.

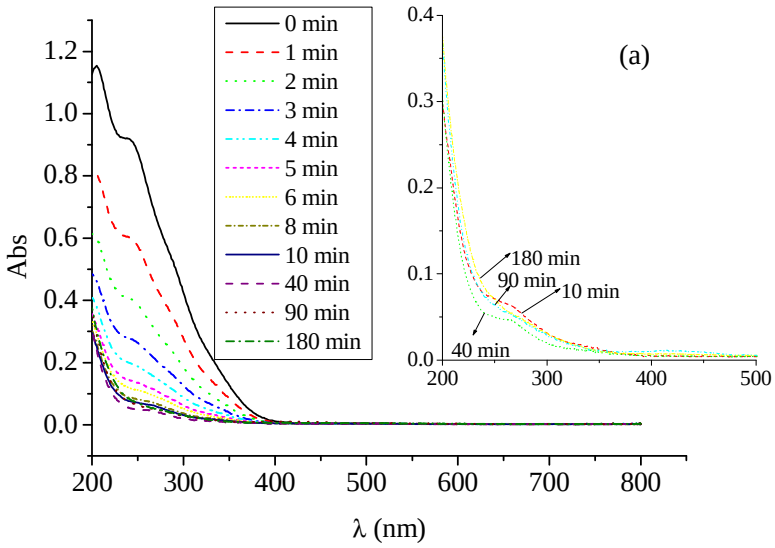
0 min
1 min
2 min
3 min
4 min
5 min
6 min
8 min
10 min
40 min
90 min
180 min
Abs
λ (nm)
(a)
180 min
90 min
10 min
40 min

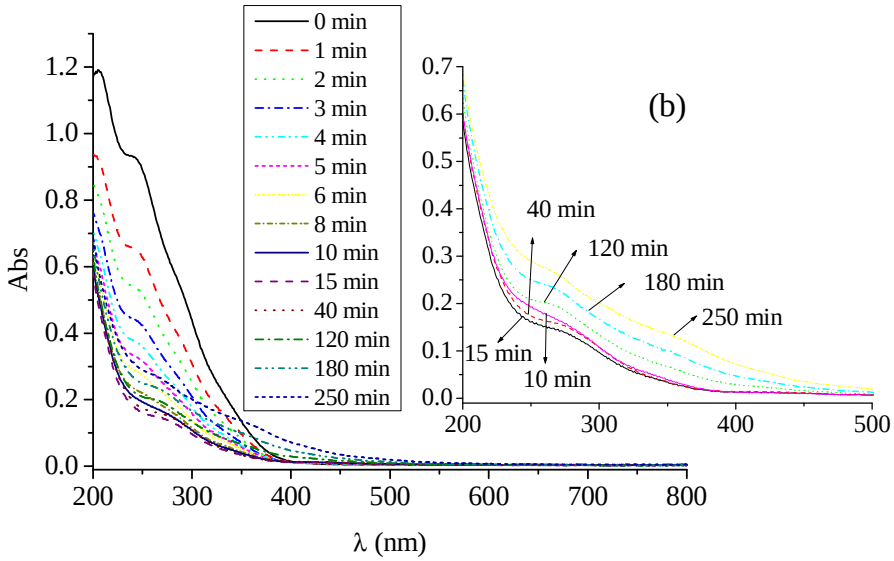
0 min
1 min
2 min
3 min
4 min
5 min
6 min
8 min
10 min
15 min
40 min
120 min
180 min
250 min
Abs
λ (nm)
(b)
40 min
120 min
180 min
250 min
15 min
10 min

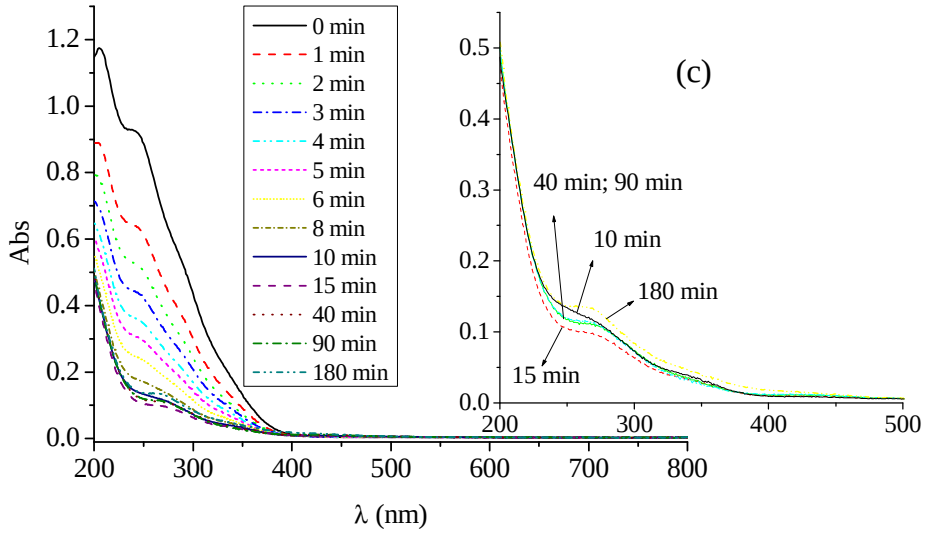
0 min
1 min
2 min
3 min
4 min
5 min
6 min
8 min
10 min
15 min
40 min
90 min
180 min
Abs
λ (nm)
(c)
40 min; 90 min
10 min
180 min
15 min

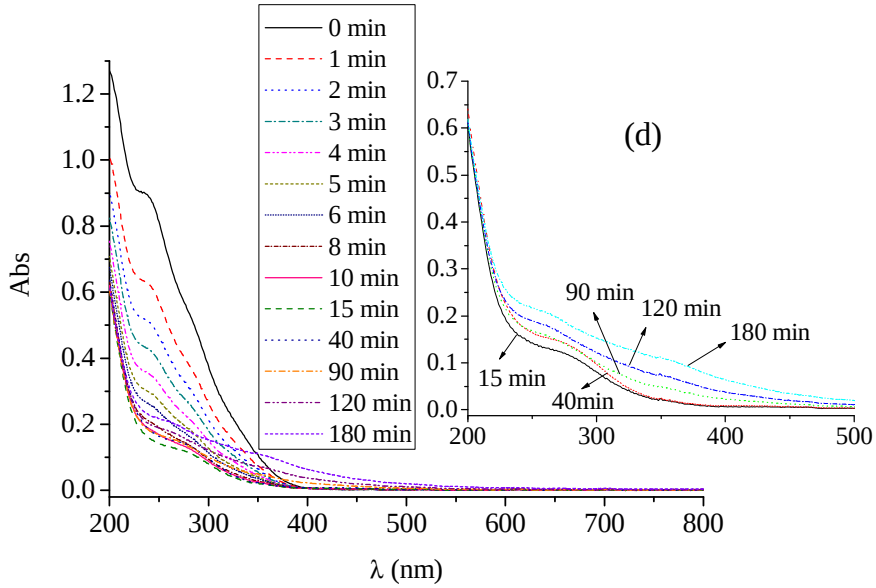
0 min
1 min
2 min
3 min
4 min
5 min
6 min
8 min
10 min
15 min
40 min
90 min
120 min
180 min
Abs
λ (nm)
(d)
90 min
120 min
180 min
15 min
40min

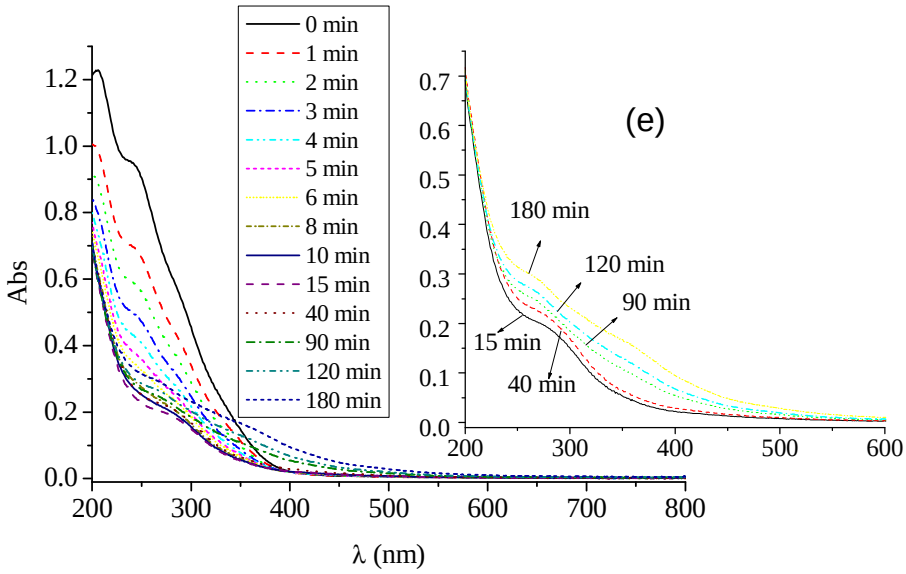

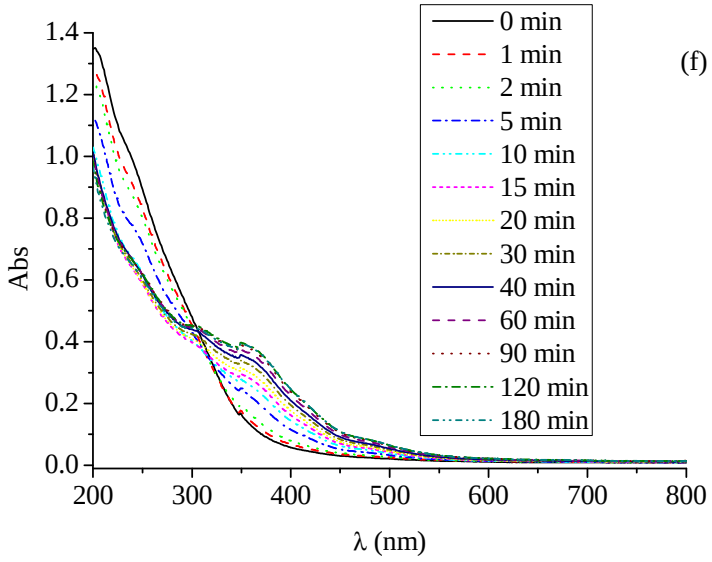

Figure IV-A-9 UV-Vis spectrum of monochromatic irradiation of Fe(III)-EDDS solutions at different pH (Fe(III)-EDDS 0.1 mM, λ = 365 nm, Monochromator (Xe Schöffel 1600W) (a) pH 3; (b) pH 4; (c) pH 5.1; (d) pH 6; (e) pH 7; (f) pH 9.1.

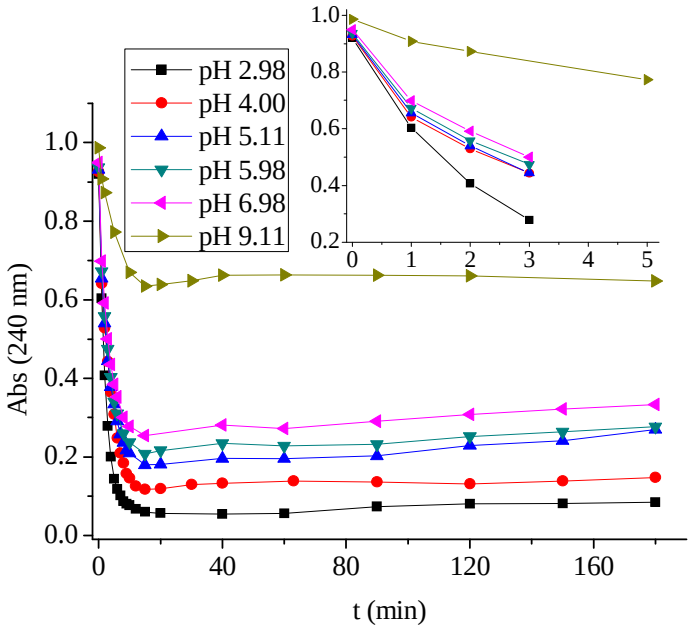

Figure IV-A-10 The $A_{\lambda = 240\ nm}$ (Fe(III)-EDDS) at the different time under the different pH

A-3 Characterization of the minerals

In this thesis, KSF, NM, Goethite are chosen as the model minerals, that is due to their quite different surface properties and composing the different concentration level of free iron ions and structural iron in the minerals, which would help understanding the iron role in photochemical process of mineral-EDDS system. The chemical compositions of KSF and NM were determined by XRF (shown in Table IV-A-4). SiO_2 and Al_2O_3 are the main constituent of KSF and NM. Goethite is composed by Fe_2O_3. KSF and NM also contain relative high and similar amount of Fe_2O_3, which is 4.76% and 4.28% respectively. But there are more amount of free iron ions in KSF than that in NM. In 1 g L^{-1} KSF suspensions at pH 3, about 100 μM iron is detected. In 1 g L^{-1} NM suspension at pH 3, almost no iron could be detected. Thus, the most iron in NM is structural iron. In 1 g L^{-1} Goethite suspension at pH 3, about 10 μM is detected, which is very small.

Table IV-A-4 Chemical compositions of the minerals

component	NM	KSF	Goethite
Na_2O	2.22	0.0573	
MgO	2.44	4.31	
Al_2O_3	21.8	16.3	
SiO_2	66.4	49.1	
P_2O_5	0.0508	0.0547	
SO_3	0.72	22.3	
K_2O	0.522	0.495	
CaO	1.24	2.30	
TiO_2	0.166	0.210	
MnO	0.0134	0.0191	
Fe_2O_3	**4.28**	**4.76**	**100**
NiO		0.00529	
CuO	0.00701	0.00756	
ZnO	0.0112	0.0153	
Ga_2O_3	0.00486	0.00372	
Rb_2O		0.00376	
SrO	0.0388	0.00838	
Y_2O_3	0.00705	0.00731	
ZrO_2	0.0356	0.0503	
BaO	0.0300	0.0680	
Cl	0.0141		
Nb_2O_5	0.00535		
$Tb4O_7$	0.000616		
PbO	0.00533		
ThO_2	0.00584		
Compton	0.96	0.89	
Rayleigh	1.34	1.3	

The surface area and porous volume of the minerals were shown in Table IV-A-5. Goethite displays a relatively high surface area whereas KSF appears as non-porous solid. The surface area measured for NM is in agreement with values reported in the literature for untreated Montmorillonite.

Table IV-A-5 Surface area analysis

	S_{BET} m^2 g^{-1}	V_{porous} cm^3 g^{-1}
KSF	5	0.005
NM	32.0	0.09
Goethite	71	0.23

The XRD patterns of the minerals are shown in Figure IV-A-11. For the goethite we

synthesized, the XRD pattern mainly displays the typical diffraction lines of pure goethite. For the NM, the diffraction lines characteristic of Montmorillonite are observed on the XRD pattern conjointly with lines corresponding to quartz (2θ =26.8), not completely removed during the clay purification. The 001 line corresponds to the expected interlayer value of 1.22 nm for Na^+ intercalated montmorillonite. For the KSF, diffraction lines correspond to the Smectite clay characteristic lines (similar to NM) but we note many additional diffraction lines due to impurities. XRD patterns of KSF/NM/Goethite after irradiation of the minerals, noted KSF/NM/Goethite IRR, were also recorded. No difference was observed on the XRD patterns before and after irradiation evidencing that the irradiation did not modify the mineral structure.

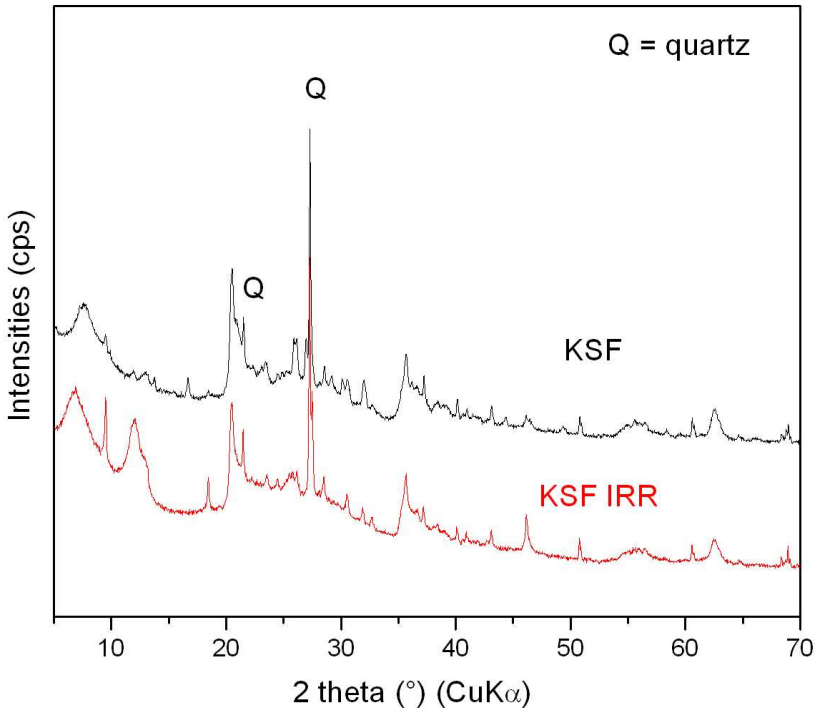

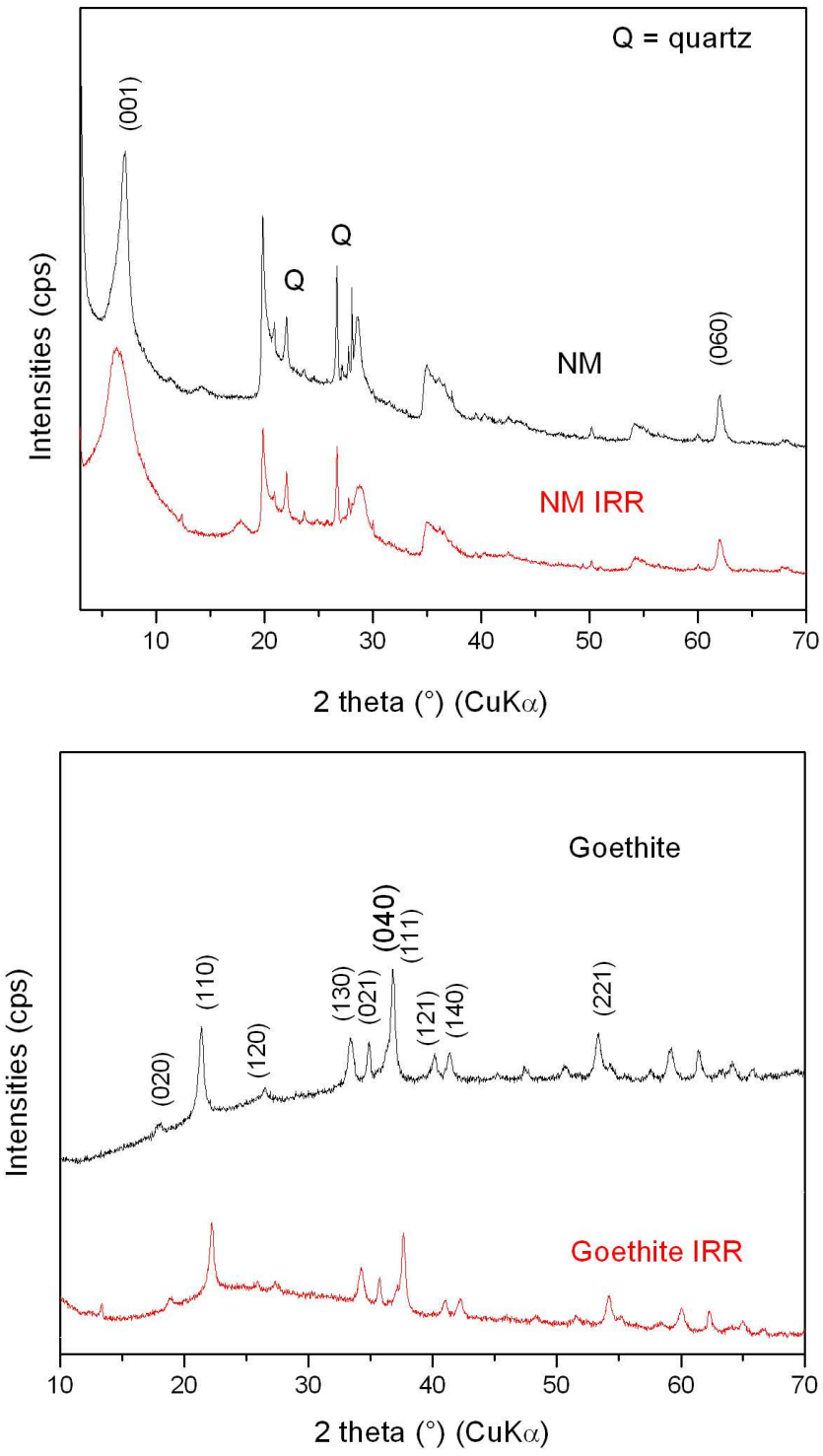

Figure IV-A-11 Powder XRD pattern of the montmorillonite KSF, NM, Goethite.

FT-IR spectra of the minerals before and after irradiation, with and without EDDS are shown in Figure IV-A-11. On the IR spectra of NM, the band at 3620 cm^{-1} can be attributed at the OH stretching vibration whereas the band at 1636 cm^{-1} correspond to the interlayer water deformation vibration. The band at 1112 cm^{-1} is due to the Si-O stretching. For the KSF, most of the bands are similar to those observed on the NM spectra. However, we note a

net modification of the vibration due to hydroxyl group, with a large band between 2600 cm^{-1} and 3300 cm^{-1}. For the goethite, the band between 3600–3300 cm^{-1} is assigned to the H---O---H vibration (ν_1). This band is a typical mode of non-stoichiometric hydroxyl units (excess of water) in the goethite structure. This type of hydroxyl units can be incorporated into goethite structure and adsorbed onto the crystal surface during the process of synthesis. Goethite can also adsorb hydroxyl units from the atmosphere. The most intense band at 3300–3000 cm^{-1} is assigned to the O---H stretching vibration (ν_2). Finally, the band at 890 cm^{-1} and 620 $cm^{-1}$are assigned to O-H bending vibration and Fe-O stretching vibration respectively.

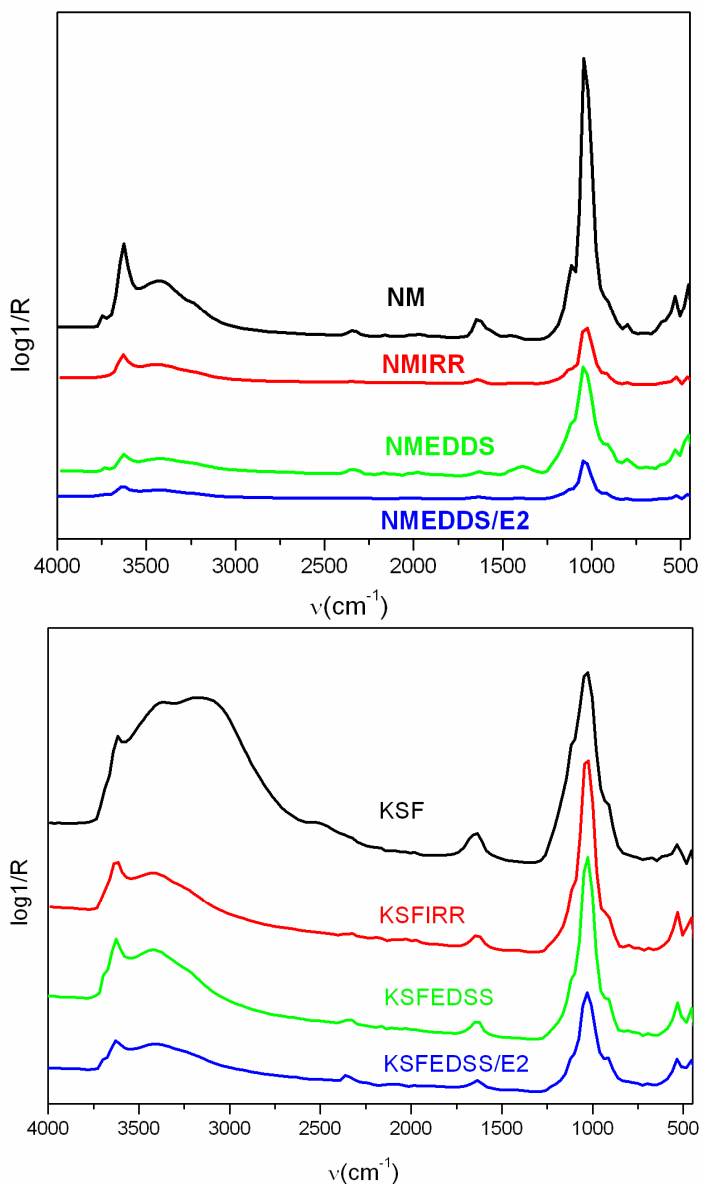

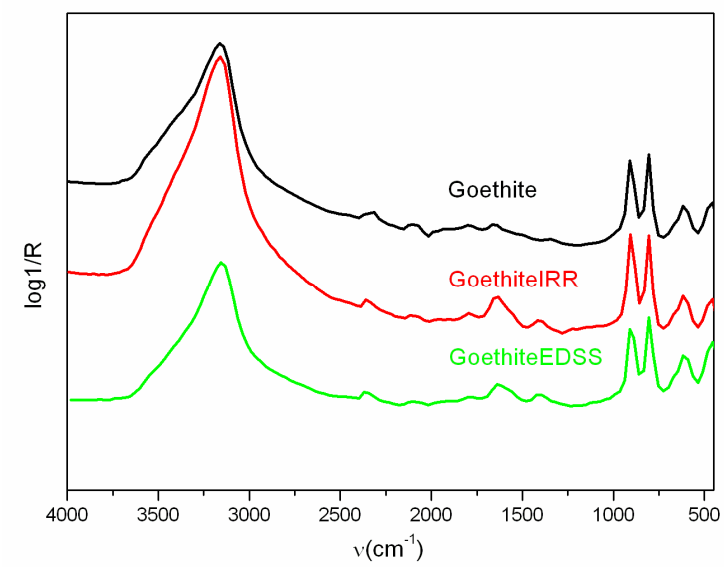

Figure IV-A-12 FT-IR spectra of KSF, NM, Goethite

The isoelectric points (PI) of the minerals are also detected. As shown in Figure IV-A-13, the measures of zeta potential are not satisfactory for KSF. It have been reported the PI of KSF is 5. For the NM, the isoelectric point is lower than 3. The isoelectric point of natural Montmorillonite is reported to be around 2. In the case of goethite, the isoelectric point was observed around pH 4.0. The zeta potential is relatively low in magnitude at high pH that indicates that the repulsive force between particles is relatively low. The PI values of goethite reported in the literature are higher in the range from 7.4 to 9.5.

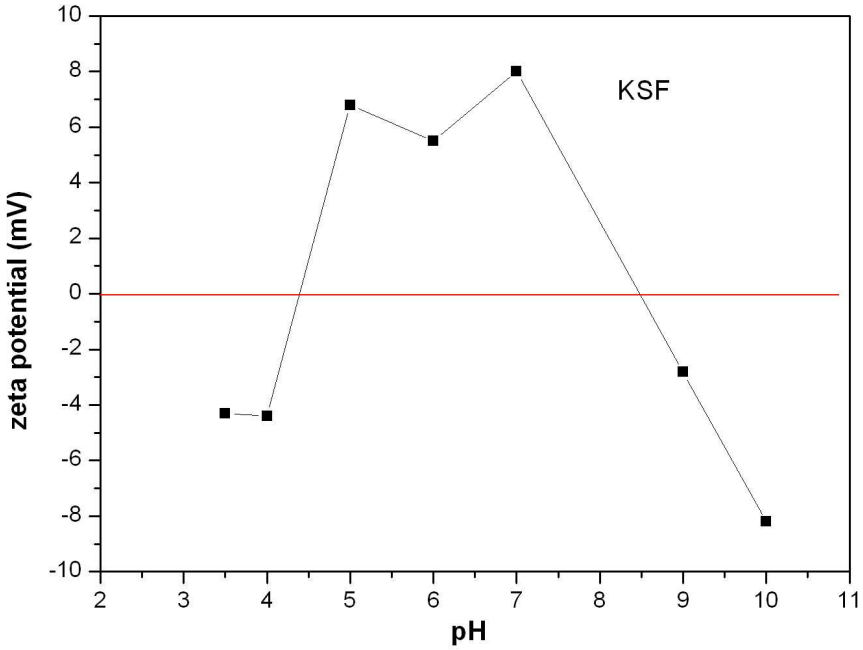

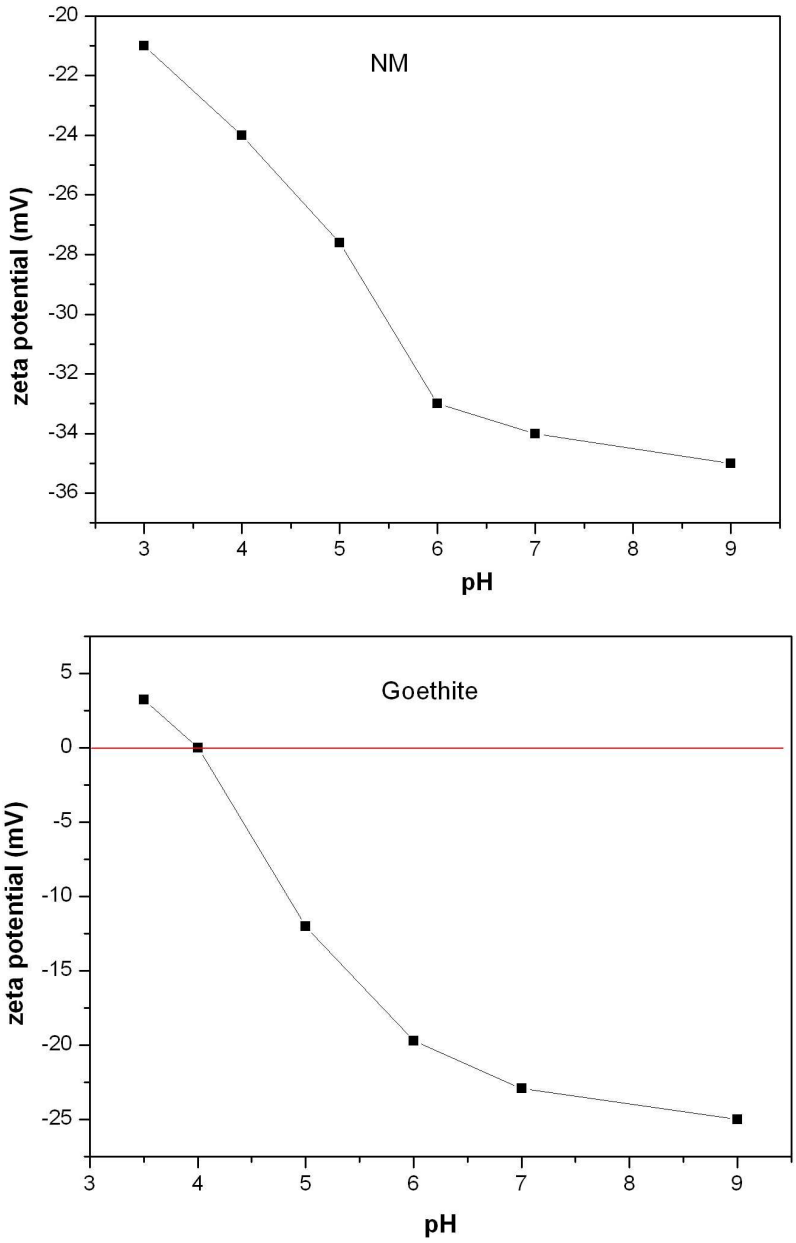

Figure IV-A-13 The isoelectric point (PI) of the minerals

Transmission electron microscopic (TEM) images of the minerals are shown in Figure IV-A-14/15/16. In the case of KSF, small particles ill-defined strongly associated together are observed, this clay does not swell in water. Even after two days of stirring, homogenous dispersion is not obtained and big aggregates are still present in the solution. For the NM, we note the presence of large platelets associated in submicronic aggregates. Concerning the synthetic goethite, the TEM images show the formation of well-defined small needle like particles stacked face to face with sizes in the range of 30 nm to 70 nm.

Note that the acido-basic properties of the surface of the three solids are rather different. Indeed, once in suspension the solid modified the solution pH. Values of 7.7, 9.0 and 3.7 are respectively measured for Goethite, NM and KSF.

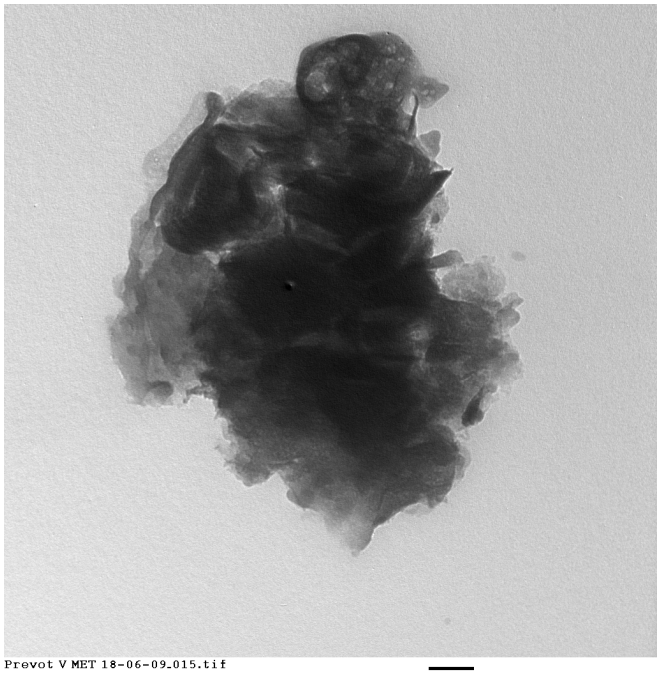

Figure IV-A-14 TEM image of KSF

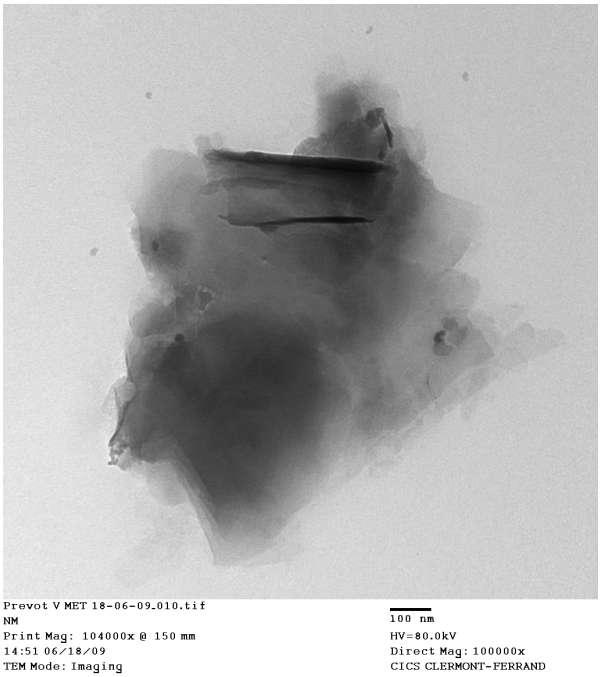

Figure IV-A-15 TEM image of NM

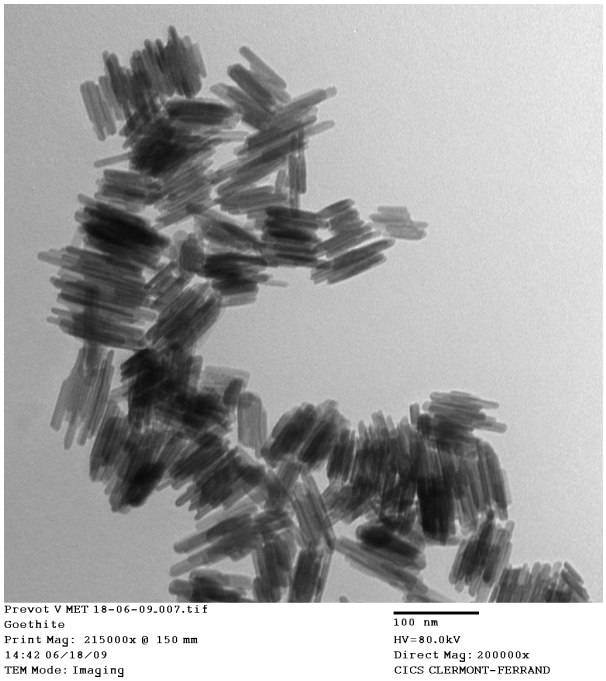

Figure IV-A-16 TEM image of Goethite

IV-B Photodegradation of E2 in the Fe(III)-EDDS complexes solution

In this part, the photochemical impact of Fe(III)-EDDS complex on the quantum yield of $^{\bullet}OH$ formation and on the degradation of 17β-estradiol (E2) was investigated. The reaction rate constants with $^{\bullet}OH$ of E2 and EDDS were also evaluated. The photoproduction of E2 identified in the Fe(III)-EDDS complex solution during the irradiation.

B-1 Quantum yields of $^{\bullet}OH$ formation in Fe(III)-EDDS complex

In this work, the quantum yields of $^{\bullet}OH$ formation from Fe(III)-EDDS complex solution under irradiation was investigated. The main influencing factors, such as pH, the concentrations of Fe(III)-EDDS, irradiation wavelength and O_2 were examined.

The stoichiometric ratio of the Fe(III)-EDDS complex is 1:1, which was established by the molar ratio method (Zhang, 2008). The UV-Vis absorption spectra of Fe(III)-EDDS aqueous solutions is not pH dependent in the domain $3 < pH < 7$. Between 7 and 9, a small decrease of absorbance was observed at wavelengths higher than 230 nm. Absorption started at 400 nm with a shoulder at 239 nm (ε = 6530 M^{-1} cm^{-1}), exhibiting an important overlap with solar emission (Figure IV-B-1). The irradiation experiments were mainly performed at 365 nm. This wavelength is sufficiently energetic to cause the photochemical process of

Fe(III)-EDDS. For TA, no significant absorption was detected above 295 nm. The absorption of TA did not interfere at the irradiation wavelengths used.

The Fe(III)-EDDS complex was stable in the dark and at room temperature for at least 10 days. But under irradiation Fe(III)-EDDS was quickly photodecomposed. The UV-Visible absorption spectra of Fe(III)-EDDS solution at pH 3.0 under monochromatic irradiation at λ = 365 nm is shown in Figure IV-B-2. The Fe(III)-EDDS complex was almost completely decomposed after 10 min of irradiation.

The mixture of TA and Fe(III)-EDDS was thermally stable. There was neither precipitation nor redox reaction in the dark at room temperature. No TAOH formation was observed in the dark in the TA and Fe(III)-EDDS mixture solution. TAOH was detected in the Fe(III)-EDDS and TA solution under irradiation, which proved the formation of $^{\bullet}OH$ by the photochemical reaction of Fe(III)-EDDS.

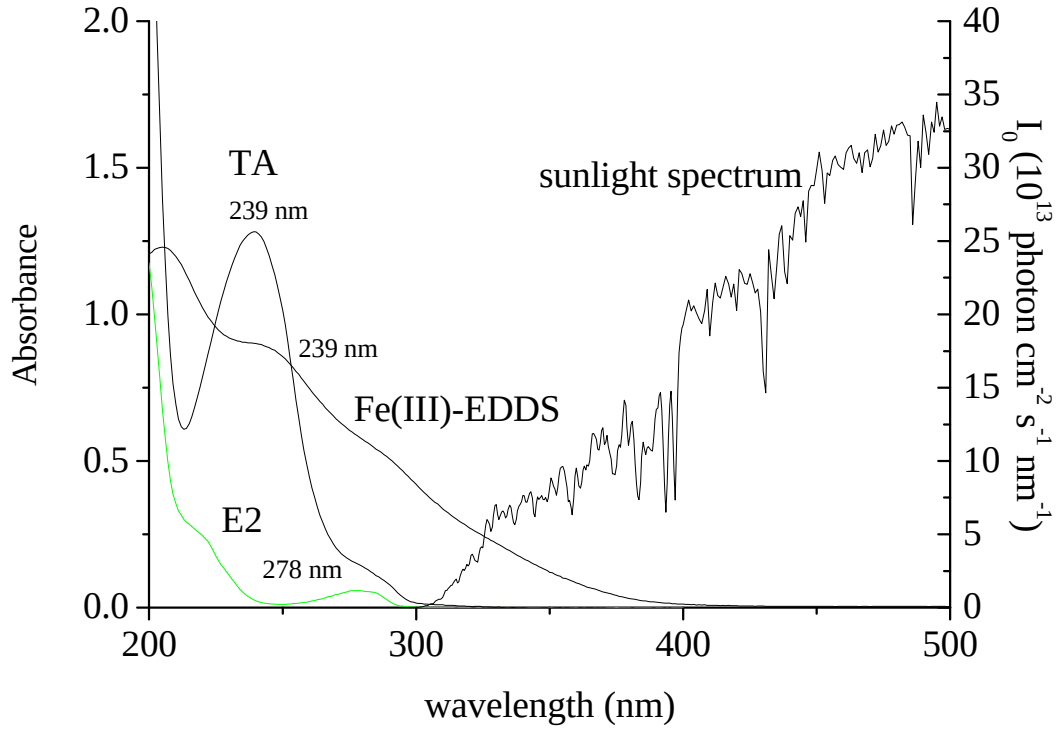

Figure IV-B-1 UV-visible absorption spectrum of E2 (6 µM), Fe(III)-EDDS (100 µM), TA (100 µM) and emission spectrum of sunlight

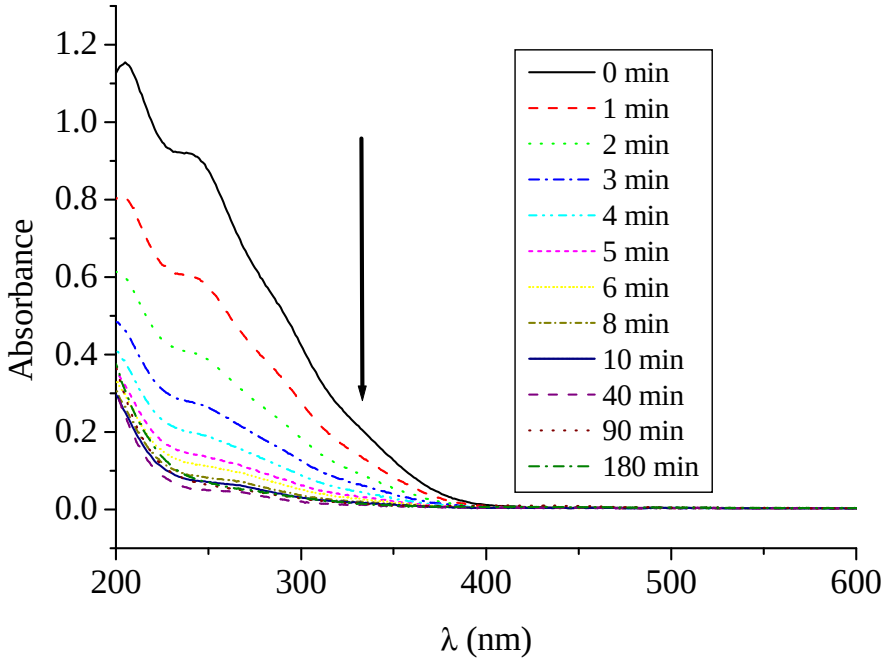

Figure IV-B-2 UV-Visible absorption spectra of Fe(III)-EDDS solution at pH = 3.0 during irradiation ([Fe(III)-EDDS] = 1×10^{-4} M, λ_{irr} = 365 nm)

B-1-1 Effect of Fe(III)-EDDS complex concentration

Quantum yields of $^{\bullet}OH$ (Φ_{OH}) from photolysis of Fe(III)-EDDS complexes were measured with different Fe(III)-EDDS concentrations at pH 6 (λ_{irr} = 365 nm). As shown in Table IV-B-1, Φ_{OH} was independent of the Fe(III)-EDDS concentration. When the concentration of Fe(III)-EDDS complex is high, the flux of absorbed photons is larger, which generates more $^{\bullet}OH$ radicals, so the generation rate of $^{\bullet}OH$ radicals increases. The increase of $^{\bullet}OH$ formation rate is the consequence of the increase of I_a caused by the increase of the optical density $OD_{\lambda irr}$ of the solution, resulting in an invariant quantum yield.

Table IV-B-1 Quantum yields of $^{\bullet}OH$ as a function of Fe(III)-EDDS concentration (pH = 6, λ_{irr} = 365 nm)

[Fe(III)-EDDS] (μM)	25	50	75	100
Φ_{OH}	0.021	0.024	0.026	0.025

B-1-2 Effect of pH

The pH is a very important parameter that affects the species and stability of the Fe(III)-EDDS complex in solution, and consequently may have considerable influence on the photochemistry reaction of Fe(III)-EDDS. In contrast to earlier studies published, which were carried out only at low pHs, we investigated the Fe(III)-EDDS system over the entire environmentally relevant pH range: $3.0 \leq pH \leq 9.0$. As shown in Table IV-B-2, the quantum yield of $^{\bullet}OH$ increased with the increase in pH. This result is unexpected and interesting. In previous studies, the quantum yield of $^{\bullet}OH$ was much higher at acidic pH, and the optimum pH for the formation of $^{\bullet}OH$ was limited between pH 3.0 and 4.0, whatever the Fe(III) aquacomplexes or the Fe(III)-carboxylate complexes (Fe(III)-oxalate, Fe(III)-citrate) solutions (Wu *et al.*, 1999). At higher pHs, the quantum yield decreased and was negligible at pHs close to 7.0. On the contrary, in the presence of Fe(III)-EDDS complexes, the quantum yield of $^{\bullet}OH$ radical formation was higher at higher pHs more relevant to the natural environment. This interesting result could be explain by the formation of H_2O_2 (reactions (3) to (6)) which is mainly governed by the reactions (3) and (5). At higher pH (higher than 4.8, the pKa of the couple $HO_2^{\bullet}/O_2^{\bullet-}$) where $O_2^{\bullet-}$ becomes the dominant reactive oxygen species, the formation of H_2O_2 is an order of magnitude faster than at lower pH. Moreover, the $^{\bullet}OH$ radical formation depends also to the possible formation of Fe(II)-polycarboxylate complex, formed with the starting organic compounds or its oxidation compounds obtained after the first photochemical reaction. In the case of ferrioxalate complex the formation of $^{\bullet}OH$ with H_2O_2 is 3 to 4 orders of magnitude higher than with Fe(II) aquacomplexes (comparison of rate constants of reactions (9) and (10)) (Sedlak and Hoigne, 1993). The speciation of such Fe(II) complexes (not known for EDDS) could explain the difference observed between EDDS and other polycarboxylate complexes for the quantum yield of $^{\bullet}OH$ radical as a function of pH.

$$\text{Fe(III)-L} + h\nu \rightarrow [\text{Fe(III)-L}]^{*} \rightarrow \text{Fe(II)} + L^{\bullet} \qquad (1)$$

$$L^{\bullet} + O_2 \rightarrow O_2^{\bullet-} + L' \qquad (2)$$

$$\text{Fe(II)} + O_2^{\bullet-} + 2\,H_2O \rightarrow \text{Fe(III)} + H_2O_2 + 2\,OH^- \quad k = 1.0 \times 10^7\ M^{-1}s^{-1} \qquad (3)$$

$$\text{Fe(II)} + HO_2^{\bullet} + H_2O \rightarrow \text{Fe(III)} + H_2O_2 + OH^- \quad k = 1.2 \times 10^6\ M^{-1}s^{-1} \qquad (4)$$

$$HO_2^{\bullet} + O_2^{\bullet-} + H_2O \rightarrow H_2O_2 + O_2 + OH^- \quad k = 9.7 \times 10^7\ M^{-1}s^{-1} \qquad (5)$$

$$HO_2^{\bullet} + HO_2^{\bullet} \rightarrow H_2O_2 + O_2 \quad k = 8.3 \times 10^5\ M^{-1}s^{-1} \qquad (6)$$

$$Fe(III) + HO_2^{\bullet} \rightarrow Fe(II) + O_2 + H^+ \quad k < 1 \times 10^3\ M^{-1}s^{-1} \quad (7)$$

$$Fe(III) + O_2^{\bullet-} \rightarrow Fe(II) + O_2 \quad k = 5 \times 10^7\ M^{-1}s^{-1} \quad (8)$$

$$H_2O_2 + Fe(II) \rightarrow Fe(III) + {}^{\bullet}OH + OH^- \quad k = 63\ M^{-1}s^{-1} \quad (9)$$

$$Fe^{II}(C_2O_4) + H_2O_2 \rightarrow Fe^{III}(C_2O_4)^+ + {}^{\bullet}OH + OH^- \quad k = 3.1 \times 10^4\ M^{-1}s^{-1} \quad (10)$$

Table IV-B-2 Quantum yields of $^{\bullet}$OH as a function of pH ([Fe(III)-EDDS] = 10^{-4} M, λ_{irr} = 365 nm)

pH	3.0	4.0	5.1	6.0	7.0	8.0	9.0
Φ_{OH}	0.0025	0.0091	0.019	0.025	0.034	0.051	0.069

B-1-3 Effect of wavelength

The influence of irradiation wavelength on the quantum yields of $^{\bullet}$OH formation (Φ_{OH}) from Fe(III)-EDDS complex photolysis was examined at 296, 313 and 365 nm ([Fe(III)-EDDS] = 1×10^{-4} M, pH = 6.0). As shown in Table IV-B-3, the quantum yields of $^{\bullet}$OH obviously increased with the decrease of wavelength. This result was attributed to the kinetic energy required for the ejection of $^{\bullet}$OH radicals from the solvent cage (Benkelberg and Warneck, 1995). Decrease of the wavelength increased the level of excitation, thus raising the quantum yield of $^{\bullet}$OH.

Table IV-B-3 Quantum yields of $^{\bullet}$OH formation as a function of wavelength ([Fe(III)-EDDS] = 10^{-4} M, pH = 6.0)

λ (nm)	365	313	296
Φ_{OH}	0.025	0.037	0.040

B-1-4 Effect of oxygen

Oxygen is an important parameter in the photochemical processes. Experiments were carried out to study the oxygen effects on the quantum yield of $^{\bullet}$OH formation ([Fe(III)-EDDS] = 1×10^{-4} M, pH = 6.0, λ_{irr} = 365 nm). As shown in table IV-B-4, the quantum yields of $^{\bullet}$OH in deaerated solution is very low, almost twenty times lower than that in aerated solutions. Therefore oxygen is involved in the photocatalytic process of Fe(III)-EDDS to form $^{\bullet}$OH. According to reaction (2), oxygen trapped the electron on the carbon centered radical formed after the Fe(III)-(amino)polycarboxylate complex photoredox process, then the $O_2^{\bullet-}$ formed rapidly reacted to finally result in the formation of hydroxyl radical (reactions (3) to (9), (10)).

Table IV-B-4 Effect of oxygen on the quantum yields of $^{\bullet}OH$ formation ([Fe(III)-EDDS] = 1×10^{-4} M, pH = 6.0, λ_{irr} = 365 nm)

	Aerated solution	Deaerated solution
Φ_{OH}	0.025	0.0011

B-1-5 Comparison with the aquacomplex $Fe(OH)^{2+}$

The quantum yield of $^{\bullet}OH$ formation was also measured by photolysis of $Fe(OH)^{2+}$ in our experimental conditions ([Fe(III)] = 1 mM, λ_{irr} = 365 nm). Among iron aquacomplexes, $Fe(OH)^{2+}$ is the most active species for photochemical production of hydroxyl radicals. Under our experimental conditions, we obtained the value of 0.044, which is approximately twenty times higher than the quantum yield of $^{\bullet}OH$ formation during the photolysis of Fe(III)-EDDS at pH 3 (Table IV-B-2). The quantum yields of $^{\bullet}OH$ formation for Fe(III)-aquacomplex photochemical reactions have been reported in several studies. It was reported that the quantum yield for photolysis of $Fe(OH)^{2+}$ was 0.01-0.07 at the wavelength of 360-370 nm (Wu *et al*., 1999, Sedlak *et al*., 1993); for Fe^{3+}, the quantum yield was 0.065 at 254 nm (Wu *et al*., 1999) and approximately 0.05 at wavelengths below 300 nm (Wu *et al*., 1999); for $Fe_2(OH)_2^{4+}$, the quantum yield was 0.007 at 350 nm (Benkelberg and Warneck, 1995). The quantum yield of $^{\bullet}OH$ formation by photolysis of $Fe(OH)^{2+}$ obtained in this study is in good agreement with the literature values at the wavelength of 365 nm obtained in the previous studies. When comparing the value of 0.044 with the quantum yield of $^{\bullet}OH$ formation by Fe(III)-EDDS at pHs higher than 5, the values are of the same order of magnitude. In addition, the quantum efficiency for the photolysis of Fe(III)-EDDS is higher at higher pHs, so the effect of Fe(III)-EDDS is more relevant to the natural environment. Moreover, it is important to note that the concentration of soluble iron aquacomplexes is negligible at pHs higher than 5.0 and consequently the quantum yield of $^{\bullet}OH$ radical formation is negligible too.

B-2 The rate constants for the reaction of $^{\bullet}OH$ with E2 and EDDS

The reaction rate constants with $^{\bullet}OH$ of E2 and EDDS, which could allow an assessment of their relativity, are not available. The rate constants were measured by competition kinetics with 2-propanol, a compound of known reaction rate constant with the hydroxyl radical.

Nitrate photolysis was used as source of $^{\bullet}OH$, which would induce the following reactions in a system containing also 2-propanol and E2 or EDDS:

$$NO_3^- + H^+ \xrightarrow{h\nu} {}^{\bullet}OH + {}^{\bullet}NO_2 \quad [R_{\bullet OH}] \quad (\lambda = 313 \text{ nm}) \qquad (1)$$

$$CH_3\text{-}CHOH\text{-}CH_3 + {}^{\bullet}OH \rightarrow CH_3\text{-}CHO^{\bullet}\text{-}CH_3 + H_2O \qquad [k_2 = 1.9 \times 10^9\ M^{-1}s^{-1}] \qquad (2)$$

$$EDDS + {}^{\bullet}OH \rightarrow \text{Photoproducts}\ [k_{EDDS,\bullet OH}] \qquad (3)$$

$$E2 + {}^{\bullet}OH \rightarrow \text{photoproducts}\ [k_{E2,\bullet OH}] \qquad (4)$$

The application of the steady-state approximation to [$^{\bullet}OH$] yields to the following equation to describe the initial degradation rate of E2 or EDDS, as a function of its initial concentration and of that of 2-propanol, [2Pr]:

$$-\frac{d[E_2/EDDS]}{dt} = \frac{R_{\bullet OH} k_{E2/EDDS,\bullet OH}[E2/EDDS]}{k_{E2/EDDS,\bullet OH}[E2/EDDS] + k_2[2Pr]} \qquad (5)$$

Figure IV-B-3 and Figure IV-B-4 report the initial degradation rate of E2 and EDDS upon UV-vis irradiation of 0.1 M NO_3^- at pH 3, as a function of the initial concentration of 2-propanol. An almost complete inhibition of the degradation of E2 and EDDS was observed at the highest adopted concentration of 2-propanol, suggesting that the transformation of E2 or EDDS is mainly due to the reaction with $^{\bullet}OH$. This finding is consistent with the results of control runs, which showed that the direct photolysis of E2 or EDDS was negligible compared to the degradation rate observed in the presence of nitrate. The possible reaction between E2 or EDDS and $^{\bullet}NO_2$, which in not affected by 2-propanol, is also negligible compared to $^{\bullet}OH$.

The fitting of the experimental data of Figure IV-B-3 and Figure IV-B-4 with equation (5) yield $k_{E2,\bullet OH} = 6.7\times10^9\ M^{-1}s^{-1}$ and $k_{EDDS,\bullet OH} = 2.0\times10^8\ M^{-1}s^{-1}$. The value of $R_{\bullet OH}$ derived from the fit was 8.6×10^{-9} and 8.4×10^{-9} M s^{-1} respectively, which is almost the same in the two cases as expected under the adopted experimental set-up.

The reaction rate constant of $k_{E2,\bullet OH}$ is about ten times higher than the $k_{EDDS,\bullet OH}$, but in our experiments, the concentration of EDDS used is normally more than ten times higher than the concentration of E2, so the competition between EDDS and E2 reacting with $^{\bullet}OH$ should not be ignored.

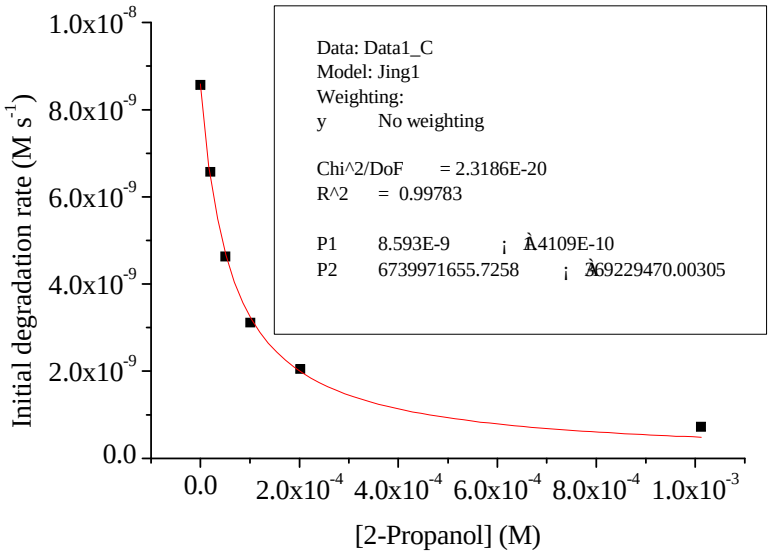

Figure IV-B-3 Initial degradation rate of 17.2 µM E2 upon monochromatic irradiation (λ = 313 nm) of 0.1 M NO_3^- ($NaNO_3$), at pH 3, as a function of the initial concentration of 2-propanol. The experimental data were fitted with equation (5) to get $k_{E2,\bullet OH} = 6.7\times10^9$ $M^{-1}s^{-1}$, $R_{\bullet OH} = 8.6\times10^{-9}$ M s^{-1}.

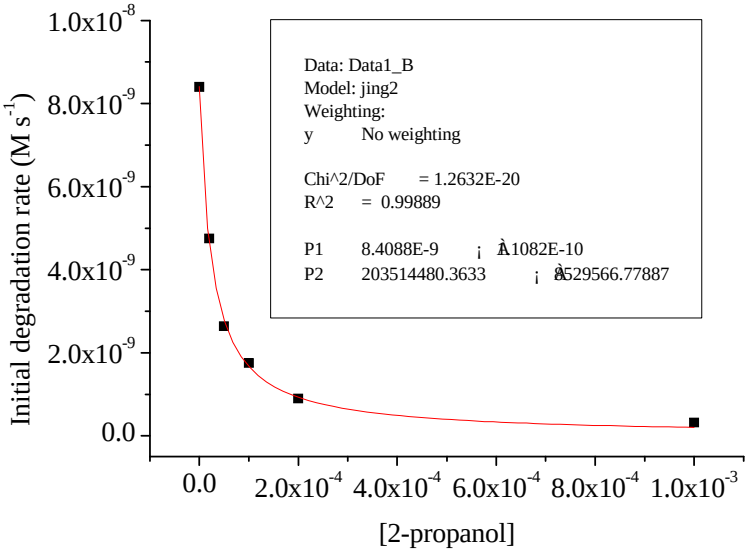

Figure IV-B-4 Initial degradation rate of 232 µM EDDS upon monochromatic irradiation (λ = 313 nm) of 0.1 M NO_3^- ($NaNO_3$), at pH 3, as a function of the initial concentration of 2-propanol. The experimental data were fitted with equation (5) to get $k_{EDDS,\bullet OH} = 2.0\times10^8$ $M^{-1}s^{-1}$, $R_{\bullet OH} = 8.4\times10^{-9}$ M s^{-1}

B-3 Photodegradation of E2 in the Fe(III)-EDDS complex solutions

We used E2 as a model pollutant to investigate the photocatalytic activity of the Fe(III)-EDDS complex and the main influencing factors, such as pH, the concentrations of Fe(III)-EDDS, Fe(III) and O_2 were examined.

The UV-Vis absorption spectrum of E2 in aqueous solution displayed one band at 278 nm (ε = 1900 M^{-1} cm^{-1}) (Figure IV-A-1). No absorption was observed at λ > 300 nm. There was a pKa at 10.4 (Shareef *et al*., 2006) and the solubility in water is evaluated at 20 μM. Under our experimental conditions and in the dark, no degradation of E2 was observed in the absence or in the presence of Fe(III)-EDDS. Similarly, there was no photodegradation of E2 under irradiation without Fe(III)-EDDS.

B-3-1 Effect of Fe(III) -EDDS concentration

Figure IV-B-5 shows the kinetics of E2 disappearance at different initial concentrations of Fe(III)-EDDS 0, 5×10^{-5}, 1×10^{-4}, 2×10^{-4} and 1×10^{-3} M at pH 3.0. The rate of E2 degradation increased with increasing concentrations of Fe(III)-EDDS in the range of 0 - 2×10^{-4} M, but much higher concentration of Fe(III)-EDDS such as 1×10^{-3} M inhibited E2 degradation (Table IV-B-5). These results gave clear evidence that photolysis of Fe(III)-EDDS could induce the degradation of E2. $^{\bullet}$OH is formed during photolysis of Fe(III)-EDDS. $^{\bullet}$OH could react with both E2 and Fe(III)-EDDS. When the concentration of Fe(III)-EDDS is high, the role of Fe(III)-EDDS as a competitor for $^{\bullet}$OH reaction is much more important, and as a consequence inhibits E2 degradation. Therefore, the appropriate concentration of Fe(III)-EDDS should be chosen for E2 degradation. Fe(II) formation was also monitored during the irradiation time (Figure IV-B-6). The generation of Fe(II) by Fe(III)-EDDS complex photochemical reactions was very fast. For Fe(III)-EDDS 5×10^{-5} and 1×10^{-4} M, almost all of the Fe(III) was transformed to Fe(II) in the first hour, and the concentration of Fe(II) remained constant up to 8 hours. But for Fe(III)-EDDS 2×10^{-4} and 1×10^{-3} M, it was observed that the concentration of Fe(II) decreased with irradiation after quick initial generation. This phenomenon can be due to the increase of pH during the irradiation time. A very fast increase in the pH of the solution was detected when irradiation had just started and then remained constant. The higher concentration of Fe(III)-EDDS resulted in the greater increase in the solution pH during irradiation, for example, initial pH 3 to 4 for [Fe(III)-EDDS] = 10^{-4} M and to 6.4 for [Fe(III)-EDDS] = 10^{-3} M after 3 h of irradiation

(Figure IV-B-7).

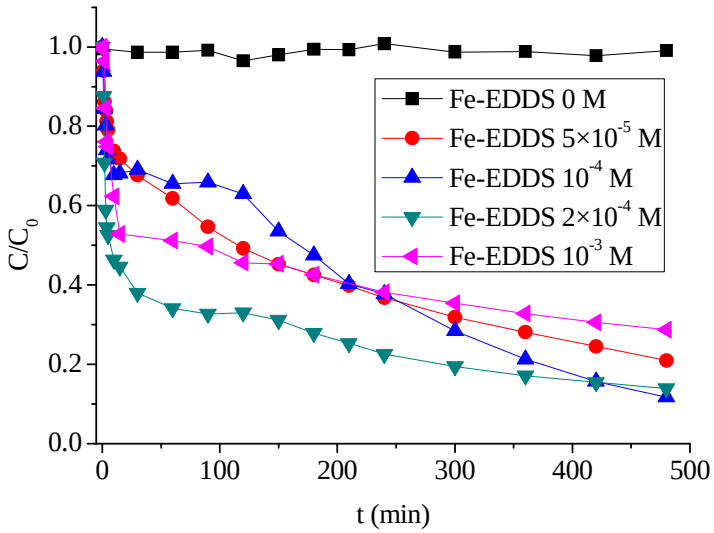

Figure IV-B-5 Effect of Fe(III)-EDDS concentration on the degradation of E2 ([E2] = 5 µM, pH = 3.0).

Table IV-B-5 The initial rate of E2 degradation at different Fe(III)-EDDS concentration

Concentration (Fe(III)-EDDS)	5 x 10^{-5} M	10^{-4} M	2 x 10^{-4} M	10^{-3} M
Initial rate (µmol L^{-1} min^{-1})	0.25	0.32	0.64	0.34

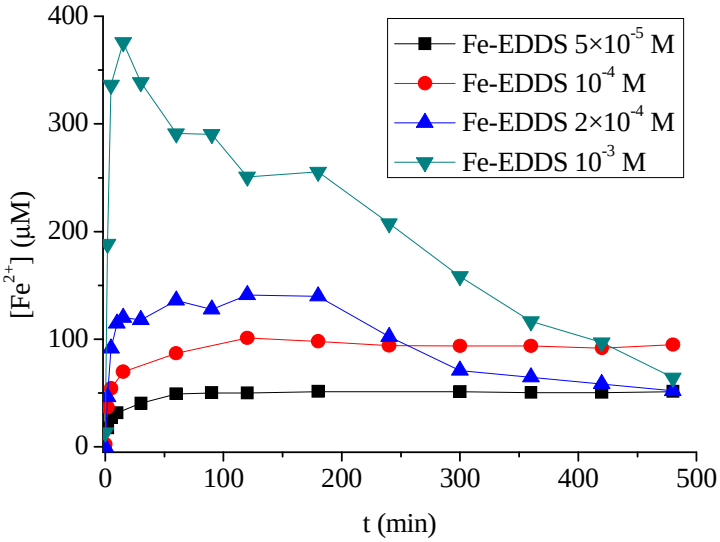

Figure IV-B-6 Photogeneration of Fe (II) as function of Fe(III)-EDDS concentration ([E2] = 5 µM, pH = 3.0).

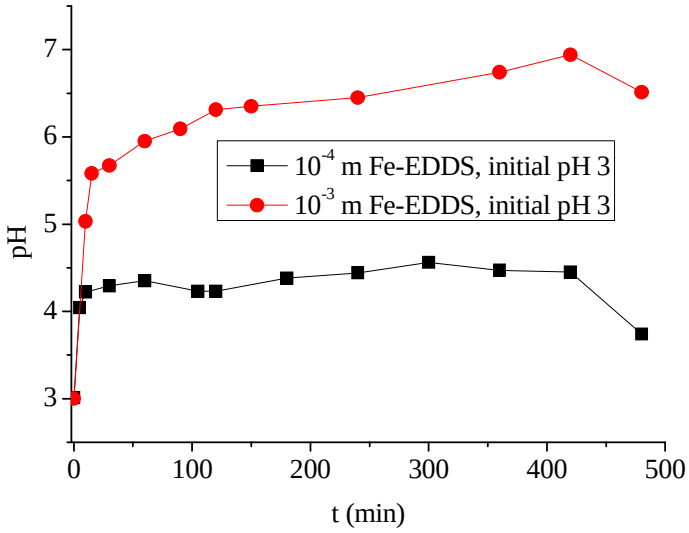

Figure IV-B-7 Change of the pH during the irradiation

B-3-2 Effect of pH

Figure IV-B-8 shows the kinetics of E2 degradation at different initial pHs with the same concentration of Fe(III)-EDDS (1×10^{-4} M) as a function of irradiation time. For pH 4.0, 5.2, 6.1 and 8.0, after very fast initial photodegradation of E2 in the first few minutes, the degradation of E2 then slowed down and stopped at about 90 min of irradiation, reaching a plateau value without further degradation. At an initial pH of 3.1, the degradation of E2 showed similar behavior during the first 90 min, but after the plateau, photodegradation of E2 started again and continued for the remaining irradiation time. The initial quick photodegradation of E2 was due to the photoredox process of Fe(III)-EDDS which induced the formation of $^{\bullet}$OH and also the decomposition of EDDS. With the decomposition of EDDS, the rate of photodegradation of E2 slowed down and finally stopped. After the first period of time and complete decomposition of Fe(III)-EDDS, the photodegradation of E2 depends on the species of Fe(III)/Fe(II) aquacomplexes in the solution. It is well known that the species $Fe(OH)^{2+}$, mainly present between pH 3.0 to 4.0, is the most photoactive iron aquacomplex. Except under the condition of initial pH = 3.1 where the pH of the solution increased to pH = 4.0, it was observed with other initial pHs that during irradiation the solution pH increased or decreased to neutral pH in the first few minutes (Figure IV-B-9). So we observed the continuous degradation of E2 after the plateau only for the initial pH = 3.1. However, before 90 min of irradiation, the efficiency of photodegradation of E2 was pH 8.0

> pH 6.1 > pH 5.2 > pH 4.0 > pH 3.1, which is in agreement with the quantum yield of $^{\bullet}OH$ formation as a function of pH.

The concentration of Fe(II) and Fe(tot) during irradiation was also detected (Figure IV-B-10). At pH 3.1 and 4.0, the major part of initial iron (Fe(III)) present in the solution was reduced to Fe(II) within a short period of irradiation. At pH = 5.2 and higher pHs, almost no Fe(II) was detected in the solution. This result could be explain by the fact that at higher pH Fe(II) aquacomplexes is easily oxidized by dissolved oxygen and by the hypothesis of the formation of Fe(II)-polycarboxylate complexes and a fast reaction with H_2O_2. Moreover, at these pHs the amount of Fe(tot) dissolved in the aqueous solution decreased very fast due to the degradation of EDDS which can maintain iron ions in solution. No new organic species formed from the degradation of EDDS are able to complex iron and avoid its precipitation. In the previous studies of iron carboxylate complex photochemistry, the formation of Fe(II) is positively related to the degradation of organic pollutants (Ou *et al.*, 2008). But no correlation was apparently observed between Fe(II) formation and E2 disappearance in our work. So it is supposed that the dominant factor that influences the photodegradation of E2 is not the amount of Fe(II) formation.

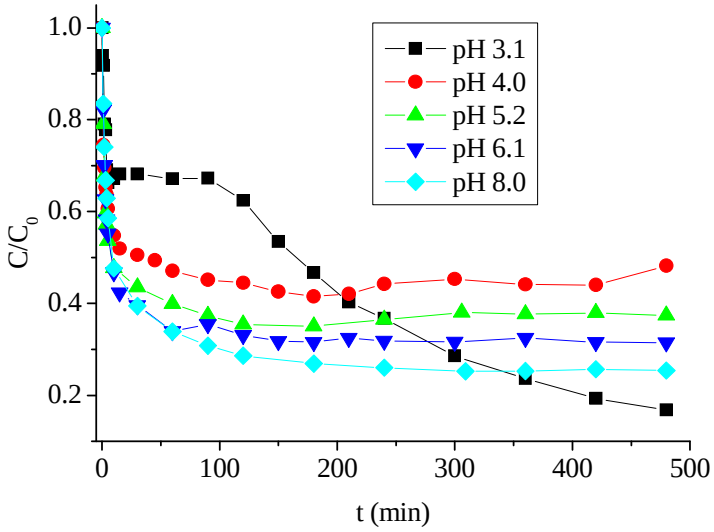

Figure IV-B-8 Effect of pH on the degradation of E2 ([Fe(III)-EDDS] = 1×10^{-4} M, [E2] = 5 µM).

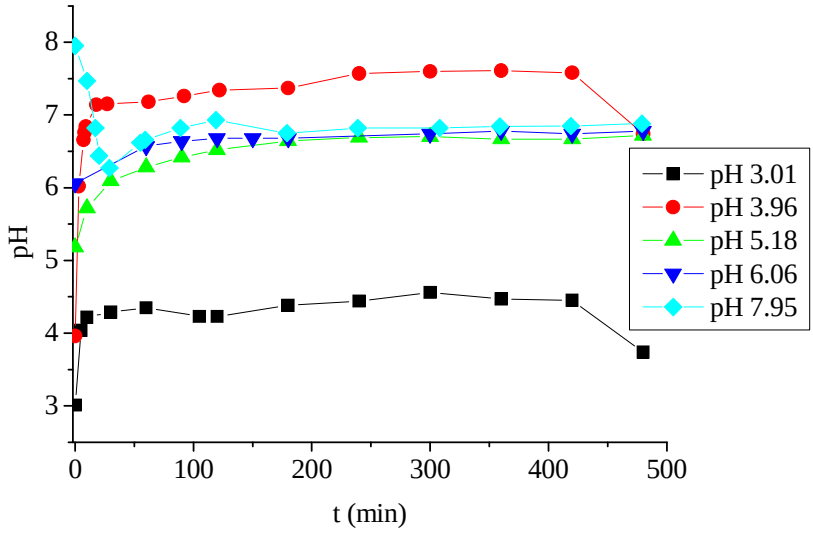

Figure IV-B-9 The change of pH during the irradiation at different pH

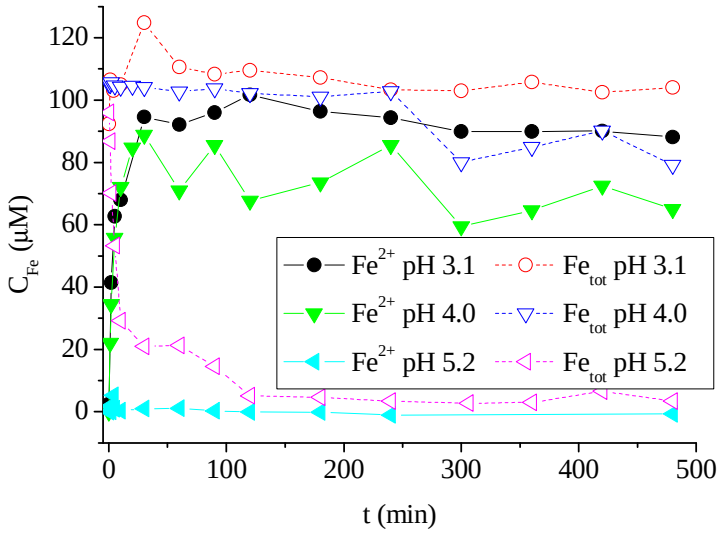

Figure IV-B-10 Concentration of Fe(II) and Fe(tot) during the irradiation (Fe(III)-EDDS 10^{-4} M, E2 5 μM)

B-3-3 Effect of oxygen

As shown in Figure IV-B-11, O_2 plays a crucial role in the degradation of E2. With solution purging with N_2, there was almost no degradation of E2 during irradiation. The photodegradation rate of E2 was much higher with solution purging with O_2 than in air-saturated solution. This result is in agreement with the effect of O_2 on the quantum yield of $^{\bullet}OH$. On the contrary, in the conditions with air, oxygen saturated, and without oxygen,

most Fe(III) were quickly transformed to Fe(II) and Fe (tot) remaining constant during irradiation (Figure IV-B-12). Therefore, O_2 has no effect on the photoredox process of iron complexes. Combined with section IV-B-3-2, this proves that the photoredox of iron complexes as the starting reaction (Fe(III)-L + hν → [Fe(III)-L] * → Fe(II) + L$^{\bullet}$) is fast and total, but not the key reaction controlling the amount of $^{\bullet}$OH formation.

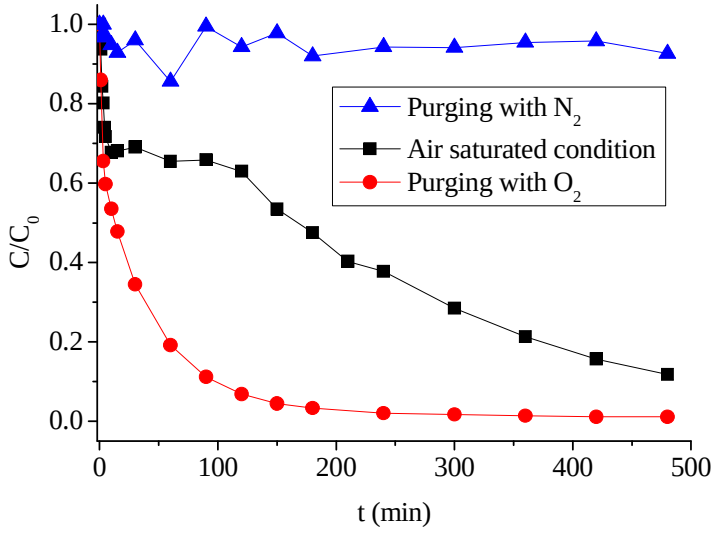

Figure IV-B-11 Effect of oxygen on the degradation of E2 ([E2] = 5 µM, [Fe(III)-EDDS] = 1×10^{-4} M, pH = 3.0).

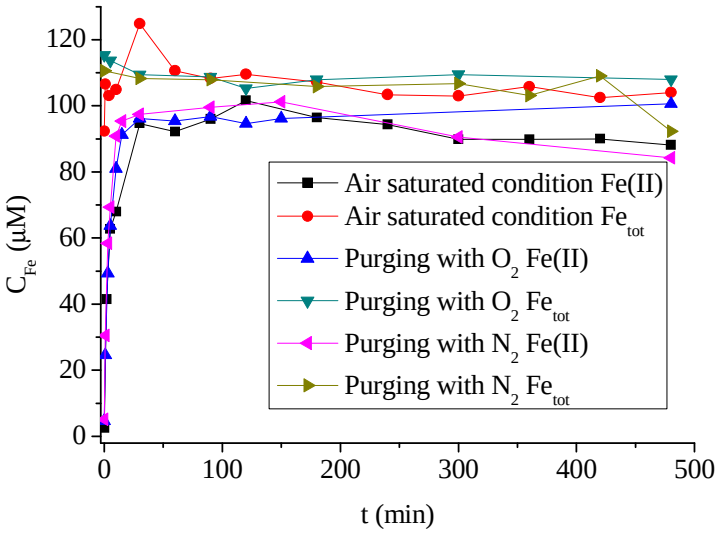

Figure IV-B-12 Concentration of Fe(II) and Fe(tot) during the irradiation ([Fe(III)-EDDS] = 10^{-4} M, [E2] = 5 µM)

B-3-4 Effect of iron concentration

According to the results for the pH and oxygen effect, the ratio between Fe(III) and EDDS concentrations seems to be very important for understanding the photochemical reaction of Fe(III)-EDDS. So the photodegradation of E2 with different concentrations of Fe(III) and the same concentration of EDDS was investigated. As shown in Figure IV-B-13, there was no degradation of E2 without Fe(III) in the irradiation solution. The initial degradation rate was increased with a higher concentration of Fe(III), but the final photodegradation efficiency after 8 h of the irradiation had the opposite trend. With the higher concentration of Fe(III) in the solution, a higher concentration of Fe(III)-EDDS complex was formed, so faster photodegradation of E2 was observed at the beginning of irradiation. But along with the quick photodegradation of E2, EDDS was also quickly decomposed. After complete photodegradation of EDDS, Fe(III)-EDDS was no longer present in the solution. Thus, when the concentration of Fe(III) was lower, although the starting efficiency of Fe(III)-EDDS was lower due to the low concentration of Fe(III)-EDDS, the reaction of Fe(III)-EDDS could be present a longer time. So even the much lower concentration of Fe(III) in the solution could achieve better photodegradation efficiency at the end.

After the first photochemical reaction (Fe(III)-L + hν → [Fe(III)-L] * → Fe(II) + L$^{\bullet}$), Fe(III) is reduced into Fe(II) and EDDS is oxidized. But if some EDDS is still present in solution, Fe(II) is easily reoxidized into Fe(III) through the formation of Fe(III)-EDDS complex. Therefore, the formation of $^{\bullet}$OH radicals and as a consequence the degradation of E2 photoinduced by Fe(III)-EDDS complex can continue (Scheme IV-B-1).

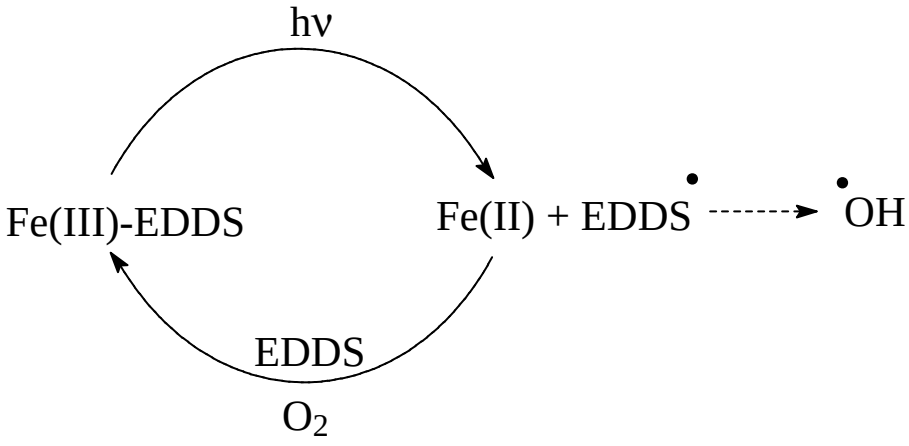

Scheme IV-B-1 The cycle of photochemical process of Fe(III)-EDDS in the presence of an excess of EDDS

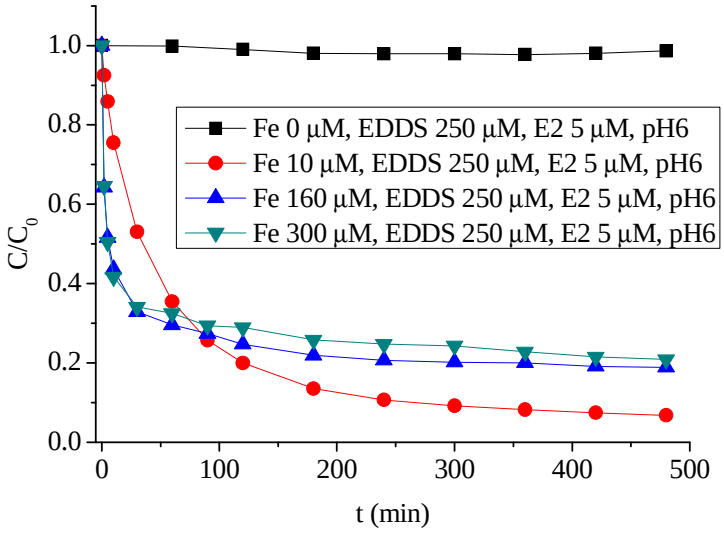

Figure IV-B-13 Effect of iron concentration on the degradation of E2 ([E2] = 5 µM, pH = 6.0)

B-4 Photoproducts

In the Fe(III)-EDDS system and under irradiation, E2 was attacked by the active radicals, especially •OH radicals. LC-MS was used to identify the intermediate photoproducts. After 3h of irradiation, the total ions chromatogram of reaction solution of E2 and Fe(III)-EDDS is presented in Figure IV-B-14. Several photoproducts are formed. The mass spectra of E2 and its photoproducts (A, B, C, D, E, F, G) are shown in Figure IV-B-15. Peak A present mass spectra with a molecular ion at 303 m/z, which is identified to be 10-hydroperoxy-17-hydroxy-13-methyl-7,8,11,12,13,15,16,17-octahydro-6*H*-cyclopenta[α] phenanthren-3(9*H*,10*H*,14*H*)-one. Peak B, C, D, E show identical mass spectra with a molecular ion at 285 (100%), 287 (100%), i.e. + 16 uma with respect to E2. This can correspond to several possibilities: formation of an *ortho* quinone derivative or formation of a hydroxylation product of the aromatic ring of estrone, or formation of hydroxyquinone derivative. B, C, D, E are indentified to be estra-1,3,5(10)-triene-3,6,17-triol-(6α,17*β*)-(ETT) (ETT), 3,17-dihydroxy-13-methyl-7,8,9,11,12,13,14,15,16,17-decahydrocyclopenta[α]phe-nanthren-6-one (ETO), 10ε-17β-dihydroxy-1,4-estradien-3-one (DEO), 2-hydroxyestradiol (2-OH-E2). Peaks F and G show identical mass spectra with a molecular ion at 269 and 267 m/z, which was estra-1,3,5-(10),9(11)-tetraene-3,17-diol-(17β)-(ETD-9) (ETD-9) and estrone (E1) respectively. According to mass information, an overall scheme of E2 degradation is proposed in Figure IV-B-16.

The main pathway of E2 involved ·OH radicals. There are two possible sites for the attack of ·OH radicals: the aliphatic rings and the aromatic ring in the E2 structure. When ·OH radicals attack the aliphatic rings, a number of intermediates (alcohols, ketones, and olefins) maybe formed during the photocatalytic degradation of E2, such as ETT, ETO, and ETD-9. These single aromatic intermediates are presumably further oxidized through ring opening reactions into aliphatic compounds containing acids and acetaldehyde. The attack of ·OH radicals on the aromatic ring led to the formation of dihydroxy photoproducts and quinone-like products, such as 2-HO-E2, and DEO. These products subsequently underwent ·OH and HO_2· attack, leading to complete mineralization.

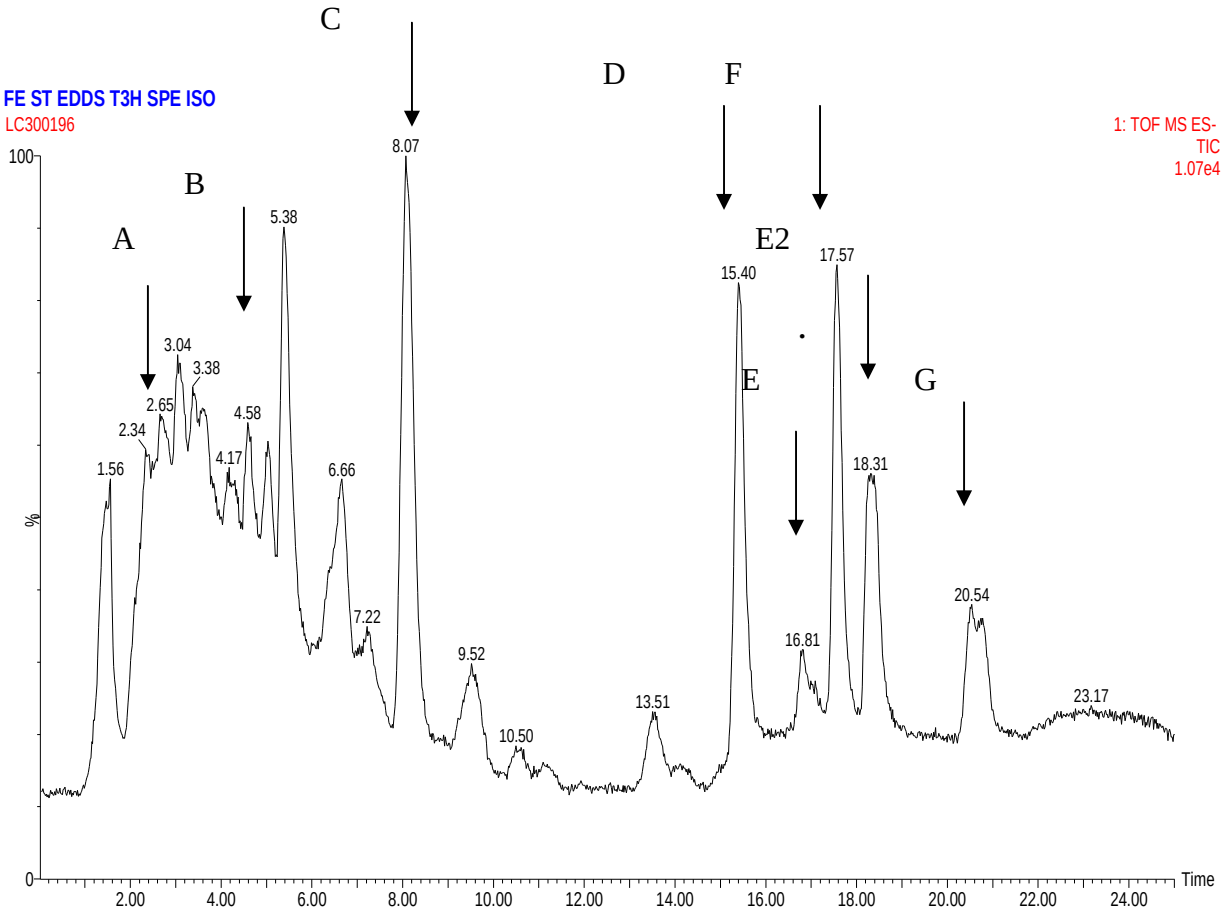

Figure IV-B-14 Total ions chromatogram of reaction solution of E2 and Fe(III)-EDDS after 3h of irradiation

FE ST EDDS T3H SPE ISO

LC300196 127 (2.356)

1: TOF MS ES-
73

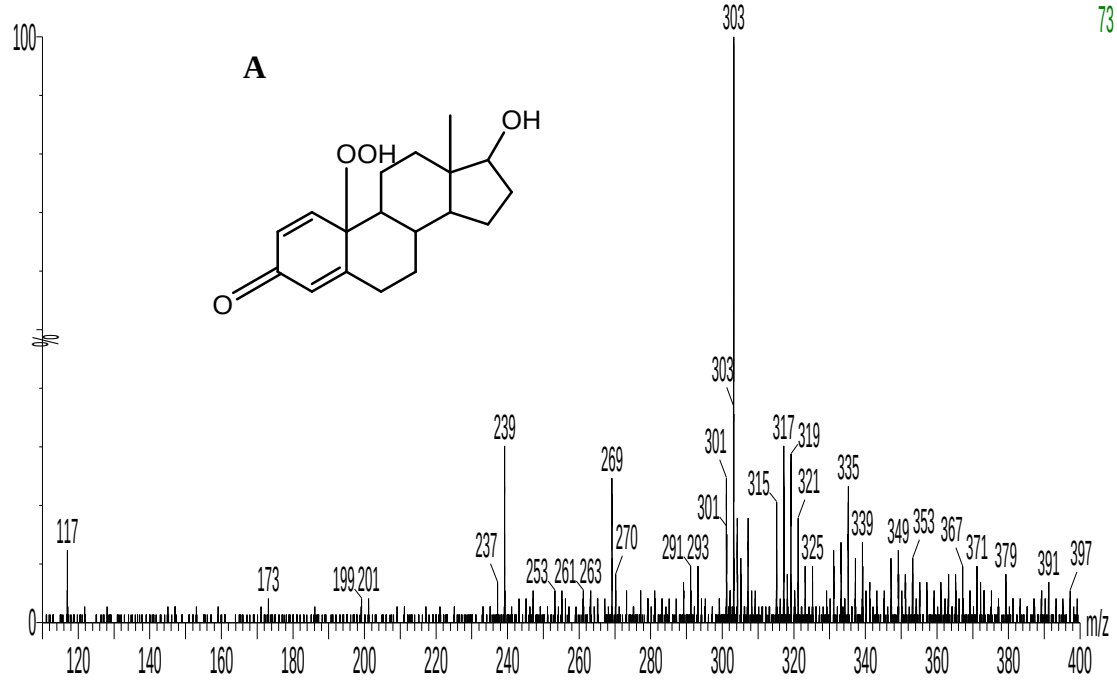

FE ST EDDS T3H SPE ISO

LC300196 248 (4.601)

1: TOF MS ES-
171

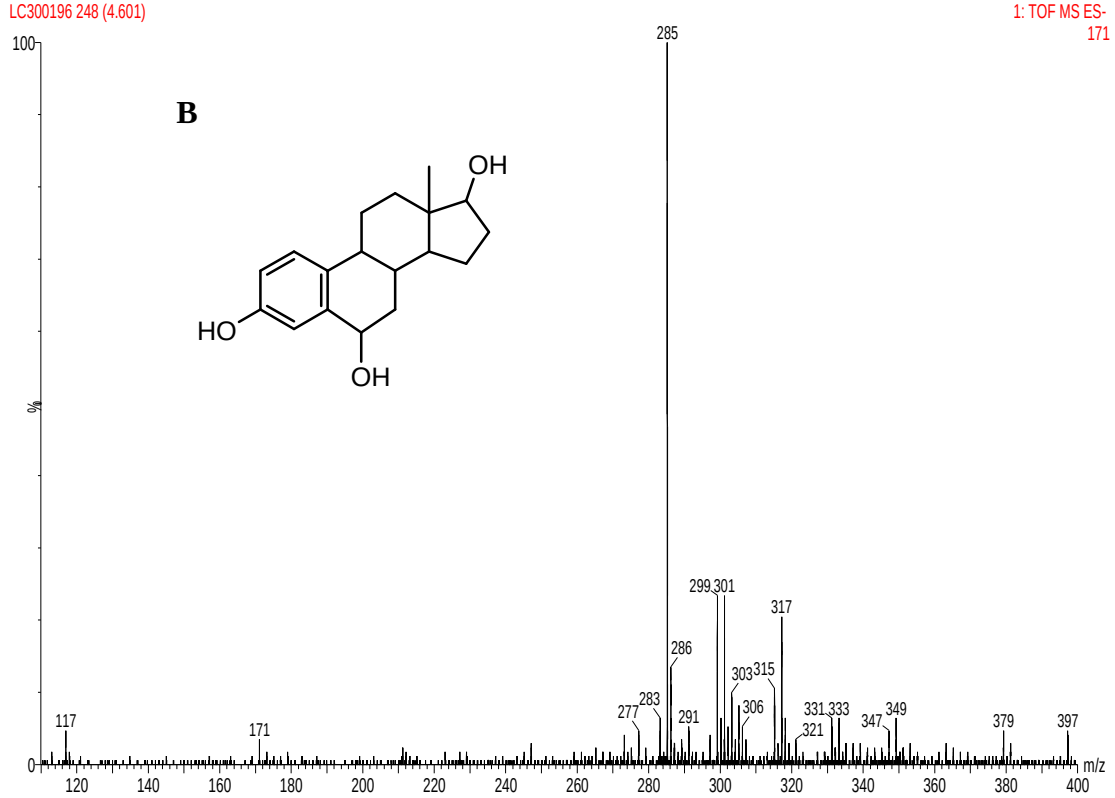

FE ST EDDS T3H SPE ISO

LC300196 436 (8.088)

1: TOF MS ES-
833

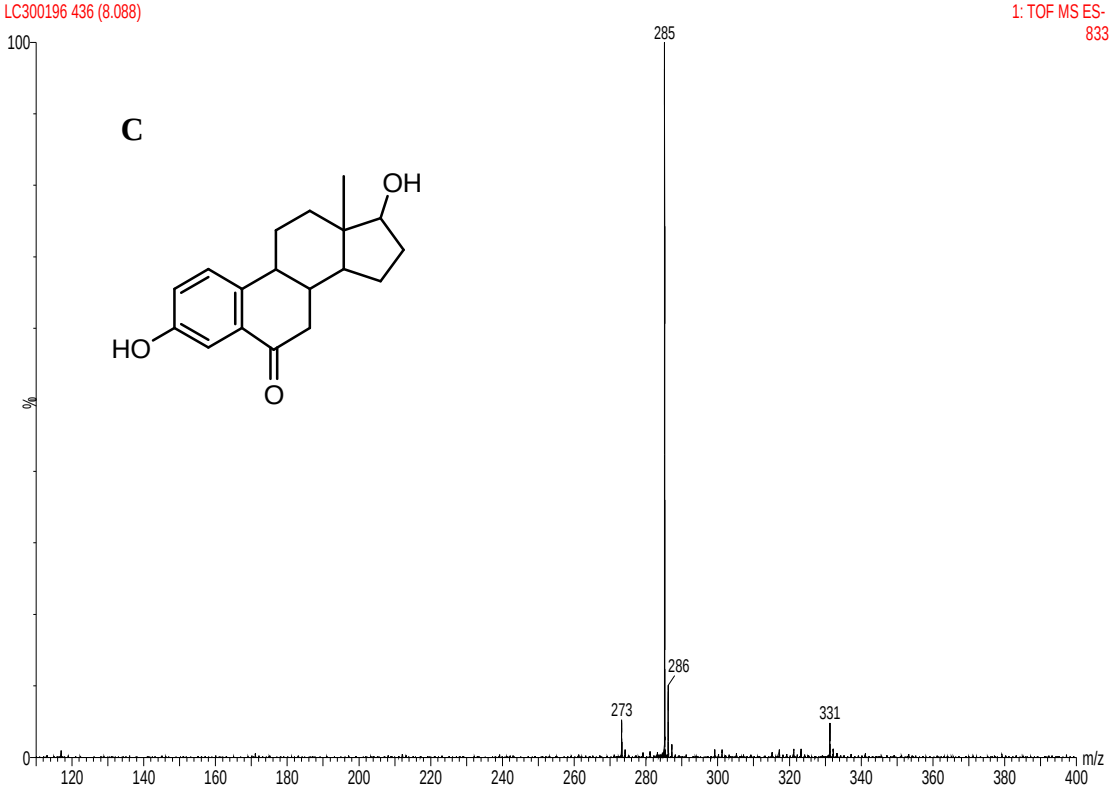

FE ST EDDS T3H SPE ISO

LC300196 830 (15.398)

1: TOF MS ES-
713

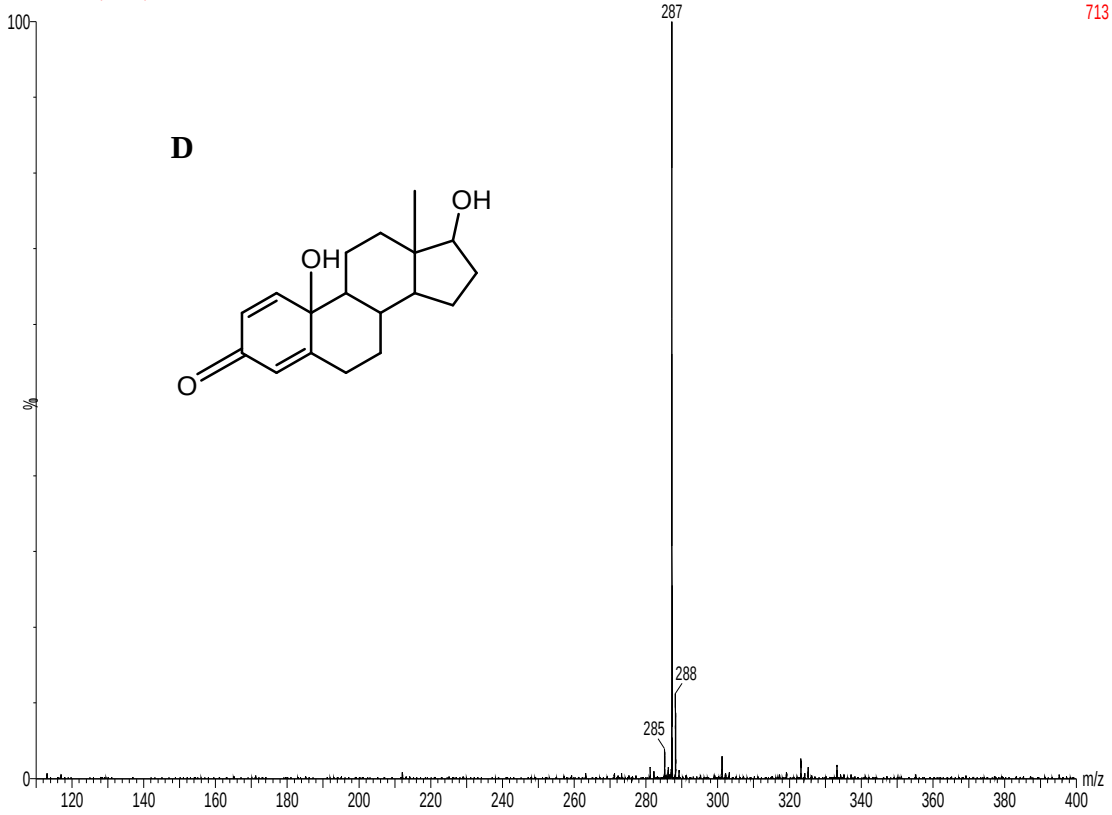

FE ST EDDS T3H SPE ISO

LC300196 905 (16.790)

1: TOF MS ES-
79

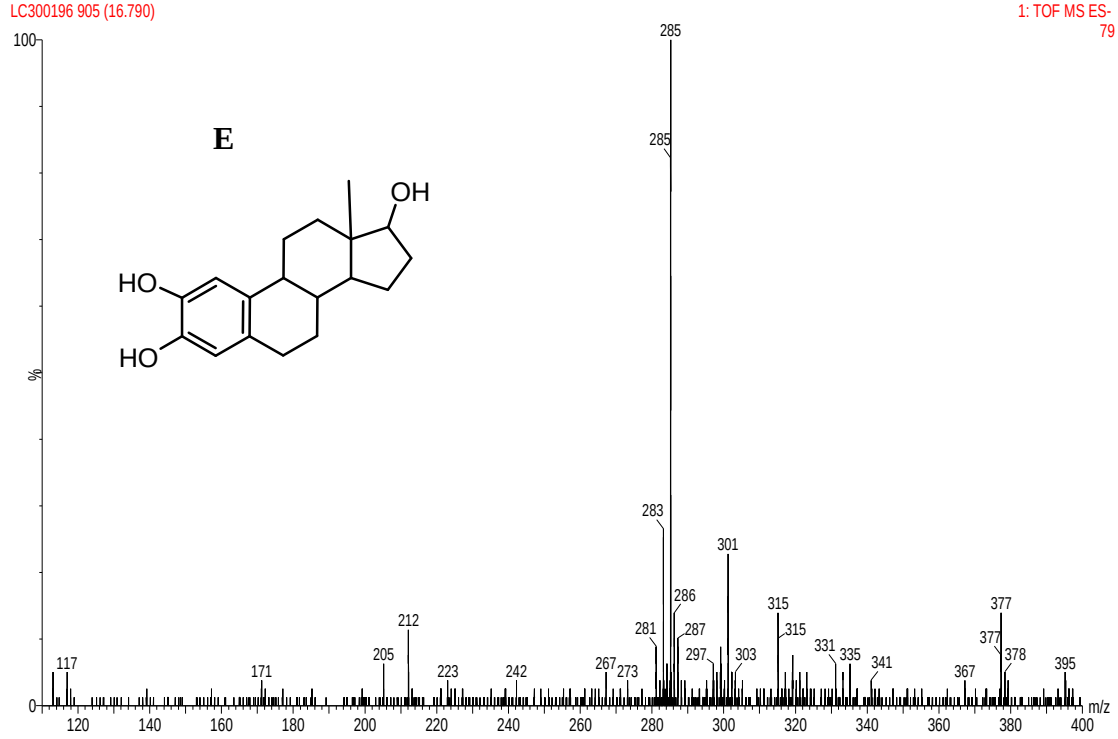

FE ST EDDS T3H SPE ISO

LC300196 947 (17.569)

1: TOF MS ES-
564

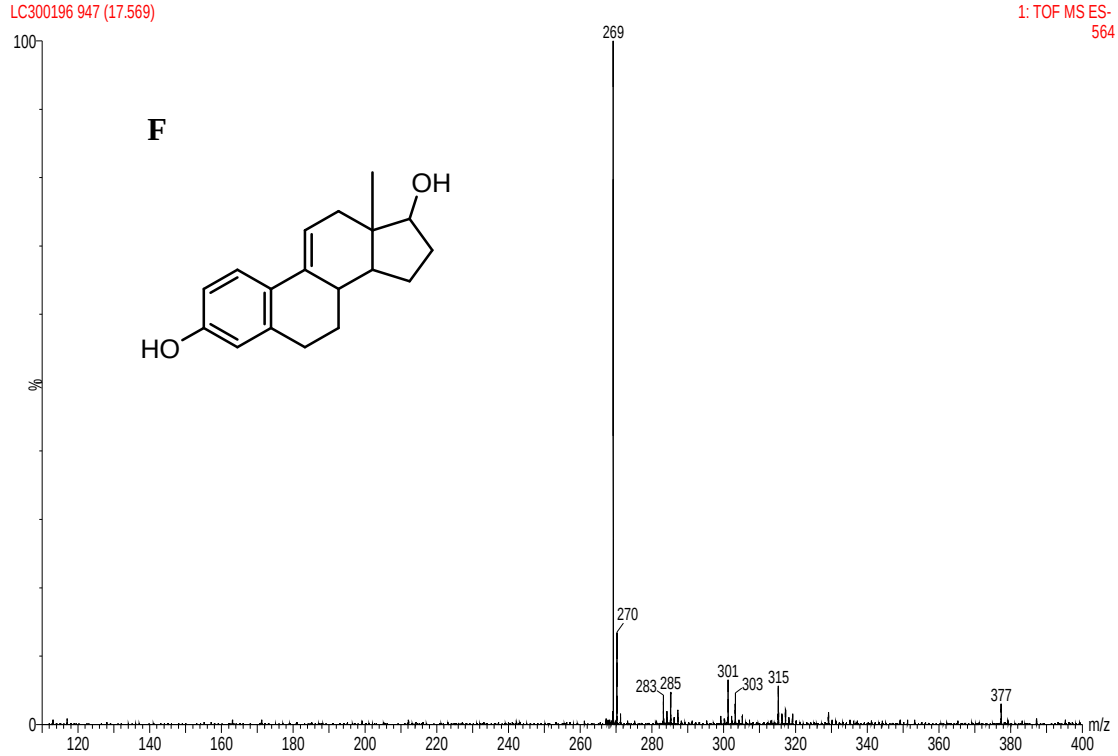

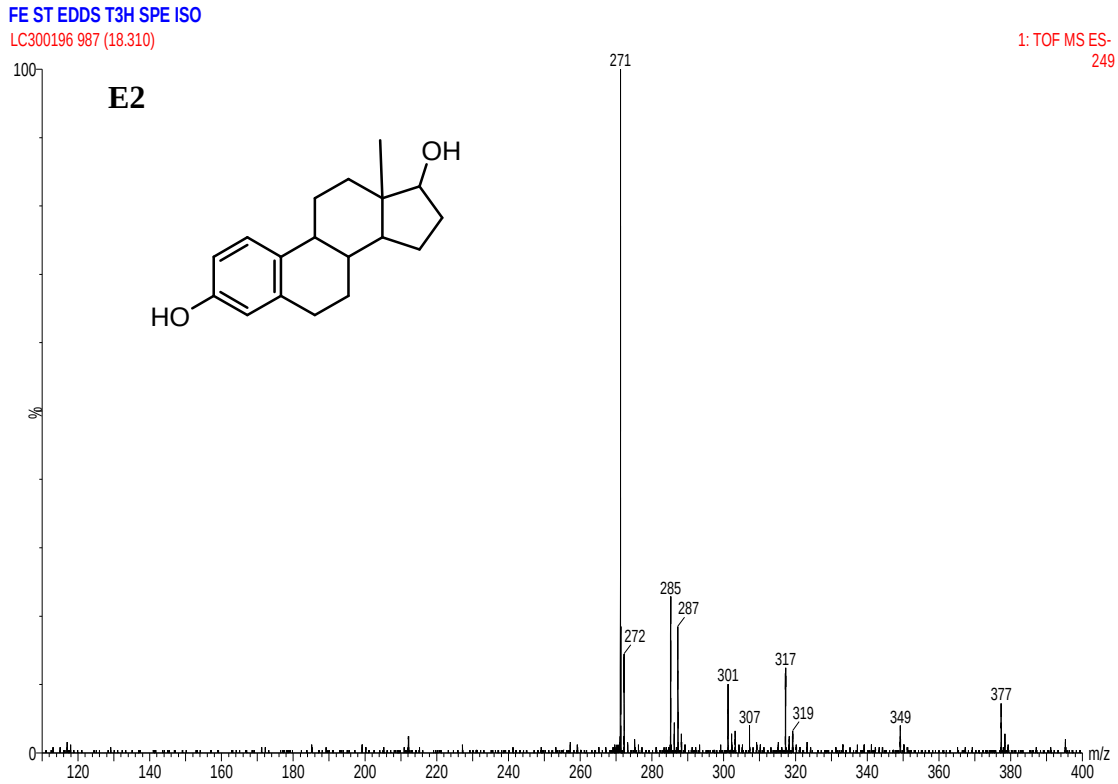

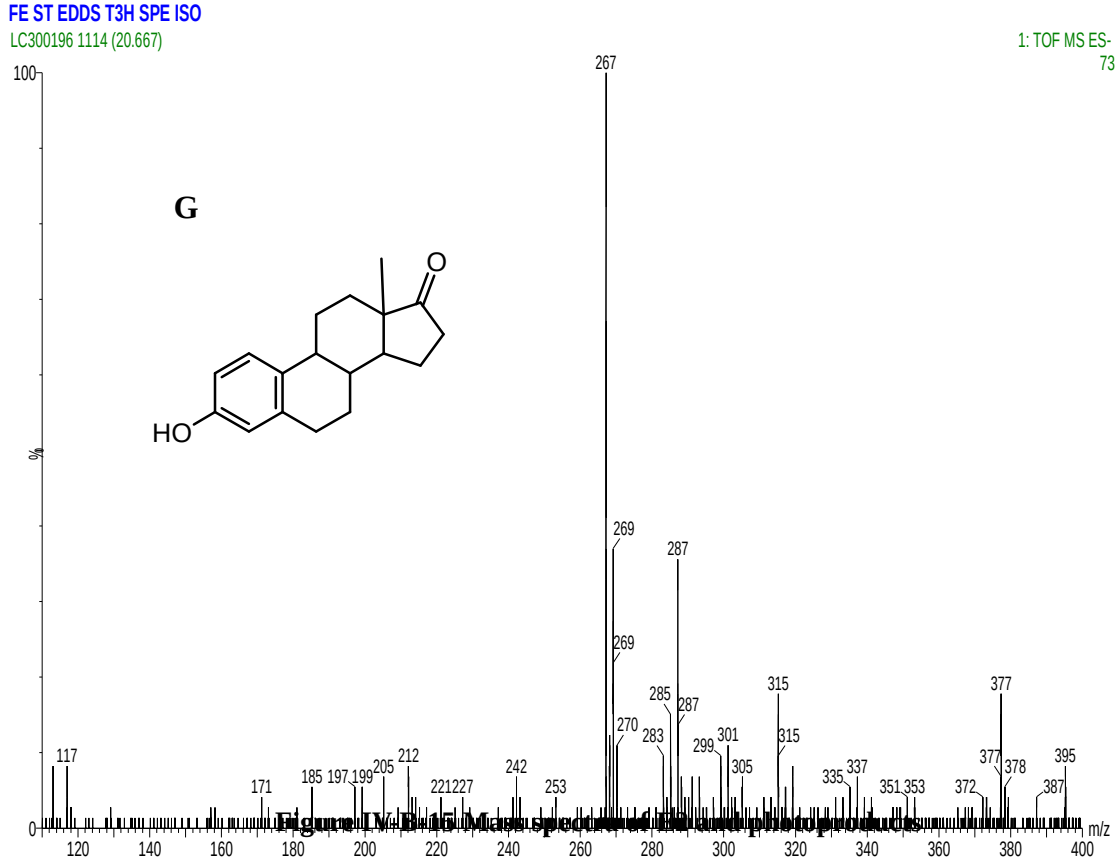

Figure IV-B15 Mass spectra of E2 and its products

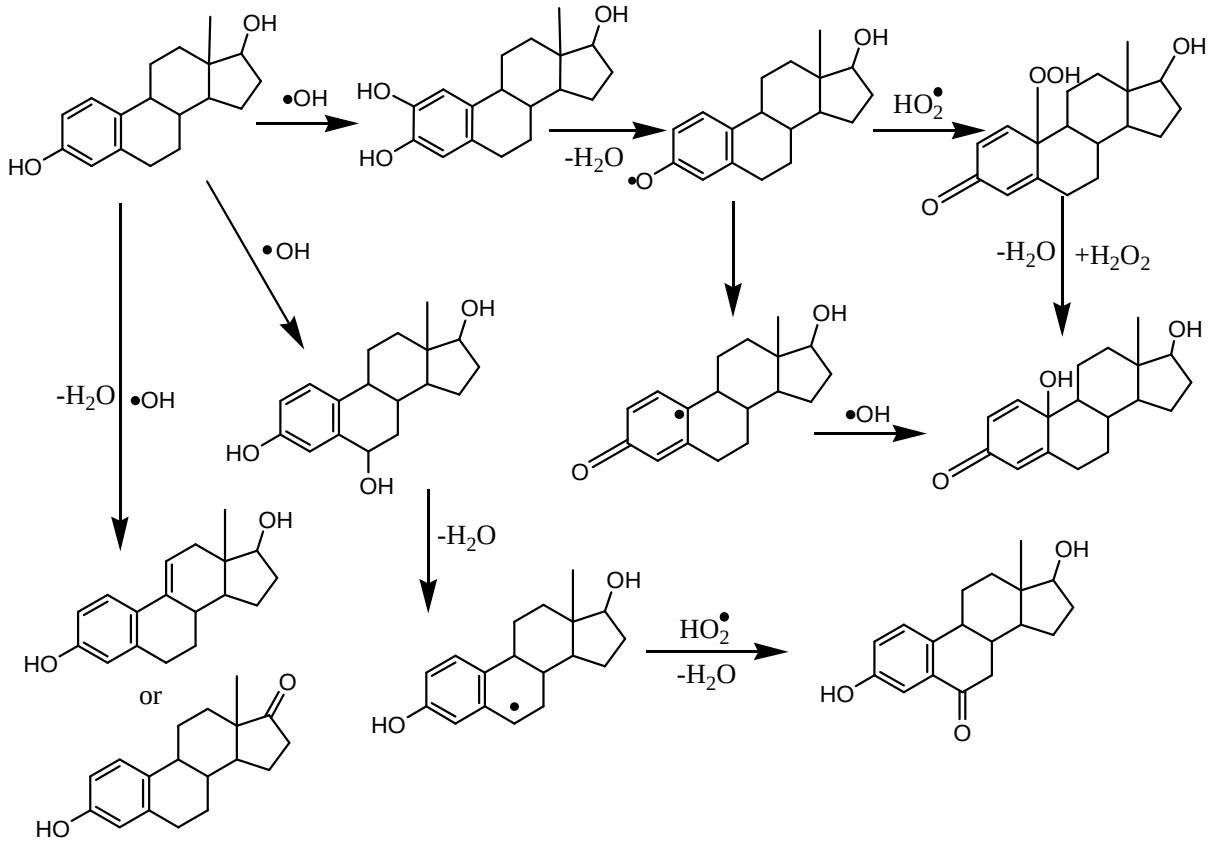

Figure IV-B-16 Proposed photodegradation scheme of E2

Conclusions

This study gives evidence of the potential role of Fe(III)-EDDS as a photoactive species in natural waters. For the first time, the quantum yield of $^{\bullet}OH$ was detected by photolysis of Fe(III)-EDDS. The quantum yield of $^{\bullet}OH$ was independent of the concentration of Fe(III)-EDDS. The effect of O_2 and irradiation wavelength on the quantum yield of $^{\bullet}OH$ are very well known and are the same as for any other iron species. On the contrary, the effect of pH is not obvious for this Fe(III)-EDDS complex. The quantum yield of $^{\bullet}OH$ radical formation was higher at higher pHs between 3.0 and 9.0. This result is particularly interesting in terms of the natural environment. Correspondingly, E2 could be photodegraded by the photolysis of Fe(III)-EDDS, which is influenced by the concentration of Fe(III)-EDDS, pH, O_2 and the concentration of Fe(III). The rate of E2 degradation increased with the increasing concentrations of Fe(III)-EDDS in the range of $0\text{-}2\times10^{-4}$ M, but much higher concentration of Fe(III)-EDDS such as 1×10^{-3} M inhibited E2 degradation. The effect of pH is complex. Before 90 min of irradiation, the efficiency of photodegradation of E2 was pH 8.0 > pH 6.1 > pH 5.2 > pH 4.0 > pH 3.1 as the formation of

$^{\bullet}$OH. High concentration of oxygen is favorable for the photodegradation of E2. From the photoproduction of E2 identified by the LC-MS, we can see that the main pathway of E2 was attacted by $^{\bullet}$OH radicals. The Fe(III)-EDDS complex would be of importance for the transformation of organic compounds in the environment due to its higher photoactivity at pHs more relevant to the environment.

IV-C-Photochemical formation of hydroxyl radicals catalyzed by montmorillonite

In this work, we quantified the photochemical formation of $^{\bullet}$OH in aqueous suspensions containing Montmorillonite (Shaoxing, Zhejiang, PRC) under irradiation with metal halide lamp (MHL) that produced near UV and visible light ($\lambda \geq 365$ nm). The hydroxylation of benzene to phenol was selected to demonstrate the formation of hydroxyl radicals, and benzene was used as a probe to demonstrate the oxidative reaction induced by illuminated clay. The influence of clay concentration, pH, carboxylate anions on the hydroxyl radical formation were checked. The mechanism of hydroxyl radical formation was proposed.

C-1 Oxidation of benzene to phenol

Figure IV-C-1 shows the HPLC chromatogram of centrifuged sample from the irradiated benzene for 2 hours in the presence of 20.0 g L^{-1} of Montmorillonite at pH 6.0. It is confirmed that phenol was produced, which shows that the photoinduced formation of $^{\bullet}$OH occurs in aqueous suspensions of Montmorillonite clay and $^{\bullet}$OH radicals oxidize benzene to phenol. However, phenol couldn not be detected in the dark condition. Gournis *et al*. (2002) reported the formation of hydroxyl radicals catalyzed by clay surfaces but no quantification data was provided. In their work, Laponite and Montmorillonite were suspended for only 30 min in the presence of DMPO and formate and the $^{\bullet}$OH radicals were determined by electron paramagnetic resonance (EPR). However, Gournis *et al*. (2002) did not describe if the experiments were carried out in dark or not. Oxidation of benzene to phenol in the presence of clay also indicates that clay may play its role in oxidation of organic compounds by producing $^{\bullet}$OH. Kong and Ferry (2003; 2004) believed only $^{1}O_2$ was responsible for the enhanced photooxidation of the polycyclic aromatic hydrocarbon chrysene in aqueous suspensions of the Smectite clay. It is possible that the types of clays and the organic

compounds could make differences in the photodegradation pathways of the organic compounds in the presence of clay.

Figure IV-C-2 shows the variation of the benzene concentration in aqueous clay suspensions under irradiation and in the dark. In the suspensions containing 20 g L^{-1} of Montmorillonite, 250 μM initial benzene concentrations, pH 3.0, the apparent first-order rate constants of benzene photodegradation ($k_{obs,\ benzene}$) was calculated to be 2.43×10^{-5} s^{-1} from the result in Figure IV-C-2. The $^{\bullet}OH$ concentration at steady state ($[^{\bullet}OH]ss$) was determined using equation 1.

$$\frac{d[benzene]}{dt} = -k_{obs,\ benzene}[benzene] = -k[\cdot OH]_{ss}[benzene] \qquad (1)$$

where k is the second-order rate constant of the reaction of benzene with $^{\bullet}OH$, $k = 7.6 \times 10^{9}$ M^{-1} s^{-1} (Kochany and Bolton, 1992). Thus,

$$k_{obs,benzene} = k\ [OH]ss \qquad (2)$$

It is calculated that $[OH]ss = 3.2 \times 10^{-15}$ M, which is similar to the steady-state concentrations of $^{\bullet}OH$ (6.7×10^{-15} M) in illuminated surface water samples (a stream approximately 3 km west of Brazil, Indiana) reported by Allen *et al*. (1996).

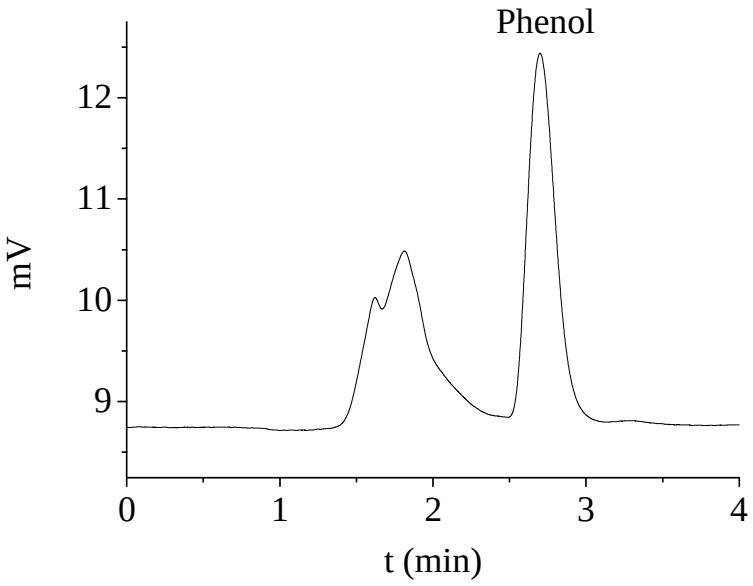

Figure IV-C -1 HPLC chromatogram of phenol produced from scavenging of hydroxyl radicals by benzene in clay suspension. The experimental conditions were as follows: [Montmorillonite] = 20.0 g L^{-1}, [benzene] =7 mM, pH = 6.0, irradiation time 2 hours, retention time of phenol = 2.70 min.

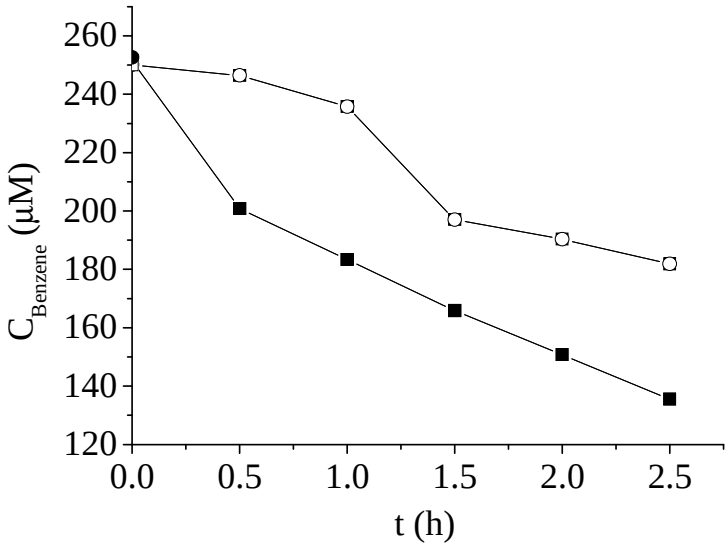

Figure IV-C -2 Concentration decrease of benzene in aqueous clay suspensions under irradiation and in the dark. Experimental conditions were as follows: clay concentrations = 20 g L^{-1}; pH = 3.0; initial benzene concentration = 250 μM; 250 W (○) Montmorillonite in the dark (■) Montmorillonite under irradiation.

C-2 Effect of clay concentration

The amount of clay is certainly a very important factor for the photochemical production of $^{\bullet}OH$ in clay suspensions through the variation of the quantity of photoreactive species in clays, adsorption of benzene onto clay surfaces, light absorption and/or light scatter. Experiments to study the effects of Montmorillonite concentration on the photochemical production of $^{\bullet}OH$ were carried out. The Montmorillonite concentration in suspensions ranged from 4.0 to 25.0 g L^{-1}. The pH value of Montmorillonite suspensions was not adjusted and it was about 9.8. As shown in Figure IV-C-3, $^{\bullet}OH$ concentration increased with increasing the concentration of clay in aqueous solutions in the range of 0 ~ 20.0 g L^{-1}, but higher concentration of clay like 25.0 g L^{-1} inhibited the $^{\bullet}OH$ production. Moreover, control experiments were carried out and the results showed that phenol was not found in an aqueous solution of benzene without clays after illumination under 250 W MHL (t = 0 ~ 6 hours). So we think that appropriate clay concentration facilitates the formation of $^{\bullet}OH$ in clay suspensions. But when clay concentration was raised to a certain high value, clay greatly reduced the light absorption into the suspensions due to light scattering. Thus, the photochemical reaction is restricted and the photochemical production of $^{\bullet}OH$ radicals is

decreased.

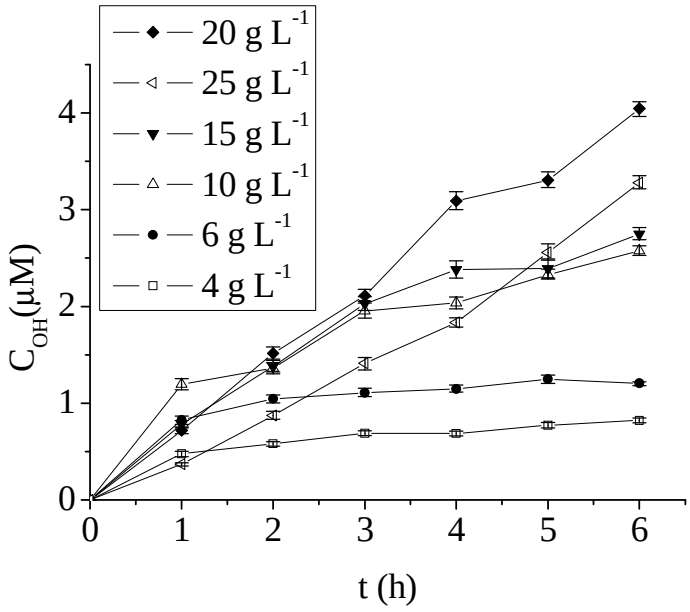

Figure IV-C -3 Influence of clay concentration on the hydroxyl radicals formation in aqueous suspensions containing Montmorillonite (4.0 to 25.0 g L^{-1}). The experimental conditions were as follows: [benzene] = 7 mM, irradiation time 6 hours, pH = 9.8 (without adjusting).

C-3 Effect of initial pH

The variation of initial pH value of the clay suspension changes the clay particle properties like surface charge and surface hydroxyl group. Also, pH changes the amount of the photoactive species dissolved from the clay into the suspended solutions. It is thought that pH value of the Montmorillonite suspension has strong influence on the photochemical formation of $^{\bullet}OH$. Experiments were carried out to study the pH effect on the photochemical production of $^{\bullet}OH$ in aqueous clay suspensions. As shown in Figure IV-C-4, the $^{\bullet}OH$ concentrations increase with reducing the pH of Montmorillonite suspensions in the range of 2.0 to 10.0. The $^{\bullet}OH$ concentration sharply decreased by 9.6 times in Montmorillonite suspensions from pH 2.0 to 4.0 after 6 hours of irradiation, but much less in the higher pH range of 4.0 to 10.0. This pH-dependent trend of photochemical formation of $^{\bullet}OH$ is quite similar to that of ferric ions, $Fe(OH)^{2+}$, which has higher photoactivity in acidic pH near 3 (Wu and Deng, 2000).

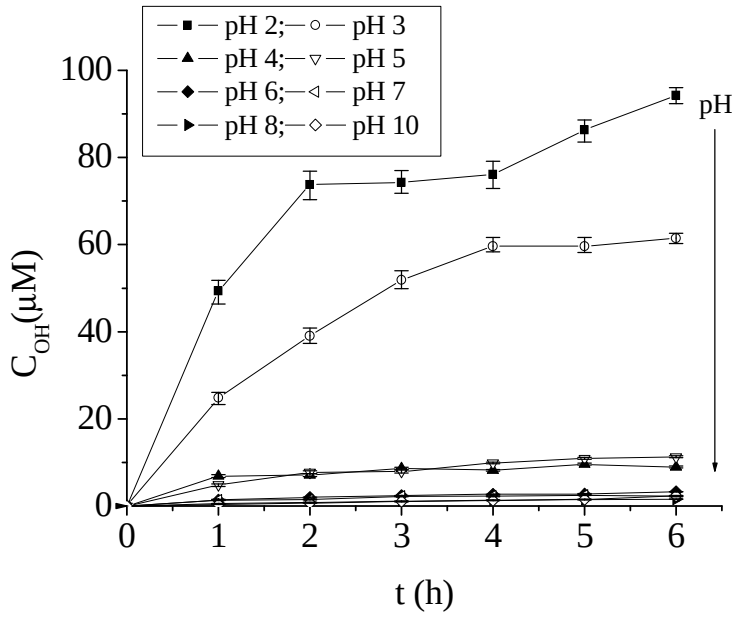

Figure IV-C-4 Influence of pH on the hydroxyl radicals formation in aqueous suspensions containing Montmorillonite at pH values in the range of 2.0 to 10.0. The experimental conditions were as follows: [Montmorillonite] = 20.0 g L^{-1}, [benzene] = 7 mM, irradiation time 6 hours.

C-4 Effect of citrate ions

It is known that citrate ions form complexes with iron as Fe(III)-citrate complex which has higher photoreactivity to produce hydroxyl radicals under irradiation with visible light (Wu and Deng, 2000). Since X-ray fluorescence analysis showed that Montmorillonite used in this work was iron-rich, in order to test the idea that iron is one of the important sources of $^{\bullet}$OH, the effect of citrate ions in the clay suspensions on the formation of $^{\bullet}$OH radicals was investigated. Results in Figure IV-C-5 show that the production of $^{\bullet}$OH increases significantly by adding 0.2 mM of citrate ions to the aqueous clay suspensions. However, high concentration of citrate ions (5 mM) added to the clay suspension does not accelerate the formation of $^{\bullet}$OH. And the addition of too much citrate ions (500 mM) results in the reduction of $^{\bullet}$OH. It is well-known that citrate ion is also a very effective $^{\bullet}$OH scavenger, besides a complexing agent for Fe(III)/(II). An initial citrate ions concentration of 5 mM, especially 500 mM, greatly exceeded the coordination site saturation of Fe(III)/(II), thus some $^{\bullet}$OH were consumed by citrate ions. The citrate concentration of 0.2 mM is small and the reaction rate of citrate ions with $^{\bullet}$OH ($k = 1.2 \times 10^8$ M^{-1} s^{-1}) at 298K (Zepp *et al*., 1992) is much lower than that of benzene with $^{\bullet}$OH ($k = 7.6 \times 10^9$ M^{-1} s^{-1}) (Kochany and Bolton,

1992), so citrate ions should not compete with benzene for acting as •OH scavenger. Therefore, iron species in the clay suspensions is believed to be one of the important factors for •OH formation, and the amount of citrate ions adding to the clay suspensions affected the concentration of •OH.

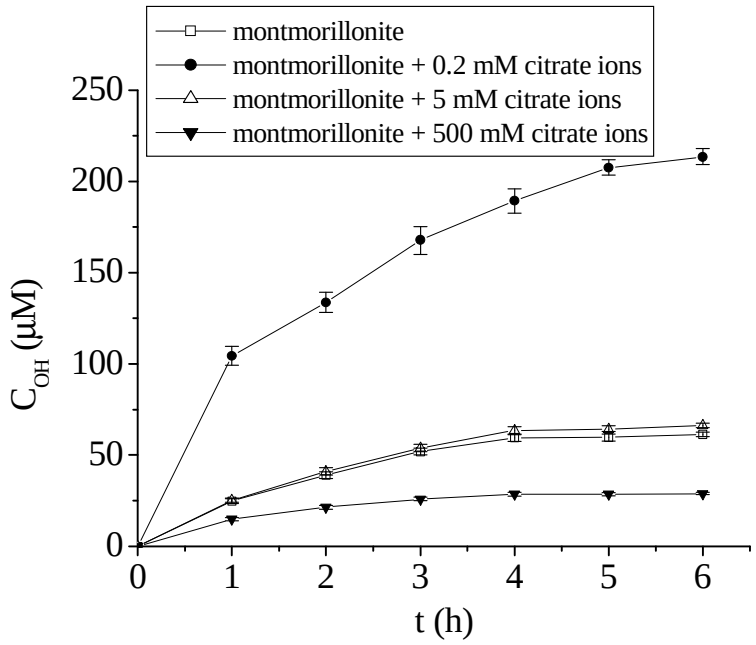

Figure IV-C-5 Influence of citrate concentration on the formation of hydroxyl radicals in the suspensions containing clays. The experimental conditions were as follows: [Montmorillonite] = 20.0 g L^{-1}, [benzene] = 7 mM, pH = 3.0.

C-5 Mechanism of hydroxyl radicals formation

C-5-1 Charged surface of nano clay

The surface of nanoparticles of clays possesses a large number of either homolytically or herterolytically broken bonds. As shown in equation 3, Gournis *et al*. (2002) have suggested that the charged surface states are highly reactive and can, as potential catalysts, activate O_2 through chemisorption or polarization and produce $O_2^{\bullet-}$. The formation of $O_2^{\bullet-}$ leads through reactions (4) to (7) to the formation of other reactive oxygen species $HO_2^{\bullet}$, H_2O_2 and •OH. However, the rate constant for production of •OH radicals is negligible. It is believed that Fe (II) complexes can catalyze this reaction through Fenton reaction mechanisms (equation 8). Even though, the amount of •OH radicals produced in the Montmorillonite suspensions may

be extremely depended on the amount of $O_2^{\bullet-}$ derived from O_2. Obviously, in the absence of light□the amount of $^{\bullet}OH$ radicals is too small to be detectable by HPLC because the amount of $O_2^{\bullet-}$ is not enough.

C-5-2 Free iron ions in clays

Montmorillonite contains metal impurities resulting from isomorphous substitution, for instance, Al^{3+} or Fe^{3+} substitution for Si^{4+}, and Fe^{2+}, Mg^{2+} or Zn^{2+} substitution for Al^{3+}. X-ray fluorescence analysis showed that total iron in Montmorillonite was 2.24% (equivalent to Fe_2O_3). Iron species in Montmorillonite include free iron ions and structural iron. The free iron ions including Fe^{2+} and Fe^{3+} dissolved in the suspensions were determined and the results are listed in Table IV-C-1. The total amount of free iron ions increased with the acidifying of the suspensions from pH 4.0 to 2.0. In the pH range of 2.0 to 4.0, Fe^{2+} ions are more abundant than Fe^{3+} ions.

$$O_2 \xrightarrow{\text{Charged surface on nano clay}} O_2^{\bullet-} \quad (3)$$

$$O_2^{\bullet-} + H^+ \rightarrow HO_2^{\bullet} \quad (4)$$

$$2\ HO_2^{\bullet} \rightarrow H_2O_2 + O_2 \quad (5)$$

$$H_2O_2 + O_2^{\bullet-} \rightarrow O_2 + OH^- + {}^{\bullet}OH \quad (6)$$

$$H_2O_2 + {}^{\bullet}OH \rightarrow H_2O + O_2^{\bullet-} + H^+ \quad (7)$$

$$Fe^{2+} + H_2O_2 \rightarrow Fe^{3+} + {}^{\bullet}OH + OH^- \quad (8)$$

$$H_2O_2 \xrightarrow{h\upsilon} 2\ {}^{\bullet}OH \quad (9)$$

Table IV-C-1 Amount of iron ions dissolved in clay suspensions

	Concentration of iron ions(μM)					
Montmorillonite	pH 2		pH 3		pH 4	
suspension	Fe^{3+}	Fe^{2+}	Fe^{3+}	Fe^{2+}	Fe^{3+}	Fe^{2+}
(20 g L^{-1})*	0.56	111.84	1.97	55.63	2.96	13.23

*: Total iron in Montmorillonite is 2.24% calculated on the basis of Fe_2O_3 by X-ray fluorescence analysis. The concentration of total iron ions in 20 g L^{-1} of Montmorillonite suspension could be calculated to be 5.6 mM. In pH 2, there is the higher amount of iron ions dissolved in Montmorillonite suspension, but the concentration of free iron ions (0.11 mM) is still much lower that the concentration of total iron ions (5.6 mM).

In the presence of light, the reactions in the acidic Montmorillonite suspensions were promoted and enough •OH radicals were detected. It is clear that photoinduced Fenton reaction (equation 8) and the photolysis of H_2O_2 (equation 9) occurred which produce much more •OH radicals than that in the dark. Certainly, the photo-Fenton reaction is dependent on the pH value of the solutions (Shemer *et al.*, 2006). In this work, pH has very significant effect on the amount of •OH radicals produced in the Montmorillonite suspensions. It is believed that pH has relationship with the speciation of iron. Table IV-C-1 shows that the total amount of soluble iron (free iron) increased with pH value decreased from 4.0 to 2.0 which has the same pH-dependent trend of the amount of •OH radicals. Therefore, the total amount of iron may has very important effect on the formation of •OH radicals. Then, the question is which iron species play most important role in such processes, Fe (III) ions versus. Fe (II) ions, and free iron versus structural iron. As we know, ferric ions has photoactivity especially in the form of $Fe(OH)^{2+}$ in acidic solutions at pH near 3.0. It is reasonably to assume that free ferric ions are responsible for the formation of •OH radicals in the pH range of 2.0 to 4.0. However, the amount of free Fe(III) ions increased with increasing pH values from 2.0 to 4.0, which presented an opposite trend as the formation of •OH radicals. This result indicated that ferrous ions also had contribution to the formation of •OH radicals. To further test this idea, the amount of •OH radicals was determined in the solutions initially containing only ferrous ions at pH 3.0. The results showed that •OH radicals produced and the amounts of •OH radicals increased with initial ferrous ions concentrations from 20 to 80 μM as well as irradiation time (Figure IV-C-6). It is believed that in the presence of dissolved oxygen, ferrous ions are oxidized to ferric ions and the latter undergoes photolysis to produced •OH radicals. The variation of concentration of ferrous ions and ferric ions was also examined (Figure IV-C-7). It was found that during the period of photoreaction in 90 minutes, the ferrous ions transformed to ferric ions, and then Fe (III) and Fe(II) are in equilibrium. Even when the Fe (III)/Fe(II) equilibrium was achieved, the formation of •OH radicals continued. Reactions (10), (11) and (12) are thought to be important for producing •OH radicals through photochemical cycle of Fe(III)/Fe(II). Thus, free ferrous ions in Montmorillonite plays the key role in photochemical formation of •OH radicals in the presence of dissolved oxygen.

$$Fe(OH)^{2+} \xrightarrow{h\upsilon} Fe^{2+} + {}^{\bullet}OH \qquad (10)$$

$$Fe^{3+} + H_2O \xrightarrow{h\upsilon} Fe^{2+} + {}^{\bullet}OH + H^{+} \qquad (11)$$

$$4\,Fe^{2+} + O_2 + 8OH^{-} + 2H_2O \rightarrow 4Fe(OH)_3 \qquad (12)$$

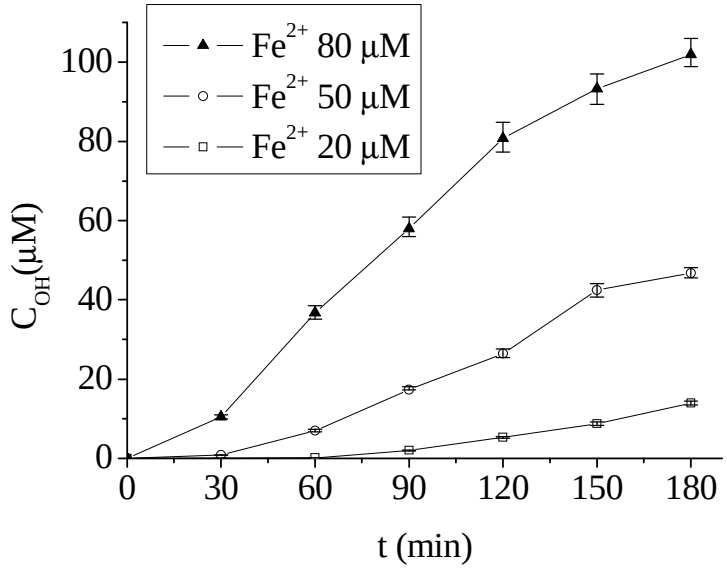

Figure IV-C-6 Influence of the concentration of Fe^{2+} on the hydroxyl radical formation in aqueous solutions containing Fe^{2+} at different concentrations 20, 50 and 80 µM. The experimental conditions were as follows: [benzene] = 7 mM, irradiation time 3 hours, pH =3.0.

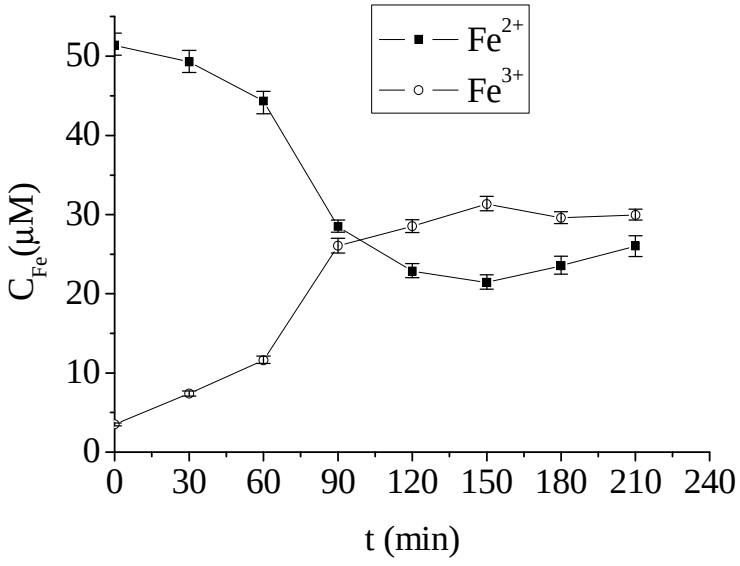

Figure IV-C-7 Concentrations of Fe^{2+} and Fe^{3+} versus irradiation times in irradiated Fe^{2+} suspensions. The experimental conditions were as follows: initial Fe^{2+} concentration = 50 µM, [benzene] = 7 mM, irradiation time 3.5 hours, pH =3.0.

C-5-3 Structural iron in the clays

Table IV-C-1 shows that the amount of total iron in Montmorillonite is much higher than the free iron ions. Structural iron is the predominant iron species and its amount is about 50 times more than that of the free iron. It is well-known that iron oxides and zinc oxides act as photocatalyst in generating hydroxyl radicals. But the iron and zinc ions in the clay lattice are in the chemical environments different from that in the iron or zinc oxides. Gournis *et al*. (2002) reported the formation of hydroxyl radicals catalyzed by Laponite and Montmorillonite. Except for the charged nano clay surface, they preferred that structural ferrous ions were also responsible for the hydroxyl radical formation through reaction (13). However, Song *et al*. (2006) reported that free iron (or soluble iron) in clay surface efficiently catalyzed the decomposition of H_2O_2 under UV light irradiation, but the structural iron in the octahedral lattice showed poor reactivity (equation 14).

$$\text{Structural-Fe}^{2+} + O_2 \rightarrow \text{Structural-Fe}^{3+} + O_2^{\bullet-} \qquad (13)$$

$$\text{Structural-Fe}^{2+} + H_2O_2 \rightarrow \text{Structural-Fe}^{3+} + {}^{\bullet}OH + OH^- \qquad (14)$$

To make sure whether the structural iron contributes to the formation of $^{\bullet}OH$ radicals in the Montmorillonite suspensions, iron in Montmorillonite was removed by 0.1 M HCl for 1 hour and washed by pure water 5 times and the Montmorillonite was dried at 105 ± 1^{o}C. The treated Montmorillonite is named as the acid-washed Montmorillonite. The acid-washed Montmorillonite was illuminated in suspension with and without citrate ions and the $^{\bullet}OH$ radicals were determined. Results in Figure IV-C-8 showed that the acid-washed Montmorillonite produced very small amount of $^{\bullet}OH$ radicals (ca. 2 μM). Furthermore, by adding citrate ions into acid-washed Montmorillonite suspension, much more $^{\bullet}OH$ radicals (ca. 36.6 μM) were detected. It seems that structural iron also has contribution to the photochemical formation of $^{\bullet}OH$ radicals especially through complexation with carboxylate ligands. The following reactions are proposed to be involved in the photochemical reaction of structural iron in the Montmorillonite:

$$\text{Structural-Fe}^{2+} + O_2 \xrightarrow{h\upsilon} \text{Structural-Fe}^{3+} + O_2^{\bullet-} \qquad (15)$$

$$\text{>Fe(III)-OH} \xrightarrow{h\upsilon} \text{>Fe(II)-OH} + {}^{\bullet}OH \qquad (16)$$

$$\text{>Fe(III)-L} \xrightarrow{h\upsilon} \text{>Fe(II)-L} + {}^{\bullet}OH + \text{L'} \qquad (17)$$

□> represents surface complex, L and L' represent organic ligand and its oxidized product respectively□

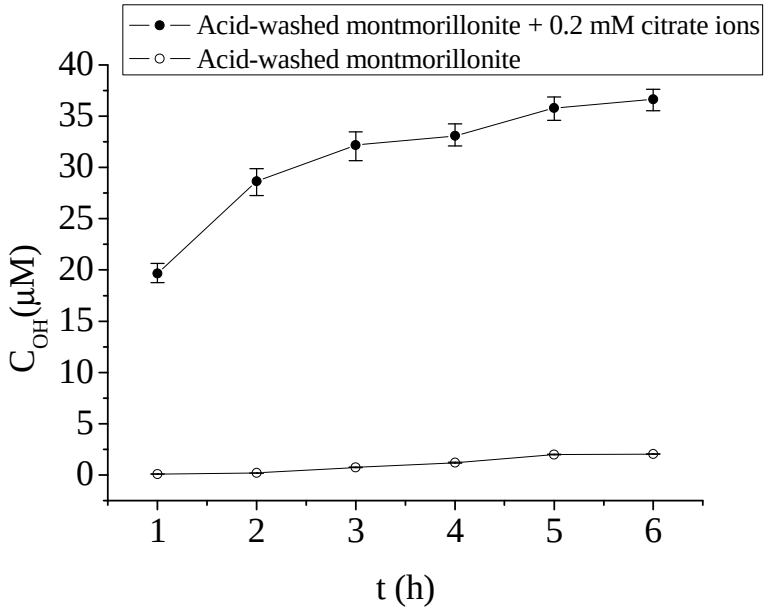

Figure IV-C-8 Effect of citrate on the formation of hydroxyl radicals in the solutions containing acid-washed clays. The experimental conditions were as follows: [Montmorillonite] = 20.0 g L^{-1}, [benzene] = 7 mM, pH = 3.0.

Conclusions

It is confirmed that •OH radicals are formed in the Montmorillonite suspensions under irradiation of a 250 W metal halide lamp ($\lambda \geq 365$ nm). The pH dependent trend and citrate ion effects on the amount of •OH radicals demonstrate that iron play a very important role in the •OH radicals formation. Both free iron and structural iron contribute to the amount of •OH radicals under illumination, moreover, ferrous and ferric species initially occurring in the Montmorillonite are both capable of producing •OH radicals upon photolysis in the presence of dissolved oxygen. The •OH concentration increased with increasing the concentration of Montmorillonite as well as irradiation time. However, too high concentrations like 25.0 g L^{-1} of Montmorillonite inhibited the •OH production, probably by reducing the light absorption of the suspension. The formation of •OH from Montmorillonite under irradiation with near UV and visible light infers that iron-rich Montmorillonite clays have important role in the interaction between the chemicals and soil surfaces as well as that the environmental behavior of chemicals through oxidation on the surface of clay particles

in air, water, soil or even top sediments.

IV-D Degradation of E2 photoinduced by KSF and KSF-EDDS

E2 was used as model compound in this work to study the photochemical properties of KSF and KSF-EDDS complex. Experiments were carried out under polychromatic irradiation (emission between 300 and 500 nm). Parameters such as KSF, EDDS, oxygen, 2-propanol, E2 concentrations and pH were all studied in the work.

D-1 Adsorption of E2 on KSF

The adsorption of E2 on KSF was rapid and high. Most of the reaction occurred within the first minutes. But E2 adsorption required one day to reach its maximum. Figure IV-D-1 shows the adsorption isotherms of E2 on the KSF at pH 6. Both of the Langmuir model for monolayer adsorption and the Freundlich model for multilayer adsorption were applied to fit the experimental data. It was found that the Langmuir model described the adsorption of E2 to KSF better. The Langmuir model is shown as

$$C_{is} = \frac{K_{eq} b C}{1 + K_{eq} C}$$

Where, C is the concentration in the clay solution after equilibration; C_{is} is the amount adsorbed on the clay; K_{eq} is the equilibration constant and b is the maximum amount adsorbed on the clay. Fitting the L equation, K_{eq} and b are calculated to be 0.0412 L μmol^{-1} and 8.02 $\mu mol\ g^{-1}$. There were no obvious differences between the E2 adsorption on the KSF in the presence of EDDS and that in the absence of EDDS.

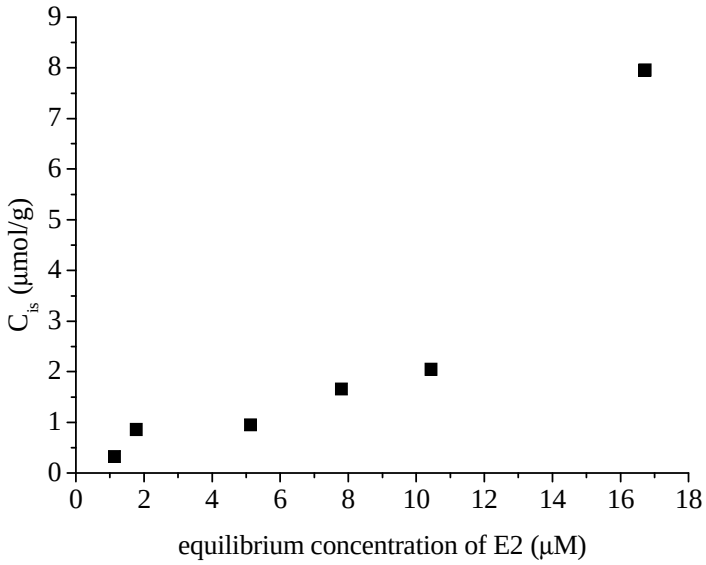

Figure IV-D-1 Adsorption isotherm of E2 onto the Montmorillonite KSF ([KSF] = 1 g L^{-1}, pH = 6.0)

The adsorption of E2 on KSF influenced by the pH was also detected. As shown in figure IV-D-2, pH has an obvious effect on the E2 adsorption. The acid pH favors to the adsorption. At the isoelectric point of KSF (about 5), the adsorption is the lowest.

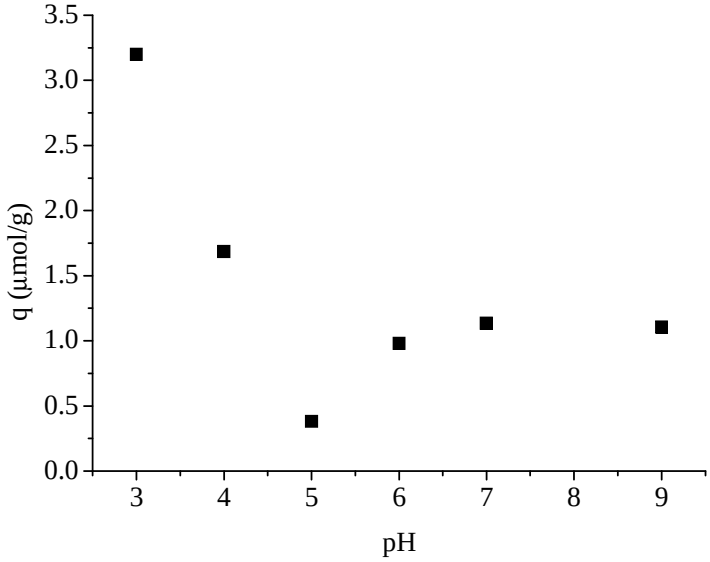

Figure IV-D-2 Effect of pH on the E2 adsorption on KSF ([KSF] = 1 g L^{-1}, [E2] = 6 µM)

D-2 Photodegradation of E2 in KSF solutions

The photodegradation of E2 was studied in the KSF solutions. Irradiation was performed with polychromatic tubes emitting between 300 and 500 nm. Effect of concentration of KSF and pH were studied in this work. Under our experimental conditions and in the dark, no degradation of E2 was observed in the absence and in the presence of KSF. Similarly, there was no photodegradation of E2 without KSF under irradiation.

D-2-1 Effect of KSF concentration on the degradation of E2

The effect of KSF concentration on the photodegradation of E2 (5 µM) was studied in the range from 0 to 6.0 g L^{-1} at pH 3. As shown in Figure IV-D-3, the photodegradation efficiency of E2 increased when the concentration of KSF in aqueous solutions was increased in the range from 0 to 2 g L^{-1}. At higher concentrations such as 4.0 and 6.0 g L^{-1} of KSF, the photodegradation efficiency of E2 was reduced. Thus an appropriate KSF concentration facilitates the degradation of E2 in clay suspensions. However, when the KSF concentration was raised to a threshold value, the suspended clay particles considerably weakened light penetration into the suspensions due to a shielding effect (Lu *et al*., 2004; Chiou and Juang, 2007). Consequently the degradation rate of E2 decreased. In our experimental conditions, the optimal concentration of KSF was around 1.0 g L^{-1}.

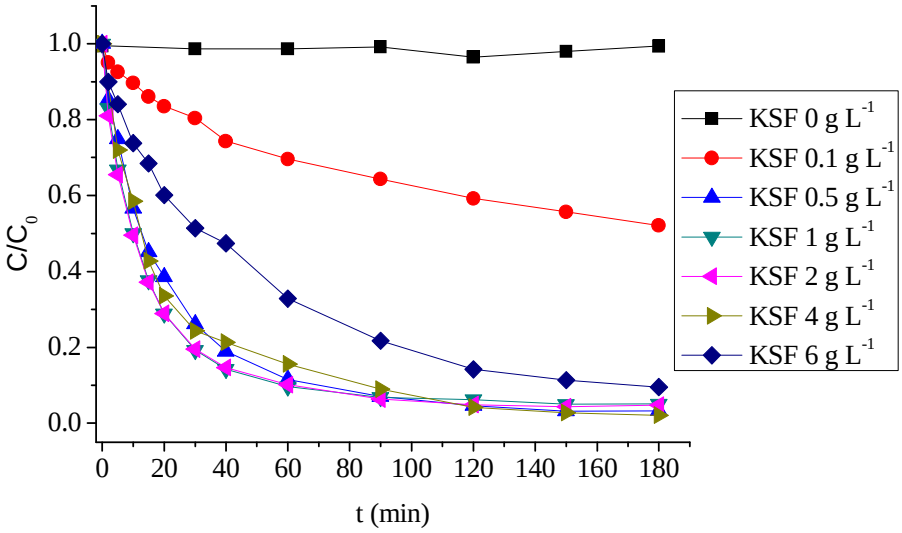

Figure IV-D-3 Influence of KSF concentration on the photodegradation of E2 in aqueous solutions containing KSF at different concentrations in the range of 0 - 6.0 g L^{-1}. The experimental conditions were as follows: [E2] = 5 µM, irradiation time 3 h, pH = 3.0.

During the irradiation, the concentration of iron was also detected. As shown in Figure

IV-D-4, the concentration of Fe(II) and Fe(tot) increased slightly during the irradiation, which indicated that there was only a very small amount of iron in the KSF photodissolved into the solution during the irradiation.

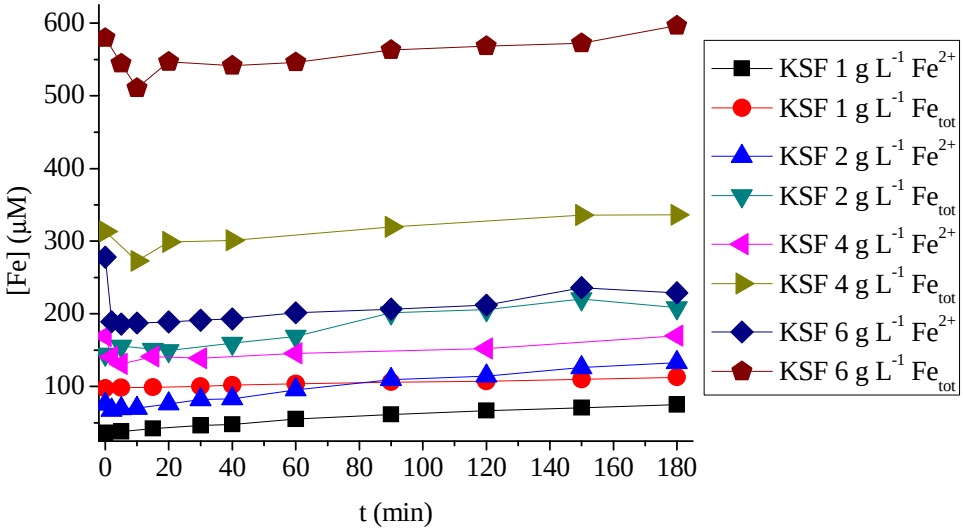

Figure IV-D-4 Concentration of Fe during the irradiation ([E2] = 5 μM, irradiation time 3 h, pH = 3.0)

D-2-2 Effect of pH on the degradation of E2

Montmorillonite KSF is acid-activated clay containing relatively high amount of iron. Variation of the initial pH value of the clay suspension changes the clay particle properties such as surface charge, surface area and surface hydroxyl group (Jozefaciuk and Bowanko, 2002) and the amount of photoactive iron species dissolved from the clay into the solutions. To observe the effect of pH on the photodegradation of E2, five experiments were conducted with the same initial E2 concentration of 5 μM, KSF concentration of 1 g L^{-1} but at different pH values (2.0, 3.0, 4.0, 5.0, and 7.0). As shown in Figure IV-D-5, the results show that the E2 degradation rate is strongly pH-dependent. Obviously, the optimal initial pH value for the photodegradation of E2 was 3 (Figure IV-D-6). The degradation of E2 would be inhibited when the initial pH value was beyond 3, and especially, E2 was almost not degraded when the initial pH value was above 5. KSF contains 4.76% of the iron component that is composed of free iron oxides that distribute randomly on the clay surface, and structural iron in the octahedral lattice (Stucki *et al.*, 2002). We detected the amount of free iron ions, including Fe^{2+} and Fe^{3+}, dissolved in the suspensions at different pH values during the irradiation. As shown in Figure IV-D-7, the total amount of free iron ions was increased by

acidifying the suspensions from pH 5.0 to 2.0. At pH 3, the higher amount of Fe(II) was formed during the irradiation. At higher pH than 5, there is almost no soluble iron in the suspended solutions. The ferric ion species, especially $Fe(OH)^{2+}$, are the most important photochemical sources of hydroxyl radical and are more abundant at acid pH in the region of 3.0 (Wu and Deng, 2000), which could lead to the formation of $^{\bullet}OH$ via reaction (1). Therefore, the variation of degradation efficiency of E2 was mainly attributed to the pH dependence of the amount of iron ions and their speciation. The pH effect reflects that iron present in the clay is the most important photochemical source of $^{\bullet}OH$ radicals which induce the photodegradation of E2.

$$Fe(OH)^{2+} \xrightarrow{h\upsilon} Fe^{2+} + {}^{\bullet}OH \quad (1)$$

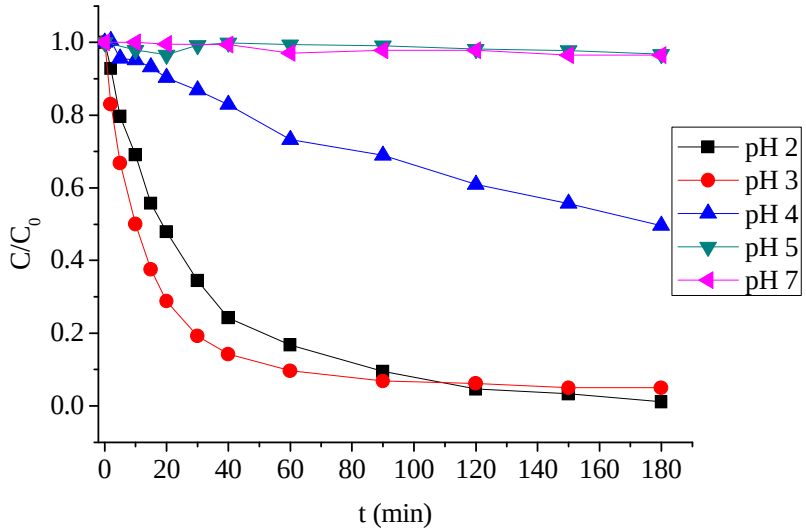

Figure IV-D-5 Influence of pH on the photodegradation of E2 in aqueous solutions containing KSF. The experimental conditions were as follows: [E2] = 5 µM, [KSF] = 1 g L^{-1}, irradiation time 3 h.

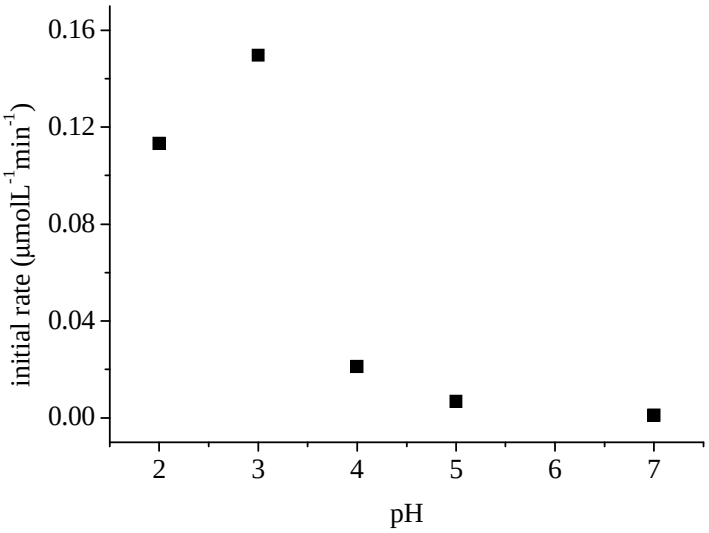

Figure IV-D-6 Initial degradation rate of E2 at different pH ([E2] = 5 µM, [KSF] = 1 g L^1, irradiation time 3 h).

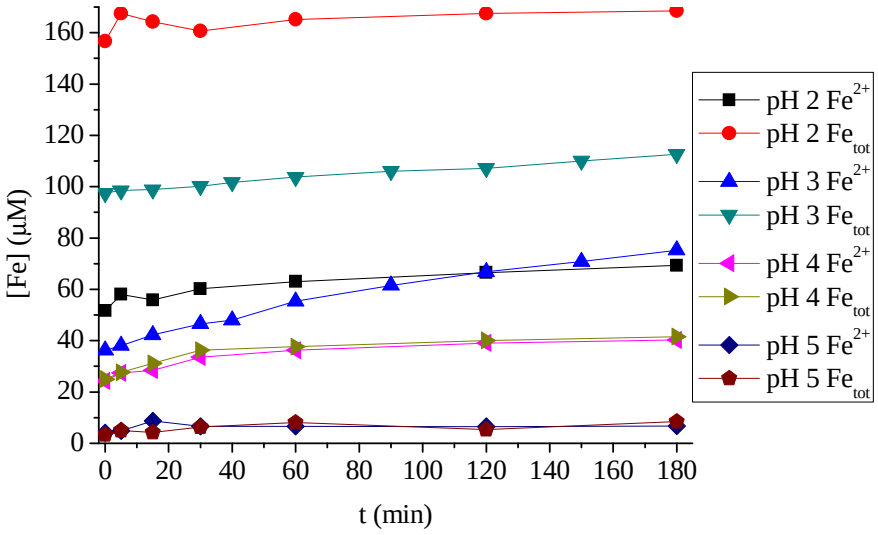

Figure IV-D-7 Concentration of iron during the irradiation ([E2] = 5 µM, [KSF] = 1 g L^{-1}, irradiation time 3 h).

D-3 Photodegradation of E2 in KSF solutions in the presence of EDDS

The photodegradation of E2 was studied in the KSF solutions in the presence of EDDS. Irradiation was performed with polychromatic tubes emitting between 300 and 500 nm. Effect of KSF, EDDS, E2, oxygen, 2-propanol concentrations and pH were all studied in this work. Under our experimental conditions and in the dark, no degradation of E2 was

observed in the absence and in the presence of KSF-EDDS. Similarly, there was no photodegradation of E2 without KSF-EDDS under irradiation.

D-3-1 Effect of KSF concentration on the degradation of E2

The effect of KSF concentration on the photodegradation of E2 (5 μM) in the presence of EDDS was studied in the range from 0 to 1.0 g L^{-1} at pH 5.0. As shown in Figure IV-D-8, the initial degradation rate of E2 increased with the increasing of KSF concentration in the range of 0 - 1.0 g L^{-1}. This result is attributed to the higher formation of Fe(III)-EDDS complex with the higher concentration of KSF in the solutions. Fe(III)-EDDS complex could undergo rapid photochemical reactions under irradiation leading to the formation of oxidative species. But the efficiency of E2 photodegradation, for the irradiation time between 30 and 180 minutes, was 0.1 g L^{-1} > 0.4 g L^{-1} > 1 g L^{-1}. At higher concentration of KSF, although the higher concentration of Fe(III)-EDDS was formed in the solutions and the initial degradation of E2 was faster, at the same time EDDS was also decomposed more quickly. After complete photodegradation of EDDS, Fe(III)-EDDS was no longer present in the solution. Thus, when the concentration of KSF was lower, although the starting efficiency of Fe(III)-EDDS was lower, the formation and reaction of Fe(III)-EDDS could continue during a longer time. So the lower concentration of KSF in the solution (0.1 g L^{-1}) could achieve better photodegradation efficiency at the end.

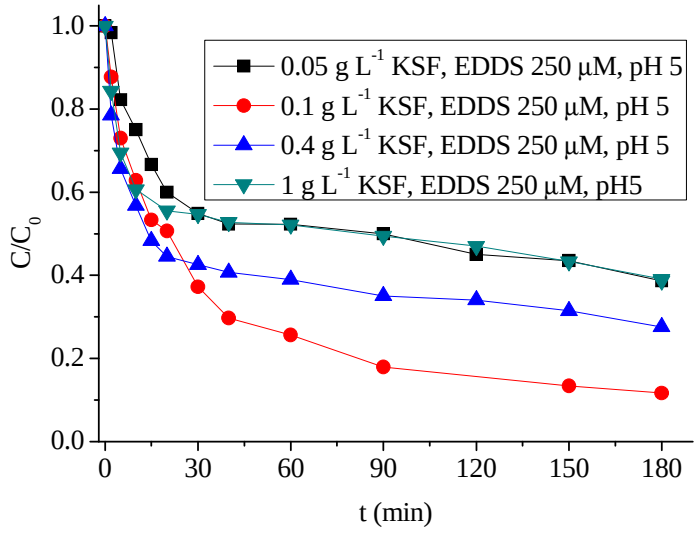

Figure IV-D-8 Influence of KSF concentration on the photodegradation of E2 in the presence of EDDS. The experimental conditions were as follows: [E2] = 5 μM, irradiation time 3 h, pH = 5.0.

D-3-2 Effect of pH on the photodegradation of E2

The effect of pH on the photodegradation of E2 in the presence of EDDS was studied with KSF at 1 g L^{-1}, initial concentration of E2 of 5 μM, EDDS concentration of 250 μM. As shown in Figure IV-D-9, the photodegradation of E2 was strongly dependent on the pH. Obviously, the optimal initial pH value for the photodegradation of E2 was 6.0. At pH lower than 6.0, the initial degradation rate of E2 was higher at pH 6.0 than pH 5.0 than pH 3.0 and than pH 4.0. At pH higher than 6.0, the initial degradation rate of E2 decreased with increasing the pH. However, we shown that the initial photodegradation rate of E2 was higher at higher pH in Fe(III)-EDDS complex solutions. EDDS could not just form complex with iron in the solutions, if there is an excess of EDDS, but also adsorb on the KSF surface and dissolve iron in solution. As shown in Figure IV-D-10, the amount of Fe(tot) at pH 3 in the KSF suspensions with EDDS before irradiation is about two times more than that in the KSF suspensions without EDDS. But the amount of Fe(II) is almost the same in these two conditions, which means that the dissolved iron is present as Fe(III) (Figure IV-D-11). And at lower pH there are more iron dissolved in the KSF solutions. So it is observed that the photodegradation of E2 was decreased at pH higher than 6. The reason for the degradation rate of E2 at pH 3 higher than that at pH 4 maybe due to the higher concentration of Fe(III) and Fe(II) formation at pH 3. During the irradiation, the concentration of EDDS was also detected. As shown in Figure IV-D-12, the degradation of EDDS was very fast at the first 20 minutes and then stopped. Except at pH 9 the degradation of EDDS was a little slower than that at other pHs, no obvious differences were found at different pH for the loss of EDDS.

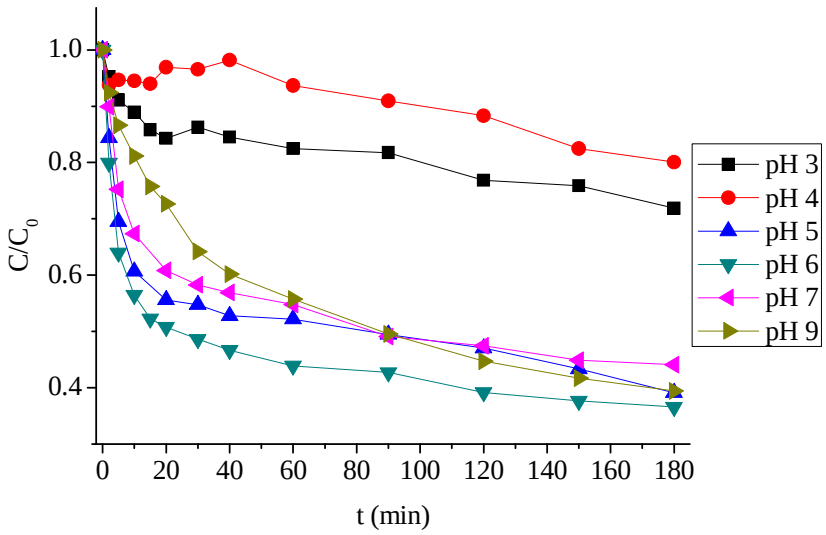

Figure IV-D-9 Influence of pH on the photodegradation of E2 in KSF suspensions in the presence of EDDS. The experimental conditions were as follows: [KSF] = 1 g L^{-1}, [E2] = 5 µM, [EDDS] = 250 µM, irradiation time 3 h.

Figure IV-D-13 indicated the comparison of the photodegradation of E2 without EDDS and with EDDS in KSF solutions. At pH 3.0 and 4.0, the photodegradation of E2 is strongly higher with the addition of EDDS in the solutions, especially at pH 3.0. At pH higher than 5.0, the photodegradation of E2 is also increased significantly in the presence of EDDS. Without EDDS, the optimal pH for the degradation of E2 was around 3.0. With EDDS in the KSF suspensions, the optima pH for the degradation of E2 was shift to the circumneutral pH and the degradation efficiency at basic pH was also very good. Thus, adding EDDS to the KSF suspensions, extended the pH for the degradation in this photochemical system is a way to remove the contaminants present in the natural aquatic environments.

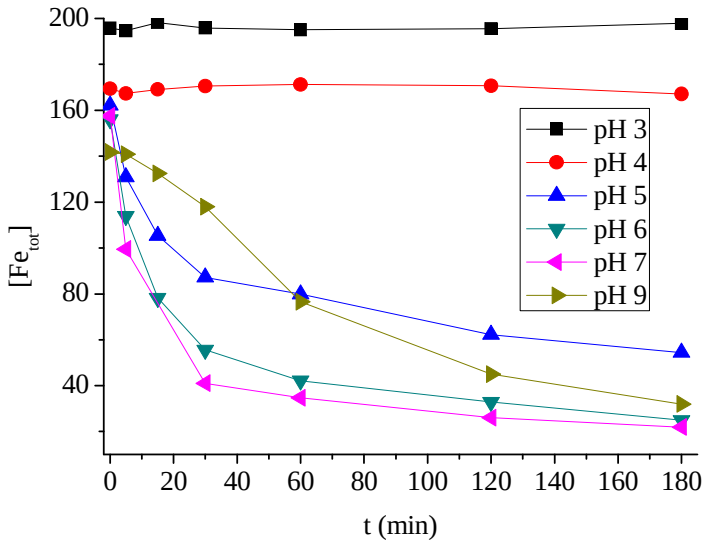

Figure IV-D-10 Concentration of Fe(tot) during the irradiation ([KSF] = 1 g L^{-1}, [E2] = 5 µM, [EDDS] = 250 µM, irradiation time 3 h).

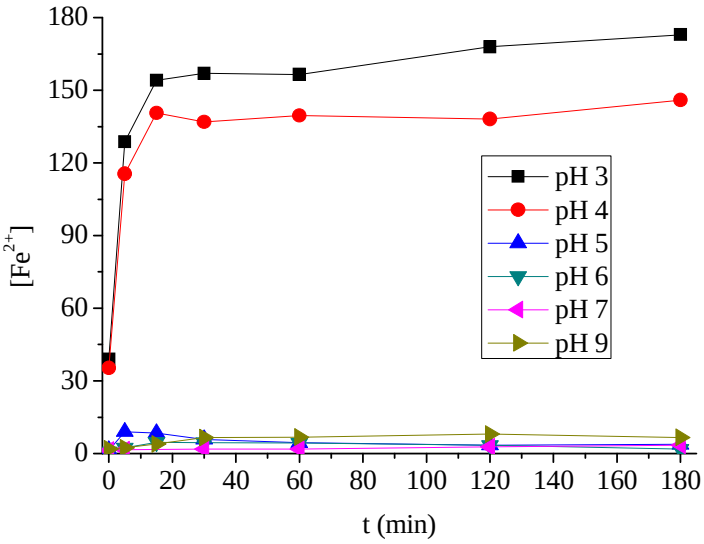

Figure IV-D-11 Concentration of Fe(II) during the irradiation ([KSF] = 1 g L^{-1}, [E2] = 5 µM, [EDDS] = 250 µM, irradiation time 3 h).

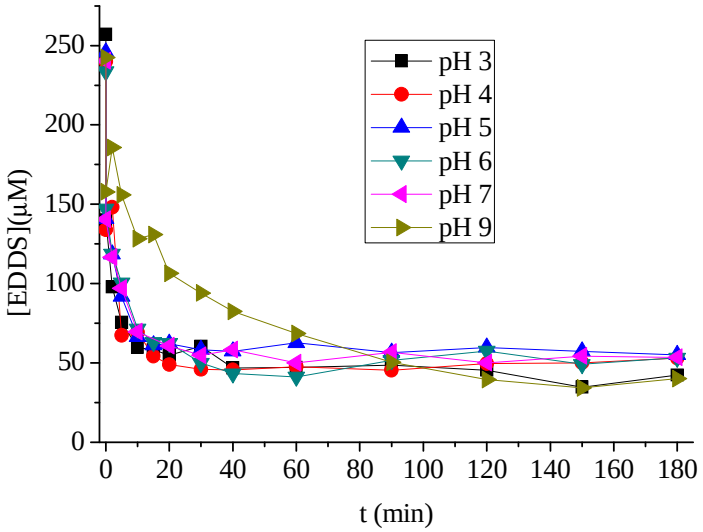

Figure IV-D-12 Concentration of EDDS during the irradiation ([KSF] = 1 g L^{-1}, [E2] = 5 µM, [EDDS] = 250 µM, irradiation time 3 h).

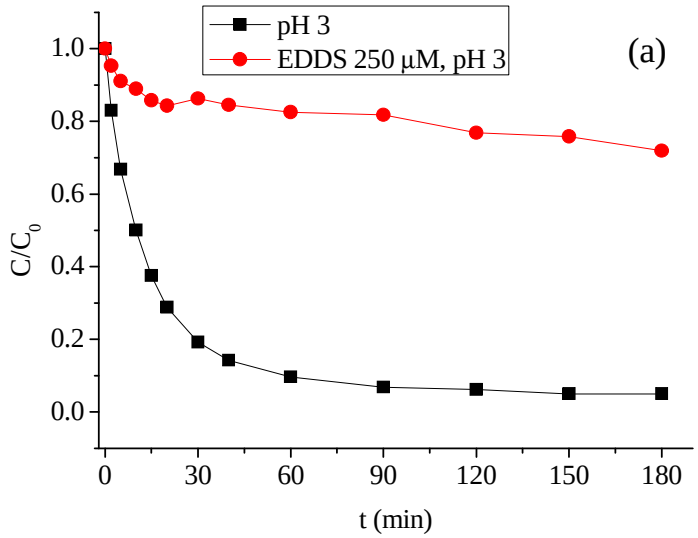
pH 3
EDDS 250 µM, pH 3
(a)
C/C0
1.0
0.8
0.6
0.4
0.2
0.0
0
30
60
90
120
150
180
t (min)

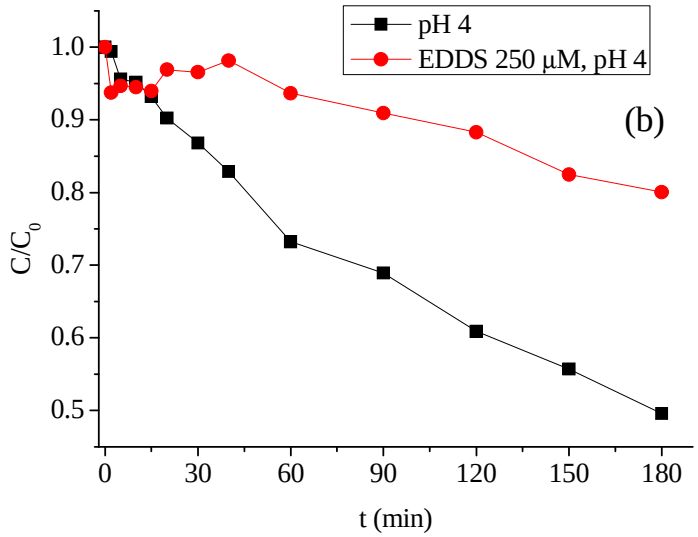
pH 4
EDDS 250 µM, pH 4
(b)
C/C0
1.0
0.9
0.8
0.7
0.6
0.5
0
30
60
90
120
150
180
t (min)

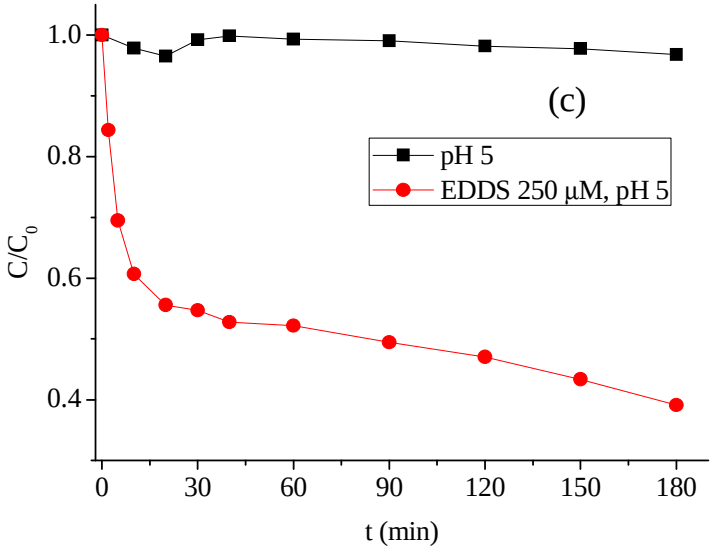
1.0
0.8
0.6
0.4
C/C0
(c)
pH 5
EDDS 250 µM, pH 5
0
30
60
90
120
150
180
t (min)

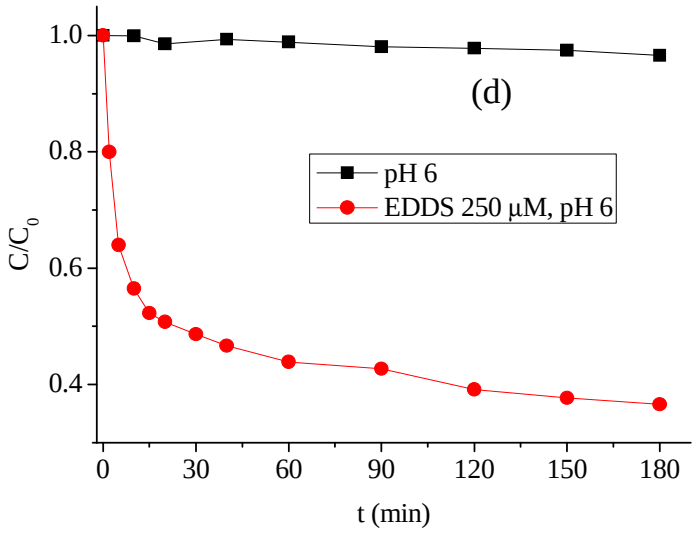
1.0
0.8
0.6
0.4
C/C0
(d)
pH 6
EDDS 250 µM, pH 6
0
30
60
90
120
150
180
t (min)

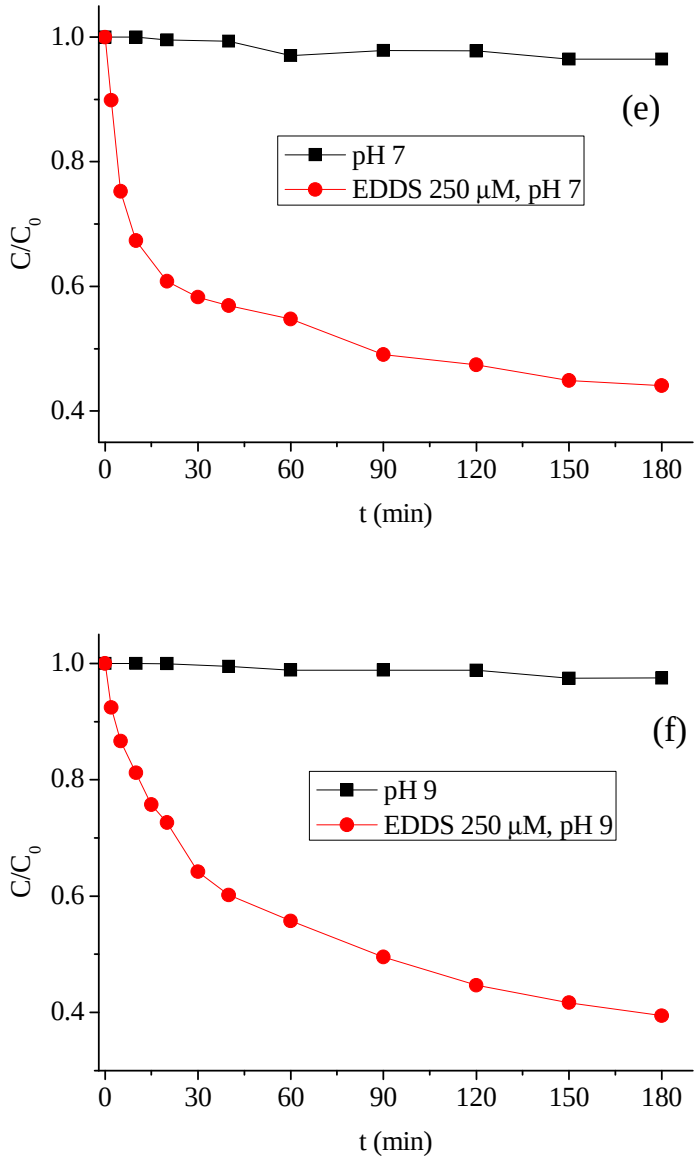

Figure IV-D-13 Comparison of the photodegradation of E2 with and without EDDS at different pHs. (a): pH 3; (b) pH 4; (c) pH 5; (d) pH 6; (e) pH 7; (f) pH 9 ([KSF] = 1 g L^{-1}, [E2] = 5 µM, [EDDS] = 250 µM, irradiation time 3 h).

D-3-3 Effect of EDDS concentration on the degradation of E2

EDDS plays a crucial role in photochemical system with KSF. To study the effect of EDDS on the photodegradation of E2, a set of experiments were performed with KSF 1 g L^{-1}, E2 5 µM, pH 6.0, and different initial concentrations of EDDS in the range of 0 - 5 mM. As shown in Figure IV-D-14, it is very obvious that the presence of EDDS could greatly enhance the E2 photodegradation in KSF suspensions at pH 6.0. The results showed that E2 degradation

was significantly increased with the increase of EDDS concentration in its low range, but it was slightly inhibited with an excessive amount of EDDS. EDDS could form complexes with iron as Fe(III)-EDDS complex which is more photoreactive for producing hydroxyl radicals under irradiation. Also, it has been reported that iron oxide in clay minerals could dissolve more easily in the presence of carboxylates under irradiation (Goldberg *et al.*, 1993; Waite and Morel, 1984). So, the degradation efficiency of E2 was enhanced when greater amounts of photoactive iron ions were present in the KSF suspensions. However, excessive EDDS would also act as scavengers of hydroxyl radicals and then compete with E2 for $^{\bullet}OH$ reactivity. As shown in Figure IV-D-15, more EDDS was degraded with higher initial concentration of EDDS. Therefore, when the concentration of EDDS is high enough (of the order of 1 mM), the photodegradation rate of E2 starts to be inhibited.

During the irradiation, the concentration of Fe(tot) and Fe(II) was also detected. At pH 6.0, the main soluble forms of iron in the suspension must be Fe(III)-EDDS complex. So, the initial concentration of Fe(tot) detected in the KSF suspension increased with the concentration of EDDS in the range of 0 - 5000 μM (Figure IV-D-16). During the irradiation, with the lost of EDDS which could stabilize the iron in the solutions, the concentration of Fe(tot) was decreased. The amount of Fe(II) detected in the solution during the irradiation is very low (Figure IV-D-17), which may be due to the more easily oxidation of Fe(II) to Fe(III) at high pH.

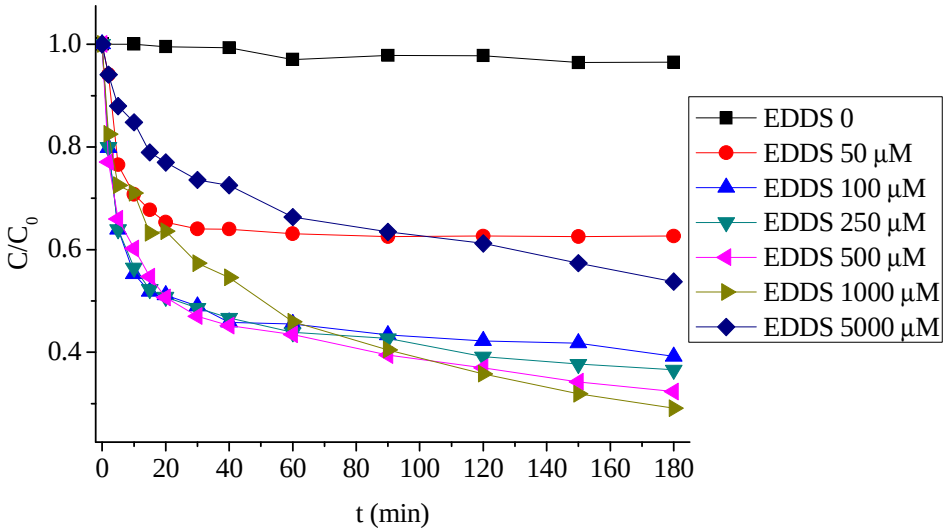

Figure IV-D-14 Influence of EDDS concentration on the photodegradation of E2 in KSF solutions in the presence of EDDS. The experimental conditions were as follows: [KSF] = 1 g L^{-1}, [E2] = 5

µM, pH 6.0, irradiation time 3 h.

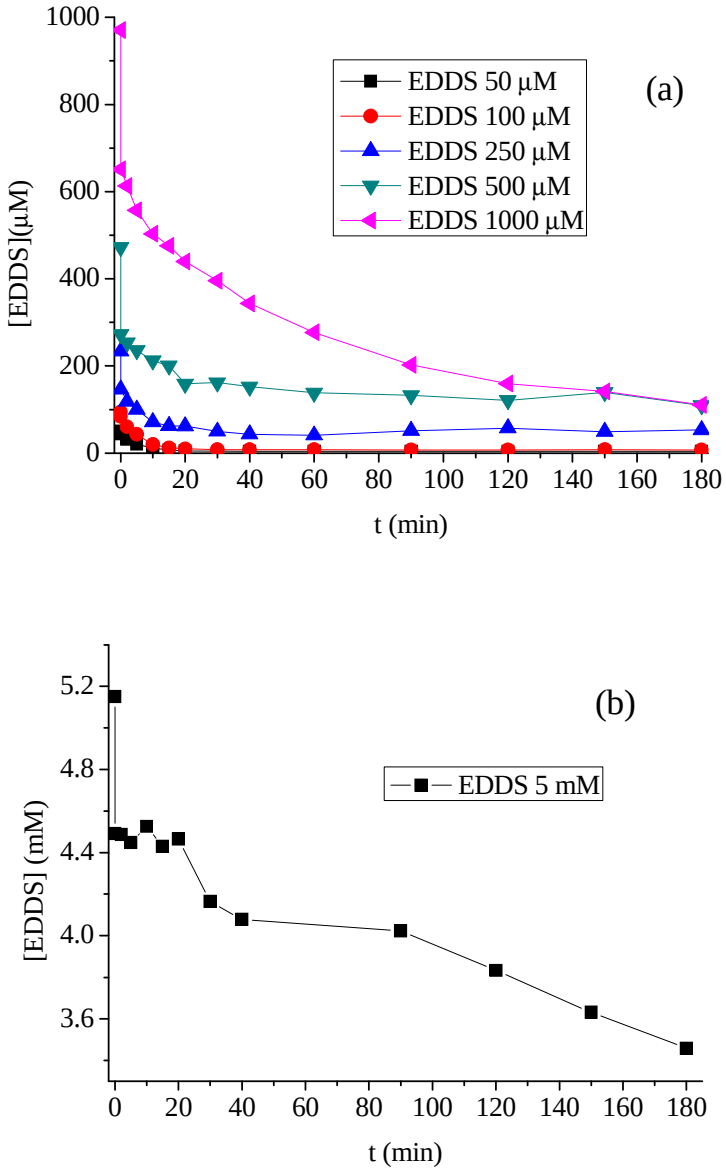

Figure IV-D-15 Concentration of EDDS during the irradiation ([KSF] = 1 g L^{-1}, [E2] = 5 µM, pH 6.0, irradiation time 3 h).

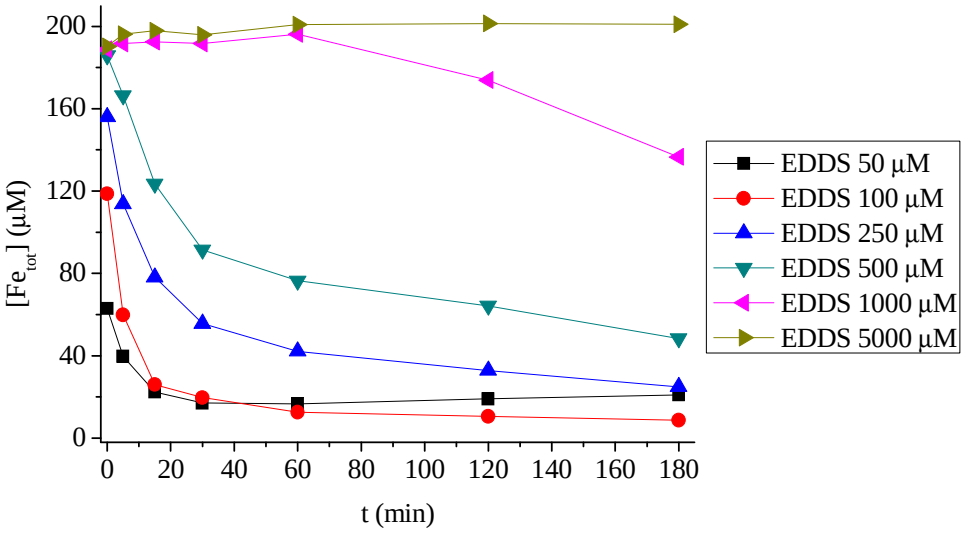

Figure IV-D-16 Concentration of Fe(tot) during the irradiation ([KSF] = 1 g L^{-1}, [E2] = 5 µM, pH 6.0, irradiation time 3 h).

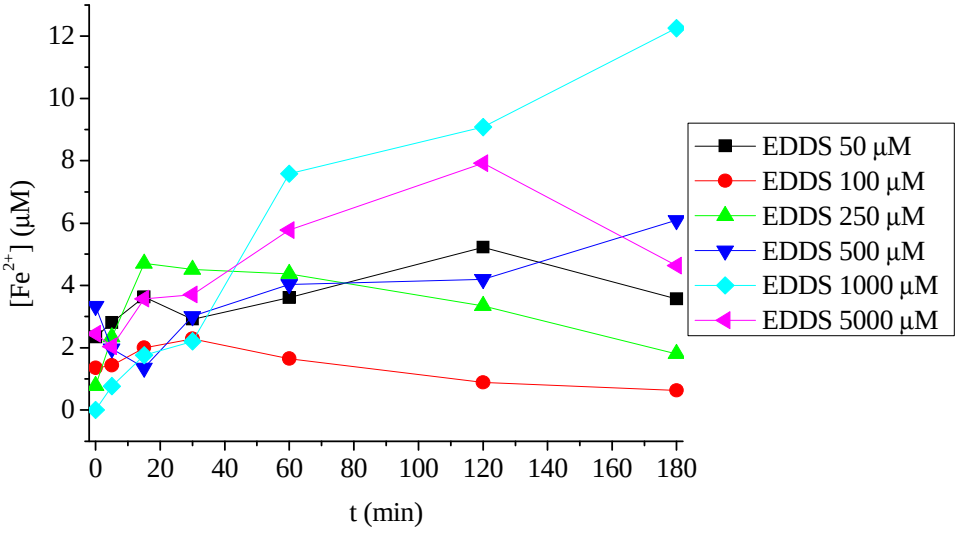

Figure IV-D-17 Concentration of Fe(II) during the irradiation ([KSF] = 1 g L^{-1}, [E2] = 5 µM, pH 6.0, irradiation time 3 h).

D-3-4 Effect of oxygen on the degradation of E2

Oxygen generally is an important parameter in the photochemical process. Experiments were carried out to study the oxygen effects on the photodegradation of E2. Different conditions were used by bubbling oxygen or nitrogen 30 minutes into the solutions before irradiation. As shown in Figure IV-D-18, in the deaerated solution (N_2), the

photodegradation rate of E2 was much lower compared to that in the presence of oxygen. Oxygen can enhance the photolysis of Fe(III)-Carboxylate complexes by trapping the electron on the carbon centered radical formed after the photoredox process. Then the formed $O_2^{\bullet-}$ radicals rapidly react to yield H_2O_2 and finally leads to the formation of hydroxyl radical. Thus oxygen is quite necessary to produce the reactive species that cause E2 degradation. The slight loss of E2 under nitrogen might be due to the presence of some O_2 traces in the solution, since the experimental set-up used did not allow to work under 100% deaerated conditions.

During the irradiation, the concentration of Fe(tot) decreased. The decrease is faster in the present of oxygen (Figure IV-D-19). It corresponds to the decrease of EDDS concentration during the irradiation (Figure IV-D-20). Although there would be more Fe(III)-EDDS in the solution under nitrogen, the hydroxyl radicals can not be formed without oxygen.

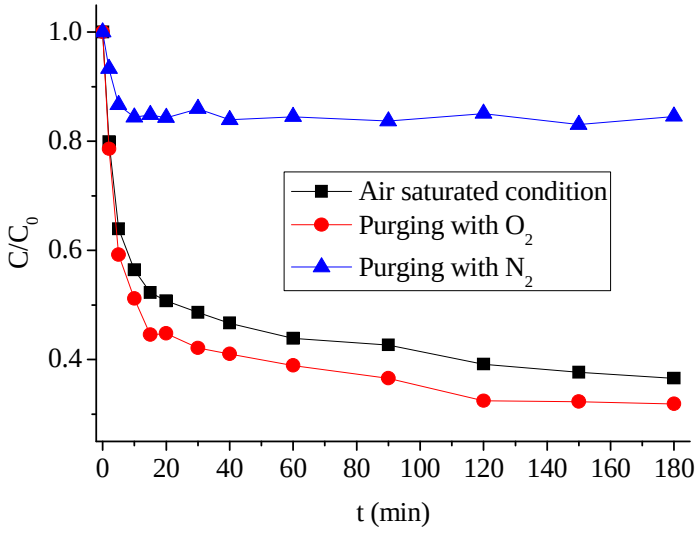

Figure IV-D-18 Influence of oxygen on the photodegradation of E2 in KSF solutions in the presence of EDDS. The experimental conditions were as follows: [KSF] = 1 g L^{-1}, [EDDS] = 250 µM, [E2] = 5 µM, pH = 6.0, irradiation time 3 h.

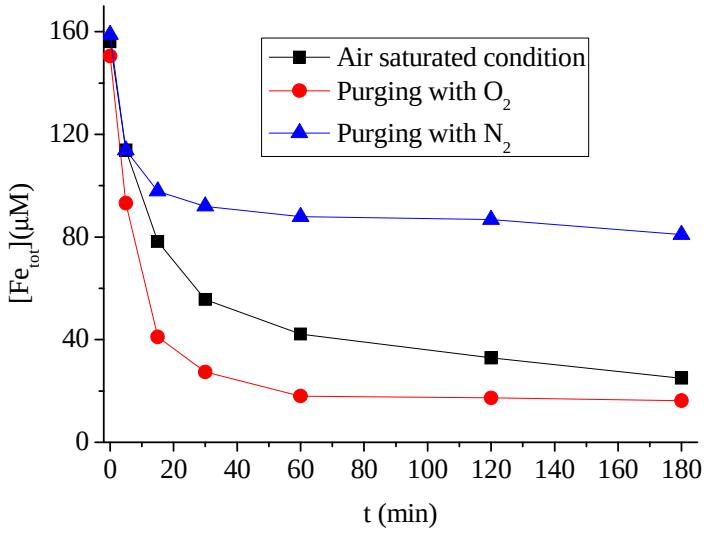

Figure IV-D-19 Concentration of Fe(tot) during the irradiation ([KSF] = 1 g L^{-1}, [EDDS] = 250 μM, [E2] = 5 μM, pH = 6.0, irradiation time 3 h).

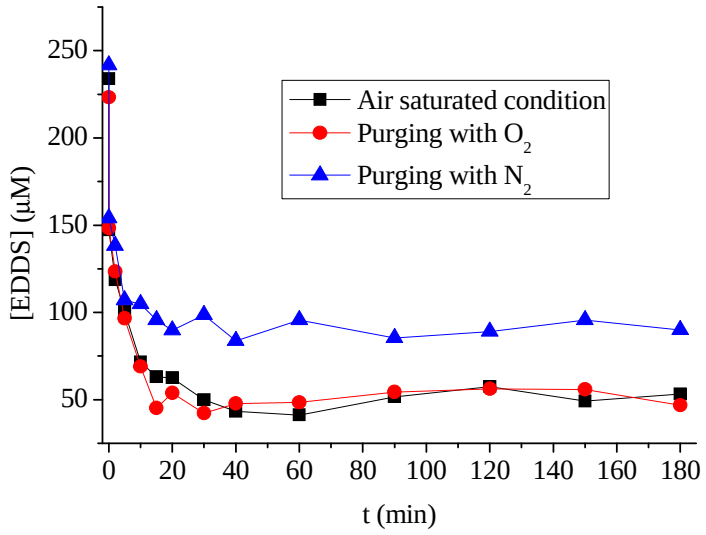

Figure IV-D-20 Concentration of EDDS during the irradiation ([KSF] = 1 g L^{-1}, [EDDS] = 250 μM, [E2] = 5 μM, pH = 6.0, irradiation time 3 h).

D-3-5 Effect of 2-propanol on the degradation of E2

The effect of 2-propanol on the degradation of E2 was studied with KSF 1 g L^{-1}, EDDS 250 μM, E2 5 μM, 0.1% 2-propanol and pH 6.0. As shown in Figure IV-D-21, only 6% of E2 is degraded in the presence of 0.1% of 2-propanol after 3 h of irradiation. In contrast, E2 degradation occurred rapidly in the absence of 2-propanol under the same conditions.

2-propanol is a very effective •OH scavenger. This result indicated that in the KSF-EDDS system, the main degradation pathway of E2 is due to the attack by •OH.

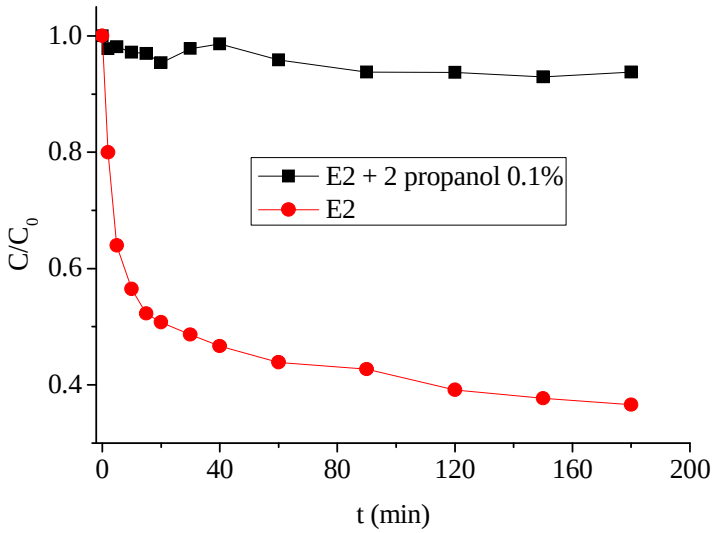

Figure IV-D-21 Influence of 2-propanol on the photodegradation of E2 in KSF solutions in the presence of EDDS. The experimental conditions were as follows: [KSF] = 1 g L^{-1}, [EDDS] = 250 μM, [E2] = 5 μM, pH 6.0, irradiation time 3 h.

D-3-6 Effect of initial concentration of E2

Under the conditions of 1 g L^{-1} KSF, EDDS 250 μM and at pH 3.8, the effect on photodegradation of the initial E2 concentration in the range of 0.94 to 12.93 μM was analyzed. Figure IV-D-22 shows the concentration profile variation of E2 at different initial concentrations in KSF-EDDS suspensions. The initial rates of the reaction were determined by extrapolating the tangent (based on the linear fit of the first four points) of the concentration profile back to initial conditions. The slopes calculated at the initial three to five points were almost identical, indicating the accuracy of the initial rates obtained in this study.

It is well known that heterogeneous photocatalytic degradation of organic pollutants follows Langmuir-Hinshelwood (L-H) kinetics (Alaton and Balcioglu, 2001).

$$R = -\frac{dC}{dt} = \frac{kKC}{1+KC} \qquad (1)$$

Where C is the concentration of the organic compound at time t, and *k* and *K* are rate constant and the adsorption coefficient respectively. As shown in table IV-D-1, the initial

rates of E2 degradation increased with increasing the initial concentrations of E2 and the initial reaction rate and initial concentration fitted well into the L-H equation. *k* and *K* are calculated to be 3.591 μmol·L^{-1}·min^{-1}and 0.0199 L·μmol^{-1} respectively.

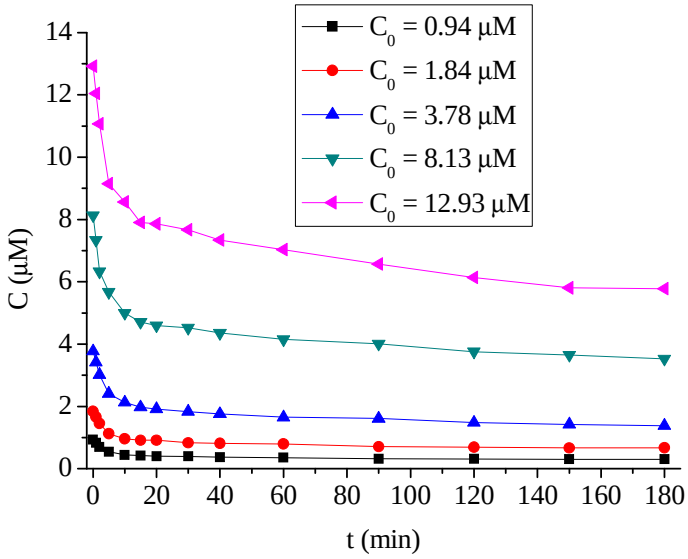

Figure IV-D-22 Influence of the initial concentration of E2 on E2 photodegradation in the KSF suspensions in the presence of EDDS. The experimental conditions were as follows: initial concentration of E2: 0.94, 1.84, 3.78, 8.13, and 12.93 μmol·L^{-1}, [KSF] = 1.0 g L^{-1}, [EDDS] = 250 μM, irradiation time 3 h, pH = 6.0.

Table IV-D -1 Initial rates at different initial concentration of E2

C (μmol·L^{-1})	Initial rate (μmol·L^{-1}·min^{-1})	Kinetic equation □L-H□	Reaction rate constant *k* (μmol·L^{-1}·min^{-1})
0.94	0.0765	$R = \frac{0.0714C}{1+0.0199C}$	
1.84	0.141		
3.78	0.266		3.591
8.13	0.470	(R^2=0.995)	
12.93	0.746		

Conclusions

The photodegradation of E2 in aqueous solutions catalyzed by KSF with or without EDDS was studied. In the KSF suspensions, the optima pH for the degradation of E2 was limited around 3. In the KSF-EDDS suspensions, the optima pH for the degradation of E2 was shift to the circumneutral pH and the degradation efficiency at basic pH was also very good. Thus,

the KSF-EDDS photochemical system is a promising way for the removal of contaminants in the natural aquatic environments. In the KSF-EDDS system, the degradation kinetics of E2 follows the Langmuir-Hinshelwood rate law. The initial photodegradation rate of E2 was studied with different KSF concentrations in the range of 0 - 1.0 g L^{-} in the presence of 250 μM of EDDS. The final efficiency of E2 photodegradation was in this order for KSF concentration 0.1 g L^{-1} > 0.4 g L^{-1} > 1 g L^{-1} ≈ 0.05 g L^{-1}. Thus, the appropriate concentration of KSF needs to be fixed according to the experimental conditions. E2 degradation was significantly increased with the increased of EDDS concentration in its low range, but it was slightly inhibited with an excessive amount of EDDS. Oxygen is a key factor influencing the reactive species formation. Without oxygen, the E2 degradation is obviously depressed. Thus the concentration of KSF and EDDS, solution pH and oxygen must be taken into account as major parameters to improve the efficiency of the KSF-EDDS process.

IV-E Degradation of E2 photoinduced by NM and NM-EDDS

E-1 Adsorption of E2 on NM

The adsorbed amounts of E2 on the NM at the first 30 min were approaching 95% of the amounts of adsorption equilibrium at 24 h, implying that the adsorption rates are quite fast during the first 30 min and it can be used as a preliminary adsorption time prior to photoreaction.

Figure IV-E-1 shows the adsorption isotherms of E2 on the NM at pH 5.0. Both of the Langmuir model for monolayer adsorption and the Freundlich model for multilayer adsorption were applied to fit the experimental data. It was found that the Freundlich model described the adsorption of E2 well. The Freundlich adsorption isotherm is $\log C_{is} = \log K_f + (1/n) \log C$, where C_{is} is the amount of E2 adsorbed on the NM, C is the concentration of E2 in the NM suspensions after equilibration; K_f is adsorption capacity; n is the adsorption intensity. Freundlich adsorption isotherm and the calculated fitting parameters are presented in Figure IV-E-2 and Table IV-E-1 respectively. It can be seen from Figure IV-E-2 that the adsorption of E2 on the NM with EDDS was a little more than that without EDDS. That is because the adsorption of EDDS increased the amount of organic carbon in the interlayer of NM, which is in favor to the adsorption of E2. However, the adsorption amount of E2 with 1 mM EDDS was less than that with 0.25 mM EDDS, which maybe due to the competitive

adsorption between EDDS and E2, when the concentration of EDDS is so high.

The adsorption isotherm of EDDS alone by 6 g L^{-1} NM at pH 5.0 is shown in Figure IV-E-3. The Langmuir model described the adsorption of EDDS well. The Langmuir model is shown as

$$C_{is} = \frac{K_{eq} b C}{1 + K_{eq} C}$$

Where, C is the concentration in the clay solution after equilibration; C_{is} is the amount adsorbed on the clay; K_{eq} is the equilibration constant and b is the maximum amount adsorbed on the clay). Fitting the L equation, K_{eq} and b are calculated to be 0.05437 L μmol^{-1} and 4.73 $\mu mol\ g^{-1}$.

The adsorption of E2 on NM influenced by the pH was also detected. As shown in Figure IV-E-4, the adsorption of E2 decreased with increasing the pH. The acid pH is in favor to the adsorption of E2. Montmorillonite bears a large permanent negative charge, so the main factor affecting the changes in adsorption to be the effect of pH on surface charge. NM has a PZC lower than 3. The pKa of E2 was 10.4. E2 would be ionized to the phenoxide and also the surface of NM is deprotonated to the negative ions causing repulsion with substrate when pH > pHzpc, especially pH > 10 (pKa of E2).

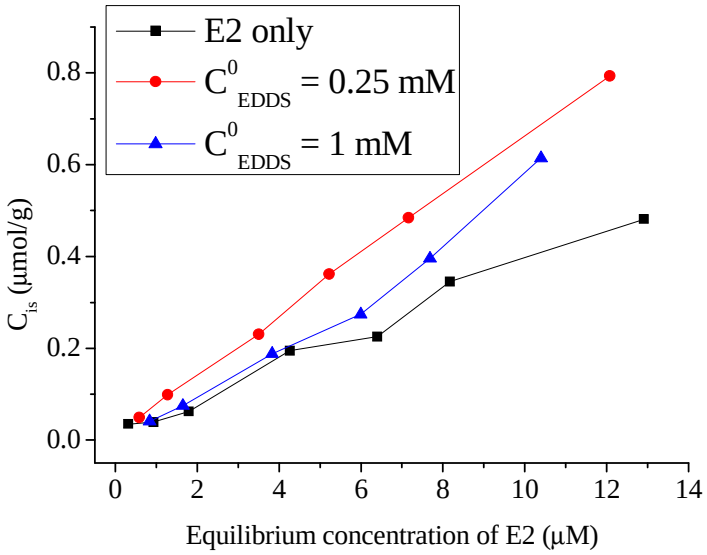

Figure IV-E-1 Adsorption isotherm of E2 in suspensions of 6 g L^{-1} of NM in the absence and in the presence of different concentration of EDDS (pH = 5.0).

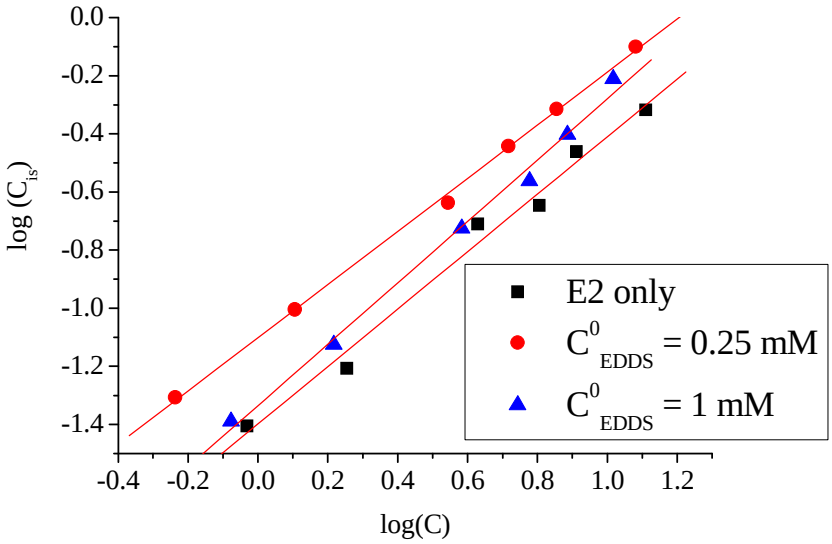

Figure IV-E-2 Freundlich adsorption isotherm in suspensions of 6 g L^{-1} of NM in the absence and in the presence of different concentration of EDDS (pH = 5.0).

Table IV-E-1 Relevant fitting parameters for Figure IV-E-2

	Equation	R	K_f
EDDS 0	$Log(C_{is}) = -1.3981 + 0.9885 \log (C)$	0.993	0.03998
EDDS 0.25 mM	$Log(C_{is}) = -1.1014 + 0.9139 \log (C)$	0.999	0.07918
EDDS 1 mM	$Log(C_{is}) = -1.3351 + 1.0561 \log (C)$	0.997	0.04623

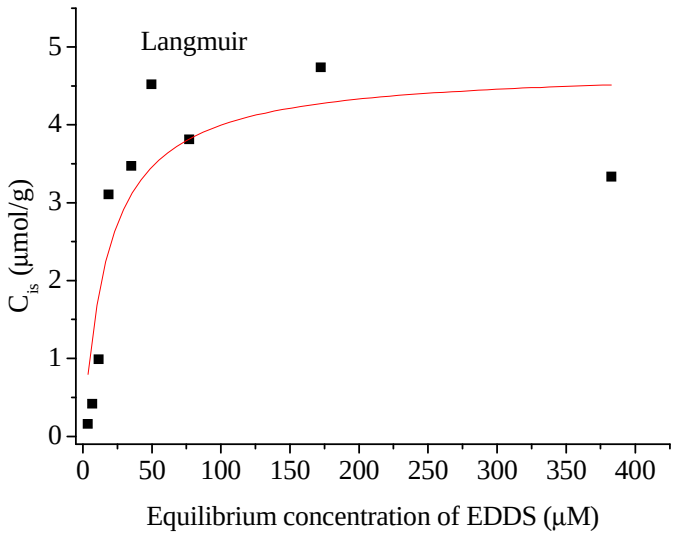

Figure IV-E-3 Adsorption isotherm of EDDS in suspensions of 6 g L^{-1} of NM (pH = 5.0).

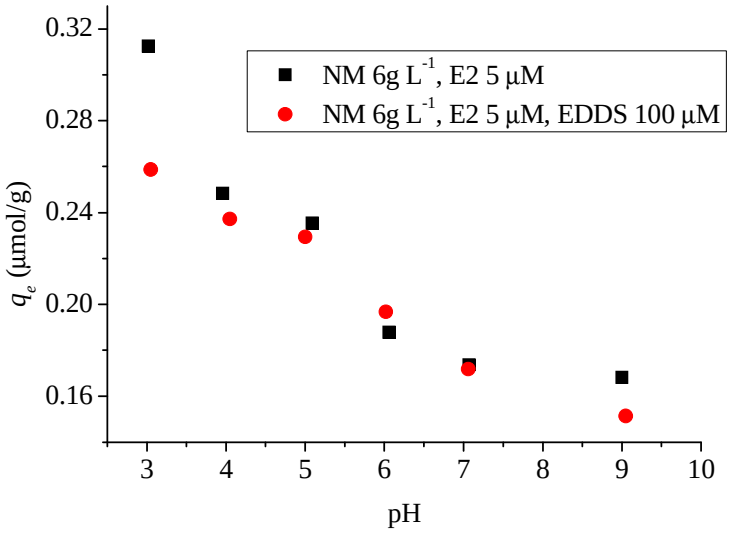

Figure IV-E-4 Influence of pH on the adsorption of E2.

E-2 Photodegradation of E2 in the NM suspensions

The photodegradation of E2 was studied in the NM suspensions. Irradiation was with polychromatic tubes emitting between 300 and 500 nm. Effect of concentration of NM and pH were studied in this work. Under our experimental conditions and in the dark, no degradation of E2 was observed in the absence and in the presence of NM. Similarly, there was no photodegradation of E2 without NM under irradiation.

E-2-1 Effect of the clay concentration on the photodegradation of E2

Figure IV-E-5 shows the photodegradation of E2 under different NM concentrations. Obviously, without NM, no degradation of E2 was found. The degradation of E2 increased with increasing the concentration of NM in aqueous solutions in the range of 1 - 6.0 g L^{-1}. This is due to increase in the number of NM particles, which increases the quantity of photoreactive species in clays and the number of the E2 molecules adsorbed. However, when the NM concentration increases from 6 to 8 g L^{-1} the degradation of E2 was inhibited. Increase of the NM concentration beyond 6 g L^{-1} may cause light scattering and screening effects, which reduce the photocatalytic activity of the catalyst (Lea and Adesina, 1998). In our experimental conditions, the optimal concentration of NM was 6 g L^{-1}.

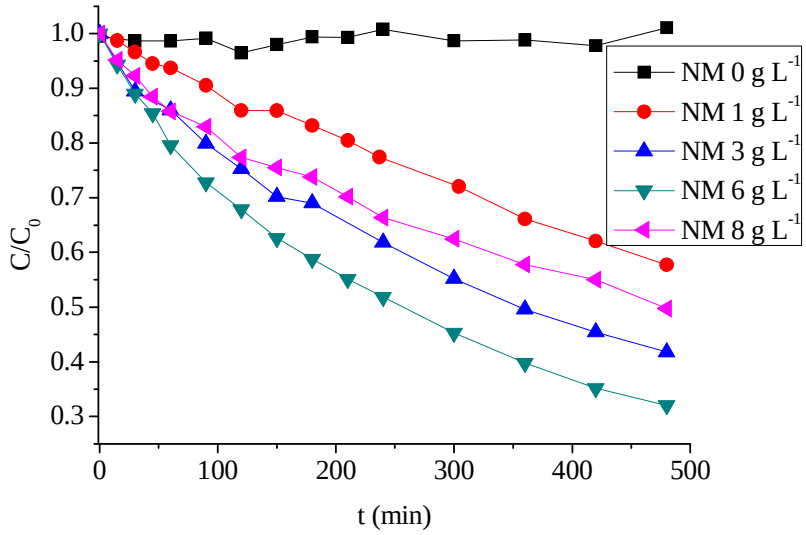

Figure IVE-5 Influence of NM concentration on the photodegradation of E2 in aqueous solutions. The experimental conditions were as follows: [E2] = 5 μM, irradiation time 8 h, pH = 3.0.

E-2-2 Effect of pH on the photodegradation of E2

Figure IV-E-6 shows E2 degradation at various pH values in irradiated suspensions containing initially 6 g L^{-1} of NM and 5 μM of E2. The degradation efficiency of E2 was maximal at pH 3 and decreased above and below this pH value gradually. NM contains 4.28% of the iron component. But not like KSF, the most of iron oxides is structural iron in the octahedral lattice. At pH higher than 3, no iron in the solution was detected. At pH 3, there is just very small amount of iron detected in the suspensions (Figure IV-E-7). As we know that the most photoactive ferric ion species, $Fe(OH)^{2+}$ is more abundant at pH 3.0, which could lead to the formation of $^{\bullet}OH$. Therefore, although the amount of iron in NM suspension is very low, the pH effect reflects that iron present in NM should be the most important photochemical source. But except iron, the degradation of E2 maybe attribute to the reactions at the NM surface.

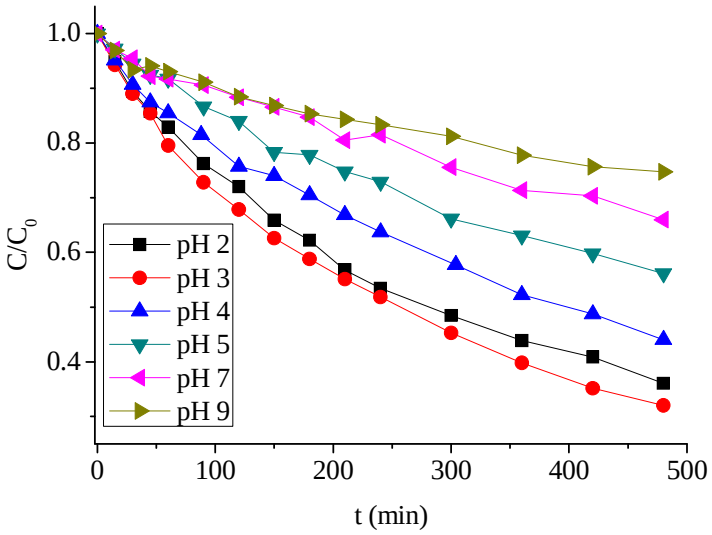

Figure IV-E-6 Influence of pH on the photodegradation of E2 in aqueous solutions containing NM. The experimental conditions were as follows: NM = 6 g L^{-1}, [E2] = 5 µM, irradiation time 8 h.

At the meantime, the pH value was simultaneously determined under the same conditions. The variations of pH versus reaction time are plotted in Figure IV-E-8. The results showed that the pH increased very fast at the first 20 minutes and then keep at constant under irradiation.

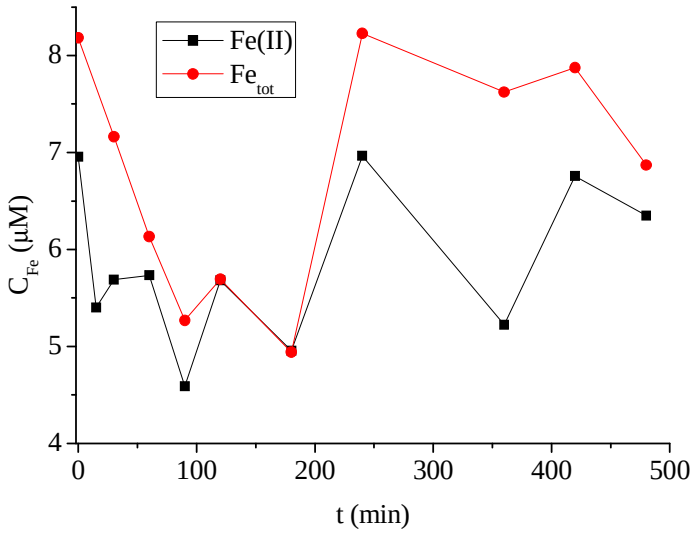

Figure IV-E-7 Concentration of Fe(II) and Fe(tot) during the irradiation ([NM = 6 g L^{-1}, [E2] = 5 µM, pH = 3.0)

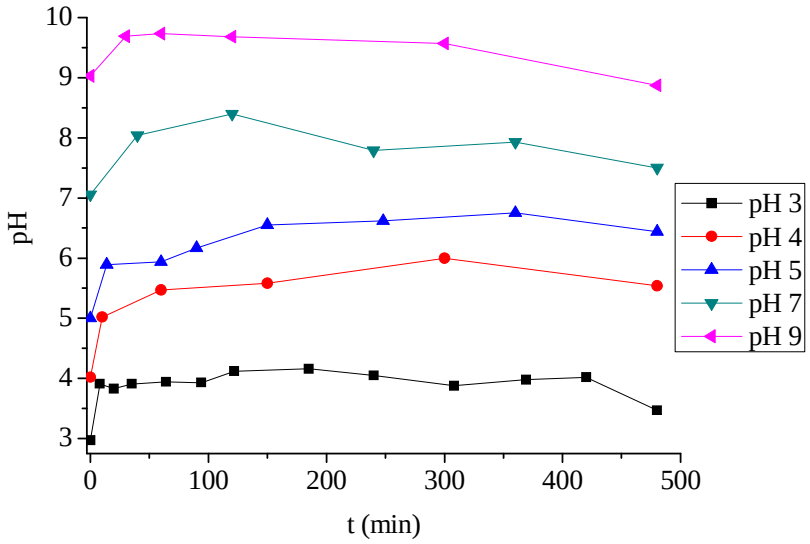

Figure IV-E-8 Change of pH during the irradiation at different starting pHs.

E-3 Photodegradation of E2 in NM-EDDS suspensions

The photodegradation of E2 was studied in the NM solutions in the presence of EDDS. Irradiation was performed with polychromatic tubes emitting between 300 and 500 nm. Effect of NM, EDDS, oxygen, 2-propanol and E2 concentrations and pH were all studied in this work. Under our experimental conditions and in the dark, no degradation of E2 was observed in the absence and in the presence of NM-EDDS. Similarly, there was no photodegradation of E2 without NM-EDDS under irradiation.

E-3-1 Effect of NM concentration on the photodegradation of E2

Figure IV-E-9 shows E2 degradation at various NM concentration in irradiated suspensions containing initially 5 μM of E2, 250 μM of EDDS at pH = 5.0. The initial degradation rate of E2 was increased with increasing the concentration of NM from 0.1 g L^{-1} to 10 g L^{-1}. However, the final degradation efficiency after 8 h of irradiation has the opposite trend. With the higher concentration of NM, there is more Fe(III)-EDDS complex formed in the solutions or on the NM surface, which induced the faster initial degradation rate of E2. But with the faster degradation of E2, in the same time, EDDS was also more quickly decomposed. When EDDS is completely decomposed, the photochemical reaction of Fe(III)-EDDS is stopped. So we can see from the Figure IV-E-9 that with the higher

concentration of NM, the photodegradation of E2 is stopped earlier and finally the degradation efficiency is lower. We also need to note that although the maximal concentration of NM used is two orders of magnitude higher than the minimum concentration used, there is no big difference in the degradation efficiency of E2. These results indicated that for removing the organic compounds in the aqueous solutions, small amount of NM is enough to get a good degradation efficiency in the presence of EDDS.

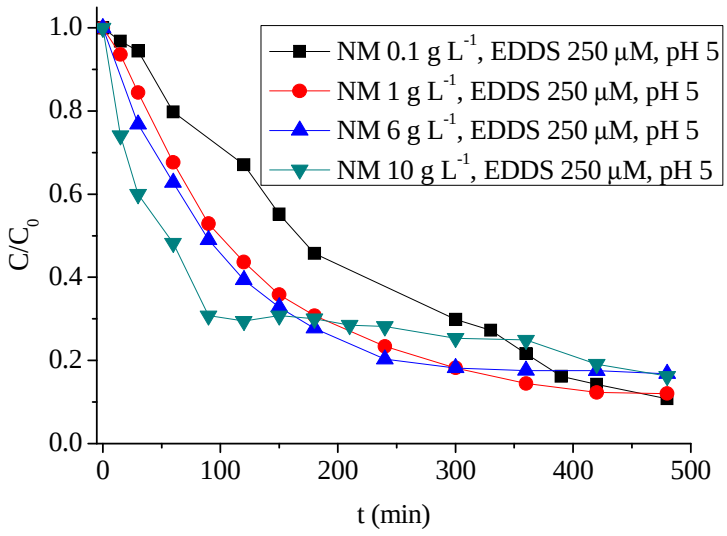

Figure IV-E-9 Influence of NM concentration on the photodegradation of E2 in the presence of EDDS. The experimental conditions were as follows: [E2] = 5 μM, [EDDS] = 250μM, irradiation time 8 h, pH = 5.0.

E-3-2 Effect of EDDS concentration on the degradation of E2

Effect of EDDS concentration on the degradation of E2 was studied with [NM] = 6 g L^{-1}, [E2] = 5 μM, at pH = 5.0 and different concentration of EDDS from 0 to 10000 μM. As shown in Figure IV-E-10, the initial degradation rate of E2 increased with increasing the concentration of EDDS in the range of 0 - 250 μM. After the maximum rate at 250 μM, the degradation rate of E2 was decreased with the concentration of EDDS. The degradation efficiency of E2 after 8 h of the irradiation has the same trend, but the maximum efficiency is achieved at the condition of 500 μM of EDDS. The initial rate and degradation efficiency after 8 hours of irradiation of E2 at different concentration of EDDS was shown in Table IV-E-2.

Table IV-E-2 Initial rate and degradation efficiency after 8 hours of irradiation of E2 at different concentration of EDDS

EDDS Concentration (μM)	0	50	100	250	500	1000	10000
Initial rate (μmol L^{-1} min^{-1})	0.00596	0.01287	0.01792	0.02036	0.01936	0.01583	0.00675
Degradation efficiency after 8 hours of irradiation	43.85%	53.93%	65.77%	83.21%	87.26%	83.60%	54.04%

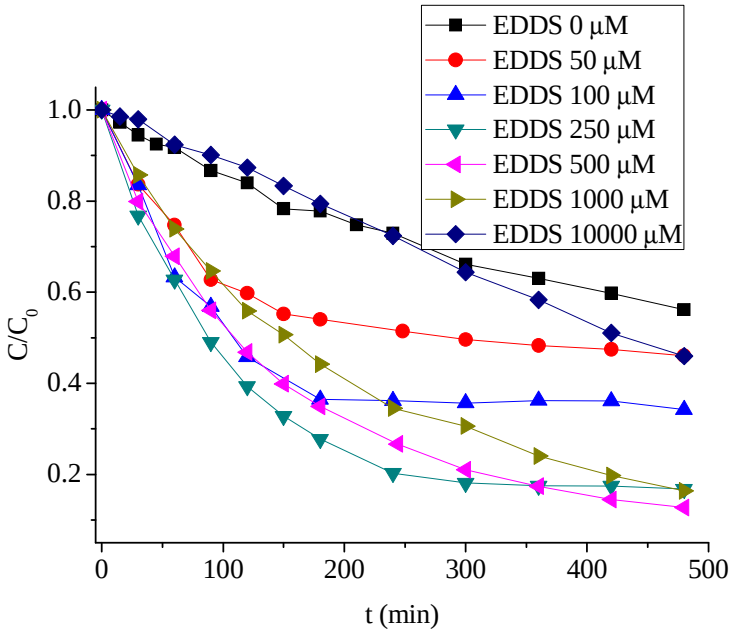

Figure IV-E-10 Influence of EDDS concentration on the photodegradation of E2 in the presence of EDDS. The experimental conditions were as follows: [NM] = 6 g L^{-1}, [E2] = 5 μM, irradiation time 8 h, pH = 5.0

EDDS could complex iron in the NM suspension and in the interlayer. Higher concentration of EDDS leads to the higher concentration of Fe(III)-EDDS complex formed which could undergo rapid photochemical reactions under irradiation leading to the formation of hydroxyl radicals. Also EDDS could react with hydroxyl radicals acting as $^{\bullet}OH$ competitor with E2. During the degradation of E2, EDDS was also degraded. Figure IV-E-11

shows the change of EDDS concentration during the irradiation under the different concentration of EDDS at pH 5. It was found that the photodegradation of EDDS and E2 have the similar trend. Figure IV-E-12 shows the comparison of the photodegradation of EDDS and E2 with different concentration of EDDS. When the degradation of EDDS stopped, the photodegradation of E2 also stopped at the same time. When there were more EDDS in the suspensions, its degradation continued, the photodegradation of E2 also continued. These results indicated that EDDS played a very important role in this photochemical system.

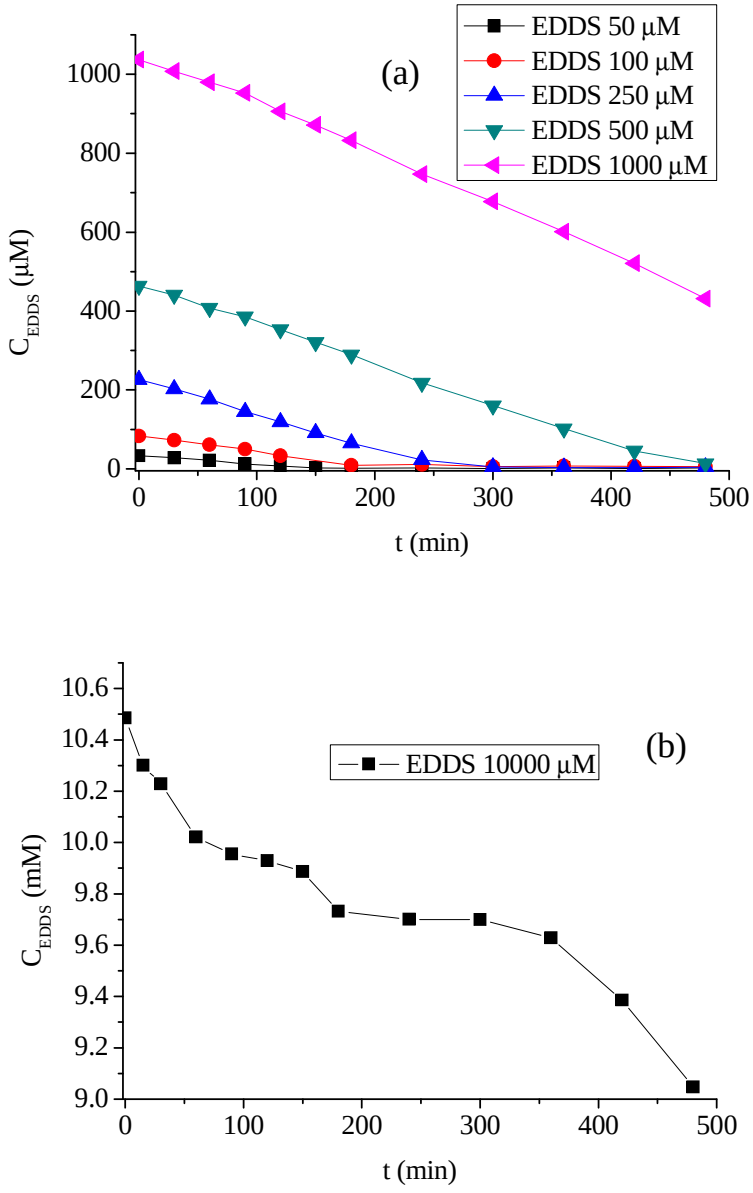

Figure IV-E-11 Change of EDDS concentration during the irradiation under the different concentration of EDDS ([NM] = 6 g L^{-1}, [E2] = 5 μM, irradiation time 8 h, pH = 5.0).

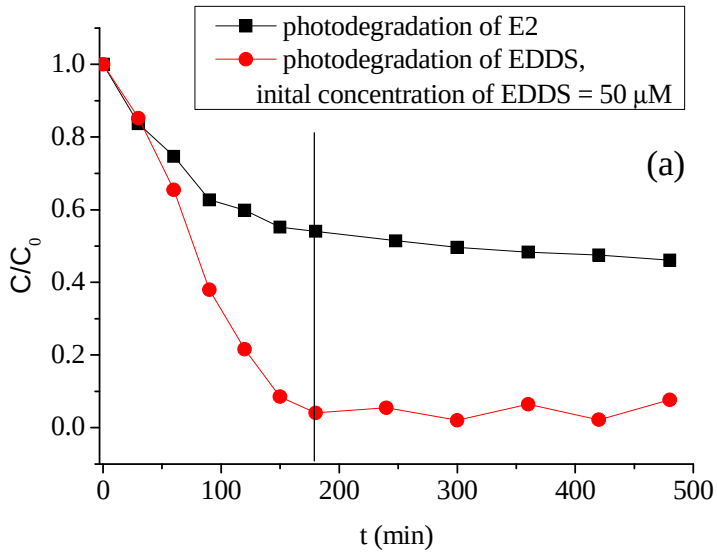
photodegradation of E2
photodegradation of EDDS,
inital concentration of EDDS = 50 μM
(a)
C/C0
t (min)
0.0
0.2
0.4
0.6
0.8
1.0
0
100
200
300
400
500

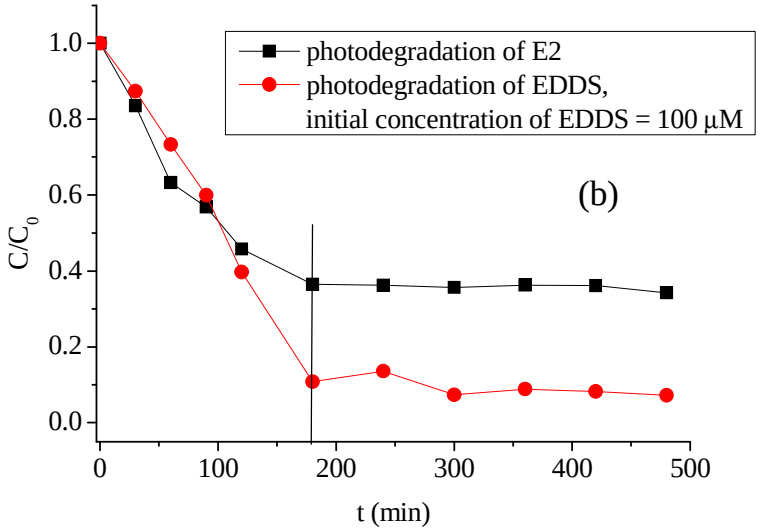
photodegradation of E2
photodegradation of EDDS,
initial concentration of EDDS = 100 μM
(b)
C/C0
t (min)
0.0
0.2
0.4
0.6
0.8
1.0
0
100
200
300
400
500

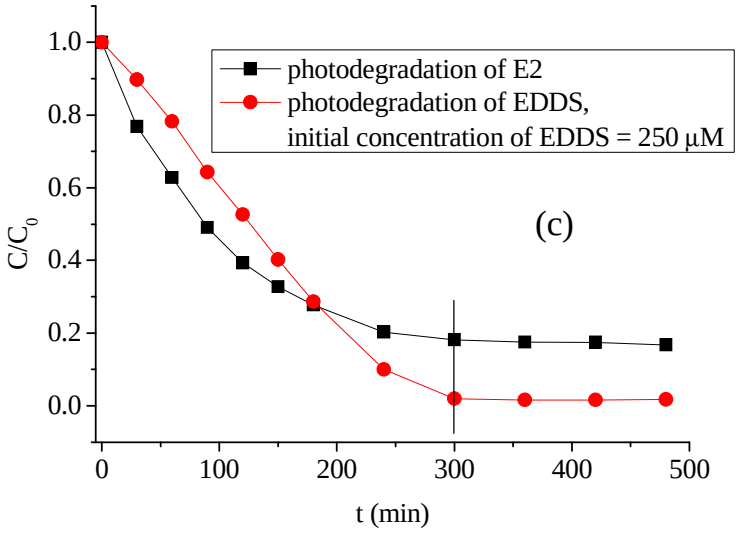
photodegradation of E2
photodegradation of EDDS,
initial concentration of EDDS = 250 μM
(c)
C/C0
t (min)
1.0
0.8
0.6
0.4
0.2
0.0
0
100
200
300
400
500

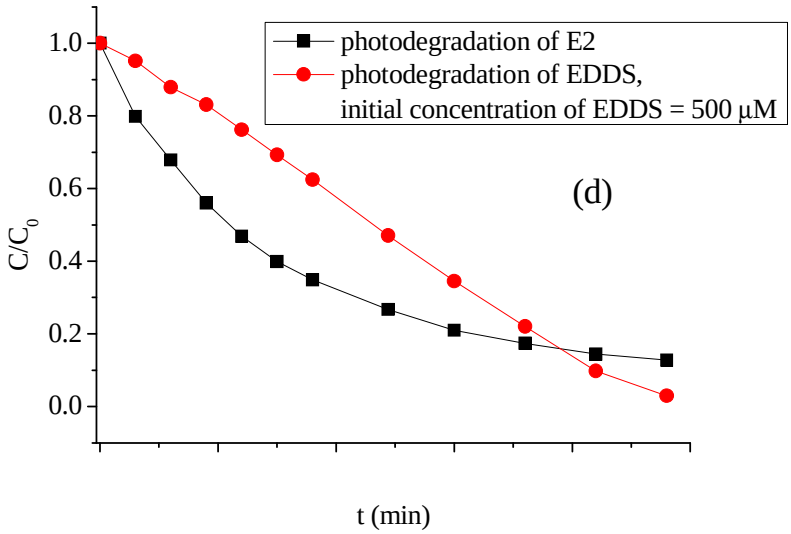
photodegradation of E2
photodegradation of EDDS,
initial concentration of EDDS = 500 μM
(d)
C/C0
t (min)
1.0
0.8
0.6
0.4
0.2
0.0

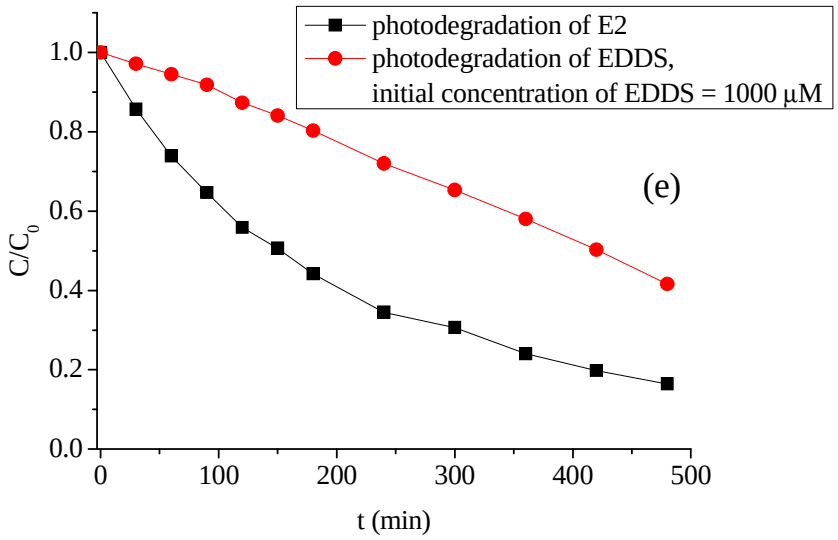

Figure IV-E-12 Comparison of the photodegradation of EDDS and E2 with different concentration of EDDS. (a): EDDS 50 μM; (b) EDDS 100 μM; (c): EDDS 250 μM; (d) EDDS 500 μM; (e) EDDS 1000 μM ([NM] = 6 g L^{-1}, [E2] = 5 μM, irradiation time 6 h, pH = 5.0).

E-3-3 Effect of pH on the degradation of E2

Figure IV-E-13 shows E2 photodegradation at various pH values in suspensions containing initially 6 g L^{-1} of NM, 5 μM of E2, 100 μM of EDDS. The initial degradation rate of E2 was maximal at pH = 6.0 and decreased above and below this pH value. Table IV-E-3 list the initial rate and degradation efficiency after 8 hours of irradiation of E2 at different pHs. At the same time, the degradaiton of EDDS was also detected. As shown in Figure IV-E-14, the influence of pH on the degradation of EDDS is similar to the influence of pH on the degradation of E2. It seems that the faster degradation of EDDS leads to the faster degradation of E2.

Comparing the photodegradation of E2 without EDDS and with EDDS under different pH in NM suspensions, we got the results that the optimal pH for the degradation of E2 without EDDS is the acid pH and that with EDDS shift to the circumneutral pH (Figure IV-E-15). At pH 3 and 9, the photodegradation of E2 was slightly depressed with EDDS in the solutions and at all other pHs, the photodegradation of E2 was increased significantly. As we mentioned in section IV-B-1-5, under the same condition, the quantum yield of $^{\bullet}OH$ formation by photolysis of $Fe(OH)^{2+}$, the most active species for photochemical production of hydroxyl radicals, was 0.044, which is approximately twenty times higher than the

quantum yield of •OH formation for photolysis of Fe(III)-EDDS at pH 3 (0.0025). So it is easy for us to understand that the photodegradation of E2 was slightly depressed with EDDS than without EDDS in pH3. At pH 9, barely no soluble Fe(III) is in the solution for the complexing with EDDS. So EDDS acts as scavenger pf hydroxyl radicals more than as a complex with Fe. Thus, although the Fe(III)-EDDS at pH 9 has a high photoactivity, we did not see the increased degradation rate of E2 with EDDS in the suspensions.

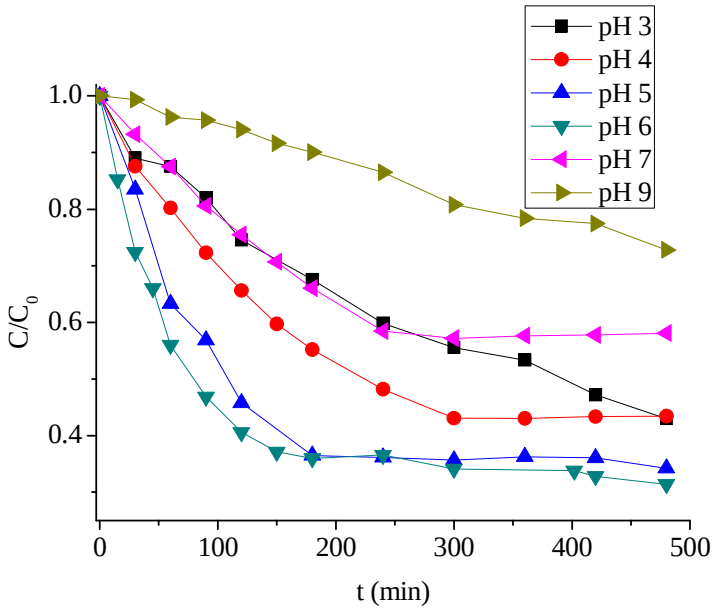

Figure IV-E-13 Influence of pH on the photodegradation of E2 in the present of EDDS. The experimental conditions were as follows: [NM] = 6 g L^{-1}, [E2] = 5 μM, [EDDS] = 100 μM, irradiation time 8 h.

Table IV-E-3 The initial rate and degradation efficiency after 8 hours of irridiation of E2 at different pH

pH	3	4	5	6	7	9
Initial rate (μmol L^{-1} min^{-1})	0.0065	0.01055	0.0179	0.0255	0.0085	0.0021
Degradation efficiency at 8 hours	57.0%	56.6%	65.8%	68.6%	41.9%	21.2%

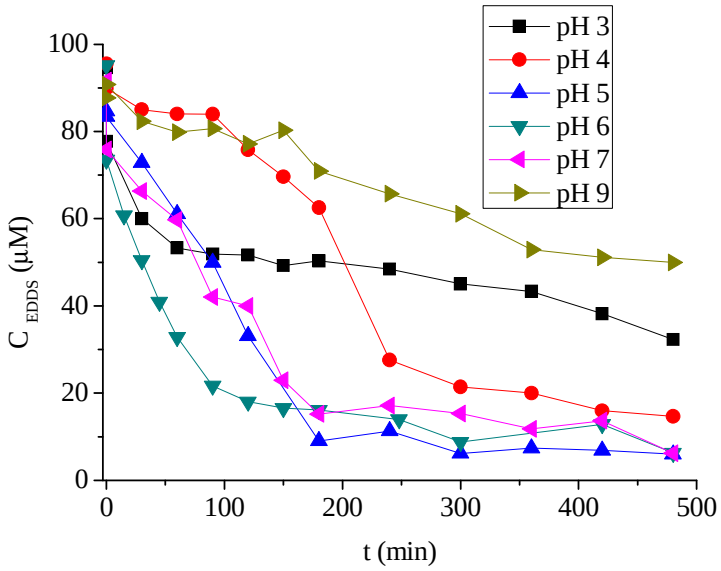

Figure IV-E-14 Change of EDDS concentration during the photodegradation of E2 under the different pHs ([EDDS] = 100 μM, [E2] = 5 μM, [NM] = 6 g L^{-1})

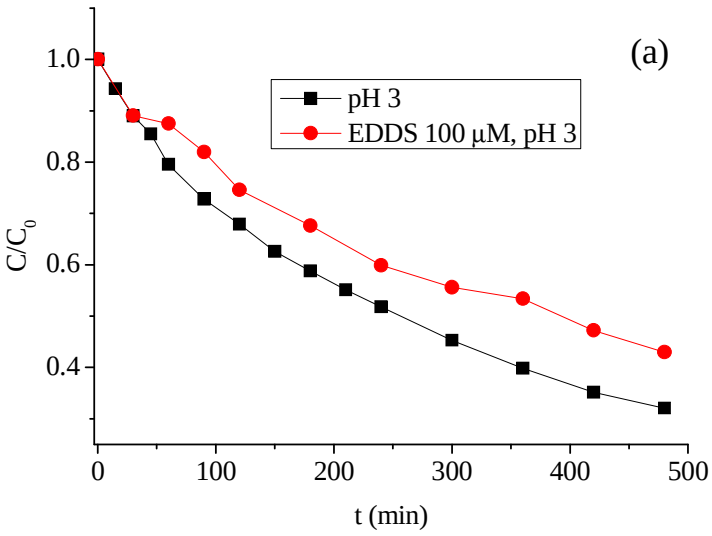

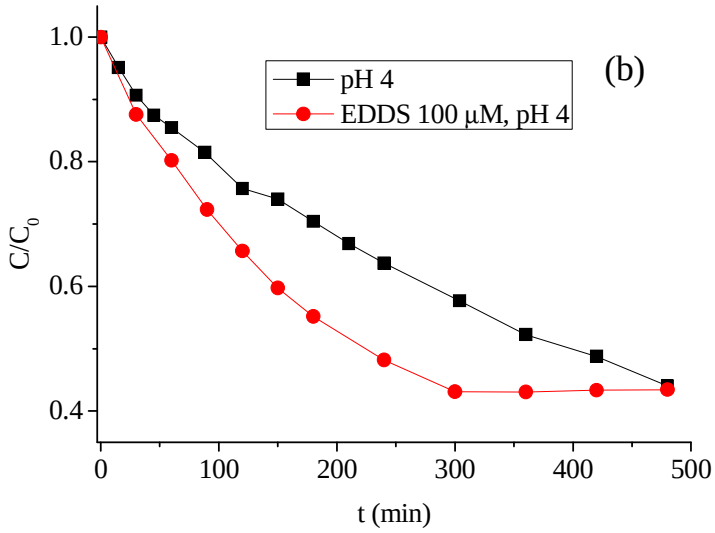
(b)
pH 4
EDDS 100 µM, pH 4
C/C0
t (min)
1.0
0.8
0.6
0.4
0
100
200
300
400
500

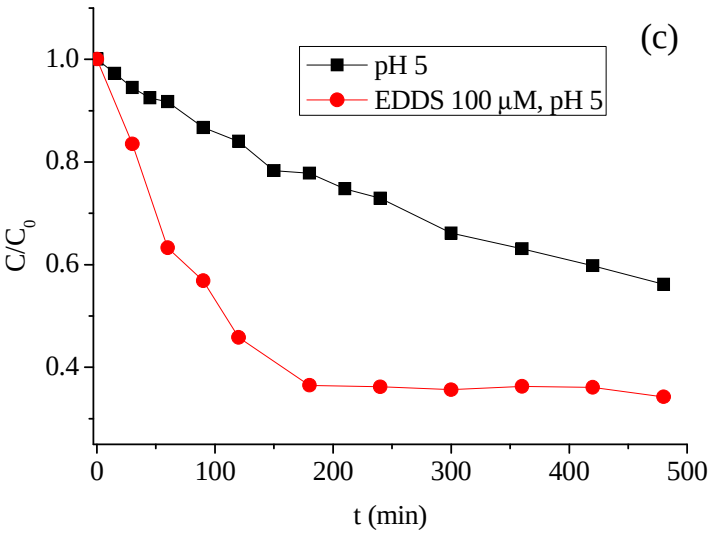
(c)
pH 5
EDDS 100 µM, pH 5
C/C0
t (min)
1.0
0.8
0.6
0.4
0
100
200
300
400
500

\

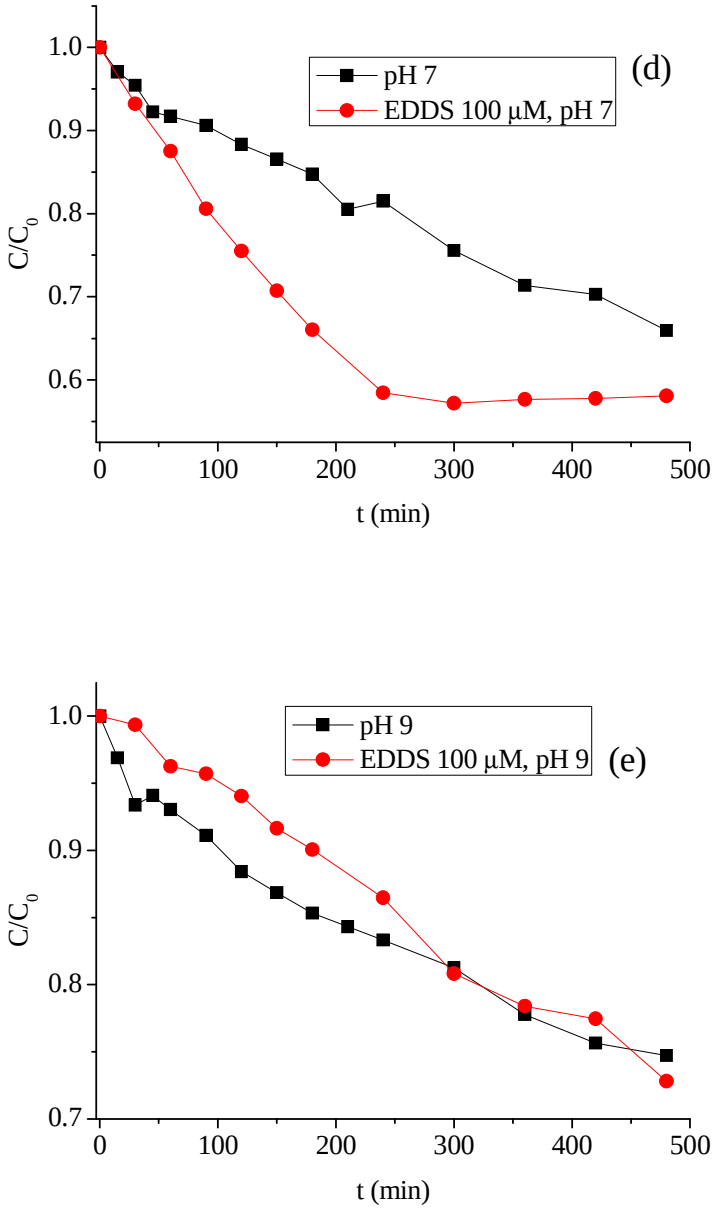

Figure IV-E-15 Comparison of the effect of pH on the photodegradaton of E2 with or without EDDS in NM suspensions. (a): pH 3; (b) pH 4; (c) pH 5; (d) pH 7; (e) pH 9 ([EDDS] = 100 µM, [E2] = 5 µM, [NM] = 6 g L^{-1}).

E-3-4 Effect of oxygen on the degradation of E2

Figure IV-E-16 shows the influence of oxygen on the photodegradation of E2 in NM suspensions in the presence of EDDS. In the deaerated solution, there was just a slight loss of E2 after 8 h of irradiation, which is much smaller than in the aerated solution and oxygen saturated solution. However, no increased rate was observed in the oxygen saturated solution

comparing with the aerated solution. These results indicated that oxygen is a very important factor that affects the photodegradation of E2 and it must take part in the photochemical process in such system. Without oxygen, the hydroxyl radicals could not be formed. However, excess oxygen also can not promote the photochemical reaction.

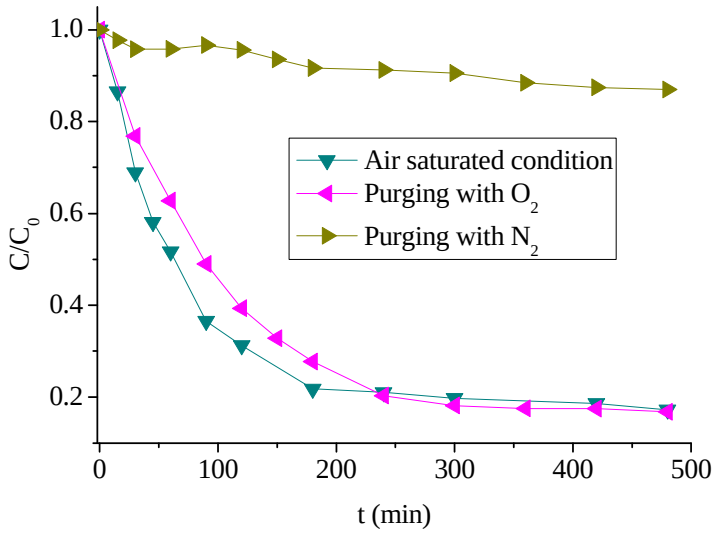

Figure IV-E-16 Influence of oxygen on the photodegradation of E2 in NM suspensions in the presence of EDDS. The experimental conditions were as followed: [NM] = 6 g L^{-1}, [EDDS] = 250 μM, [E2] = 5 μM, pH = 5.0, irradiation time 8 h.

E-3-5 Effect of 2-propanol on the photodegradation of E2

Figure IV-E-17 shows E2 degradation at two different 2-propanol concentrations in the irradiated suspensions containing NM (6 g L^{-1}), EDDS (250 μM,) and E2 (5 μM) at pH = 5.0. With 2-propanol in the solutions, the degradation of E2 was deeply depressed. 2-propanol is a very effective $^{\bullet}$OH scavenger. This result indicated that the main degradation pathway of E2 was the attack by $^{\bullet}$OH. However, a small photodegradation efficiency was observed in the irradiated suspensions with the two different concentration of 2-propanol. Thus, except the main pathway through reacting with $^{\bullet}$OH, there is another pathway for the degradation of E2, But it could be negligible compared to the $^{\bullet}$OH radical reaction.

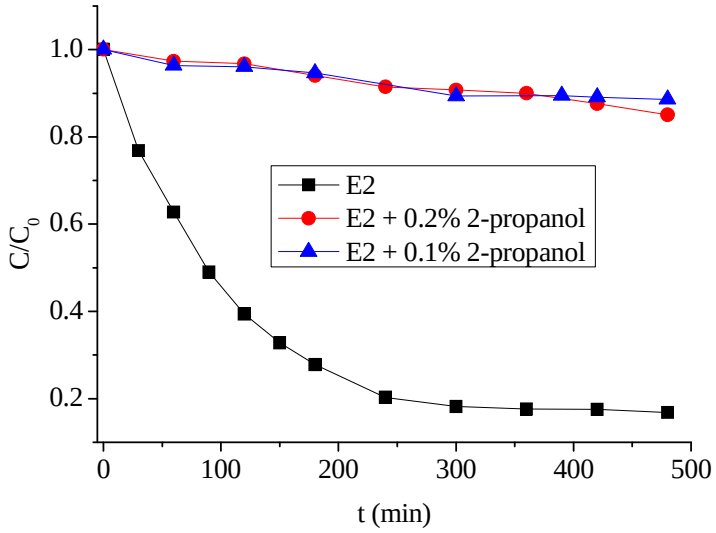

Figure IV-E-17 Influence of 2-propanol on the photodegradation of E2 in NM solutions in the presence of EDDS. The experimental conditions were as followed: [NM] = 6 g L^{-1}, [EDDS] = 250 μM, [E2] = 5 μM, pH = 5.0, irradiation time 8 h.

E-3-6 Effect of the initial E2 concentration

Under the conditions of 6 g L^{-1} of NM, EDDS of 250 μM and at pH = 5.0, the effect on photodegradation of the initial E2 concentration in the range of 0.65 to 11.32 μM was analyzed. Figure IV-E-18 shows the concentration profile variation of E2 at different initial concentrations. The degradation rate increased with increasing E2 concentration (data shown in Table IV-E-4).

E2 photodegradation by NM in the presence of EDDS was found to occur according to the Langmuir-Hinshelwood rate law (L-H equation), i.e.:

$$R = -\frac{dC}{dt} = \frac{kKC}{1+KC}$$

Where C is the concentration of E2 at time 't' and *k*, *K* are rate constant and the adsorption coefficient respectively.

As shown in Figure IV-E-19, the initial reaction rate and initial concentration fitted well into the L-H equation. *k* and *K* are calculated to be 0.173 $\mu mol \cdot L^{-1} \cdot min^{-1}$and 0.0412 $L \cdot \mu mol^{-1}$ respectively.

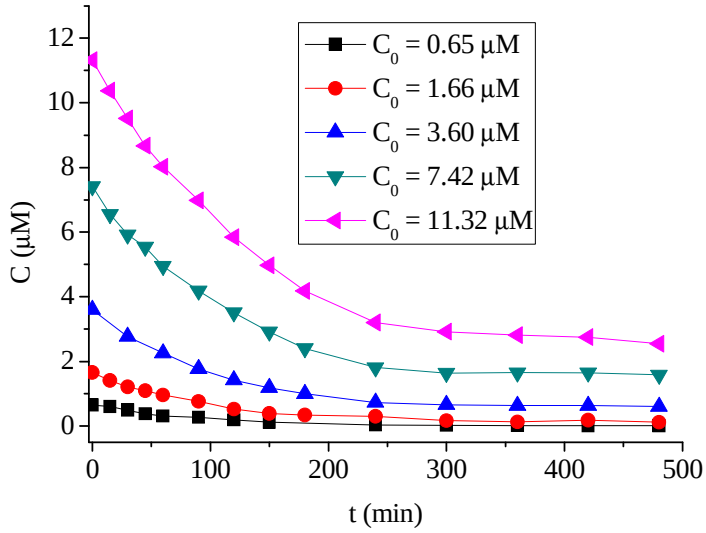

Figure IV-E-18 Influence of initial E2 concentration on the photodegradation of E2 in NM solutions in the presence of EDDS. The experimental conditions were as follows: [NM] = 6 g L^{-1}, [EDDS] = 250 µM, pH = 5.0, irradiation time 8 h.

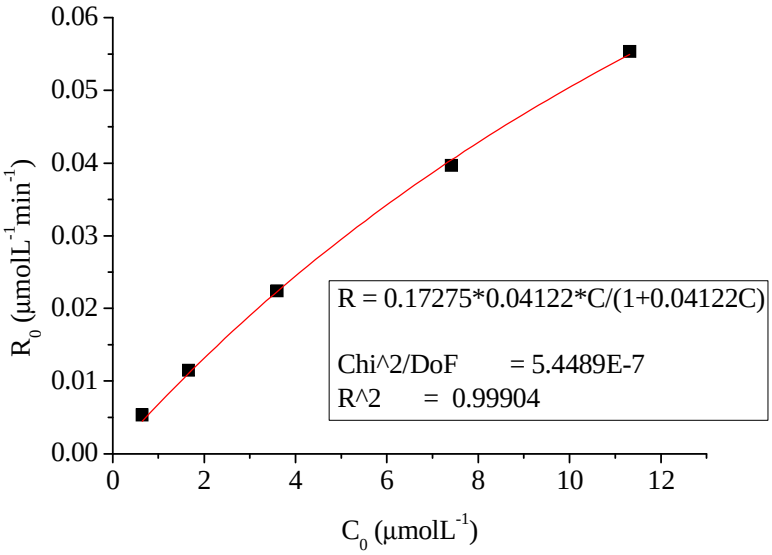

Figure IV-E-19 Plots of Ro versus Co for E2 degradation in the NM suspensions in the presence of EDDS

Table IV-E-4 Initial rates at different initial concentration of E2

C ($\mu mol \cdot L^{-1}$)	Initial rate ($\mu mol \cdot L^{-1} \cdot min^{-1}$)	Kinetic equation (L-H)	Reaction rate constant k_{LH} ($\mu mol \cdot L^{-1} \cdot min^{-1}$)
0.65	0.0053	$R = \frac{0.00712C}{1+0.04122C}$	
1.66	0.0115		
3.60	0.022		0.173
7.42	0.040	(R^2=0.999)	
11.32	0.055		

Conclusions

The photodegradation of E2 was investigated in NM suspensions in the absence and presence of EDDS. The results indicate that the NM concentration, EDDS concentration, pH, and oxygen all have an important impact on the E2 disappearance. In the NM-EDDS suspensions, the optimal pH range for the degradation of E2 was extended to the neutral and near-neutral pH ranges (pH 5-9). On the contrary without EDDS, the optimal pH is limited to the acid pH. In the NM-EDDS system, small amount of NM (0.1 g L^{-1}) is enough to get good degradation efficiency in the presence of EDDS. For achieving the best efficiency of E2 degradation, appropriate EDDS concentration should be chosen. The degradation kinetics of E2 follows the Langmuir-Hinshelwood rate law. After adding 2-propanol into the suspension, there was almost no E2 degradation, indicating that the main degradation pathway of E2 was reaction with $^{\bullet}OH$. Oxygen is a very important factor that affects the photodegradation of E2 and it must take part in the photochemical process in this system. Without oxygen, the hydroxyl radicals barely could be formed. However, excess oxygen also can not promote the photochemical reaction. Thus all these results show that NM-EDDS system could be considered as an efficient photocatalysis system for wastewater treatment.

IV-F Degradation of E2 photoinduced by Goethite and Goethite-EDDS

F-1 Adsorption of E2 on Goethite

The adsorption of E2 on Goethite was very fast, the adsorption equilibrium could be reached

in the first ten minutes. Figure IV-F-1 shows the adsorption isotherms of E2 on the Goethite at pH 5.0. Both, the Langmuir model for monolayer adsorption and the Freundlich model for multilayer adsorption were applied to fit the experimental data. It was found that the Langmuir model described the adsorption of E2 on Goethite well. The Langmuir model is shown as

$$C_{is} = \frac{K_{eq} b C}{1 + K_{eq} C}$$

Where, C is the concentration in the clay solution after equilibrium; C_{is} is the amount adsorbed on the clay; K_{eq} is the equilibrium constant and b is the maximum amount adsorbed on the clay. Fitting the L equation, K_{eq} and b are calculated to be 0.02387 L μmol^{-1} and 116.01 $\mu mol\ g^{-1}$. In the presence of EDDS, the E2 adsorption on the Goethite is a little lower than that without EDDS.

The pHzpc (pH at zero point of charge) of Goethite is detected to be 4.0, which is in the middle of the experimental pH values in our experiment. But it was found that pH has no obvious influence on the adsorption of E2 on goethite.

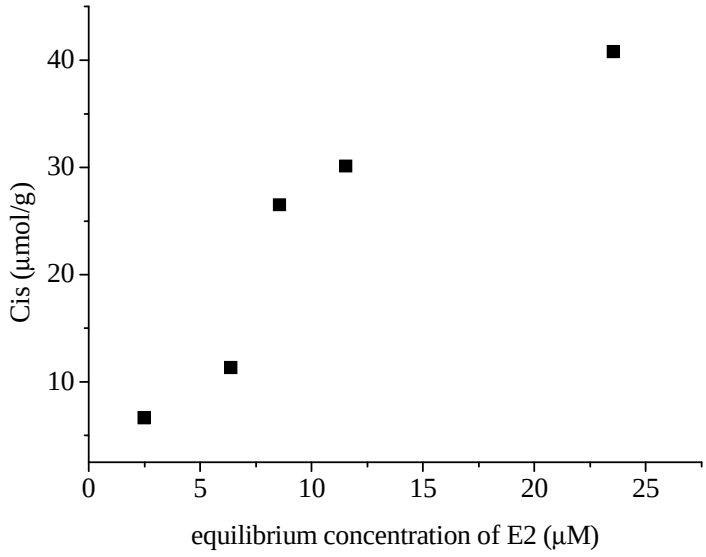

Figure IV-F-1 Adsorption isotherm of E2 onto the goethite ([Goethite] = 0.05 g L^{-1}, pH = 5.0)

F-2 Photodegradation of E2 in the Goethite suspensions

The photodegradation of E2 was studied in the Goethite suspensions. Irradiation was performed with polychromatic tubes emitting between 300 and 500 nm. Effect of concentration of Goethite and pH were studied in this work. Under our experimental

conditions and in the dark, no degradation of E2 was observed in the absence and in the presence of Goethite. Similarly, there was no photodegradation of E2 without Goethite under irradiation.

F-2-1 Effect of Goethite concentration on the photodegradation of E2

Effect of Goethite concentration on the degradation of E2 was studied with [E2] = 5 µM, at pH = 3.0 and different concentrations of goethite from 0 to 0.4 g L^{-1}. As shown in Figure IV-F-2, the kinetics of E2 degradation is strongly dependent on Goethite concentration. The disappearance of E2 became faster when the concentration of Goethite increased from 0 to 0.05 g L^{-1}. However at higher Goethite concentrations than 0.05 g L^{-1}, the rate of E2 disappearance decreased with increasing the Goethite concentration. This negative effect is attributed to the fact that excessive amount of iron oxide limits the penetration of UV light in the solution and leads to the quick decay of UV light intensity. During the irradiation, the concentration of Fe(tot) and Fe(II) was also detected at the same time. As shown in Figure IV-F-3 and IV-F-4, the concentration of Fe(tot) and Fe(II) was increased during the irradiation and was higher with higher concentration of Goethite. But even there was iron dissolved during the irradiation, the amount of iron in the suspensions is very small. The amount of Fe(tot) dissolved in the 0.05 g L^{-1} Goethite suspensions after 8 hours of irradiation was about 10 µM.

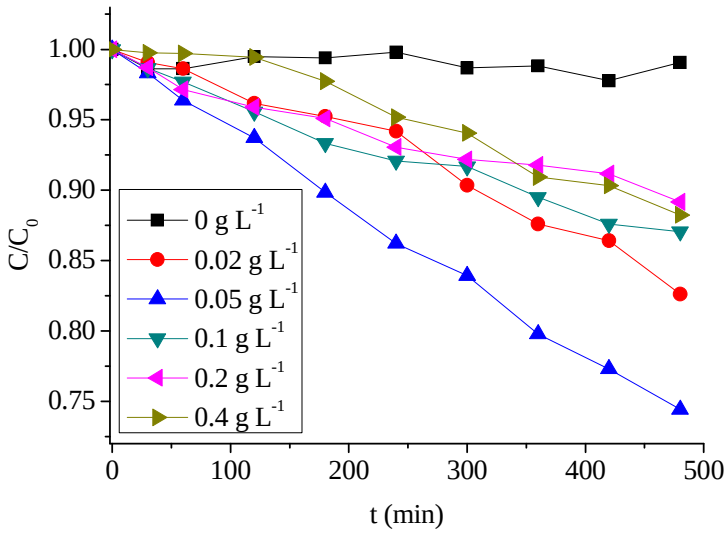

Figure IV-F-2 Influence of Goethite concentration on the photodegradation of E2 in aqueous solutions containing Goethite at different concentrations in the range of 0 – 0.4 g L^{-1}. The experimental conditions were as follows: [E2] = 5 µM, irradiation time 8 h, pH = 3.0.

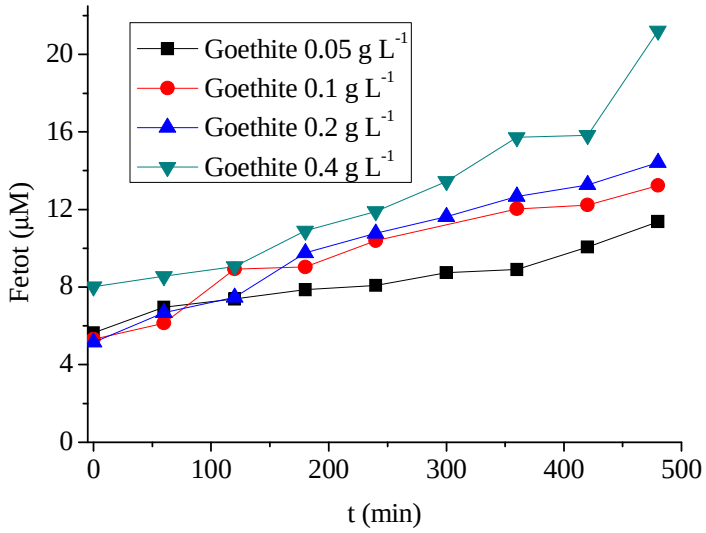

Figure IV-F-3 Concentration of Fe(tot) during the irradiation ([E2] = 5 μM, irradiation time 8 h, pH = 3.0).

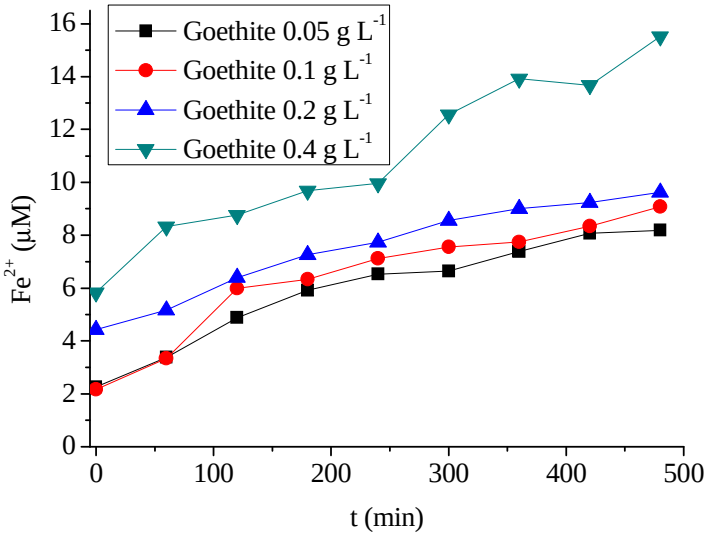

Figure IV-F-4 Concentration of Fe(II) during the irradiation ([E2] = 5 μM, irradiation time 8 h, pH = 3.0).

F-2-2 Effect of pH on the photodegradation of E2

The pH of zero-point-charge (pHzpc) of Goethite is detected to be 4.0. We varied the pH value of the suspensions below and above the pHzpc value of Goethite. Figure IV-F-5 shows the effect of pH on the photodegradation of E2 with [E2] = 5 μM, [Goethite] = 0.05 g L^{-1} and different of pH from 3 to 9. Obviously, the optimal pH for the degradation of E2 was 3.0, and

there was no significant effect on the degradation of E2 at other pHs. The changed of the pH was also investigated. As shown in Figure IV-F-6, except that the pH kept constant value near 3 for starting pH of 3.0 during the irradiation, at all other pHs, the pH decreased quickly at the first one hour and then kept constant. We also investigated the release of iron during the irradiation (Figure IV-F-7). There is more iron released at low pH in the range of 2 - 5. At pH higher than 5, no iron is detected in the suspensions.

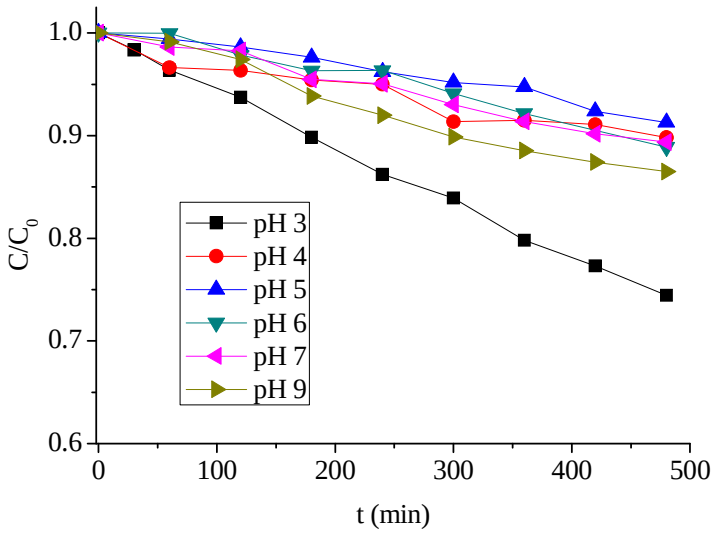

Figure IV-F-5 Influence of pH on the photodegradation of E2 in aqueous solutions containing Goethite. The experimental conditions were as follows: [E2] = 5 µM, [Goethite] = 0.05 g L^{-1}, irradiation time 8 h.

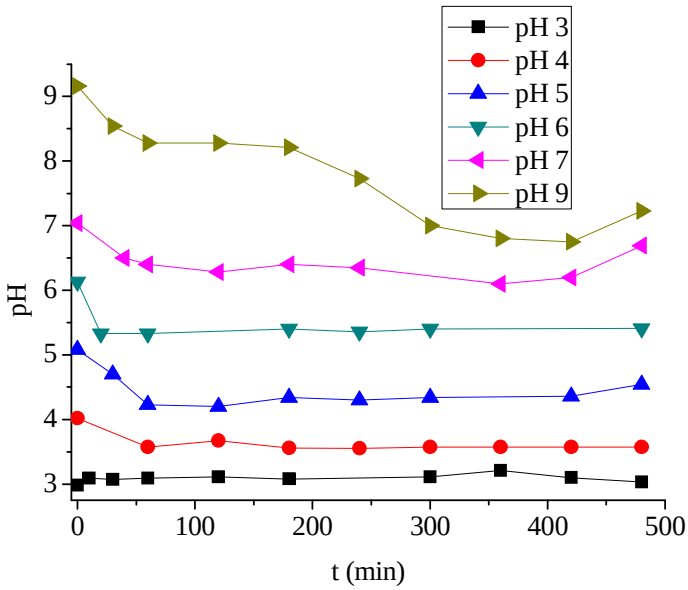

Figure IV-F-6 Changes of pH during the irradiation ([E2] = 5 µM, [Goethite] = 0.05 g L^{-1}, irradiation time 8 h).

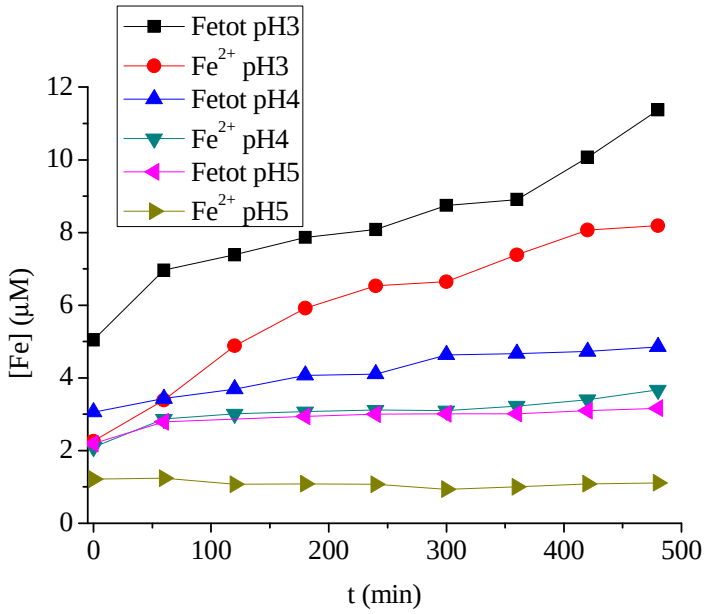

Figure IV-F-7 Concentration of iron during the irradiation ([E2] = 5 µM, [Goethite] = 0.05 g L^{-1}, irradiation time 8 h).

F-3 Photodegradation of E2 in the Goethite-EDDS complex solutions

The photodegradation of E2 was studied in the Goethite suspensions in the presence of EDDS. Irradiation was performed with polychromatic tubes emitting between 300 and 500 nm. Effect of Goethite, EDDS, oxygen, 2-propanol and E2 concentrations and pH were all studied in this work. Under our experimental conditions and in the dark, no degradation of E2 was observed in the absence and in the presence of Goethite-EDDS. Similarly, there was no photodegradation of E2 without Goethite-EDDS under irradiation.

F-3-1 Effect of Goethite concentration on the photodegradation of E2

Figure IV-F-8 shows the photodegradation of E2 in Goethite suspensions in the presence of EDDS as function of Goethite concentration. The rate of E2 degradation was increased with increasing the Goethite concentration in the rage of 0 to 0.04 g L^{-1}, but at higher Goethite concentration of 1 g L^{-1}, the rate of E2 degradation decreased. In the presence of EDDS, the effect of Goethite concentration is not that obviously comparing with that in the condition without EDDS in the suspensions.

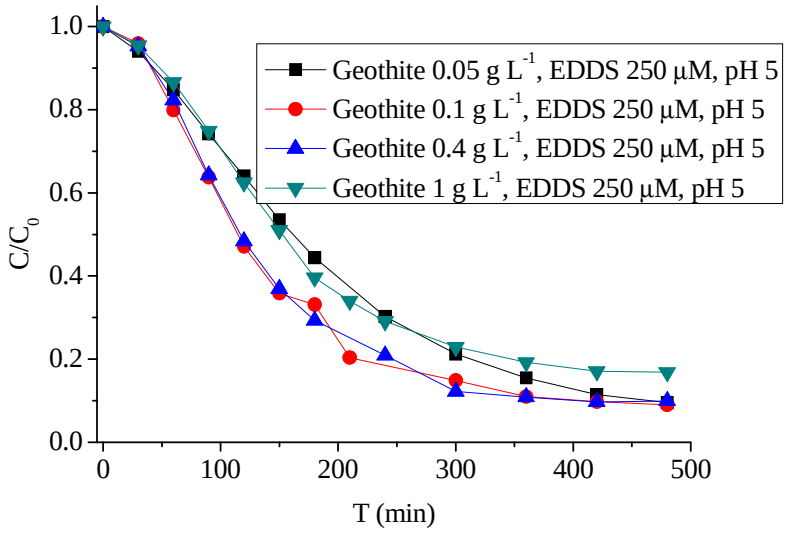

Figure IV-F-8 Influence of Goethite concentration on the photodegradation of E2 in the presence of EDDS. The experimental conditions were as follows: [E2] = 5 µM, [EDDS] = 250 µM, irradiation time 8 h, pH = 5.0.

F-3-2 Effect of EDDS concentration on the photodegradation of E2

Effect of EDDS concentration on the degradation of E2 was studied with [E2] = 5 µM, [Goethite] = 0.05 g L^{-1} at pH = 5.0 and different concentrations of EDDS from 0 to 5 mM. As shown in Figure IV-F-9, there was just near 10% of E2 degradation without EDDS in the suspensions after 8 hours of irradiation. With EDDS in the suspension, the initial degradation rate was increased significantly. In our experimental conditions, the initial degradation rate was decreased with increasing the EDDS concentration from 50 to 5000 µM, but the optimal final photodegradation efficiency after 8 hours of irradiation was achieved with 250 µM of EDDS in the suspensions. When the concentration of EDDS was less than 250 µM, the final photodegradation efficiency increased with the increase of EDDS concentration, while the final photodegradation efficiency decreased with the increase of EDDS concentration when EDDS concentration was higher than 250 µM.

EDDS could form complexes with iron in the Goethite suspension and in the interlayer as Fe(III)-EDDS complex which is more photoreactive for producing hydroxyl radicals under irradiation. Also EDDS could react with hydroxyl radicals acting a $^{\bullet}OH$ competitor with E2. In the Goethite suspensions and in the presence of EDDS, the amount of iron dissolved in the suspensions is between 3-11 µM, which is much lower than the initial concentration of

EDDS used. No big difference was found with the different concentration of EDDS in the suspensions (Figure IV-F-10). So in the initial Goethite suspension, 50 µM of EDDS is high enough to completely complex with dissolved iron. More EDDS act as the •OH competitor. Thus, we found that the initial degradation rate was decreased with increasing the EDDS concentration from 50 to 5000 µM. During the irradiation, EDDS was also decomposed, as shown in Figure IV-F-11. After complete photodegradation of EDDS, Fe(III)-EDDS was no longer present in the solution and the photodegradation of E2 was stopped. With more EDDS in the suspensions, the degradation of E2 could continue for a longer time. Thus, the best photodegradation efficiency after 8 hours of irradiation was found at the condition of 250 µM EDDS in our experimental conditions.

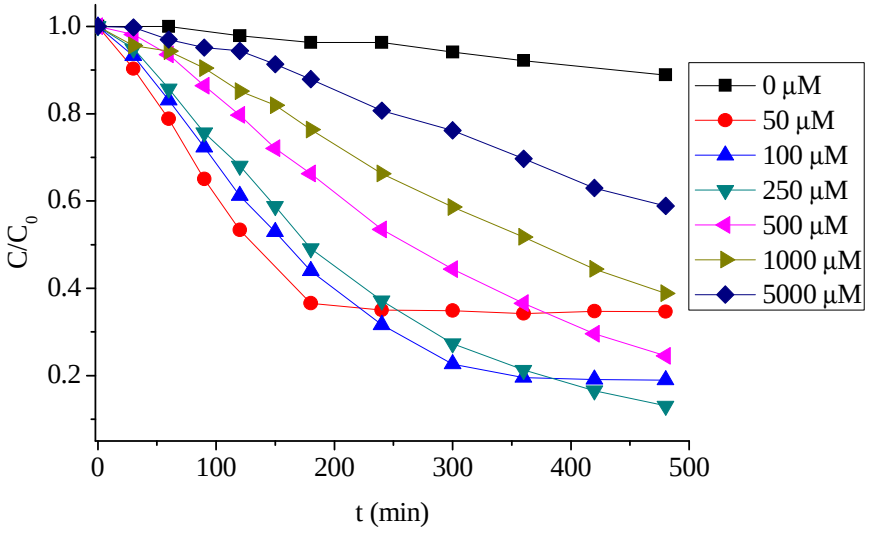

Figure IV-F-9 Influence of EDDS concentration on the photodegradation of E2 in the presence of EDDS. The experimental conditions were as follows: [Goethite] = 0.05 g L^{-1}, [E2] = 5 µM, irradiation time 8 hours, pH = 5.0.

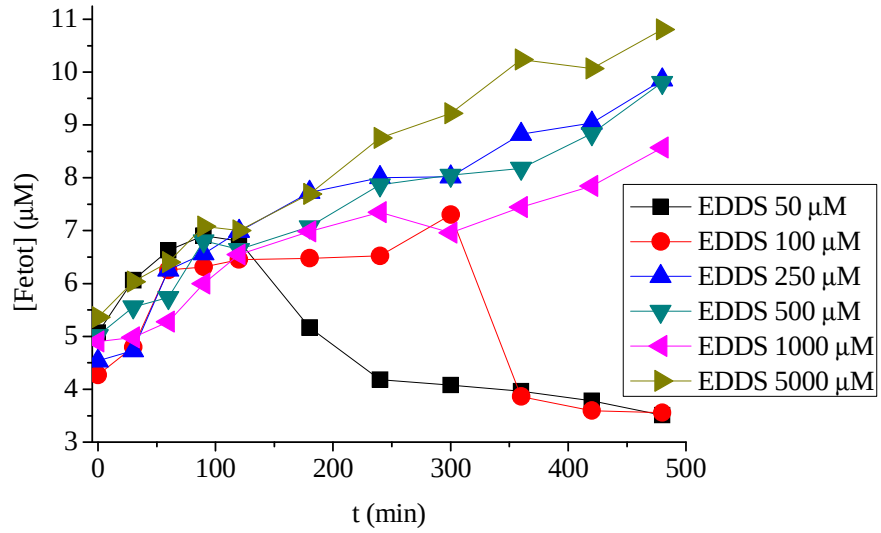

Figure IV-F-10 Concentration of iron during the irradiation ([Goethite] = 0.05 g L^{-1}, [E2] = 5 µM, irradiation time 8 hours, pH = 5.0).

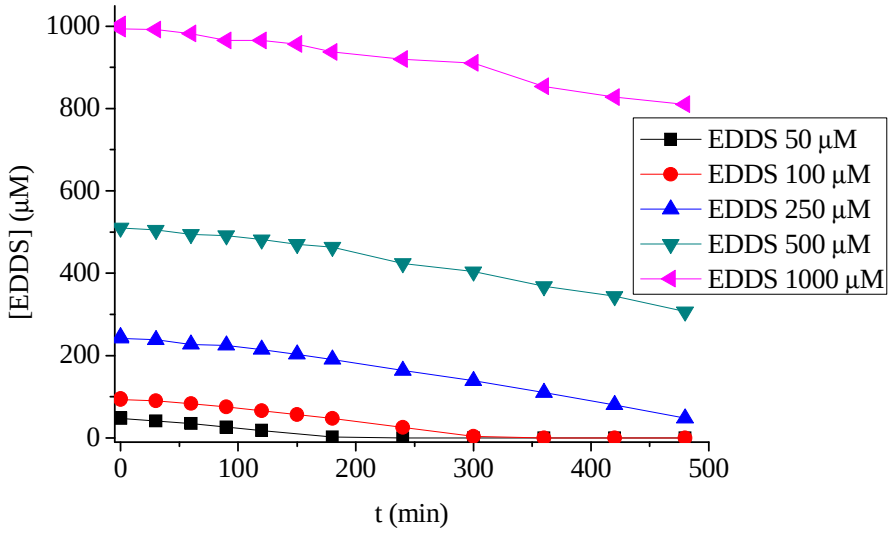

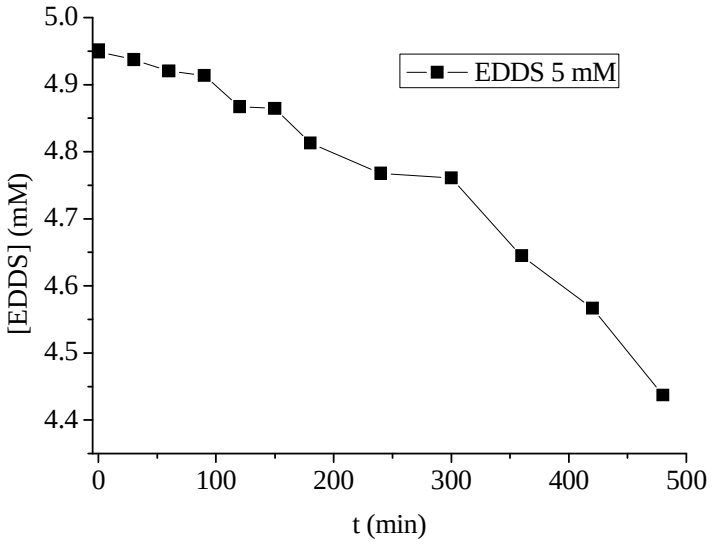

Figure IV-F-11 Change of EDDS concentration during the irradiation with different starting concentration of EDDS ([Goethite] = 0.05 g L^{-1}, [E2] = 5 μM, irradiation time 8 hours, pH = 5.0).

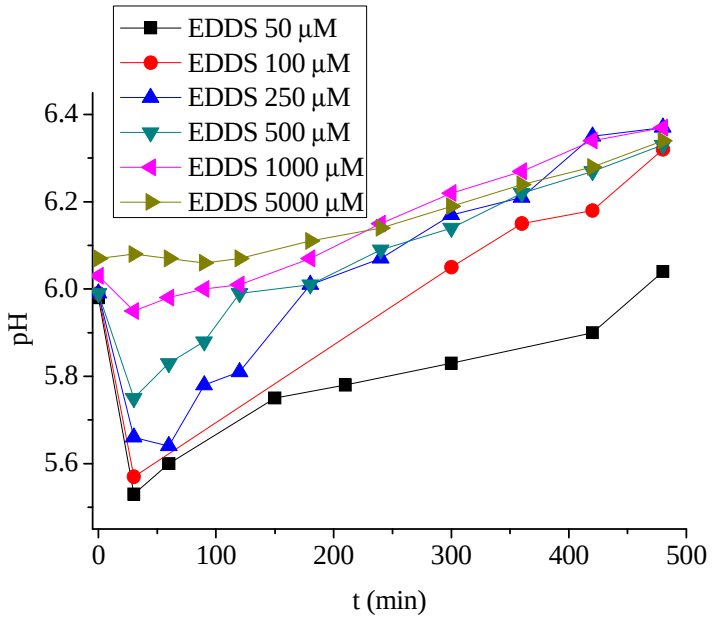

Figure IV-F-12 Changes of pH during the irradiation ([Goethite] = 0.05 g L^{-1}, [E2] = 5 μM, irradiation time 8 hours, pH = 5.0).

F-3-3 Effect of pH on the photodegradation of E2

The effect of pH on the photodegradation of E2 in the presence of EDDS was studied with Goethite at 0.05 g L^{-1}, initial concentration of [E2] = 5 μM and [EDDS] = 250 μM. As shown

in Figure IV-F-13, the photodegradation of E2 was strongly dependent on the initial pH. The optimal initial pH value for the photodegradation of E2 was obtained for pH 4.0 and 5.0. The initial degradation rate of E2 decreased above and below these optimal pH values. At the same time, the degradation of EDDS was also detected. As shown in Figure IV-F-14, the influence of pH on the degradation of EDDS is similar to the influence of pH on the degradation of E2. It seems that the faster degradation of EDDS leads to the faster degradation of E2.

Figure IV-F-15 shows the amount of iron dissolved in the suspensions during the irradiation. The amount of Fe(tot) and Fe(II) slowly increased during the irradiation, but the values were very small, the amount of Fe(II) is below 3 µM even at pH 3. Figure IV-F-16 shows that during the irradiation, the pH was slightly increased in the acid pH range and decreased in the basic pH range.

Figure IV-F-17 indicated the comparison of the photodegradation of E2 without EDDS and with EDDS in Goethite suspensions. At all the pH, the photodegradation of E2 was significantly increased after adding EDDS in the solutions, more particularly near the neutral pH. Without EDDS, the optimal pH for the degradation of E2 was limited around 3 and even at pH 3, the degradation efficiency was low. Thus, the addition of EDDS to the Goethite suspensions extended the pH for the effective degradation of E2 and increased the degradation efficiency.

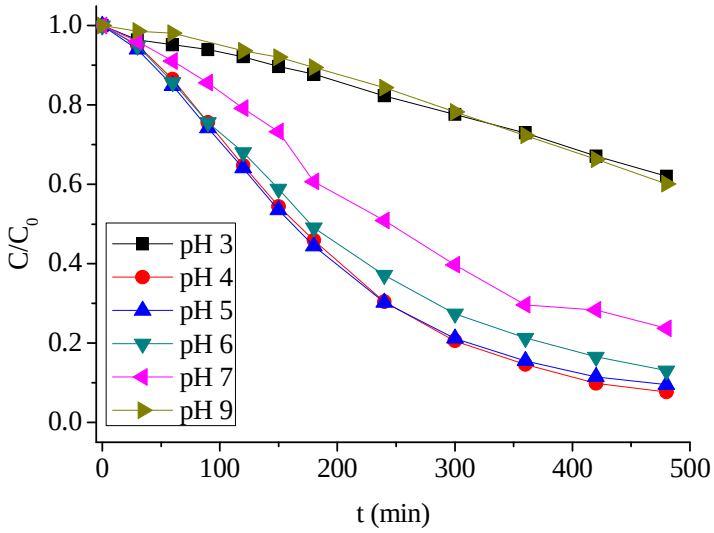

Figure IV-F-13 Influence of pH on the photodegradation of E2 in aqueous solutions containing Goethite in the presence of EDDS. The experimental conditions were as follows: [E2] = 5 µM, [Goethite] = 0.05 g L^{-1}, [EDDS] = 250 µM, irradiation time 8 hours.

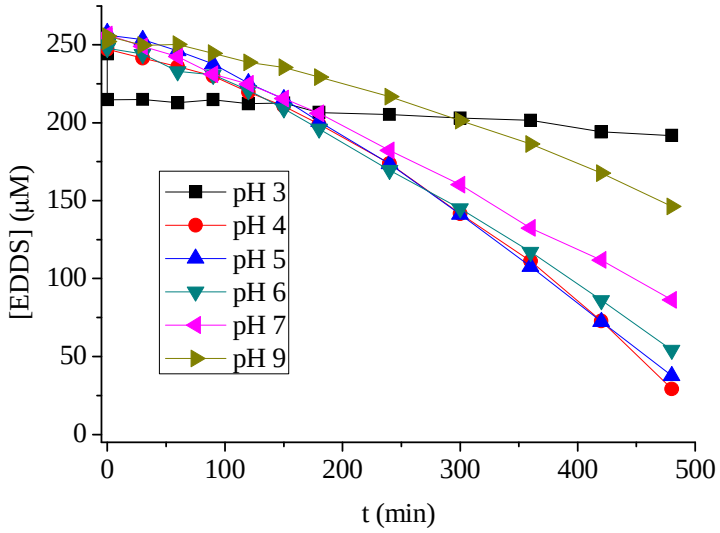

Figure IV-F-14 Change of EDDS concentration during the irradiation under the different pH ([E2] = 5 µM, [Goethite] = 0.05 g L^{-1}, [EDDS] = 250 µM, irradiation time 8 hours).

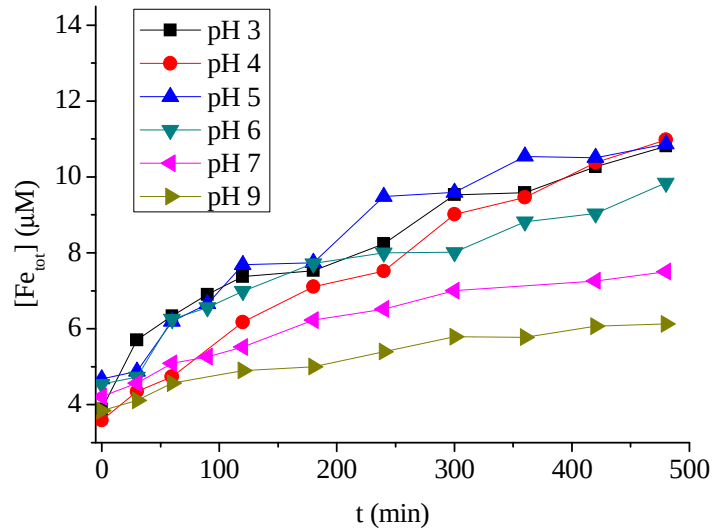

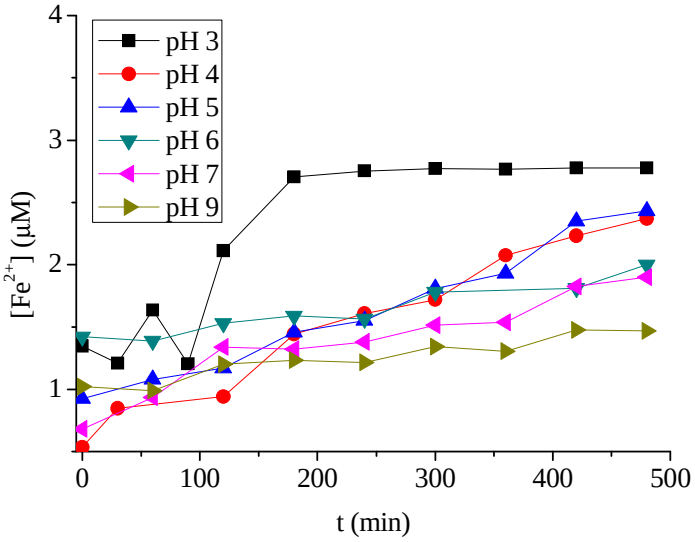

Figure IV-F-15 Concentration of iron during the irradiation ([E2] = 5 µM, [Goethite] = 0.05 g L^{-1}, [EDDS] = 250 µM, irradiation time 8 hours).

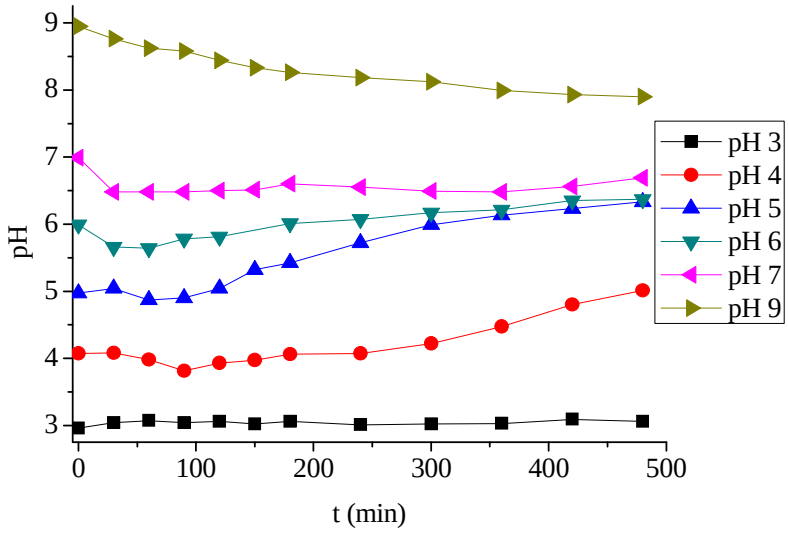

Figure IV-F-16 Changes of pH during the irradiation ([E2] = 5 µM, [Goethite] = 0.05 g L^{-1}, [EDDS] = 250 µM, irradiation time 8 hours).

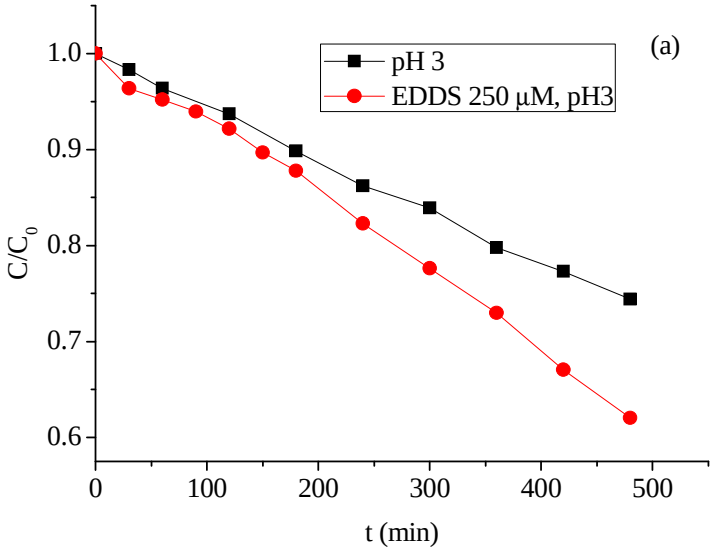
(a)
pH 3
EDDS 250 µM, pH3
C/C0
t (min)
1.0
0.9
0.8
0.7
0.6
0
100
200
300
400
500

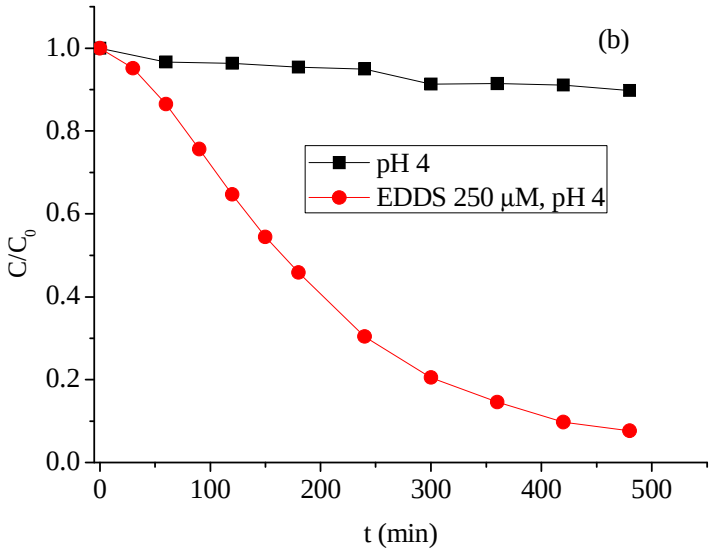
(b)
pH 4
EDDS 250 µM, pH 4
C/C0
t (min)
1.0
0.8
0.6
0.4
0.2
0.0
0
100
200
300
400
500

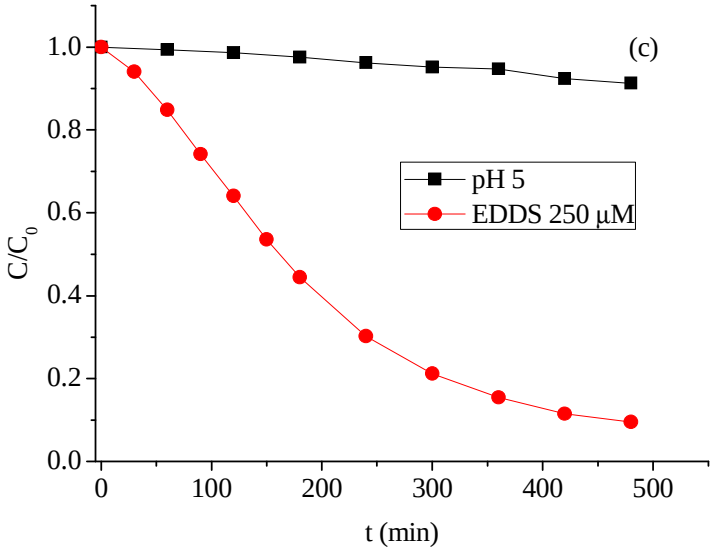
(c)
pH 5
EDDS 250 µM
C/C0
t (min)
0.0
0.2
0.4
0.6
0.8
1.0
0
100
200
300
400
500

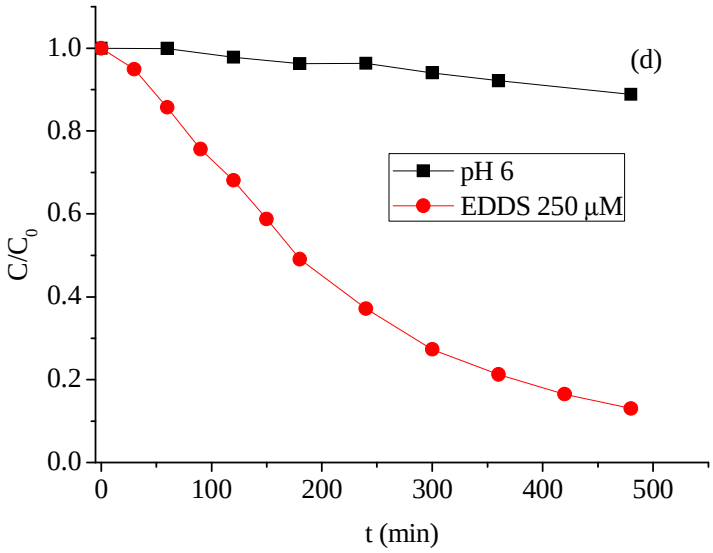
(d)
pH 6
EDDS 250 µM
C/C0
t (min)
0.0
0.2
0.4
0.6
0.8
1.0
0
100
200
300
400
500

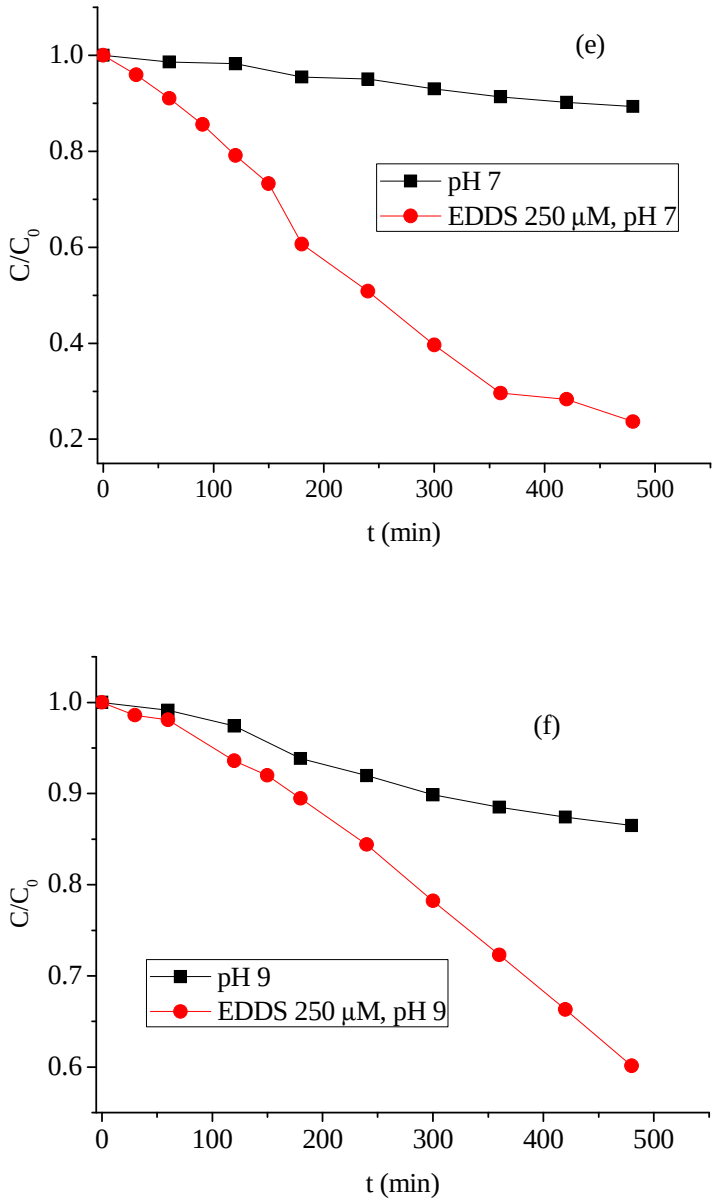

Figure IV-F-17 Comparison of the effect of pH on the photodegradation of E2 with EDDS in Goethite suspensions with or without EDDS. (a): pH 3; (b) pH 4; (c) pH 5; (d) pH 6; (e) pH 7; (f) pH 9 ([E2] = 5 µM, [Goethite] = 0.05 g L^{-1}, [EDDS] = 250 µM, irradiation time 8 hours).

F-3-4 Effect of oxygen on the photodegradation of E2

Goethite suspensions containing EDDS and E2 were irradiated in deaerated (nitrogen bubbling), aerated or oxygen saturated medium. The corresponding kinetics of E2 disappearance is represented in Figure IV-F-18. We observed an important effect of oxygen. The degradation of E2 in the absence of oxygen was very slow. Oxygen seems to be

necessary for E2 photodegradation. However, the photodegradation of E2 was not promoted in oxygen saturated suspension comparing with that in the aerated suspension. Thus, O_2 is a limited parameter for the photochemical reaction but the photodegradation rate of E2 in the Goethite-EDDS suspensions is not controlled by O_2 concentration.

During the irradiation, the concentration of EDDS was detected. As shown in Figure IV-F-19, there was no photodegradation of EDDS observed in the deoxygenated suspension. The kinetics of EDDS photodegradation in the oxygen saturated and aerated suspensions are almost the same, which is like the photodegradation of E2. Figure IV-F-20 shows the amount of iron dissolved in the suspensions. The concentrations of dissolved Fe(tot) and Fe(II) increased during the irradiation. In the aerated and oxygen saturated suspensions, the concentration of Fe(tot) was near 10 μM after 8 hours of irradiation. But in deoxygenated suspension, the concentration of Fe(tot) reached a value of 100 μM at the end of the irradiation. Thus, it is well known that light-induced dissolution of iron from Goethite oxide and more particularly in the presence of iron complex like EDDS. In deaerated suspension, EDDS was not degraded and as a consequence the concentration of dissolved iron could increase in the suspension. In the absence of oxygen the photoredox process from the iron complex is not effective. The dissolved iron detected was Fe(III), which is due to the formation of Fe(III)-EDDS complex through the reaction of the reductive Fe(II) and EDDS under the irradiation (reaction (1)).

$$\text{Goethite} \xrightarrow{h\nu} \text{dissolved Fe(II)} \xleftrightarrow{h\nu} \text{soluble Fe(III)-EDDS complex} \quad (1)$$

As other Fe(III)-carboxyl ate complexes, the first two steps of photochemical reaction of Fe(III)-EDDS complex was thought the ligand-to-metal charge transfer (LMCT) reaction producing Fe(II) and ligand-free radical and then the $O_2^{\bullet-}$ formation, as shown in following reactions:

$$\text{Fe(III)-L} + h\nu \rightarrow [\text{Fe(III)-L}]^* \rightarrow \text{Fe(II)} + L^{\bullet} \quad (2)$$

$$L^{\bullet} + O_2 \rightarrow O_2^{\bullet-} + L' \quad (3)$$

In the deoxygenated suspension, although the high amount of dissolved Fe(III) is formed, which is mean that the concentration of Fe(III)-EDDS should be high in the suspensions, the rate of E2 photodegradation was very slow. This result shows that in the photoredox process of iron complexes the starting reaction (reaction (1)) is important, but the key reaction controlling the amount of $^{\bullet}OH$ formation (leading to the degradation of organic compound like E2) is not the reaction (2) but the reaction (3).

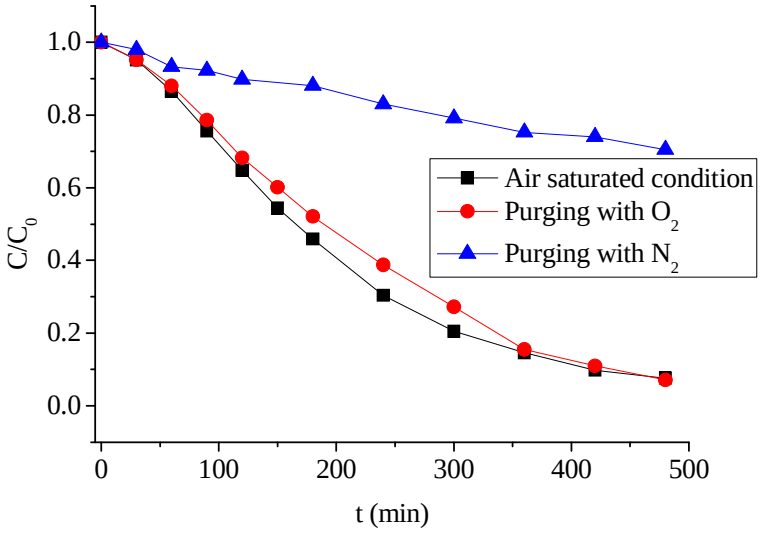

Figure IV-F-18 Influence of oxygen on the photodegradation of E2 in Goethite suspensions in the presence of EDDS. The experimental conditions were as follows: [Goethite] = 0.05 g L^{-1}, [EDDS] = 250 µM, [E2] = 5µM, pH 4.0, irradiation time 8 hours.

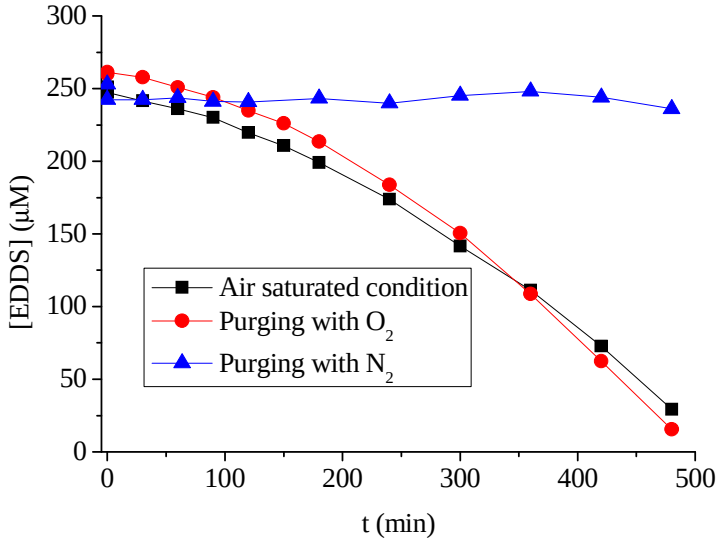

Figure IV-F-19 Change of EDDS concentration during the irradiation ([Goethite] = 0.05 g L^{-1}, [EDDS] = 250 µM, [E2] = 5µM, pH 4.0, irradiation time 8 hours).

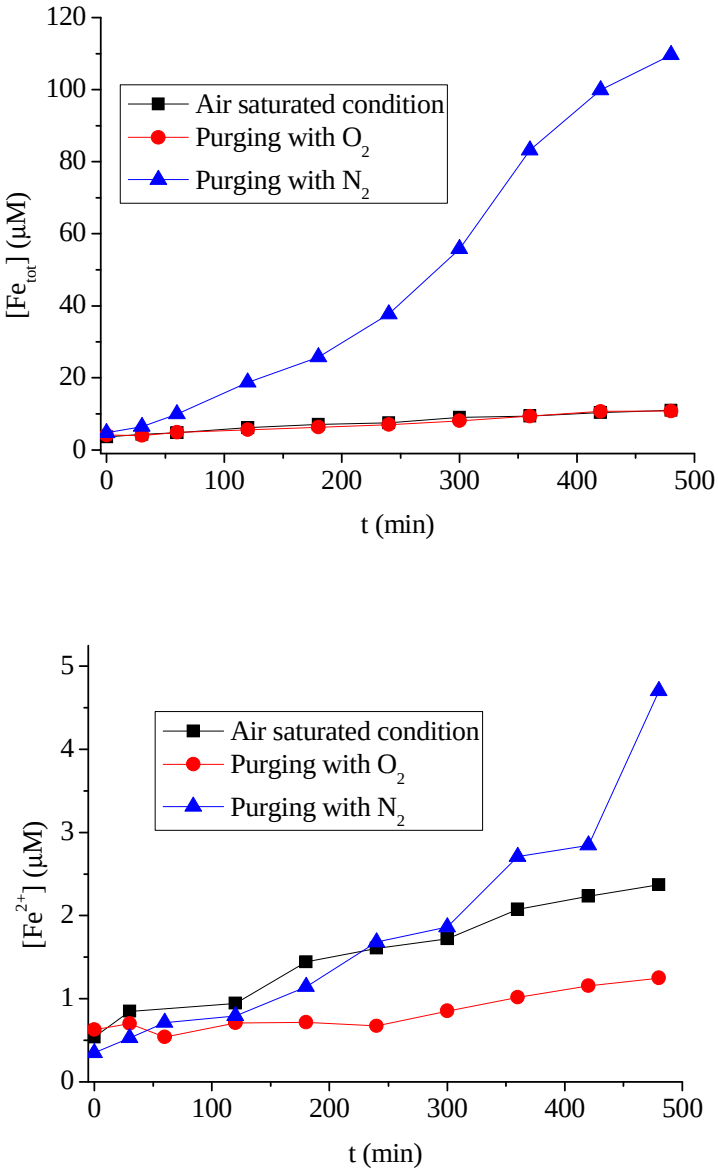

Figure IV-F-20 Concentration of iron during the irradiation ([Goethite] = 0.05 g L^{-1}, [EDDS] = 250 µM, [E2] = 5µM, pH 4.0, irradiation time 8 hours).

F-3-5 Effect of 2-propanol on the photodegradation of E2

2-propanol (0.1%) was added to some Goethite-E2 suspensions in order to give evidence for the formation of $^{\bullet}$OH radicals. Actually, 2-propanol is usually used as a hydroxyl radicals scavenger, the rate constant of reaction of these radicals on 2-propanol being close to 2×10^9 M^{-1} s^{-1} (Buxton *et al.*, 1988). The results clearly showed that the degradation of E2 was strongly affected by the presence of 2-propanol (Figure IV-F-21) demonstrated that $^{\bullet}$OH radicals are involved in the process of E2 photodegradation.

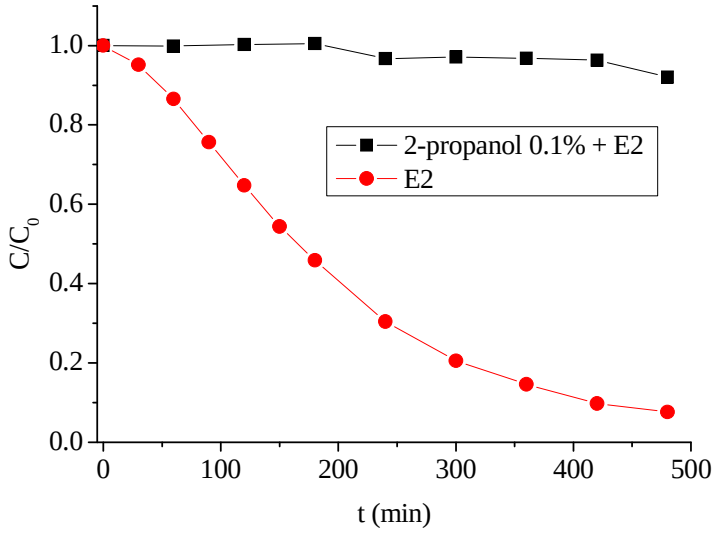

Figure IV-F-21 Influence of 2-propanol on the photodegradation of E2 in Goethite suspensions in the presence of EDDS. The experimental conditions were as follows: [Goethite] = 0.05 g L^{-1}, [EDDS] = 250 µM, [E2] = 5µM, pH 4, irradiation time 8 hours.

F-3-6 Comparison of the homogenous and heterogeneous reaction

The photochemical process in the presence of iron oxide and oxalate/citrate together has been described in detail by some researchers (Zuo and Deng, 1997; Balmer and Sulzberger, 1999; Ou *et al*., 2008). It should be noted that this photochemical process happened both on the surface of iron oxide as a heterogeneous reaction and also in the solution as a homogeneous reaction. To compare the efficiency in Goethite-EDDS heterogeneous system with that in Fe(III)-EDDS homogeneous system, a homogeneous system was set up by adding 10 µM of Fe(III) (same concentration in Goethite and EDDS suspension) and 250 µM EDDS to degrade E2 under irradiation. The results show that the E2 degradation was only 34% in homogeneous system, which is much lower than in the heterogeneous system (Figure IV-E-22). These results indicate that the E2 degradation in the Goethite-EDDS suspension was achieved at a higher efficiency than that in the homogenous system.

The photodegradation of E2 was also investigated in the KSF, NM, Goethite suspension respectively in the same condition. As shown in Figure IV-F-23, under the same condition, the initial rate of E2 degradation was higher with KSF than Goethite and than NM. This result is certainly due to the concentration of dissolved iron in the solutions which is in the same order. The concentration of dissolved iron is higher in the presence of KSF than with

Goethite and than with NM. With more iron in the solution, more Fe(III)-EDDS complex will be formed, which lead to a fast photochemical process. However, at the end of the irradiation (but not the same time of irradiation) in all the suspensions the same degradation efficiency was achieved. Thus, except the homogeneous reaction, the heterogeneous reaction must be happened, but it should be slower than the homogeneous reaction.

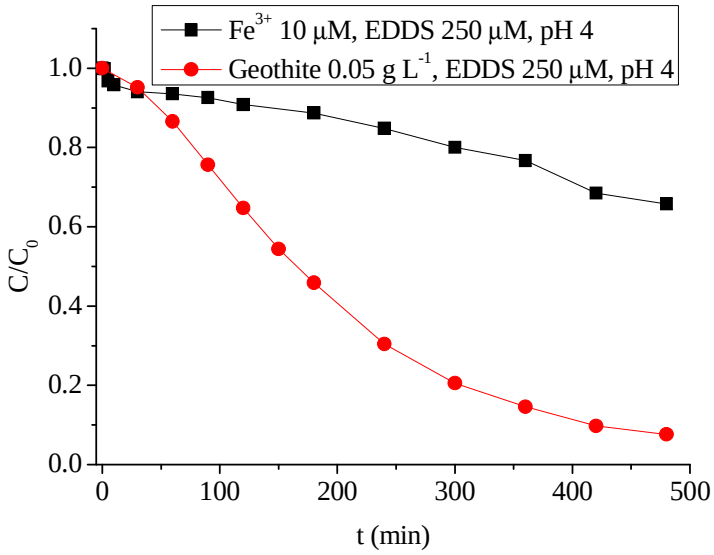

Figure IV-F-22 Photodegradation of E2 under heterogeneous system and homogeneous system

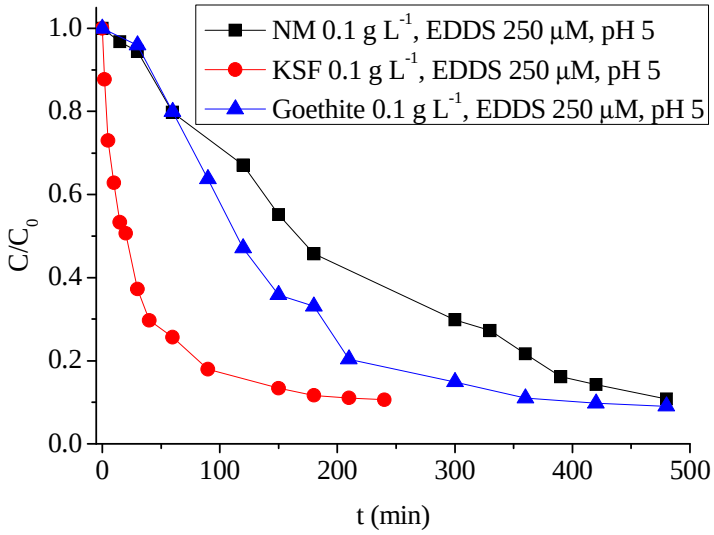

Figure IV-F-23 Photodegradation of E2 in the three different minerals- EDDS system

F-3-7 Effect of initial concentration of E2

Under the conditions of [Goethite] = 0.05 g L^{-1}, [EDDS] = 250 µM and pH 6, the effect of

initial concentration of E2 on the photodegradation of E2 was studied. Figure IV-F-24 shows the concentration profile of E2 at different initial concentrations in Goethite-EDDS suspensions. The initial rate R_0 increased upon increasing the initial concentration of E2 in the rage of 0.99-15.03 μM (data shown in Table IV-F-1). Figure IV-F-25 represents the variation of the initial rate of E2 degradation as a function of the initial E2 concentration. The curve fit well into the Langmuir-Hinshelwood rate law (L-H equation), i.e.:

$$R = -\frac{dC}{dt} = \frac{kKC}{1+KC}$$

Where C is the concentration of E2 at time 't' and *k* and *K* are rate constant and the adsorption coefficient respectively. The values obtained for *k* and *K* are 0.0979 μmol·L^{-1}·min^{-1} and 0.0308 L·μmol^{-1} respectively.

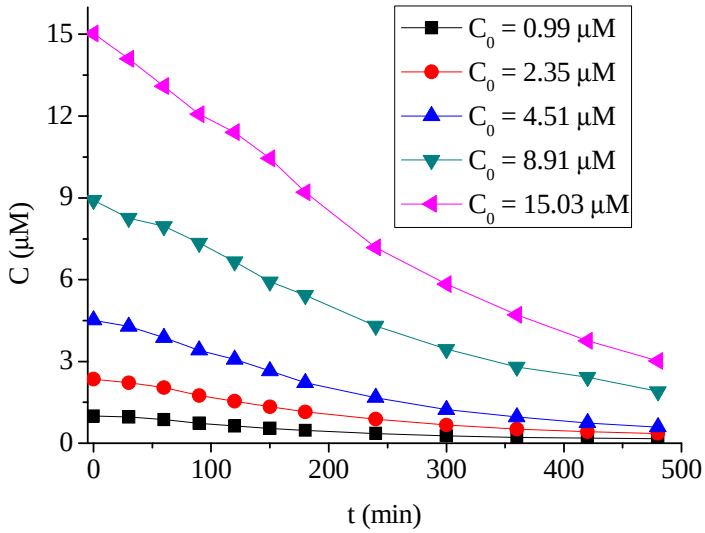

Figure IV-F-24 Influence of initial E2 concentration on the photodegradation of E2 in Goethite suspensions in the presence of EDDS. The experimental conditions were as follows: [Goethite] = 0.05 g L^{-1}, [EDDS] = 250 μM, pH 6, irradiation time 8 hours.

Table IV-F-1 Initial rate of E2 degradation for different initial E2 concentration

C (μmol·L^{-1})	Initial rate (μmol·L^{-1}·min^{-1})	Kinetic equation □L-H□	Reaction rate constant k_{LH} (μmol·L^{-1}·min^{-1})
0.99	0.00312	$R = \frac{0.00302C}{1+0.0308C}$	
2.35	0.00699		
4.51	0.01303		0.0979
8.91	0.01953	(R^2=0.991)	
15.03	0.03153		

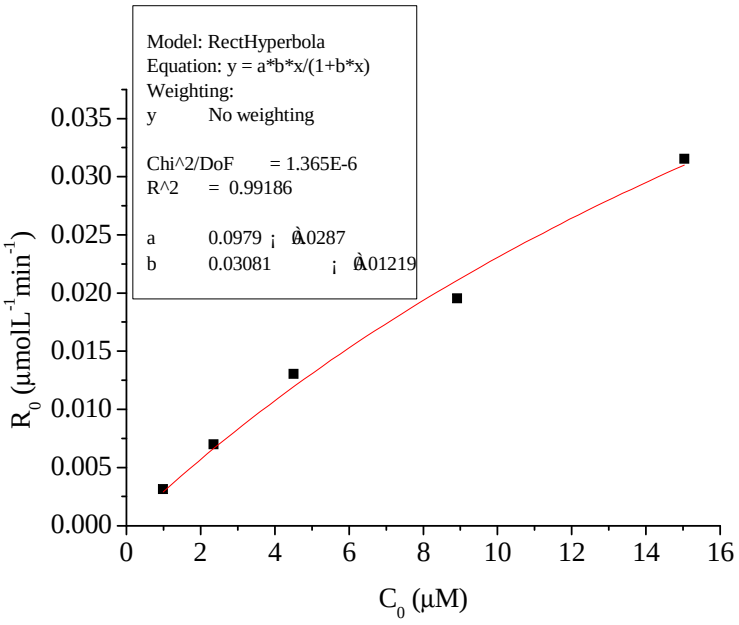

Figure IV-F -25 Plots of Ro versus Co for E2 photodegradation in the Goethite suspensions in the presence of EDDS

Conclusions

The photodegradation of E2 was investigated in Goethite suspensions in the absence and presence of EDDS. The results indicate that the Goethite concentration, EDDS concentration, pH, oxygen all have an important impact on the E2 disappearance. In the present of EDDS, the effect of Goethite concentration is not that obviously comparing with that in the condition without EDDS in the suspensions. In our experimental condition the best photodegradation efficiency after 8 hours of irradiation was found with 250 µM of EDDS. In the Goethite-EDDS suspensions, the optimal pH range for the degradation of E2 was between 4.0 and 7.0. During the irradiation, EDDS was also disappeared gradually. The influence of pH on the degradation of EDDS is similar to the influence of pH on the degradation of E2. It seems that the faster degradation of EDDS leads to the faster degradation of E2. Oxygen is found to be a limited parameter in the Goethite-EDDS photochemical system. Comparing with the Fe(III)-EDDS homogeneous system, the Goethite-EDDS system is more efficient for the E2 degradation. In the goethite-EDDS system, the main degradation pathway of E2 is proved to be reaction with $^{\bullet}OH$ reaction. Thus all these results show that goethite-EDDS system is very complex but could be considered as an efficient photocatalytic system for wastewater treatment.

V

General conclusions

V-General conclusions

In this work the photochemical performance, on the degradation of 17β-estradiol used as a probe molecule, of Fe(III)-EDDS, Montmorillonite KSF (KSF), Natural Montmorillonite (NM) and Goethite in the presence of EDDS were investigated. Our results provide some important knowledge for the fate of pollutants in the natural aquatic environment and for the photocatalytic treatment of organic pollutants. Main conclusions of this dissertation are as follows.

The photochemical impact of Fe(III)-EDDS complex on the quantum yield of $^{\bullet}OH$ formation and on the degradation of 17*β*-estradiol (E2) was investigated. For the first time, the quantum yield of $^{\bullet}OH$ was evaluated by photolysis of Fe(III)-EDDS. The quantum yield of $^{\bullet}OH$ was independent of the concentration of Fe(III)-EDDS. The effects of O_2 and irradiation wavelength on the quantum yield of $^{\bullet}OH$ are very well known and are the same as for any other iron species. On the contrary, the effect of pH is not obvious for this Fe(III)-EDDS complex. The quantum yield of $^{\bullet}OH$ radical formation was higher at higher pHs between 3.0 and 9.0. This result is particularly interesting for the natural environment. Correspondingly, E2 could be photodegraded by the photolysis of Fe(III)-EDDS, which is influenced by the concentration of Fe(III)-EDDS, pH, O_2 and the concentration of Fe(III). The Fe(III)-EDDS complex would be of importance for the transformation of organic compounds in the environment due to its higher photoactivity at pHs more relevant to the natural environment.

The reaction rate constants of $^{\bullet}OH$ on E2 and EDDS were measured by competition kinetics with 2-propanol. The reaction rate constant of $k_{E2,\bullet OH}$ and $k_{EDDS,\bullet OH}$ was 6.7×10^9 $M^{-1}s^{-1}$ and 2.0×10^8 $M^{-1}s^{-1}$ respectively. The rate constant of $^{\bullet}OH$ on E2 was about ten times faster than on EDDS. Several photoproducts were detected. Most of them formed by $^{\bullet}OH$ radicals attack on the aliphatic rings and the aromatic ring in the E2 structure.

The quantitative determination of $^{\bullet}OH$ radicals in the Montmorillonite suspensions under irradiation of a 250 W metal halide lamp ($\lambda \geq 365$ nm) was investigated. We confirmed that hydroxyl radicals were produced by illuminating Montmorillonite which was responsible for the photooxidation of benzene in aqueous suspensions of Montmorillonite. Low pH value facilitated the formation of hydroxyl radicals in the pH range of 2.0 to 10.0. The $^{\bullet}OH$ concentration increased with increasing the concentration of Montmorillonite in aqueous solutions in the range of 0 to 20.0 g L^{-1}. Higher concentration like 25.0 g L^{-1} of

Montmorillonite inhibited the •OH production. Iron, predominantly free iron in the clays, is believed to be one of the most important factors determining •OH formation. Structural irons in Montmorillonite have also contributions to •OH formation but especially in the presence of carboxylate ions. The formation of •OH from Montmorillonite under irradiation of near UV and visible light indicates that clays might play important role not only in transfer through adsorption but also in transformation through oxidation of organic compounds on the surface of clay particles in air, water, soil or even top sediments.

The adsorption and photocatalytic degradation process of E2 in the suspension of Montmorillonite KSF, Natural Montmorillonite (NM) and Goethite were studied. The adsorption of E2 on the minerals is fast and weak. The results followed the Langmuir equation in the KSF and Goethite suspensions, and the Freundlich equation in NM suspensions. EDDS influence slightly the E2 adsorption on the minerals. However, the influence of E2 adsorption on the degradation process was not found. The optimal concentration of KSF, NM and Goethite for the E2 degradation was 1.0 g L^{-1}, 6.0 g L^{-1}, 0.1 g L^{-1} respectively. The degradation of E2 was decreased with increasing the pH and in the basic pH there was almost no E2 degradation. The optimal pH for the E2 degradation was around 3.0 in all the three minerals. The results indicated that the iron in the minerals was involved in the photocatalytic process.

The photocatalytic degradation process of E2 in the suspension of Montmorillonite KSF, Natural Montmorillonite and Goethite in the presence of EDDS were studied. In these three minerals-EDDS suspensions, the degradation of E2 significantly increased at near-neutral pH and basic pH (pH 5.0 to 9.0). On the contrary without EDDS, the optimal pH is limited in the acid pH (3.0 to 4.0). These results demonstrate that the mineral-EDDS photochemical system is less limited by the pH condition and a promising way for the removal of contaminants in the natural aquatic environment. The degradation kinetics of E2 follows the Langmuir-Hinshelwood rate law in all the three minerals-EDDS system. Small amount of minerals is enough to get good degradation efficiency in the presence of EDDS, i.e. KSF 0.1 g L^{-1}, NM 0.1 g L^{-1} and Goethite 0.1 g L^{-1}. The concentration of EDDS is a very important factor influencing the efficiency of E2 degradation, which can not be too low or too high for acting as scavenger of hydroxyl radicals. During the E2 degradation, EDDS also is degraded. EDDS plays an important role for keeping ferrous iron soluble at cirumneutral pH and the photochemical process of the minerals-EDDS can continue. After adding 2-propanol into the suspension, there was almost no E2 degradation, indicating that the main degradation

pathway of E2 was the reaction with $^{\bullet}OH$. Oxygen is a very important factor that affects the photodegradation of E2. Oxygen takes part in the photochemical process in such system. Without oxygen, the hydroxyl radicals barely could be formed. Thus all these results show that the concentration of minerals and EDDS, solution pH and oxygen must be taken into account as major parameters to improve the efficiency of the mineral-EDDS photochemical process.

In this work, though study the main factors that influence the photodegradation of E2 or the formation of hydroxyl radical in EDDS-Fe(III)/mineral system, we start to understand the photochemical process of these systems. However, the mechanism of EDDS-mineral as a photochemical system is still poor understood. The photochemical process in EDDS-mineral system happened both on the surface of mineral as a heterogeneous reaction and also in the solution as a homogeneous reaction. The research of the heterogeneous reaction on the surface of the minerals should be stressed in further.

VI

APPENDIX

VI-APPENDIX

VI-1 List of tables

VI-2 List of figures

VI-3 List of scheme

VII

REFERENCES

VII-REFERENCES

Abida O., Impact complexes of iron and the solar light on the fate of pollutants in the aquatic environment, Ph.D.Thesis. University Blaise Pascal. 2005.

Abida O., Mailhot G., Litter M., Bolte M., Impact of iron-complex (Fe(III)-NTA) on photoinduced degradation of 4-chlorophenol in aqueous solution, Photochemi. Photobiol. Sci. 2006, 5: 395-402.

Achterberg E.P., Holland T.W., Bowie A.R., Mantoura R.F.C., Worsfold P.J., Determination of iron in seawater, Anal. Chim. Acta 2001, 442: 1-14.

Ahn M.Y., Filley T.R., Jafvert C.T., Nies L., Hua I., Bezares-Cruz J., Photodegradation of decabromodiphenyl ether adsorbed onto clay minerals, metal oxides, and sediment. Environ. Sci. Technol. 2006, 40: 215-220.

Alaton I.A., Balcioglu I.A., Photochemical and heterogeneous photo-catalytic degradation of waste vinylsulphone dyes: a case study with hydrolyzes Reactive Black 5, J. Photochem. Photobiol., A 2001, 141(2-3): 247-254.

Amonette J.E., Workman D.J., Kennedy D.W., Fruchter J.S., Gorby Y.A., Dechlorination of carbon tetrachloride by Fe(II) associated with goethite, Environ. Sci. Technol. 2000, 34: 4606-4613.

Amonette J.E., Iron redox chemistry of clays and oxides: environmental applications. electrochemical Properties of Clays, CMS Workshop Lectures, Aurora, Clay Minerals Society 2003, 10: 89-148.

Andreozzi R., Caprio V., Marotta R., Iron(III) (hydr)oxide-mediated photooxidation of 2-aminophenol in aqueous solution: a kinetic study, Water Res. 2003, 37: 3682-3688.

Arakaki T., Miyake T., Hirakawa T, Sakugawa H., pH dependent photoformation of hydroxyl radical and absorbance of aqueous-phase N(III) (HNO_2 and NO_2^-), Environ. Sci. Technol. 1999, 33: 2561-2565.

Arnold S.F., Klotz D.M., Collins B.M., Vonier Jr. P.M., Guillette L.J., Mclachlan J.A., Synergistic activation of estrogen receptor with combinations of environmental chemicals, Science 1996, 272: 1489-1492.

Atkinson R.J., Posner A.M., Quirk J.P., Crystal nucleation in Fe(III) solutions and hydroxide gels, J. Inorg. Nucl. Chem. 1968, 30: 2371-2381.

Baldrian, P., Merhautová, V., Gabriel, J., Nerud, F., Stopka, P., Hrubý, M., Benes, M.J., Decolorization of synthetic dyes by hydrogen peroxide with heterogeneous catalysis by mixed iron oxides, Appl. Catal. B: Environ. 2006, 66: 258-264.

Balmer M. E., Sulzberger B., Atrazine Degradation in Irradiated Iron/Oxalate Systems: Effects of pH and Oxalate, Environ. Sci. Technol. 1999, 33: 2418-2424.

Banfield J.F., Zhang H., Nanoparticles in the environment, Rev. Mineral. Geochem. 2001, 44: 1-58.

Barbeau K., Photochemistry of organic iron(III) complexing ligands in oceanic systems, Photochem. Photobiol. 2006, 82: 1505-1516.

Baronti C., Curini R., D'Ascenzo G., Corcia AD., Gentili A., Samperi R., Monitoring natural and synthetic estrogens at activated sludge sewage treatment plants and in a receiving river water, Environ. Sci. Technol. 2000, 40: 2181-2189.

Baronti C., Curini R., D'Ascenzo G., Di Corcia A., Gentili A., Samperi R., Monitoring natural and synthetic estrogens at activated treatment plants and in receiving river water, Environ. Sci. Technol. 2000, 34:5059-5066.

Baronti C., Curini R., D'Ascenzo G., Di Corcia A., Gentili A., Samperi R., 2000. Monitoring natural and synthetic estrogens at activated treatment plants and in receiving river water. Environ. Sci. Technol. 35, 5059-5066.

Barrault J., Tatibouët J.M., Papayannakos N., Catalytic wet peroxide oxidation of phenol over pillared clays containing iron or copper species, C.R. Acad. Sci. Paris, Sér. II C, Chem. 2000, 3: 777-783.

Barreto J.C., Smith G.S., Strobel N.H.P., McQuillan P.A. and Miller T.A., Terephthalic acid: A dosimeter for the detection of hydroxyl radicals in vitro, Life Sci. 1995, 56: 89-96.

Belessi V., Lanbropoulou D., Konstantinou I., Katsoulidis A., Pomonis P., Pertridis D., Albanis T., Structure and photocatalytic performance of TiO2/clay nanocomposites for the degradation of dimethachlor, Appl. Catal. B: Environ. 2007, 73: 292-299.

Belfroid A.C., Van der Horst A., Vethaak A.D., Schafer A.J., Ris G.B.J., Wegener J., et al. Analysis and occurrence of estrogenic hormones and their glucuronides in surface water and waste water in the Netherlands, Sci. Total. Environ. 1999, 225: 101-108.

Benkelberg H.J., Warneck P., Photodecomposition of iron(III) hydroxo and sulfato complexes in aqueous solution: wavelength dependence of OH and SO_4^- quantum yields, J. Phys. Chem. 1995, 99: 5214-5221.

Bielski B.H.J., Cabelli D.E., Arudi L.R., Ross A.B., Reactivity of HO_2/O_2^- radicals in aqueous solution. J. Phys. Chem. Ref. Data 1985, 14:1041-1100.

Bila D., Montalvão A.F., Azevedo D.A., Dezotti M., Estrogenic activity removal of 17β-estradiol by ozonation and identification of by-products, Chemosphere 2007, 69: 736-746.

Bobu, M., Yediler, A., Siminiceanu, I., Schulte-Hostede, S., Degradation studies of ciprofloxacin on a pillared iron catalyst, Appl. Catal. B: Environ. 2008, 83: 15-23.

Bondgaard, M., Bjerregaard, P., Association between cadmium and calcium uptake and distribution during themoult cycle of females shore crabs, Carcinus maenas: an in vivo study, Aquat. Toxicol. 2005, 72: 17-28.

Bucheli-Witschel M., Egli T., Environmental fate and microbial degradation of aminopolycarboxylic acids, FEMS Microbiology Reviews 2001, 25: 69-106.

Buerge, I. J.; Hug, S. J. Influence of mineral surfaces on chroniium(VI) reduction by iron(II). Environ. Sci. Technol. 1999, 33: 4285-4291.

Bushe´e E.L., Edwards D.R., Moore P.A., Quality of runoff from plots treated with municipal sludge and horse bedding, Trans ASAE 1998, 41: 1035-1041.

Buxton G.V., Greenstock C.L., Helman W.P., Ross A.B., Critical review of rate constants for reactions of hydrated electrons, hydrogen atoms and hydroxyl radicals in aqueous solution, J. Phys. Chem. Ref. Data 1988, 17(2): 513-886

Calvert J.G., Pitts J. N., Photochemistry, John Wiley & Sons, New York, 1966: 783.

Chamarro E., Marco A., Esplugas S., Use of Fenton reagent to improve organic chemical biodegradability. Water Res. 2001, 35 (4): 1047-1051.

Chang Hyun-Shik, Choo Kwang-Ho, Lee Byungwhan, Choi Sang-June, The methods of identification, analysis, and removal of endocrine disrupting compounds (EDCs) in water, J. Hazard. Mater. 2009, 172: 1-12.

Chatterjee S., Sarkar S., Bhattacharyya S.N., Photodegradation of phenol by visible light in the presence of colloidal Fe_2O_3, J. Photochem. Photobiol. A: Chem. 1994, 81: 199-203.

Chen Q.Q., Wu P.X., Dang Z., Zhu N.W., Li P., Wu J.H., Wang X.D., Iron pillared vermiculite as a heterogeneous photo-Fenton catalyst for photocatalytic degradation of azo dye reactive brilliant orange X-GN, Sep. Purif. Technol. 2010, 71: 315-323.

Chen Q.Q., Wu P.X., Li Y.Y., Zhu N.W., Dang Z., Heterogeneous photo-Fenton photodegradation of reactive brilliant orange X-GN over iron-pillared montmorillonite under visible irradiation, J. Hazard. Mater. 2009, 168: 901-908.

Chen X.Q., Li F.B., Xin-jun Li. Synthesis of TiO2/montmorillonite multiplex photo-catalyst and catalytic decomposition of methylene blue, Soil Environ Sci 2001, 10: 30-32.

Chen Y., Wu F., Lin Y.X., Deng N.S., Bazhin N., Glebov E., Photodegradation of glyphosate in the ferrioxalate system, J. Hazard. Mater. 2007, 148: 360-365.

Cheng M.M., Song W.J., Ma W.H., Chen C.C., Zhao J.C., Lin J., Zhu H.Y., Catalytic activity of iron species in layered clays for photodegradation of organic dyes under visible irradiation, Appl. Catal. B: Environ. 2008, 77: 355-363.

Chiou C.H., Juang R.S., Photocatalytic degradation of phenol in aqueous solutions by Pr-doped TiO2 nanoparticles, J. Hazard. Mater. 2007,149: 1-7.

Chun C.L., Hozalski R.M., Arnold W.A., Degradation of drinking water disinfection

byproducts by synthetic goethite and magnetite, Environ. Sci. Technol. 2005, 39: 8525-8532.

Chun C.L., Penn R.L., Arnold W.A., Kinetic and microscopic studies of reductive transformation of organic contaminants on goethite, Environ. Sci. Technol. 2006, 40: 3299-3304.

Cieśla P., Kocot P., Mytych P., Stasicka Z., Homegeneous photocatalysis by transition metal complexes in the environment, J. Mol. Catal. A: chem. 2004, 223: 17-33.

Clara M., Kreuzinger N., Strenn B., Gans O., Kroiss H., The solids retention time-a suitable design parameter to evaluate the capacity of wastewater treatment plants to remove micropollutants, Water Res. 2005, 39: 97-106.

Colborn T., Dumanoski D., Myers J.P., Our Stolen Future, Plume/Penguin Book: New York 1996.

Coleman H.M., Routledge E.J., Sumpter J.P., Eggins B.R., Byrne J.A., Rapid loss of estrogenicity of steroid estrogens by UVA photolysis and photocatalysis over an immobilized titanium dioxide catalyst, Water Res. 2004, 38: 3233-3240.

Cornell R.M., Schwertmann U., The iron oxides: structure, properties, reactions, occurrences, and uses. 2nd, completely rev. and extended ed., Wiley-VCH: Weinheim 2003, p188.

Daneshvar, N., Salari, D., Khataee, A.R., Photocatalytic degradation of azo dye acid red 14 in water: investigation of the effect of operational parameters, J. Photochem. Photobiol. A: Chem. 2003, 157: 111-116.

Daniel L.M., Frost R.L., Zhu H.Y., Synthesis and characterisation of clay-supported titania photocatalysts, J. Colloid Interface Sci. 2007, 316: 72-79.

D'Ascenzo G., Corcia A.D., Mancini A.G.R., Mastropasqua R., Nazzari M., Samperi R. Fate of natural estrogen conjugates in municipal sewage transport and treatment facilities, Sci. Total Environ. 2003, 302: 199-209.

De León M.A., Castiglioni J., Busssi J., Sergio M., Catalytic activity of an iron-pillared montmorillonitic clay mineral in heterogeneous photo-Fenton process, Catal. Today 2008, 133-135: 600-605.

Deborde M., Rabouan S., Duguet J.P., Legube B., Kinetics of aqueous ozone-induced oxidation of some endocrine disruptors, Environ. Sci. Technol. 2005, 39: 6086-6092.

Desbrow C., Routledge E.J., Brighty G.C., Sumpter J.P., Waldock M., Identification of estrogenic chemicals in STW effluent. 1. Chemical fractionation and in vitro biological

screening, Environ. Sci. Technol. 1998, 32: 1549-1558.

Ding X.J., An T.C., Li G.Y., Zhang S.Q., Chen J.X., Yuan J.M., Zhao H.J., Chen H., Sheng G.Y., Fu J.M., Preparation and characterization of hydrophobic TiO_2 pillared clay: The effect of acid hydrolysis catalyst and doped Pt amount on photocatalytic activity, J. Colloid Interface Sci. 2008, 320: 501-507.

Dong H., Kukkadapu R.K., Fredrickson J.K., Zachara J.M., Kennedy D.W., Kostandarithes H.M., Microbial reduction of structural Fe(III) in illite and goethite, Environ. Sci. Technol. 2003, 37: 1268-1276.

Ebina Y., Okada S., Hamazaki S., Ogino F., Li J. L., Midorikawa O., Nephrotoxicity and renal cell carcinoma after use of iron- and aluminum-nitrilotriacetate complexes in rats, J. Natl. Cancer Inst. 1986, 76: 107-113.

Erb R.E., Chew B.P., Keller H.F., Relative concentrations of estrogen and progesterone in milk and bold, and excretion of estrogen in urine, J. Anim. Sci. 1977, 46: 617- 626.

Fang X.W., Mark G., von Sonntag C., OH radical formation by ultrasound in aqueous solutions Part I: the chemistry underlying the terephthalate dosimeter, Ultrason. Sonochem. 1996, 3: 57-63.

Faust B.C., Allen J.M. Aqueous-phase photochemical formation of hydroxyl radical in authentic cloudwaters and fogwaters, Environ. Sci. Technol. 1993, 27: 1221-1224.

Faust B.C., Zepp R.G., Photochemistry of aqueous iron(III)-polycarboxylate complexes: Roles in the chemistry of atmospheric and surface waters, Environ. Sci. Technol. 1993, 27: 2517-2522.

Feng X.H., Tu J.F., Ding S.M., Wu F., Deng N.S., Photodegradation of 17β-estradiol in water by UV-vis/Fe(III)/H_2O_2 system, J. Hazard. Mater. B 2005, 127: 129-133.

Feng J., Hu X., Yue P.L., Novel Bentonite Clay-Based Fe -Nanocomposite as a Heterogeneous Catalyst for Photo-Fenton Discoloration and Mineralization of Orange II, Environ. Sci. Technol. 2004, 38: 269-275.

Feng J.Y., Hu X.J., Yue P.L., Zhu H.Y., Lu G.Q., A novel laponite clay-based Fe nanocomposite and its photocatalytic activity in photo-assisted degradation of Orange II, Chem. Eng. Sci. 2003, 58: 679-685.

Feng J.Y., Hu X.J., Yue P.L., Discoloration and mineralization of Orange II by using a bentonite clay-based Fe nanocomposite film as a heterogeneous photo-Fenton catalyst, Water Res. 2005, 39: 89-96.

Fernandez M.P., Ikonomou M.G., Buchanan I., An assessment of estrogenic organic

contaminants in Canadian wastewaters, Sci. Total Environ. 2007, 373: 250-269.

Flynn C.M., Hydrolysis of inorganic iron (III) salts, Chem. Rev. 1984, 84: 31-41.

Frank R., Rau H., Photochemical transformation in aqueous solution and possible environmental fate of ethylenediaminetetraacetic acid (EDTA), Ecotoxicol. Environ. Saf. 1990, 19: 55-63.

Gallard H., De Laat J., Legube B., Effect of pH on the oxidation rate of organic compounds by Fe^{II}/H_2O_2, Mechanism and simulation, New J. Chem. 1998, 22: 263-268.

Garrido-Ramírez E.G., Theng B.K.G., Mora M.L., Clays and oxide minerals as catalysts and nanocatalysts in Fenton-likereactions-A review, Appl. Clay Sci. 2010, 47: 182-192.

Gates W.P., Slade P.G., Manceau A., Lanson B., Site occupancies by iron in nontronites, Clays. Clay. Miner. 2002, 50: 223-239.

Giesy J.P., Hilscherova K., Jones P.D., Kannan K., Machala M., Cell bioassays for detections of aryl hydrocarbon (AhR) and estrogen receptor (ER) mediated activity in environmental samples, Mar. Pollut. Bull. 2002, 45: 3-16.

Goldberg M.C., Cunningham K.M., Weiner E.R., Aquatic photolysis: photolytic redox reactions between geothite and adsorbed organic acids in aqueous solutions, J. Photochem. Photobiol. A 1993, 73: 105-120.

Gournis D., Karakassides M.A., Petridis D., Formation of hydroxyl radicals catalyzed by clay surfaces. Phys. Chem. Miner. 2002, 29: 155-158.

Gulshan F., Yanagida S., Kameshima Y., Isobe T., Various factors affecting photodecomposition of methylene blue by iron-oxides in an oxalate solution, Water Res. 2010, doi: 10.1016/j. watres.2010.01.040.

He J., Ma W.H., He J.J., Zhao J.C., Yu J.C., Photooxidation of azo dye in aqueous dispersions of H2O2/α-FeOOH, Appl. Catal. B: Environ. 2002, 39: 211-220

Hofstetter T.B., Schwarzenbach R.P., Haderlein S.B., Reactivity of Fe(II) species associated with clay minerals. Environ. Sci. Technol. 2003, 37 (3): 51-528.

Hohenblum P., Gans O., Moche W., Scharf S., Lorbeer G., Monitoring of selected estrogenic hormones and industrial chemicals in groundwaters and surface waters in Austria, Sci. Total Environ. 2004, 333: 185-93.

Houben G.J., Iron oxide incrustations in wells. Part 2: chemical dissolution and modeling, Appl. Geochem. 2003, 18: 941-945.

Huston P.L., Pignatello J.J., Reduction of perchlorokanes by ferriox-generated carboxylate radical preceding mineralization by the photo-Fenton reaction, Environ. Sci. Technol.

1996, 30: 3457-3463.

Irmak S., Erbatur O., Akgerman A., Degradation of 17β-estradiol and bisphenol A in aqueous medium by using ozone and ozone/UV techniques, J Hazard. Mater. B 2005, 126: 54-62.

Iurascu B., Siminiceanu I., Vione D., Vicente M.A., Gil, A., Phenol degradation in water through a heterogeneous photo-Fenton process catalyzed by Fe-treated laponite, Water Res. 2009, 43: 1313-1322.

Jaeger C.D., Bard A.J., Spin trapping and electron spin resonance detection of radical intermediates in the photodecomposition of water at titanium dioxide particulate systems, J. Phys. Chem. 1979, 83: 314-3152.

Jaworska J.S., Schowanek D., Feijtel T.C.J., Environmental risk assesment for trisodium [S,S]-ethylene diamine disuccinate, a biodegradable chelator used in detergent applications, Chemosphere 1999, 38: 3597-3625.

Jeannot R., Sabik H., Sauvard E., Dagnac T., Dohrendorf K., Determination of endocrine-disrupting compounds in environmental samples using gas and liquid chromatography with mass spectrometry, J. Chromatogr. A 2002, 974: 143-159.

Johnson A.C., Belfroid A., Di Corcia A., Estimating steroid oestrogen inputs into activated sludge treatment works and observations on their removal from the effluent, Sci. Total Environ. 2000, 256: 163-173.

Joseph J.M., Varghese R., Aravindakumar C.T., Photoproduction of hydroxyl radicals from Fe(III)-hydroxy complex: a quantitative assessment, J. Photochem. Photobiol. A: Chem. 2001, 146: 67-73.

Jozefaciuk G., Bowanko G., Effect of acid and alkali treatments on surface areas and adsorption energies of selected minerals, Clays Clay Miner. 2002, 50: 771-783.

Kari F.G., Hilger S., Canonica S., Determination of the reaction quantum yield for the photochemical degradation of Fe(III)-EDTA: implication for the environmental fate of EDTA in surface waters, Environ. Sci. Technol. 1995, 29: 1008-1017.

Katagi T., Photoinduced oxidation of the organophosphorus fungicide tolclofos-methyl on clay minerals, J. Agric. Food Chem. 1990, 38: 1595-1600.

Katagi T., Photodegradation of esfenvalerate in clay suspensions, J. Agric. Food Chem. 1993, 41: 2178-2183.

Katagi T., Photodegradation of pesticides on plant and soil surfaces, Rev. Environ. Contam. Toxicol. 2004, 182: 1-189.

Katsumata H., Kawabe S., Kaneco S., Suzuki T., Ohta K., Degradation of bisphenol A in water by the photo-Fenton reaction, J. Photochem. Photobiol. A Chem. 2004, 162: 297-305.

Kavlock R., Overview of endocrine disruptor research activity in the United States, Chemosphere 1999, 39: 1227-1236.

Kawamura K., Steinberg S., Kaplan I.R., Capillary GC determination of short-chain dicarboxylic acids in rain, fog, and mist, Int. J. Environ. Anal. Chem. 1985, 19: 175-188.

Kim S.D., Cho J., Kim I.S., Vanderford B.J., Snyder S.A., Occurrence and removal of pharmaceuticals and endocrine disruptors in South Korean surface, drinking, and waste waters, Water Res. 2007, 41: 1013-1021.

Kobayashi Y., Okuda T., Yamashita N., Tanaka H., Tanaka S., Fuji S., et al. The behavior of free/conjugated estrogens during advanced wastewater treatment, Environ Sanit Eng Res 2006, 20: 55-8.

Kochany J., Bolton J.R., Mechanism of photodegradation of aqueous organic pollutants. 2. Measurement of the primary rate constants for reaction of •OH radicals with benzene and some halobenzenes using an EPR spin-trapping method following the photolysis of H_2O_2, Environ. Sci. Technol. 1992, 26: 262-265.

Kocot P., Karocki A., Stasicka Z., Photochemistry of the Fe(III)-EDTA complexe A mechanistic study, J. photochem. Photobiol. A: chem. 2006, 179: 176-183.

Kocot P., Szacilowski K., Stasicka Z., Photochemistry of the $[Fe^{III}(edta)(H_2O)^{-}]$ and $[Fe^{III}(edta)(OH)^{2-}]$ complexes in presence of environmentally relevant species, J. photochem. Photobiol. A: chem. 2007, 188: 128-134.

Kong, L., Ferry, J.L., Effect of salinity on the photolysis of the chrysene adsorbed to a smectite clay. Environ. Sci. Technol. 2003, 37: 4894-4900.

Kong, L., Ferry, J.L., Photochemical oxidation of chrysene at the Silica gel–water interface. J. Photochem. Photobiol. A: Chem. 2004, 162: 415-421.

Kriegman-King, M.R., Reinhard, M., Transformation of carbon tetrachloride in the presence of sulfide, biotite, and vermiculite, Environ. Sci. Technol. 1992, 26, 2198-2206.

Kuch H.M., Ballschmiter K., Endocrine-disrupting phenolic compounds and estrogens in surface and drink-ing water by HRGC-(NCl)-MS in the picogram per liter range, Environ. Sci. Technol. 2001, 35: 3201-3206.

Lagana A., Bacaloni A., Leva I.D., Faberi A., Fago G., Marino A., Analytical methodologies for determining the occurrence of endocrine disrupting chemicals in sewage treatment

plants and natural waters, Anal. Chim. Acta. 2004, 501: 79-88.

Lan Q., Li F.B., Sun C.X., Liu C.S., Liu C.S., Li X.Z., Heterogeneous photodegradation of pentachlorophenol and iron cycling with goethite, hematite and oxalate under UVA illumination, J. Hazard. Mater. 2010, 174: 64-70.

Laszlo P., Chemical reactions on clays, Scinece, New Series, 1987, 235: 1473-1477.

Lea J., Adesina A.A., The Photo-Oxidative Degradation of Sodium Dodecyl Sulphate in Aerated Aqueous TiO_2 Suspension, J. Photochem. Photobiol. A: Chem., 1998, 118: 111-122.

Lei J., Liu C.S., Li F.B., Li X.M., Zhou S.G., Liu T.X., Gu M.H., Wu Q.T., Photodegradation of orange I in the heterogeneous iron oxide–oxalate complex system under UVA irradiation, J. Hazard. Mater. B 2006, 137: 1016-1024.

Leland J.K., Bard A.J., Photochemistry of colloidal semiconducting iron oxide polymorphs, J. Phys. Chem. 1987, 91: 5076-5083.

Lewis R.J., Carcinogenically Active Chemicals, Van Nostrand Reinhold: New York, 1991, p131.

Li D., Yuranova T., Albers P., Kiwi J., Accelerated photobleaching of Orange II on novel ($H_5FeW_{12}O_{40}10H_2O$)/silica structured fabrics, Water Res. 2004, 38: 3541-3550.

Li F.B., Li X.Z. Li, Li X.M., Liu T.X., Dong J., Heterogeneous photodegradation of bisphenol A with iron oxides and oxalate in aqueous solution, J. Colloid Interface Sci. 2007, 311: 481-490.

Li J., Wu F., Deng N.S., Glebov E.M., Bazhin N.M., Degradation of orange II by heterogeneous photocatalytic reaction using montmorillonite KSF, React. Kinet. Catal. Lett. 2008, 95: 247-255.

Li J., Wu F., Maihot G., Deng N.S., Photodegradation of chloroform in aqueous solution: Impact of montmorillonite KSF paricles, J. Hazard. Mater. 2010, 174: 368-374.

Liu C.S., Li F.B., Li X.M., Zhang G., Kuang Y.Q., The effect of iron oxides and oxalate on the photodegradation of 2-mercaptobenzothiazole, J. Mol. Catal. A: Chem. 2006, 252: 40-48.

Liu C.X., Kota S., Zachara J.M., Fredrickson J.M., Brinkman C.K., Kinetic analysis of the bacterial reduction of goethite, Environ. Sci. Technol., 2001, 35: 2482-2490.

Liu R., Wilding A., Zhou J., Simultaneous determination of endocrine disrupting phenolic compounds and steroids in water by solid-phase extraction-gas chromatography–mass spectrometry, J. Chromatogr. A 2004, 1022: 179-189.

Liu Y.X., Li J., Wu F., Zhang C.B., Deng N.S., Insight into heterogeneous photocatalytic degradation of phenol over montmorillonite KSF, Chem. Eng. Comm. 2008a, 195:1-10.

Liu Y.X., Zhang X., Guo L., Wu F., Deng N.S., Photodegradation of Bisphenol A in the montmorillonite KSF suspended solutions, Ind. Eng. Chem. Res., 2008b, 47: 7141-7146.

Liu X.L., Wu F., Deng N.S. Photoproduction of hydroxyl radicals in aqueous solution with algae under high pressure mercury lamp, Environ. Sci. Technol. 2004, 38: 296-299.

Liu X.W., Hu M., Hu Y.H., Chemical composition and surface charge properties of montmorillonit, J. Cent. South Univ. Technol. 2008, 15: 193-197.

Liu Ze-hua, Kanjo Yoshinori, Mizutani Satoshi, Removal mechanisms for endocrine disrupting compounds (EDCs) in wastewater treatment-physical means, biodegradation, and chemical advanced oxidation: A review, Science of the total environment 2009, 407: 731-748.

Lu M.C., Chen J.N., Chang C.P., Oxidation of dichlorvos with hydrogen peroxide using ferrous ion as catalyst, J. Hazard. Mater. 1999, 65: 277-288.

Lu M.C., Oxidation of chlorophenols with hydrogen peroxide in the presence of goethite, Chemosphere 2000, 40: 125-130.

Lu P., Wu F., Deng N.S., Enhancement of TiO_2 photocatalytic redox ability by β-cyclodextrin in suspended solutions, Appl. Catal. B 2004, 53: 87-93.

Macounová K., Krýsová H., Ludvík J., Jirkovský J., Kinetics of photocatalytic degradation of diuron in aqueous colloidal solution of Q-TiO2 particles, J. Photochem. Photobiol. A: Chem. 2003, 156: 273-282.

Madhavan D., Pitchumani K., Photoreactions in clay media: singlet oxygen oxidation of electron-rich substrates mediated by clay-bound dyes, J. Photochem. Photobiol. A: Chem. 2002, 153: 205-210.

Mashlan M., Bartonkova H., Jancik D., Tucek J., Martinec P., Iron oxide modified minerals, Hyperfine Interact. 2009, 191: 151-157.

Matta R., Hanna K., Chiron S., Fenton-like oxidation of 2, 4, 6-trinitrotoluene using different iron minerals, Sci. Total Environ. 2007, 385: 242-251.

Mazeina L., Navrotsky A., Surface enthalpy of goethite. Clays clay miner. 2005, 53: 113-122.

Mazellier P., Bolte M., Heterogeneous light-induced transformation of 2,6-dimethylphenol in aqueous suspensions containing goethite, J. Photochem. Photobiol. A: Chem. 2000, 132: 129-135.

Mazellier P., Sulzberger B., Diuron Degradation in Irradiated, Heterogeneous Iron/Oxalate Systems: The Rate-Determining Step, Environ. Sci. Technol. 2001, 35: 3314-3320.

Means J.L., Kucak T., Crear A., Relative degradation rates of NTA, EDTA and DTPA and environmental applications, Environ. Pollut., Series B 1980, 1: 45-60.

Metsärinne S., Tuhkanen T., Aksela R., Photodegradation of ethylenediaminetetraacetic acid (EDTA) and ethylenediamine disuccinic acid (EDDS) within natural UV radiation range, Chemosphere 2001, 45: 949-955.

Meunier B., Metalloporphyrins as versatile catalysts for oxidation reactions and oxidative DNA cleavage, Chem. Rev. 1992, 92: 1411-1456.

Ménesi J., Körösi L., Bazsó É, Zöllmer V., Richardt A., Dékánv I., Photocatalytic oxidation of organic pollutants on titania–clay composites, Chemosphere 2008, 70: 538-542.

Miller G.C., Zepp R.G., Effects of Suspended Sediments on Photolysis Rates of Dissolved Pollutants, Water Res. 1979b, 13: 453-459.

Millington K.R., Kirschenbaum L.J., Detection of hydroxyl radicals in photoirradiated wool, cotton, nylon and polyester fabrics using a fluorescent probe, Color. Technol. 2002, 118: 6-14.

Morteani G., Moller P., Fuganti A. Paces T., Input and fate of anthropogenic estrogens and gadolinium in surface water and sewage plants in the hydrological basin of Prague (Czech Republic), Environ. Geochem. Health 2006, 28: 257-264.

Murugananthan M., Yoshihara S., Rakuma T., Uehara N., Shirakashi T., Electrochemical degradation of 17β-estradiol (E2) at boron-doped diamond (Si/BDD) thin film electrode, Electrochim. Acta 2007, 52: 3242-3249.

Nowack B., Environmental chemistry of aminopolycarboxylate chelating agents, Environ. Sci. Technol. 2002, 36: 4009-4016.

Nowack B., Sigg L., Adsorption of EDTA and Metal-EDTA complexes onto goethite, J. colloid interface sci. 1996, 177: 106-121.

Odom I.E., Smectite clay minerals: Properties and Uses, Philosophical transactions of the royal society of london, NATO ASI Ser., Ser. C 1984, 311: 391-409.

Ohko Y., Iuchi K.I., Niwa C., Tatsuma T., Nakashima T., Iguchi T., Kubota Y., Fujishima A., 17β-Estradiol degradation by TiO_2 photocatalysis as a means of reducing estrogenic activity, Environ. Sci. Technol. 2002, 36: 4175-4181.

Ooka C., Yoshida H., Suzuki K., Hattori T., Adsorption and Photocatalytic Degradation of Toluene Vapor in Air on Highly Hydrophobic TiO_2 Pillared Clay, Chem. Lett. 2003, 32:

896-897.

Orama M., Hyvönen H., Saarinen H., Aksela R., Complexation of [S,S] and mixed stereoisomers of N,N'-ethylenediaminedisuccinic acid (EDDS) with Fe(III), Cu(II), Zn(II), and Mn(II) ions in aqueous solution, J. Chem. Soc., Dalton Trans., 2002, 4644-4648.

Ou X.X., Quan X., Chen S., Zhang F.J., Zhao Y.Z., Photocatalytic reaction by Fe(III)–citrate complex and its effect on the photodegradation of atrazine in aqueous solution, J. Photochem. Photobiol. A: Chem. 2008, 197: 382-388.

Pan X.M., Schuchmann M.N., Von Sonntag C., Oxidation of benzene by the OH radical A product and pulse radiolysis study in oxygenated aqueous solution. J. Chem. Soc., Perkin Trans. 1993, 2: 289-297.

Panias D., Taxiarchou M., Paspaliaris I., Kontopoulos A., Mechanisms of dissolution of iron oxides in aqueous oxalic acid solutions, Hydrometallurgy 1996, 42: 257-265.

Panter G.H., Thompson R.S., Sumpter J.P., Adverse reproductive effects in male fathead minnows (Pimephales promelas) exposed to environmentally relevant concentrations of the natural oestrogens, oestradiol and oestrone, Aquat. Toxicol. 1998, 42: 243-253.

Panter G.H.; Thompson R.S.; Sumpter J.P., Intermittent exposure of fish to estradiol, Environ. Sci. Technol. 2000, 34: 2756-2760.

Parida K., Das J., Studies on ferric oxide hydroxides II. Structural properties of goethite samples (α-FeOOH) prepared by homogeneous precipitaton from $Fe(NO_3)_3$ solution in the prsence of sulfate ions, J. colloid interface sci. 1996, 178: 586-593.

Pavelčik F., Kettmann V., The crystal and molecular structure of calcium (S,S)-ethylenediamine-N,N'-disuccinatoferrate octahydrate, Collect. Czech. Chem. Commun. 1983, 48: 1376-1389.

Peterson E.W., Davis R.K., Orndorff H.A., 17β-estradiol as an indicator of animal waste contamination in mantled karst aquifers, J. Environ. Qual. 2000, 29: 826-834.

Pinnavaia T.J., Intercalated clay catalysts, Science 1983, 220: 365-371.

Qin H.L., Zhang S.M., Liu H.J., Xie S.B., Yang M.S., Shen D.Y., Photo-oxidative degradation of polypropylene/montmorillonite nanocomposites, Polymer 2005, 46: 3149-3156.

Ramírez J.H., Costa C.A., Madeira L.M., Mata G., Vicente M.A., Rojas-Cervantes M.L., López-Peinado A.J., Martín-Aranda R.M., Fenton-like oxidation of Orange II solutions using heterogeneous catalysts based on saponite clay, Appl. Catal. B Environ. 2007, 71: 44-56.

Robert F.C., Suri R.P.S., Fu H.X., Free synthetic and natural estrogen hormones in influent and effluent of three municipal wastewater treatment plants, Water Environ. Res. 2007, 79: 969-974.

Roefer P., Snyder S., Zegers R.E., Rexing D.J., Fronk J.L., Endocrine-disrupting chemicals in a source water, J AWWA 2000, 92: 52-58.

Routledge E.J., Sheahan D., Desbrow C., Brighty G.C., Waldock M., Sumpter J.P., Identification of estrogenic chemicals in STW effluent. 2. In vivo responses in trout and roach, Environ. Sci. Technol. 1998, 32: 1559–1565.

Silva M.R.A., Trovó A.G., Nogueira R.F.P., Degradation of the herbicide tebuthiuron using solar photo-Fenton process and ferric citrate complex at circumneutral pH, J. Photochem. Photobiol. A: Chem. 2007, 191: 187-192.

Tabak H., Bloomhuff R.N., Bunch R.L., Steroid hormones as water pollutants II. Studies on the persistence and stability of natural urinary and synthetic ovulation-inhibiting hormones in untreated and treated wastewaters, Dev. Ind. Microbiol. 1981, 22: 497-519.

Tabata A., Kashiwa S., Ohnishi Y., Ishikawa H., Miyamoto N., Itoh M., et al. Estrogenic influence of estradiol-17β, p-nonylphenol and bisphenol A on Japanese Medaka (Oryzias iatipes) at detected environmental concentrations, Water Sci. Technol. 2001, 43: 109-116.

Tandy S., Bossart K., Mueller R., Ritschel J., Hauser L., Schulin R., Nowack B., Extraction of heavy metals from soils using biodegradable chelating agents, Environ. Sci. Technol. 2004, 38: 937-944.

Taylor R.W., Shen S., Bleam W.F., Tu S.I., Chromate removal by dithionite-reduced clays: evidence from direct x-ray absorption near edge spectroscopy (XANES) of chromate reduction at clay surfaces, Clays Clay Miner. 2000, 48: 648-654.

Schmidt C.K., Fleig M., Sacher F., Brauch H.-J., Occurrence of aminopolycarboxylates in the aquatic environment of Germany, Environ. Pollut. 2004, 131: 107-124.

Schwertmann U., Cornell R.M., Iron oxides in the laboratory, V.C.H. Publisher, Inc 1991, p137.

Sedlak D.L., Hoigne J., The role of copper and oxalate in the redox cycling of iron in atmospheric waters, Atmos. Environ. 1993, 27: 2173-2185.

Servos M.R., bennie D.T., Burnison B.K., Jurkovie A., McInnis R., Neheli T., et al. Distribution of estrogens, 17β-estradiol and estrone, in Canadian municipal wastewater treatment plants, Sci. Total Environ. 2005, 336: 155-170.

Shareef A., Angove M.J., Wells J.D., Johnson B.B., Aqueous solubilities of Estrone,

17β-Estradiol, 17α-Ethynylestradiol, and Bisphenol A, J. Chem. Eng. Data 2006, 51: 879-881.

Shemer H., Kunukcu Y.K., Linden K.G., Degradation of the pharmaceutical metronidazole via UV, Fenton and photo-Fenton processes. Chemosphere 2006, 63: 269-276.

Shichi T., Takagi, K., Clay minerals as photochemical reaction fields, J. Photochem. Photobiol. C 2000, 1: 113-130.

Shore L.S., Correll D.L., Chakraborty P.K., Relationship of fertilization with chick manure and concentrations of estrogens in small streams. In: Steele K, editor. Animal waste and the land–water interface, Boca Raton, FL: CRC Press 1995, p 155- 162.

Song W.J., Cheng M.M., Ma J.H., Ma W.H., Chen C.C., Zhao J.C., Decomposition of hydrogen peroxide driven by photochemical cycling of iron species in clay, Environ. Sci. Technol. 2006, 40: 4782-4787.

Song W.J., Ma J.H., Ma W.H., Chen C.C., Zhao J.C., Photochemical production or depletion of hydrogen peroxide controlled by different electron transfer pathways in methyl viologen intercalated clays, J. Photochem. Photobiol. A: Chem. 2006, 183: 31-34.

Sposito G., Skipper N.T., Sutton R., Park S.-h., Soper A.K., Greathouse J.A., Surface Geochemistry of the clay minerals, P. Natl. Acad. Sci. USA, 1999, 96: 3358-3364.

Stucki J.W., Lee K., Zhang L.Z., Larson R.A., Effects of iron oxidation state on the surface and structural properties of smectites, Pure Appl. Chem. 2002, 74: 2145-2158.

Stumm W., Chemistry of the solid-water interface, John Wiley and Sons: New York 1992, p13-41.

Sum O.S.N., Feng J.Y., Hu X.J., Yue P.L., Pillaredlaponite clay-based Fe nanocomposites as heterogeneous catalysts for photo-Fenton degradation of acid black 1, Chem. Eng. Sci. 2004, 59: 5269-5275.

Sun Y.F., Pignatello J.J., Photochemical reactions involved in the total mineralization of 2,4-D by Fe3+/H2O2/UV, Environ. Sci. Technol. 1993, 27: 304-310.

Sun Z.S., ChenY.X., Ke Q., Photocatalytic degradation of cationic azo dye by TiO_2/bentonite nanocomposite, J. Photochem. Photobiol. A: Chem. 2002, 149: 169-174.

Swartz C.H., Reddy S., Benotti S.J., Yin H., Barber L.B., Brownawell B.J., et al. Steroid estrogens, nonylphenol ethoxylate metabolites and other wastewater contaminants in ground water affected by a residential septic system on Cape Cod, MA. Environ. Sci. Technol. 2006, 40: 4894-4902.

Thomas J.K., Physical aspects of radiation-induced processes on SiO_2,-Al_2O_3, zeolites, and

clays, Chem. Rev. 2005, 105: 1683-1734.

United States Environmental Protection Agency (USEPA). Special report on environmental endocrine disruption: an effects assessment and analysis, Washington, DC: Office of Research and Development, EPA/630/R-96/012, 1997, p6.

Vandevivere P., Saveyn H., Verstraete W., Feijtel T.C.J., Schowanek D., Biodegradation of metal-[S,S]-EDDS complexes, Environ. Sci. Technol. 2001, 35: 1765-1770.

Velupula N.J., Tedros G.J., Andrew M.C., Determination of Copper and Iron Using [S,S]-Ethylenediaminedisuccinic Acid as a Chelating Agent in Wood Pulp by Capillary Electrophoresis, Anal. Sci. 2007, 23: 493-496.

Voelker B.M., Morel F.M.M., Sulzberger B., Iron redox cycling in surface waters: effects of humic substances and light, Environ. Sci. Technol. 1997, 31: 1004-1011.

Waite T.D., Morel F.M.M., Photoreductive dissolution of colloidal iron oxide: effect of citrate, J. Colloid Interface Sci. 1984, 102: 121-137.

Walling C., Amaranth K., Oxidation of mandelic acid by Fenton's reagent, J. Am. Chem. Soc. 1982, 104: 1185-1189.

Wang L., Zhang C., Wu F., Deng N. Glebov E. M., Bazhin N. M. Determination of hydroxyl radroxyl radicals from photolysis of fe(III)-pyruvate complexes in homogeneous aquous solution, React. Kinet. Catal. Lett. 2006, 89: 183-192.

Wang X.G., Liu C.S., Li X.M., Li F.B., Zhou S.G., Photodegradation of 2-mercaptobenzothiazole in the γ-Fe_2O_3/oxalate suspension under UVA light irradiation, J. Hazard. Mater. 2008, 153: 426-433.

Wang Y., Liu C.S., Li F.B., Liu C.P., Liang J.B., Photodegradation of polycyclic aromatic hydrocarbon pyrene by iron oxide in solid phase, J. Hazard. Mater. 2009, 162: 716-723.

Wang Z.H., Ma W.H., Chen C.C., Zhao J.C., Light-assisted decomposition of dyes over iron-bearing soil clays in the presence of H_2O_2, J. Hazard. Mater. 2009, 168: 1246-1252.

Wiederhold J.G., Kraemer S.M., Teutsch N., Borer P.M., Halliday A.N., Kretzschmar R., Iron isotope fractionation during proton-promoted, ligand-controlled, and reductive dissolution of goethite, Environ. Sci. Technol. 2006, 40: 3787-3793.

Wicks C., Kelley C. Peterson E., Estrogen in a karstic aquifer ground water, GroundWater 2004, 42: 384-389.

Wu F., Deng N.S., Zuo Y.G., Discoloration of dye solutions induced by solar photolysis of ferrioxalate in aqueous solutions, Chemosphere 1999 39: 2079-2085.

Wu F., Deng N.S., Photochemistry of hydrolytic iron (III) species and photoinduced

degradation of organic compounds. A minireview, Chemosphere 2000, 41: 1137-1147.

Wu F., Li J., Peng Z.E, Deng N.S., Photochemical formation of hydroxyl radicals catalyzed by montmorillonite, Chemosphere 2008, 72: 407-413.

Wu K., Xie Y., Zhao J., Hidaka H., Photo-Fenton degradation of a dye under visible light irradiation, J. Mol. Catal. A: Chem. 1999, 144: 77-84.

Wu W.C., Wang S.L., Tzou Y.M., Chen J.H., Wang M.K., The adsorption and catalytic transformations of chromium on Mn substituted goethite, Appl. Catal. B 2007, 75: 272-280.

Xiao J.R., Peng T.Y., Dai K., Zan L., Peng Z.H., Hydrothermal synthesis, characterization and its photoactivity of CdS/Rectorite nanocomposites, J. Solid State Chem. 2007, 180: 3188-3195.

Ying G.G., Kookana R.S., Ru Y.J., Occurrence and fate of hormone steroids in the environment, Environ. Int. 2002, 28: 545-551.

Yost E.C., Anderson M.A., Absence of phenol adsorption on goethite, Environ. Sci. Technol. 1984, 18: 101-106.

Zen J.M., Kumar A.S., The prospects of clay mineral electrodes, Analytical Chemistry, 2004, 76: 205A-211A.

Zepp R. G., Hoigné J., Bader H. Nitrate-induced photooxidation of trace organic chemicals in water, Environ. Sci. Technol. 1987, 21: 443-450.

Zepp R.G., Faust B.C., Hoigne J., Hydroxyl radical formation in aqueous reactions (pH 3-8) of iron(II) with hydrogen peroxide: the photo-Fenton reaction. Environ. Sci. Technol. 1992, 26: 313-319.

Zhang C.B., Photodegradation of organic pollutants induced by iron-carboxylate complexes in aqueous solutions, pHD thesis, n^{o} DU 1925, Université Blaise Pascal, Clermont-Ferrand (France).

Zhang C.B., Wang L., Pan G., Wu F., Deng N.S., Mailhot G., Mestankova H., Bolte M., Degradation of atrazine photoinduced by Fe(III)-pyruvate complexes in the aqueous solution, J. Hazard. Mater. 2009, 169: 772-779.

Zhang L.H., Zhu Z.L., Zhang R.H., Zheng C.S., Zhang H., Qiu Y.L., Zhao J.F., Extraction of copper from sewage sludge using biodegradable chelant EDDS, J. Environ. Sci. 2008, 20: 970-974.

Zhang Y., Zhou J.L., Ning B., Photodegradation of estrone and 17β-estradiol in water, Water Res. 2007, 41: 19-26.

Zhao Y.P., Hu J.G., Jin W., Transformation of oxidation products and reduction of estrogenic activity of 17β-estradiol by heterogeneous Photo-Fenton reaction, Environ. Sci. Technol. 2008, 42: 5277-5284.

Zheng W., Yates S.R., Bradford S.A., Aanylsis of Steriod hormones in a typical dairy wast disposal system, Environ. Sci. Technol. 2008, 42: 530-535.

Zhou D.N., Wu F., Deng N.S., Fe(III)-oxalate complexes induced photooxidation of diethylstilbestrol in water, Chemosphere 2004, 57: 283-291.

Zhou J.L., Liu R., Wilding A., Hibberd A., Sorption of selected endocrine disrupting chemicals to different aquatic colloids, Environ. Sci. Technol. 2007, 41: 206-213.

Zhu H.Y., Li J.Y., Zhao J.C., Churchman G.J., Photocatalysts prepared from layered clays and titanium hydrate for degradation of organic pollutants in water, Appl. Clay Sci. 2005, 28: 79-88.

Zuo Y.G., Deng Y.W., Iron(II)-catalyzed photochemical decomposition of oxalic acid and generation of H_2O_2 in atmospheric liquid phases, Chemosphere, 1997, 35: 2051-2058.

Paper published

F. Wu, **J. Li**, N.S. Deng, Photochemical formation of hydroxyl radicals catalyzed by montmorillonite, Chemosphere, 2008, 72(3): 407-413.

J. Li, F. Wu, N.S. Deng, E.M. Glebov, N.M. Bazhin, Degradation of orange II by heterogeneous photocatalytic reaction using montmorillonite KSF, Reaction Kinetics and catalysis letter, 2009, 95(2): 247-255.

J. Li, F. Wu, G. Mailhot, N.S. Deng, Photodegradation of chloroform in aqueous solution:

Impact of Montmorillonite KSF particles, Journal of Hazardous Material, 2010, 174: 368-374.

J. Li, G. Mailhot, F. Wu, N.S. Deng, Photochemical efficiency of Fe(III)-EDDS complex: OH radical production and 17β-estradiol degradation, Journal of Photochemistry and Photobiology A: Chemisty, 2010, 212: 1-7.

J. Li, Y.X. Lu, F. Wu, N.S. Deng, Determination of hydroxyl radicals in aqueous kaolinite suspensions under irradiation, Environmental Chemistry 2007, 26(5): 651-653.

J. Li, Y.X. Liu, F. Wu, N.S. Deng, Determination of hydroxyl radicals in aqueous kaolinite suspensions under irradiation, presented at the Program 2nd International Workshop on Sustainable Asia, 2006.

Y.X. liu, **J. Li,** F. Wu, C.B. Zhang, N.S. Deng, Insight into heterogeneous photocatalytic degradation of phenol over montmorillonite KSF, Chemical Engineering Communications, 2008, 195: 988-997.

Z.'e Peng, **J. Li**, F. Wu, N.S. Deng, H.Z. Yang, Photodegradation of 4-Octylphenol induced by algae in aqueous solution, Fresenius Environmental bulletin, 2009, 18(4): 399-405.

Z.P. Wang, L.Z. Huang, J.W. Su, **J. Li**, G.H. Liu, Z. Zhang, Removal of cyanides in coking wastewater by ferrate pre-oxidization followed by photochemical process, Fresenius Environmental bulletin, 2008, 17(8a): 1082-1087.

Y. Chen., **J. Li**, W.Y. Huang, Photodegradation of Dichlorophen in Montmorillonite Suspension, Environmental Science & Technology(in China), 2009, 32(3): 135-138.

Tire français :

Dégradation du 17β-estradiol photoinduite par des complexes et des oxydes de fer et par des argiles : effet d'un agent complexant l'acide éthylènediamine-N,N'-disuccinique

Résumé français:
La photodégradation du 17β-estradiol (E2), un perturbateur chimique endocrinien, est réalisée en présence d'un complexe de fer, d'argiles et d'un oxyde de fer. L'impact d'un agent complexant du fer l'acide éthylènediamine-N,N'-disuccinique (EDDS) est aussi étudié. Après la détermination des propriétés physicochimiques du complexe Fe(III)-EDDS, les rendements quantiques de formation des $^{\bullet}OH$ et de dégradation de E2 ont été évalués en fonction de différents paramètres (pH, $[O_2]$, [Fe(III)-EDDS], [Fe(III)]). Pour la première fois, les rendements quantiques de production d'$^{\bullet}OH$ ont été mesurés *via* la photolyse du complexe Fe(III)-EDDS en utilisant l'acide téréphtalique comme sonde. Dans une seconde partie, les processus d'adsorption et de dégradation photocatalytique de E2 dans des suspensions de Montmorillonite KSF, de Montmorillonite naturel et de Goethite sont étudiés. L'adsorption de E2 sur les minéraux est rapide et faible. La vitesse de photodégradation de E2 est influencée par la concentration en minéraux et le pH. Le processus de dégradation photocatalytique de E2 dans ces systèmes a par la suite été étudié en présence d'EDDS. Dans les trois suspensions et en présence d'EDDS, la photodégradation de E2 augmente significativement dans la zone de pH neutre et basique (de 5,0 à 9,0). Au contraire, sans EDDS le pH optimal est limité aux pHs acides (entre 3,0 et 4,0). Les cinétiques de dégradation de E2 suivent un loi de vitesse du modèle Langmuir-Hinshelwood pour les trois systèmes. Sur la base de nos résultats, il est possible de conclure que les systèmes EDDS-Fe(III)/minéraux sont photocatalytiquement efficaces pour l'élimination de polluants organiques dans l'eau.

Titre anglais:

17β-estradiol degradation photoinduced by iron complex, clay and iron oxide minerals: effect of the iron complexing agent ethylenediamine-N,N'-disuccinic acid

Résumé anglais:
In this study the photodegradation of the 17β-estradiol (E2), an endocrine-disrupting chemicals (EDCs), is investigated in the presence of iron complex, clay and iron oxide minerals. The impact of one iron complexing agent ethylenediamine-N,N'-disuccinic acid (EDDS) in such systems is also investigated . After the determination of the physicochemical properties of Fe(III)-EDDS complex, the quantum yields of $^{\bullet}OH$ formation and of E2 degradation are evaluated as a function of different parameters (pH, $[O_2]$, [Fe(III)-EDDS], [Fe(III)]). For the first time, the quantum yields of $^{\bullet}OH$ production are measured *via* photolysis of Fe(III)-EDDS with terephthalic acid as probe. In a second part of the work, the adsorption and photocatalytic degradation processes of E2 in the suspensions of Montmorillonite KSF, Natural Montmorillonite (NM) and Goethite are studied. The adsorption of E2 on the minerals is fast and weak. The E2 photodegradation rate is influenced by the concentration of minerals and pH. The photocatalytic degradation process of E2 in the suspensions of Montmorillonite KSF, Natural Montmorillonite and Goethite in the presence of EDDS are studied. In these three minerals-EDDS suspensions, the photodegradation of E2 significantly increases at near-neutral pH and basic pH (pH 5.0 to 9.0). On the contrary, without EDDS, the optimal pH is limited in the acid pH (3.0 to 4.0). The degradation kinetics of E2 follows the Langmuir-Hinshelwood rate law in all the three minerals-EDDS system. Based on the above results, EDDS-Fe(III)/mineral systems are effective photocatalysis system

for the removal of the organic pollutants from water.

Mots clés :
Oxydes de fer ; Argiles ; EDDS ; Radicaux hydroxyles ; 17β-estradiol ; Photodégradation